

Trinity College Dublin
Coláiste na Tríonóide, Baile Átha Cliath
The University of Dublin

Methods in Reducing The Risk of Fatal Injury During Subway Train to Pedestrian Collisions

---

Daniel Hall

Supervisor: Dr. Ciaran Simms

Department of Mechanical, Manufacturing & Biomedical Engineering
School of Engineering
Trinity College Dublin, *the University of Dublin*
D02 PN40
Ireland

March 2025

A PhD Thesis submitted to the University of Dublin in partial fulfillment of the requirements for the degree Doctor of Philosophy in Biomechanical Engineering *(PhD)*

Declaration

I have read and I understand the plagiarism provisions in the General Regulations of the University Calendar for the current year, found at http://www.tcd.ie/calendar.
I have also completed the Online Tutorial on avoiding plagiarism 'Ready Steady Write', located at http://tcd-ie.libguides.com/plagiarism/ready-steady-write.

Your name, Month Year

Abstract

Significant advancements in pedestrian safety have been achieved in automotive design over the past century, as evidenced by the adoption of rounded vehicle shapes, increased bumper coverage, and the implementation of policies such as speed limits and vehicle safety assessment programmes. In contrast, subway-to-pedestrian collisions remain a growing concern, receiving comparatively less attention regarding passive safety measures. While collision avoidance interventions such as Platform Screen Doors have proven effective, they are not always feasible in older subway networks, such as the NYC subway system.

At the onset of this research, the most recent epidemiological data for NYC subway-to-pedestrian collisions covered incidents from 1990–2007. This study seeks to update and expand upon that previous work by analysing 185 subway-to-pedestrian incident reports from 2019, as provided by the Public Transportation Safety Board (PTSB), to offer biomechanically relevant insights that were previously unavailable in academic literature. The updated data refines the distribution of incidents by sex, age, and geographic area, demonstrating nearly equivalent distributions of standing, jumping, and lying pedestrian postures at the moment of impact. It identifies 12m/s as the most common impact velocity, with 97% of incidents occurring within 60m of a station platform. Elevated stations showed a higher fatality rate (40%) compared to below-ground stations (27%), with drainage troughs highlighted as a potential mitigating factor.

The literature review identified a lack of PMHS (post-mortem human subject) or ATD (anthropomorphic test device) data specific to subway-to-pedestrian collisions. At present, the characteristics of pedestrians predominantly dictate the effective contact stiffness in such impacts; however, the introduction of energy-absorbing countermeasures alters this dynamic. To mitigate this gap, nine controlled impact tests were performed utilising a cylindrical headform and DC-coupled accelerometer. The derived force-penetration relationships for foam, as well as foam encased in 1mm aluminium or 3mm ABS shells at impact velocities of

7.5, 10, and 11.5m/s were validated using multibody modelling software (MADYMO). This validation demonstrates its effectiveness for future countermeasure modelling.

The first baseline subway-to-pedestrian model was developed to evaluate the current risks associated with head and run-over injuries. Using 1920 simulated scenarios informed by the PTSB data, the model revealed a significant risk of wheel contact during run-over events, irrespective of train entry velocity. The incorporation of a 0.5m drainage trough resulted in a 50% reduction in run-over risk, thereby validating its safety advantages. These findings indicate that policies which concentrate exclusively on reducing train entry speed would have minimal impact on the reduction of run-over injuries.

Three countermeasure designs were evaluated using a reduced simulation test matrix: three impact velocities (8, 10, and 12m/s) and a trough depth of 0.75m. Modular panels attached to the train front significantly reduced head injury risk (90%) and pedestrian-to-train wheel contact risk (58%), with greater effectiveness observed when a larger frontal area was covered. A rail guard design successfully decreased secondary contact injuries; however, it inadvertently heightened the risks of run-over and amputation due to altered pedestrian kinematics.

This research represents an advancement in the field of subway-to-pedestrian collision safety, providing key insights into biomechanics and engineering design across four pillars of biomechanical safety research. By addressing previously unexplored aspects of impact dynamics, pedestrian injury mechanisms, and countermeasure efficacy, this thesis establishes a foundational framework for enhancing subway safety worldwide. The findings highlight that targeted design interventions, such as energy-absorbing countermeasures and optimised drainage troughs, can significantly reduce the risks of fatal head injuries and train wheel contact during subway-to-pedestrian collisions. This work not only bridges the gaps in biomechanical understanding but also lays the groundwork for future policy, design, and simulation-based advancements aimed at mitigating subway-related fatalities and injuries in both legacy and modern transit networks.

List of Publications

The research presented in this thesis has resulted in the following journal publications.

Based on Chapter 3

- Hall, D., Linogao, J., Zentz, L., Shaw, G., Lamb, T. and Simms, C., 2023. Detailed analysis of New York City subway pedestrian incidents from 2019. Transportation research record, 2677(11), pp.642-650.

Based on Chapter 5

- Hall, D., Gildea, K. and Simms, C., 2024. Drainage Troughs as a Protective Measure in Subway–Pedestrian Collisions: A Multibody Model Evaluation. Applied Sciences, 14(22), p.10738.

Acknowledgements

I would like to thank all those who have helped and supported this research with particular attention given to Prof Ciaran Simms, my PhD supervisor. Prof Simms has gone far beyond what is expected of a supervisor and has facilitated my academic, career and personal growth throughout the course of my PhD. I have been introduced to so many people through Prof Simms and he always made me feel welcome and like a peer. Ciaran genuinely cares for the development of his students beyond the completion of the PhD programme. The balance Prof Simms has struck between teaching, supervision and personal responsibilities is incredibly admirable and he always made the time to offer support for any issue that might arise. His reputation as one of the best supervisors, as well as his reputation in the field of biomechanics, is well earned. I look forward to continued work and learning from him in the future.

Growing up in a single parent household and as the first one in my family to attend third level education let alone go on to pursue a PhD, my mother has sacrificed a lot to ensure my success and for that I am forever grateful. She gave me the tools and confidence to put myself into positions I never would have thought possible. Without both my mother's (Sharon Hall) and grandmother's (Pauline Hall) help, both personally and financially I would not have been able to achieve this no matter how hard I tried. I hope to continue making them both proud and inspire my little brother (Adam Hall) to never doubt what is possible as he grows up.

Dr Kevin Kildea, a former PhD student under Ciaran Simms has acted as an academic rolemodel for me throughout my career. Kevin acted as a Teaching Assistant (TA) while I was in my undergraduate and through him, I was introduced to the world of PhD work and publishing (and I still chose to do one). Kevin and I have worked together on multiple projects and I hope to continue this in the future.

The staff at Trinity College Dublin have been a huge benefit to my overall PhD experience. Not only did the technical staff (Robert Dunbar, Alex Kearns, Brendan Caffrey, Nithin

Ajayanand Brian O'Dwyer) manufacture the components necessary for this research, but their attitude and overall interest in the application of these tools heightened the experience.

The new senior technical officer Dr Patrick Lynch also deserves special attention. Patrick has given a huge amount of his time to help me with the experimental sensors and equipment used in this thesis. From late nights trying to diagnose issues with calibration to talking about undergraduate memories and dungeons and dragons, Patrick has always been open and willing to help and I thank him for this.

This project is funded as part of a larger collaborative effort under FTA-2020-004-TRI-SRD: Research effort entitled "FY20 SRD-Designed for Impact – An Innovative Approach to Train Safety and Collision Fatality Reduction". As part of this work I have been introduced to many professionals in this field such as John Kraljic from idk3 and the faculty and alumni of the University of Virginia (UVA). I was fortunate to spend some time at the Center for Applied Biomechanics (CAB) at UVA during my PhD and have learned a lot from Dr Greg Shaw, Dr Bronislaw Gepner, Dr Daniel Perez, Katarzyna Rawska and Logan Zentz. I look forward to continued experience working with CAB in the future.

Contents

Declaration **i**

Acknowledgements **vii**

List of Figures **xix**

List of Tables **xxii**

Nomenclature **xxv**

1 Introduction **1**

1.1 Background 2

1.2 Research Approach and Thesis Structure 4

1.2.1 Funding 4

1.2.2 Objectives 4

1.2.3 Thesis Structure 7

2 Literature Review **9**

2.1 Introduction 10

2.2 Head Injury Metrics 10

2.2.1 Background 10

2.2.2 Gadd Severity Index 11

2.2.3 Head Injury Criterion 12

2.2.4 Rotational Based Head Injuries 14

2.2.5 Abbreviated Injury Scale 15

2.3 Epidemiology and Data Collection 16

2.3.1 Background 16

2.3.2 Search Criteria 16

2.3.3 Pedestrian Information 18

2.3.4 Fatality Rates and Injury Information 18

2.3.5 Station Environment . . . 21
2.4 Impact Testing . . . 25
2.4.1 Background . . . 25
2.4.2 Post-Mortem Human Surrogates Testing . . . 26
2.4.3 Anthropomorphic Test Devices . . . 31
2.5 Numerical and Computational Modelling . . . 33
2.5.1 Background . . . 33
2.5.2 MADYMO Multibody Modelling . . . 33
2.5.3 Finite Element Modelling . . . 43
2.6 Impact Energy Mitigation . . . 45
2.7 Summary and Research Gap . . . 50

3 A Detailed Analysis of New York City Subway Pedestrian Incidents from 2019 53

3.1 Introduction . . . 54
3.2 Methodology and Data Collection . . . 56
3.3 Results . . . 58
3.3.1 Literature Comparison . . . 58
3.3.2 Event Type and Location . . . 59
3.3.3 Impact Data . . . 60
3.4 Discussion . . . 63
3.4.1 Event Type and Location . . . 63
3.4.2 Impact Data . . . 64
3.4.3 Countermeasure Summary . . . 65
3.4.4 Limitations . . . 66
3.5 Conclusion . . . 67

4 Experimentally Derived Contact Characteristics for Hard Shell Energy Absorbing Material: Application to Subway-to-Pedestrian Collisions 69

4.1 Introduction . . . 70
4.2 Material Selection . . . 71
4.2.1 Analytical model . . . 71
4.2.2 Quai-static Compression Testing . . . 73
4.3 Full Testing Methodology . . . 76
4.3.1 Acceleration . . . 76

4.3.2 Impact . . . 80
4.3.3 Containment . . . 82
4.3.4 Instrumentation . . . 83
4.3.5 Test Matrix . . . 83
4.4 Post Processing . . . 85
4.5 Results . . . 86
4.5.1 Impact Test Results . . . 86
4.5.2 Force Penetration Characteristics . . . 88
4.5.3 Viscoelastic Behaviour . . . 88
4.5.4 MADYMO Reconstruction . . . 90
4.6 Discussion . . . 91
4.6.1 Limitations . . . 92
4.7 Conclusions . . . 93

5 Baseline Multibody Model of Subway-to-Pedestrian Collisions: Effect of Impact Velocity and Drainage trough Depth on Injury Risk 95

5.1 Introduction . . . 96
5.2 Methodology . . . 97
5.2.1 Multibody Train Model and Impact Velocity . . . 97
5.2.2 Adapted MADYMO Human Pedestrian Model . . . 99
5.2.3 Pedestrian Position and Pose . . . 101
5.2.4 Simulation Test Sample (STS) . . . 101
5.3 Injury Criteria & Contact Score . . . 103
5.4 Weighted Injury Scores (WIS) . . . 104
5.5 Sensitivity Study . . . 105
5.6 Results . . . 106
5.6.1 Sensitivity Study . . . 106
5.6.2 Baseline Run-Over Risk . . . 107
5.6.3 Baseline Head Injury Risk . . . 109
5.6.4 STS Run-Over Risk . . . 111
5.6.5 STS Head Injury Risk . . . 111
5.7 Discussion . . . 112
5.7.1 Main Findings . . . 112

5.7.2 Baseline Run-Over Risk . . . 113
5.7.3 Effect of drainage trough on Run-Over Risk . . . 114
5.7.4 Baseline Head Injury Risk . . . 115
5.7.5 Limitations . . . 116
5.8 Conclusion . . . 117

6 Subway to Pedestrian Collision Safety: Multibody Models of Energy Absorbing Countermeasure Designs 119

6.1 Introduction . . . 120
6.2 Countermeasure Design . . . 121
6.2.1 Design Targets . . . 121
6.2.2 Train Front Panels (FP) . . . 122
6.2.3 Full Frontal Guard (FFG) . . . 124
6.2.4 Rail Guard (RG) . . . 125
6.2.5 Simulation Test Matrix . . . 126
6.3 Results . . . 126
6.4 Discussion . . . 129
6.4.1 Head Injury Risk . . . 129
6.4.2 Run-Over Risk . . . 130
6.4.3 Overall Fatality Risk . . . 132
6.4.4 Limitations . . . 132
6.5 Conclusions . . . 133

7 Discussion 135

7.1 Discussion of Results . . . 136
7.1.1 Background . . . 136
7.1.2 Epidemiology - A Detailed Analysis of New York City Subway Pedestrian Incidents from 2019 . . . 136
7.1.3 Impact Testing - Experimentally Derived Contact Characteristics for Hard Shell Energy Absorbing Material: Application to subway-to-pedestrian Collisions . . . 137
7.1.4 Computational Modelling - Drainage Troughs as a Protective Measure in subway-to-pedestrian Collisions: A Multibody Model Evaluation . . . 139

7.1.5 Safety Device Design - subway-to-pedestrian Collision Safety: Multi-body Models of Energy Absorbing Countermeasure Designs 141
7.2 Limitations 143
7.3 Addition To Known Literature 144

8 Conclusions **147**
8.1 Main Conclusion 148
8.2 Future Work 150
8.3 Final Statement 150

A Quasi-static Compression Testing Used in Chapter 4 **165**
A.1 Firm Foam F2H 40F 166
A.2 Mixed Firm and Memory Foam F2H 36M 167

B DYNATEST Operational Procedure Used in Chapter 4 **169**

C Construction of Containment Unit Used in Chapter 4 **171**

D Effect of Z Axis Acceleration on Foam Impact Tests [Chapter 4] **175**
D.1 Investigation of Multi-Axis Rotational Effects on Acceleration Time History . 176

List of Figures

1.1 Visual road and rail vehicle design progression over 100 year time span 2
1.2 Thesis structure schematic 7

2.1 Wayne State Tolerance Curve (WSTC) [Rowson and Duma, 2022] 11
2.2 The relationship between the GSI and its scaling factor [Nokes et al., 1995] . 12
2.3 Logistic Regression of HIC to Skull Fracture [Vander Vorst et al., 2003] . . . 13
2.4 Comparison of linear and rotation based head injury criterions [Marjoux et al., 2008] 14
2.5 Relationship between HIC score and AIS [Mackay, 2007] 15
2.6 Incidents involving persons under London Underground trains (1973-1990). Survival according to line and presence of drainage troughs [O'Donnell and Farmer, 1994a] 22
2.7 Railway suicides by railway system in Hong Kong, 1997–2007 [Law et al., 2009] 24
2.8 Evacuation time of a train compartment [O'Donnell and Farmer, 1994a] . . . 25
2.9 Vehicles used in PMHS tests 28
2.10 Sequences of vehicle-pedestrian impact for the six cadaver tests 29
2.11 Summary of head injuries for vehicle and ground contact 30
2.12 Pilot Tram Hybrid III Impact Setup 31
2.13 Impact between Hybrid III and a T6A5 ČKD Tatra tram 32
2.14 Ellipsoid pedestrian models, from left to right; 3-year-old child, 6-year-old child, small female, mid-size male and large male 35
2.15 The vehicle models used in [Shi et al., 2018a] with simplified MADYMO models 36
2.16 The initial postures of PMHS pedestrians and the corresponding scaled multi-body models 36
2.17 Comparison between PMHS and MADYMO HIC scores 38

2.18 Initial joint angle effect on aHIC and BrIC from ground contact for Test 01 . 38
2.19 Tramway front end modeled using 2 portions of planes (blue = windshield, green = fairing) 39
2.20 All scenarios involved a tram speed of 20 km/h and the AM50 model 40
2.21 Pedestrian stances for different gait parameters (%) 41
2.22 Comparison of the distribution of head contact point on different vehicle for different vehicle velocity and pedestrian gait 42
2.23 All scenarios involved a tram speed of 20 km/h and the AM50 model 43
2.24 Primary stage of impact of modified front on the dummy in the simulation . 44
2.25 Illustration of overall test configuration 45
2.26 Tata SE 1613 Turbo EX BS II Truck with attached with DEA frontal system 47
2.27 Plot for HIC at different speeds during first and secondary impacts for pedestrian rear impacts 48
2.28 Primary impact HIC vs gait with DEA (Right) and without DEA (Left) . . . 49
2.29 Summary of literature review findings 52

3.1 Fatality data comparison between Gershon et al., 2008 and 2019 data 58
3.2 KABCO Accident vs Suicide for NYC Subway 2019, n = 159 59
3.3 KABCO proportions vs track type for NYC Subway 2019, n = 178 60
3.4 Pre-Impact behaviour for for NYC Subway 2019, N = 159 61
3.5 Impact positions for for NYC Subway 2019, N = 125 61
3.6 2019 NYC Subway data with estimated impact velocity (mph), N = 65 . . . 62
3.7 2019 NYC Subway KABCO data with primary contact area, N = 170 62
3.8 2019 NYC Subway KABCO data with pedestrian final position, N = 175 . . 63
3.9 Elevated and Below ground NYC Subway Stations. Images taken by Author . 64

4.1 Analytical model ramp function schematic 71
4.2 Analytical model estimates for a 15kN/m EAC with a 4.5kg mass at 12m/s . 72
4.3 Instron 3366 compression test machine using Bluehill software package . . . 73
4.4 Bound Foam with Memory Foam Topper 74
4.5 Full scale, quasi static compression test setup 75
4.6 Pedestrian headform ATD from Humanetics 76
4.7 Pedestrian headform dimensioned drawings for fabrication at TCD 77

4.8 Dynatest 500 Impact System 78
4.9 Dynatest 500 Impact System operating principles 78
4.10 Dynatest 500 headform mount, dimensioned drawing for fabrication at TCD . 79
4.11 Solidworks render of foam EAC held within mount on crash barrier 80
4.12 Solidworks part drawing for EAC hard shell covers 81
4.13 All energy absorbing countermeasure surfaces 81
4.14 Solidworks render of containment unit 82
4.15 Completed containment unit 82
4.16 Instrumentation schematic for headform impact tests 83
4.17 Recording apparatus used for impact testing 84
4.18 Positions of markers used for impact velocity calculations 84
4.19 Accelerometer data processing 85
4.20 Acceleration data for each test condition 86
4.21 Position of tracking points throughout the loading phase shown as red circles 87
4.22 Penetration time histories during the impact loading phase 87
4.23 Derived force penetration relationship for each test condition 88
4.24 Headform linear velocities for foam EAC force penetration curves [Impact Velocities, bottom to top 7.5-10-11,5m/s] 89
4.25 Viscoelastic behaviour observed for dynamic tests only 89
4.26 Real (solid) and simulated (dashed) acceleration time histories 90

5.1 MADYMO Multibody Model of an R160 Subway Train 98
5.2 NYC flat track bed with no crossties & multibody model (Images taken by author) 99
5.3 NYC track bed with drainage trough and crossties & multibody model (Images taken by author) 99
5.4 Force-Penetration data for the existing AM50 model compared to calculated linear stiffness [Shi et al., 2018b] 100
5.5 Representative stills from YouTube videos, illustrating 2D keypoints, 3D keypoints, and the subsequent MADYMO pe-destrian modeling configuration via KinePose [Gildea et al., 2022] 101
5.6 Pedestrian position and poses used in full STS 102
5.7 Contact phases for jumping case at 16m/s impact velocity 103

5.8 Sensitivity study pedestrian impact position and posture 105
5.9 Sensitivity study contact scores at different hysteresis values 107
5.10 Contact Scores and Weighted Contact Scores for baseline model. All impact positions 107
5.11 Overall combined Contact Scores and Weighted Contact Scores for Baseline Simulation Test Sample 108
5.12 Effect of impact velocity on contact scores (weighted*) 108
5.13 Baseline Simulation Test Sample (BSTS) primary and secondary HIC_{15} scores 109
5.14 Baseline Simulation Test Sample proportion of jumping and standing $HIC_{15} <$ 2000 110
5.15 Full Simulation Test Sample contact scores separated by impact position and drainage trough depth 111
5.16 Relationship between drainage trough depth and secondary contact HIC_{15} score for jumping and standing impact scenarios 112
5.17 Standing (blue) and jumping (yellow) kinematics for a 16m/s impact 114

6.1 Multibody model of subway pedestrian collision with front panel EAC concept 123
6.2 Solidworks renderings of modular front panels countermeasure design 123
6.3 Multibody model of standing pedestrian to subway collision with full frontal guard countermeasure concept 124
6.4 Solidworks rendering of rail guard design 125
6.5 Range of HIC_{15} scores for each countermeasure design 126
6.6 HIC_{15} scores for each countermeasure design 127
6.7 Contact scores for each countermeasure deign 128
6.8 Countermeasure effect on head injury and run-over risk [Hatched = No run-over] 128
6.9 Baseline (yellow) and front panels (green) effect on fall kinematics 130
6.10 Baseline (yellow) and rail guard (green) effect on fall kinematics 131

7.1 Summary of literature review findings 146

A.1 Firm foam compression test results 166
A.2 Firm foam with memory compression test results 167

C.1 Dynatest 500 impact ram with containment unit and EAC mounting block . 173

D.1 Effect of incorporating Z axis acceleration to 7m/s foam impact tests 176

List of Tables

2.1 Abbreviated Injury Scale classifications and associated head injury risk 15
2.2 Review of 13 epidemiological studies involving subway to pedestrian collisions 17
2.3 Review of 13 epidemiological studies involving subway to pedestrian collisions 18
2.4 Subway related injury patterns at a level 1 adult trauma centre in Toronto Canada 2010-2018 19
2.5 Type and location of injuries at Bellevue Hospital, New York City from 2001 to 2016 20
2.6 Injury Type (Fatalities) and Location from NYC OCME 2003-2007 21
2.7 Published studies regarding effectivness of drainage troughs 22
2.8 PMHS test details 28
2.9 Estimated hypothetical HIC scores for tram pedestrian collisions 32
2.10 Anthropometry of the ellipsoid pedestrian model 34
2.11 Anthropometry of the ellipsoid pedestrian model 35
2.12 Pendulum Head Side Impact with 25 mm offset from CG 5th percentile female Hybrid III Head and Neck 46
2.13 Free Fall Head Impacts 50% male Hybrid III 5.4 m/s and 25 mm CG offset . 47
2.14 Secondary impact HIC scores 50

3.1 1990-2003 NYC fatality data 55
3.2 2003-2007 NYC fatality data 55
3.3 Relevant information recorded from PTSB incident reports 57
3.4 1990-2003 Gershon et al. [2008a], 2003-2007 Lin and Gill [2009] and 2019 Data 59
3.5 2019 NYC Subway incidents by station type and location 60
3.6 Summary of possible countermeasures based on findings 66

4.1 Impact Test Matrix 84

5.1 Age and Sex percentage for NYC Subway fatalities [Gershon et al., 2008b] [Lin and Gill, 2009] [Hall et al., 2023] 100
5.2 Full Simulation Test Sample (N = 1920) 102
5.3 All Impact Scenario Proportions (ISPs) for baseline model 104
5.4 Sensitivity study initial conditions and variables 105
5.5 Sensitivity study, simulations with modelling instabilities with various fracture joint damping 106

6.1 Countermeasure design simulation test sample N = 216 126

Nomenclature

Acronyms

AIS Abbreviated Injury Score

*AM*50 Adult Male 50th Percentile

ASTM American Society for Testing and Materials

ATD Anthropomorphic Test Devices

BrIC Brain Injury Criterion

BSTS Baseline Simulation Test Sample

CG Centre of Gravity

CPSC Consumer Product Safety Commission

CSA Canadian Standards Association

CSO Central Statistics Office

CVS Crash Victim Simulation

DEA Deformable Energy Absorber

DEA Deformable Energy Absorbing

ERA European Railway Agency

EU European Union

Euro NCAP European New Car Assessment Programme

FE Finite Element

FRA Federal Railroad Administration

$GIDAS$ German In-Depth Accident Study

GSI Gadd Severity Index

HBM Human Body Model

HGV Heavy Goods Vehicle

HIC Head Injury Criterion

HIP Head Impact Power

ISS Injury Severity Score

LRV Light Rail Vehicle

LTV Light Truck Vehicle

$MADYMO$ MAthematical DYnamic MOdels

$MAIS$ Maximum Abbreviated Injury Score

MB Multibody

$MBIM$ Model Based Image Mapping

MPV Multi-Purpose Vehicle

$NBLEH$ Normalized Bonnet Leading Edge Height

$NCAP$ New Car Assessment Programme

$NHTSA$ National Highway Traffic Safety Administration

NYC New York City

$OCME$ Office of Chief Medical Examiner

$PMHS$ Post-Mortem Human Subject

PSD Platform Screen Doors

STS Simulation Test Sample

SUV Sports Utility Vehicle

$THUMS$ Total Human Model for Safety

URV Urban Rail Vehicle

USA United States of America

UVA University of Virginia

$WSTC$ Wayne State Tolerance Curve

Chapter 1

Introduction

1.1 Background

Since the rise and widespread adoption of road vehicles in the early 20th century, pedestrians have been at risk of injury, with the first reported pedestrian fatality in 1899 [Tiwari, 2020]. This growing concern has spurred decades of research and development aimed at reducing pedestrian fatalities and injuries. Pedestrian safety advancements can be seen both visually (Figure 1.1(a)) in the evolution of vehicle designs (e.g. rounded edges, crumple zones, and external airbags) and statistically through a marked decrease in pedestrian fatality rates over time [Buehler and Pucher, 2021, Eid and Abu-Zidan, 2015]. Organisations such as the United States New Car Assessment Programme (US NCAP) or European New Car Assessment Programme (EURO NCAP) have become synonymous with crash testing and safety ratings.

There are other forms of transportation which have been increasing in usage in large cities. According to the International Association of Public Transport, 14 new cities opened a metro system between 2018 and 2020, taking the total number to 193, of which 15 had a length exceeding 250km [Brief, 2022]. The New York City (NYC) Subway, one of the oldest and largest in the world, transports 5.5 million daily passengers as of 2019. Despite the global increases in metro, subway and rail transportation use, the pedestrian safety measures in this domain have not witnessed the same degree of advancement 1.1(b).



(a) Road vehicle design progression 1920-2020



(b) NYC Subway design progression 1920-2020

Figure 1.1: Visual road and rail vehicle design progression over 100 year time span

Unique challenges, such as the high rate of intentional incidents including suicides and the extreme severity of run-over or secondary contact injuries (amputations), distinguish rail safety research from that of road traffic. In Europe, there were a total of almost 3000 annual occurrences of rail suicides between 2012 and 2016, accounting for 73% of all European rail-related fatalities [ERA, 2018]. In the United States of America (USA), the Federal Railroad Administration (FRA) Office of Safety Analysis reports a total of 941 train collisions involving trespassing pedestrians in 2023, a 64% increase in collisions since 2013 [FRA, 2022].

The high number of pedestrians purposefully positioning themselves in the path of a rail vehicle, combined with accidental collisions caused by falls from the platform, has prompted safety researchers to separate the pedestrian station environment from the track bed. This can be achieved through increased safety infrastructure such as Platform Screen Doors (PSD) which are designed to prevent access to the track area and open only when the train has safely stopped at the station. Many different types of PSDs have been implemented across various networks globally, such as the newly constructed Victoria Line on the London Underground in the United Kingdom (UK) or in the Shanghai metro system. Half-height PSDs that are 1.5m and 1.2m high have been shown to decrease the number of rail suicides by 79.2% and 60.2% respectively, while full-height PSDs reduced the number of metro suicides by 90.9% [Chung et al., 2016b]. Platform screen doors have been hailed as a catch-all solution to subway pedestrian safety; however, while these findings are promising, the installation of PSDs into the existing subway infrastructure can be both a technical and financial challenge. The NYC Subway system, which opened in 1904, has 472 active stations (more than 1200 platform edges) with 400km of passenger route track. A 2020 investigation by New York City Transit (NYCT) into the feasibility of PSDs on the NYC Subway found that, in its current state, only 8.6% of stations could support the installation of PSDs [Metropolitan Transportation Authority Track Trespassing Task Force, 2020]. One of the limiting factors of PSDs is the requirement that all subway train doors be specifically spaced apart so that the train doors line up with the platform doors. The NYC Subway fleet currently consists of a variety of different train models with various car lengths and door spacings. The NYCT investigation found that even with no misalignment issue, the number of feasible stations would increase to a maximum of only 27% due to the physical width and structural support of the platforms.

In summary, as road vehicle prevalence increased, pedestrian safety saw major advancements through rigorous assessment programs and targeted policies, significantly reducing fatality rates. In contrast, despite subway systems becoming essential to urban transport, subway vehicle front-end designs have remained largely unchanged for decades. While platform screen doors are effective in new stations, they are often impractical for existing infrastructure like the NYC Subway. This highlights the urgent need for further research into passive safety strategies to mitigate subway-to-pedestrian collision severity.

1.2 Research Approach and Thesis Structure

1.2.1 Funding

The work presented in this thesis is part of a Collaborative Research effort funded by the FTA and Research Team Members under FTA-2020-004-TRI-SRD: a research effort entitled "FY20 SRD-Designed for Impact – An Innovative Approach to Train Safety and Collision Fatality Reduction."

1.2.2 Objectives

The biomechanical safety research approach is fundamentally grounded in accident reconstruction, often informed by epidemiological studies. This process begins with identifying the existence and extent of a safety issue, along with analyzing the initial conditions and outcomes of real-world incidents. From there, accident reconstruction techniques involve controlled physical testing using Anthropomorphic Test Devices (ATDs), such as crash test dummies, or Post-Mortem Human Subjects (PMHS) to gain a deeper understanding of impact mechanics and injury kinematics. The insights derived from these staged tests are crucial for validating numerical models, whether finite element or multibody simulations. Such simulations enable the exploration of various factors—like vehicle geometry or impact velocity—and their influence on pedestrian fatality risk, while also facilitating the evaluation of safety device designs.

In addition to the high societal costs associated with pedestrian fatalities, the US Department of Transport (DOT) recently updated the Value of Statistical Life (VSL) to $13.2 million as of 2023 [U.S. Department of Transportation, 2023]. This metric is used to quantify the economic benefits of reducing fatalities in transportation-related policies and projects. With an estimated 50-60 fatalities per year on the NYC Subway alone [Gershon et al., 2008b],

the total societal economic costs exceed 660 million USD per year. However, despite this cost, biomechanical safety research in subway-to-pedestrian collisions remains underexplored. This thesis aims to address this gap by contributing to each of the aforementioned research methodologies in the following structure:

1. **Literature search**

   A focused literature review will be conducted on subway-to-pedestrian incidents, covering key areas such as epidemiological analysis, staged testing, multibody modeling, and safety countermeasure development. The review will highlight the unique challenges of subway collisions compared to established automotive safety techniques, emphasizing differences in biomechanics, impact dynamics and design constraints. While global research will be considered, particular emphasis will be given to data and studies specific to the New York City subway, the primary case study for this research.

2. **Epidemiology**

   Currently, the pre impact conditions such as vehicle speed and pedestrian posture, needed for accurate representation are not well understood. An epidemiology study consisting of 263 Public Transportation Safety Board (PTSB) incident report files from 2019 was conducted. This study expanded upon the existing epidemiological literature regarding subway-to-pedestrian collisions in NYC as well as identify key factors relevant to future biomechanical impact studies.

3. **Impact Testing**

   Model validation is likely to be a reoccurring challenge and limitation to the studies in this thesis due to the lack of available ATD or PMHS and scaled test data specific to subway-to-pedestrian collisions. While PMHS test are beyond the scope of this thesis, impact tests using a cylindrical headform and various energy absorbing materials are to be conducted. The acceleration and position data from such tests will be used to experimentally derive suitable contact characteristics for application to multibody modelling techniques.

4. **Computational Modelling**

   The multibody modelling software MADYMO (MAthematical DYnamic MOdels) was be used to create the first subway-to-pedestrian baseline model. The epidemiology data provided the ability to set weighted velocities and initial conditions to determine the current head injury and run-over risk to pedestrians. This model allow for factors such as impact velocity and station geometry to be assessed in an environment which avoids confounding factors.

5. **Countermeasure Design**

   Combining all of the information from the previous studies, the effect of multiple countermeasure designs on head injury and run-over risk can be assessed compared to the baseline model. The experimentally derived contact characteristics will offer further confidence in the model and provide a first step towards future validation efforts. Both run-over and head injury risk will be considered together to provide an overall benefit estimate of each countermeasure type and recommend a direction of future studies.

The overarching aim of this research is to explore whether the perception that improving pedestrian safety in subway collisions is infeasible due to the sheer size and weight of these vehicles holds true. By investigating the potential and practicality of passive safety measures, this study seeks to assess if meaningful advancements can be achieved. A central question is whether innovative passive safety design interventions can effectively prevent fatalities in subway-to-pedestrian collisions. The goal, therefore, is to inform future research and development efforts by determining the viability of these safety improvements, thereby addressing any possible longstanding doubts in the field.

1.2.3 Thesis Structure

Figure 1.2 provides an overview of the thesis structure, detailing the key themes and contributions of each chapter.

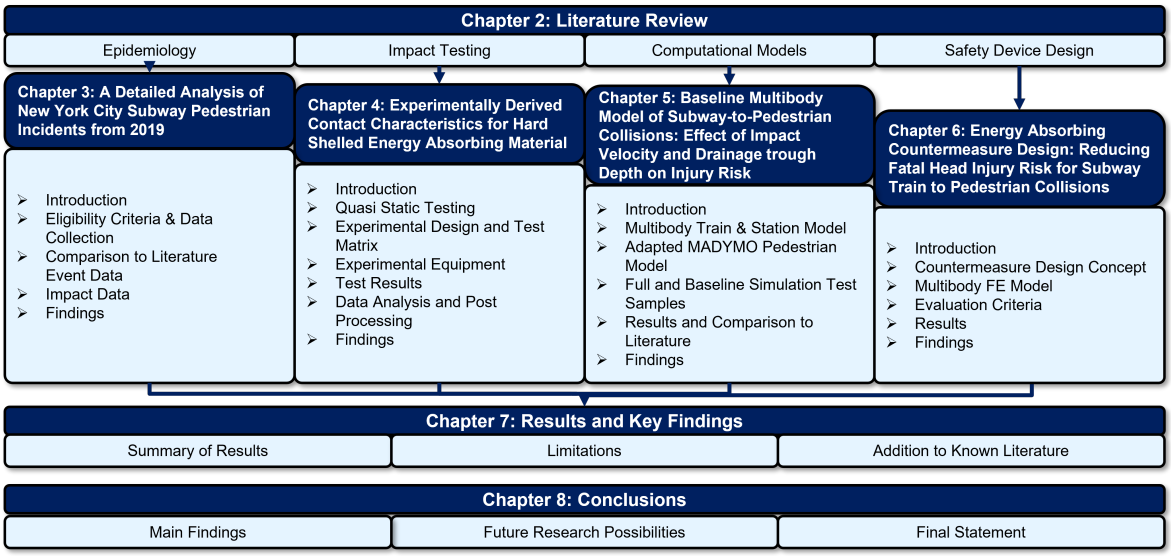

Figure 1.2: Thesis structure schematic

Chapter 2

Literature Review

2.1 Introduction

The literature review for this thesis begins by outlining the foundational biomechanical injury metrics, such as the Head Injury Criterion (HIC) and Abbreviated Injury Scale (AIS). It provides a historical overview of these metrics, detailing their evolution and application in biomechanics research, along with examples of key studies in which these metrics have been utilised. The review then delves into the existing body of research on subway-to-pedestrian collisions, categorised into four critical areas: epidemiological analysis, staged testing, multi-body modelling, and safety countermeasure development. This comprehensive approach contextualises the research within the broader biomechanical and transportation safety fields, while identifying gaps and challenges specific to subway-pedestrian interactions.

2.2 Head Injury Metrics

2.2.1 Background

Within biomechanics, understanding and quantifying head injuries is pivotal to the advancement of safety research. Injury metrics are used to evaluate automotive safety as well as protective equipment. Existing head injury metrics are based on either head kinematics (e.g., linear or angular acceleration) or intracranial parameters such as tissue stress or strain. This review will focus on kinematic head injury metrics. Many of these injury metrics are based on the Wayne State Tolerance Curve (WSTC) (Figure 2.1) based on full body cadaver and detached head drop tests conducted in the 1950s and 1960s [Gurdjian et al., 1966, Lissner et al., 1960]. These tests make up the first 1-6ms of the WSTC, with skull fracture set as the failure criterion. The curve was later updated with additional longer duration impacts (6-10ms) using both animal and cadaver data [Gurdjian, 1961, Gurdjian et al., 1966, JE and HR, 1955, Lissner et al., 1960]. The asymptote for long-duration head accelerations was determined to be 80g through non-injurious volunteer tests [Patrick et al., 1963, Stapp, 1955]. The WSTC presented evidence that the impact duration plays a substantial role in injury risk. Under a very short duration, the head may be below its tolerance level. Given the same effective linear acceleration over a longer time period, the head may now be above its tolerance level.

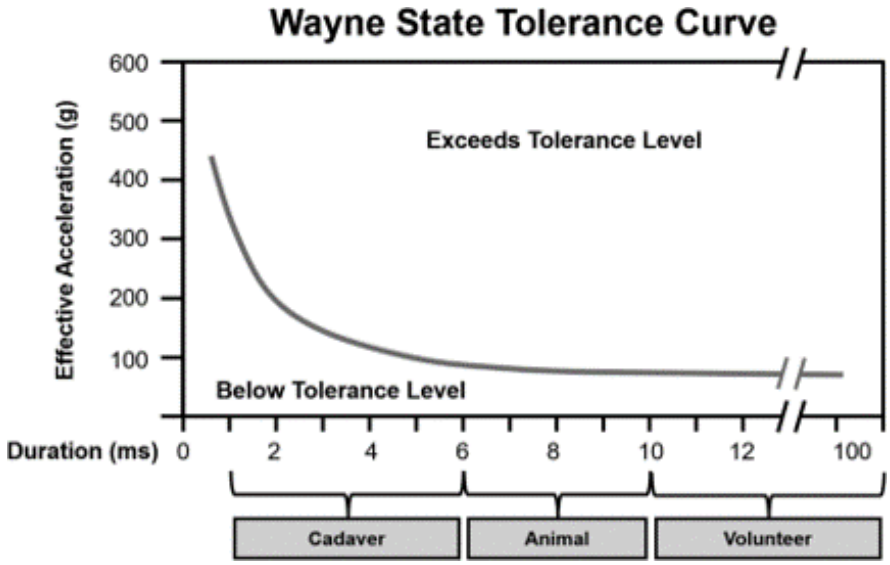

Figure 2.1: Wayne State Tolerance Curve (WSTC) [Rowson and Duma, 2022]

The WSTC has guided the development of safety standards based on a maximum allowable linear acceleration threshold. The Consumer Product Safety Commission (CPSC) set the maximum allowable linear acceleration during bicycle helmet testing to 300g. Ice hockey has similar standards of 275g set by the Canadian Standards Association (CSA) and American Society for Testing and Materials (ASTM) [Rowson and Duma, 2022].

2.2.2 Gadd Severity Index

Due to the uncertain meaning of "effective" acceleration, applying the WSTC to automotive safety applications proved difficult. The WSTC was used to create analytical approximations of the head threshold values. The first of these head injury metrics became known as the Gadd Severity Index (GSI) created by Gadd [1966]. Mathematically, the GSI represents a weighted function that depends more on the magnitude of acceleration than the impulse time (Eq 2.1).

$$GSI = \int a(t)^n dt \tag{2.1}$$

where:

a = Linear Acceleration (g)

n = Weighting factor greater than 1 (originally 2.5)

t = Time (seconds)

The original weighting factor of $n = 2.5$ used by Gadd was based on the available WSTC data at the time. It is stated in Gadd's original work that the intention of this value was to change and update as new information became available. The weighting factor could be tailored to specific cases. A value of 1000 for GSI was the threshold for serious or fatal head injury. A GSI value above 1000 corresponds to an expected loss of life. This threshold would later change with the introduction of more head injury metrics.

Although developed for automotive safety research the GSI was also used as forensic evidence in criminal legal cases. One such case in which the GSI was used involved the death of a 3 month old baby. The farther claimed he failed to catch the child while playfully throwing him in the air. The prosecution expert witness argued using the GSI that the degree of force needed to cause these injuries was not compatible with the father's version of events. Nokes et al. [1995] conducted a biomechanical review of this case to highlight the degree of care needed when using injury metrics in this manner. This paper shows that small changes to the scaling factor as well as the distance to decelerate, can cause large variations the resulting GSI (Figure 2.2). This highlights the important fact that head injury metrics should be treated as nothing more than a general indicator of total head trauma.

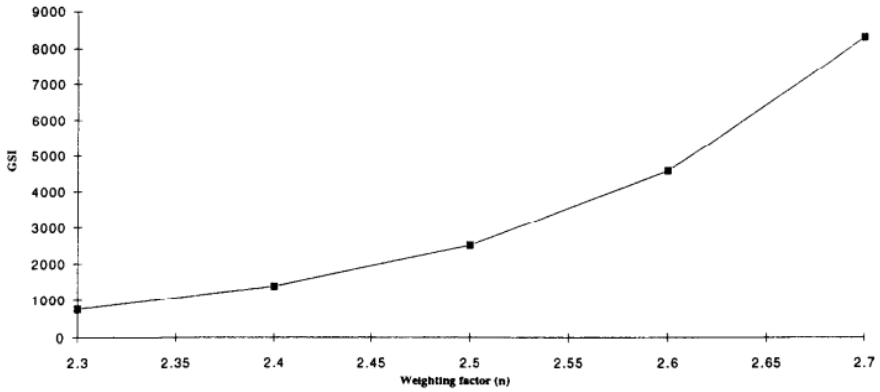

Figure 2.2: The relationship between the GSI and its scaling factor [Nokes et al., 1995]

2.2.3 Head Injury Criterion

The general form for what would later become known as the Head Injury Criterion or HIC score was proposed by Versace [1971a]. In his review of the GSI, Versace found the way the approximation of the WSTC was used in the GSI formula to be unjustified. The main suggested change was that the "effective" acceleration should be defined as the average acceleration, which led to the development of the HIC score equation (Eq 2.2)

$$HIC = max\left[\frac{1}{t_2 - t_1}\int_{t_1}^{t_2} a(t)dt\right]^{2.5}(t_2 - t_1) \tag{2.2}$$

where:

a = Linear acceleration (g)

t_1, t_2 = Time boundaries which maximise HIC (seconds)

t = Time (seconds)

The HIC score was adopted by the National Highway Traffic Safety Administration (NHTSA) which suggested limiting the time interval to 36ms (HIC_{36}) or 15ms (HIC_{15}) based on volunteer data and the WSTC. Comparisons between the (HIC_{36}) and (HIC_{15}) with thresholds of 1000 and 700 respectively found that, for short duration events, where either criteria would produce the same numerical value, HIC_{15} with its proposed 700 threshold is more stringent [Bandak et al., 1999].

The relationship between the HIC score and skull fracture risk is well documented [Bandak et al., 1999, Hertz, 1993, Vander Vorst et al., 2003]. A statistical regression analysis of head impact data was conducted by Vander Vorst et al. [2003]. The HIC correlation shows a steep rise at low probability of fracture, with a significantly wider confidence band at high fracture probability (Figure 2.3). For the data which consists of short duration impacts (< 15 milliseconds), the risk curves would be applicable to both HIC_{15} and HIC_{36} [Bandak et al., 1999]. The data shows that for a HIC_{15} score of 750, there is a 50% risk of skull fracture.

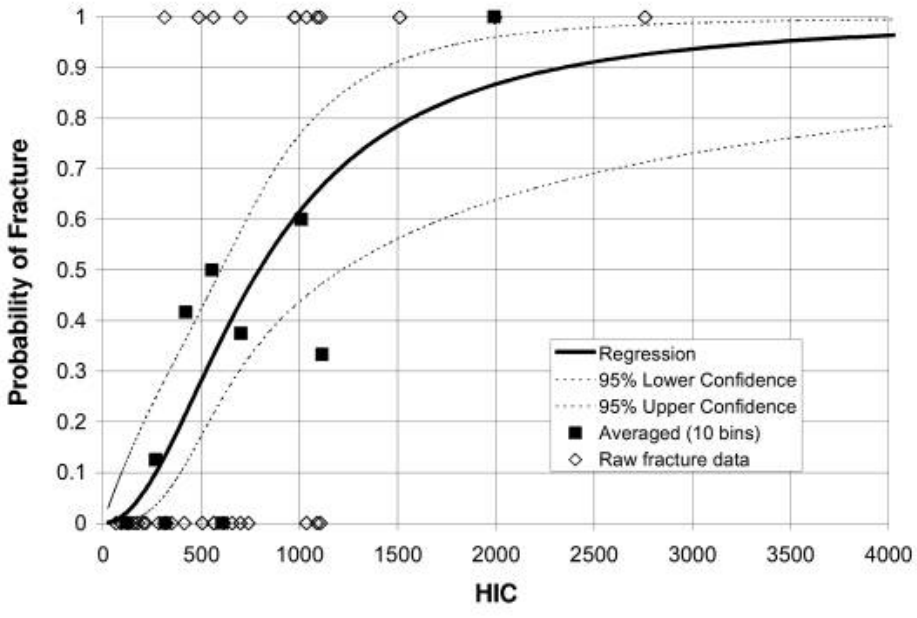

Figure 2.3: Logistic Regression of HIC to Skull Fracture [Vander Vorst et al., 2003]

2.2.4 Rotational Based Head Injuries

To account for the lack of rotational kinematics used in the HIC score, metrics such as the Brain Injury Criterion (BrIC) [Takhounts et al., 2013] or Head Impact Power (HIP) [Newman and Shewchenko, 2000] can be used, which utilize the head's angular velocity and acceleration (Equations 2.3 & 2.4).

$$BrIC = \sqrt{\left(\frac{\omega_x}{\omega_{xc}}\right)^2 + \left(\frac{\omega_y}{\omega_{yc}}\right)^2 + \left(\frac{\omega_z}{\omega_{zc}}\right)^2} \tag{2.3}$$

where:

$\omega_x, \omega_y, \omega_z$ = Maximum angular velocity ($\frac{rad}{s}$)

$\omega_{xc}, \omega_{yc}, \omega_{zc}$ = Critical angular velocities ($\frac{rad}{s}$)

$$HIP = C_1 a_x \int a_x dt + C_2 a_y \int a_y dt + C_3 a_z \int a_z dt + C_4 \alpha_x \int \alpha_x dt + C_5 \alpha_y \int \alpha_y dt + C_6 \alpha_z \int \alpha_z dt \tag{2.4}$$

where:

C_i = Mass (kg) and moments of inertia (kgm^2) for a 50th percentile human head

a_x, a_y, a_z = Linear acceleration components $\frac{m}{s^2}$

$\alpha_x, \alpha_y, \alpha_z$ = Angular acceleration components $\frac{rad}{s^2}$

A strong correlation is observed between linear and rotational head injury metrics, indicating that impacts resulting in high HIC scores are also likely to produce elevated BrIC or HIP scores [Marjoux et al., 2008]. This suggests that efforts to reduce HIC scores would similarly mitigate rotational head injury risks (Figure 2.4).

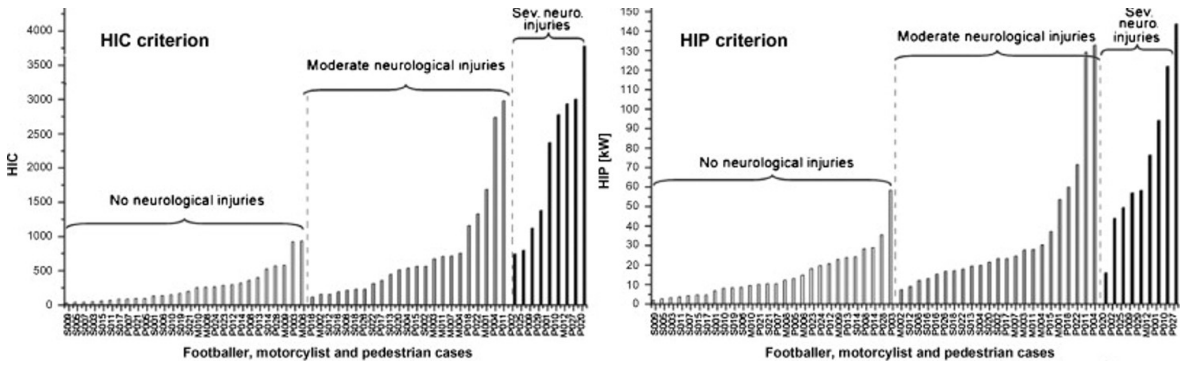

Figure 2.4: Comparison of linear and rotation based head injury criterions [Marjoux et al., 2008]

2.2.5 Abbreviated Injury Scale

The Abbreviated Injury Scale (AIS) was originally developed within the Association for the Advancement of Automotive Medicine (AAAM) in the 1960s as a way of tracking automotive injuries. Field use feedback and outcome analysis have led to several updates and revisions [Loftis et al., 2018]. The AIS system is an anatomically based, consensus derived, global severity scoring system that classifies injury severity on a 6-point scale (Table 2.1).

One strength of the AIS system is that it can represent the singular maximum injury severity (MAIS) or be used to calculate the total severity based on all injuries received, typically using the Injury Severity Score (ISS) [Baker and O'Neill, 1976]. The relationship between a head injury's AIS score and the probability of skull fracture using the HIC score (Figure 2.5) is another useful biomechanical tool for evaluating the safety of automotive vehicles.

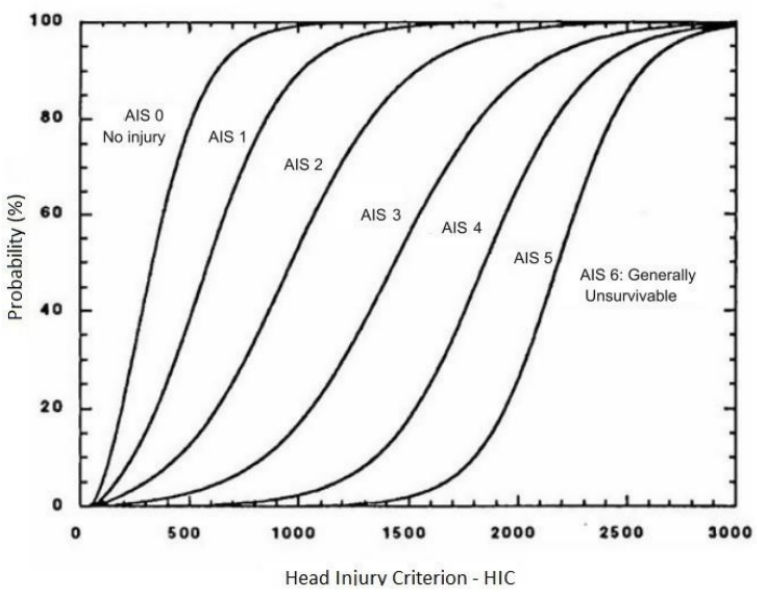

Figure 2.5: Relationship between HIC score and AIS [Mackay, 2007]

Table 2.1: Abbreviated Injury Scale classifications and associated head injury risk Mackay [2007]

AIS Code	Injury Severity
1	Minor
2	Moderate
3	Serious
4	Severe
5	Critical
6	Maximum

2.3 Epidemiology and Data Collection

2.3.1 Background

The word "epidemiology" is derived from the Latin word "epedimion" meaning to visit. The first known use of the word in modern language was in 1598 in a study on the bubonic plague [Robertson, 2015]. Epidemiology studies are typically related to the study of disease control and prevention in a population; however, the definition of epidemiology in academic research has changed and continues to change [Frérot et al., 2018]. Historically, epidemiological studies related to public health from automotive injuries and prevention have often been overlooked in academic safety research [Lemov, 2015]. In recent years, the importance of this type of research has been recognised as a key step in the development of injury prevention methods. Literature reviews have been published, aiming to identify and address the gap in published work [Norton et al., 2001] [Alexandrescu et al., 2009] [Azami-Aghdash et al., 2017]. As a first step in addressing the health concern caused by subway train to pedestrian impacts, an epidemiological literature review is presented below.

2.3.2 Search Criteria

From a biomechanical engineering perspective, the initial conditions of an impact are of great importance for accident reconstruction and the evaluation of preventative measures. Accurate pedestrian information allows future studies to ensure a representative population is used for injury prevention methods. This section reviewed 13 articles from 1972 to 2021 across Google Scholar, PubMed and Web of Science in a systematic manner. Each paper was found using the search terms "subway", "train", "rail", "pedestrian", "epidemiology", "collision", "fatality" and "suicide". The references of each study were checked to account for possible missed articles in the search criteria. Subway specific articles are highlighted for their increased relevance. Studies which focus on light surface level trams or heavier freight specific conditions were excluded. This was due to the differences in impact environment. Streetcars routinely share walkable space with pedestrians, whereas subway tracks are separated. The risk of secondary contact injuries are also likely very different due to the lack of a third rail and cross ties on street level tracks.

Table 2.2: Review of 13 epidemiological studies involving subway to pedestrian collisions

Reference	**City, Country**	**Study Period**	**Sample Size**	**Suicides (N)**	**Accidents (N)**	**Fatality Rate (%)**	**Sex (%M/F)**	**Mean Age (Years)**	**Injury Data**
Gaylord and Lester [1994]	Hong Kong	1979-1991	132	132	NA	42.4	70/30	30-40	NA
Guggenheim and Weisman [1972]	Boston, USA	1960-1967	50	50	NA	34.0	59/41	41	Death = 17(34%), Severe Injury = 12(24%), Minor Injury = 6(12%) No Injury = 14(28%)
Johnston and Waddell [1984]	Toronto, Canada	1954-1980	119	NA	NA	28	NA	20-30	Fatality Only - Neurological = 75(63%), Massive Chest = 25(21%) Both = 6(5%), Total Crush = 5(4%), Sepsis = 2(2%). 11 arrived in hospital but later died from injuries
Cocks [1987]	London, England	1981-1986	100	≈ 75	≈ 25	40	49/51	40	Fatality Only - 35% Dead on Arrival (DOA), 8% died in hospital. Affected Body Region - 44% head and neck, 11% face, 34% chest, 25% abdominal and pelvic contents, 67% limbs
O'Donnell and Farmer [1992]	Multiple See Paper	Varies on Source	NA	NA	NA	≈ 45	$\approx$ 60% male	21-30	NA
O'Donnell and Farmer [1994a]	London, England	1940-1990	3240	3240	NA	55	64/36	25-34	NA
Sonneck et al. [1994]	Vienna, Austria	1984-1992	89	89	NA	62.9	63/37	37	NA
Coats and Walter [1999]	London, England	1997	58	58	NA	44-76	NA	NA	NA
Gershon et al. [2008a]	NYC,USA	1990-2003	668	343	315	NA	84/16	35-44	NA
Lin and Gill [2009]	NYC,USA	2003-2007	211	111	76	NA	83/17	44	Cause of Death - Blunt force = 206 Electrocution = 5
Rodier et al. [2018]	NYC,USA	2001-2016	254	17	70	10	80/20	41	Torso = 34% Amputation = 21% Intracranial Hemorrhage = 27%
Maclean et al. [2006]	NYC,USA	1989-2003	41	5	16	5	79/21	37	Amputation Data - Upper extremities = 10(24%), lower = 26(63%), Both = 2(5%)
Ho et al. [2021a]	Toronto, Canada	2010-2018	51	39	10	29	69/31	41	AIS3+ - Head = 22(43%), Thorax = 17(33%), Spine = 5(10%), Upper Extremities = 4(8%), Lower Extremities = 15(29%)

2.3.3 Pedestrian Information

In 1992, O'Donnell and Farmer at the Department of Public Health and Epidemiology, University of London, contacted the largest 45 subway systems in the world at the time. The information requested included the number of suicides per year, fatality rate, age and sex. Of the 45 railways contacted, 23 (51%) supplied all or most of the information.

Tables 2.2 and 2.3 show that across most subway systems, individuals in the 30-40 age range consistently account for a notably higher proportion of both successful and unsuccessful suicide attempts. For studies conducted on the NYC subway specifically, the most common age tends towards 40 years old. In all but three systems, the majority of suicides and/or suicide attempts involved male pedestrians. This does not account for non-suicide related collisions, such as pedestrians who fell on the tracks unintentionally.

Table 2.3: Review of 13 epidemiological studies involving subway to pedestrian collisions

Adapted from O'Donnell and Farmer [1992]

Age/Location	**<20**	**21-30**	**31-40**	**41-50**	**51-60**	**61-70**	**>70**	**% Dead**	**% Male**
Athens								52	65
Boston								34	52
Budapest								37	51
Caracas	16	28	24	9	15	7	1	61	61
Helsinki								67	58
Hong Kong	9	36	34	6	8	5	1	41	66
London	4	28	19	15	16	11	7	60	64
Mexico City	4	42	37	11	2	2	4	80	54
Milan								44	66
Munich	4	26	23	21	13	7	5	59	50
Nuremberg	7	50	21	7	0	14	0	20	38
Paris	3	31	20	17	14	7	8	26	71
San Francisco	10	27	30	20	7	7	0	28	52
Sao Paulo								26	62
Tokyo	0	15	20	20	37	9	0	54	67
Toronto								48	41
Tyne & Wear	0	33	25	0	8	8	25	46	86
Vienna	2	39	22	20	2	2	12	57	62

2.3.4 Fatality Rates and Injury Information

Understanding the injury mechanisms in a collision event is an important step in safety research. This step allows researchers to focus on specific injury prevention methods and more accurately estimate the effectiveness of countermeasure designs against a baseline injury or fatality rate.

While Tables 2.2 and 2.3 show a large range of fatality rates from 5% to 80%, there are details in the methodology of each study which make direct comparisons difficult. A fatality caused by a subway to pedestrian collision may occur either at the scene of the accident or

in a hospital setting while undergoing medical attention. It is also possible that intentional collisions (suicides) and accidental collisions may yield different fatality rates and injury types. This is difficult to determine as the categorisation of suicide and accident varies across systems. Depending on access to medical records and the type of incidents under review, fatality rates should be considered within the context of each study.

Ho et al. [2021a] conducted a retrospective cohort study to identify patients who presented to the emergency department of a level 1 adult trauma centre in Toronto, Canada, with a subway related injury between 1 Jan. 2010 and 31 Dec. 2018. A total of 51 patients are reviewed in this study, in which 10 were declared dead in the emergency department, 2 after surgery, and 3 in intensive care. Despite the high overall mortality rate of 29%, the survival rate was quite high for patients who survived their initial presentation, at 88%. Patients most commonly presented with an isolated severe injury ($AIS > 3$) to the lower extremity or a combination of severe head and lower extremity injuries. One in 4 patients had a severe head injury. The fatality and injury rates presented in this study are likely an underestimation of the true fatality rate, as incidents which resulted in death at the scene are not considered.

Table 2.4: Subway related injury patterns at a level 1 adult trauma centre in Toronto Canada 2010-2018

Obtained from Ho et al. [2021a]

Pattern	**No.(%) of patients**
No severe injuries	15 (29)
Severe injury to 1 body region only	17 (33)
Lower Extremity	7 (14)
Head	6 (12)
Thorax	4 (8)
Severe injury to multiple body regions	19 (37)
Head and lower extremity	4 (8)
Head and thorax	4 (8)
Other	11 (22)

Maclean et al. [2006], conducted a retrospective trauma registry review of 41 patients who presented to Bellevue Hospital, New York City from 1989-2003, with amputations from subway accidents. All patients in this study had stable vital signs on admission. There were 14 amputated upper extremities and 42 amputated lower extremities. The most common amputation on presentation was below the knee. The patients underwent an average of three operative procedures. Two patients died in the operating room and there were no late hospital fatalities, resulting in an overall fatality rate of 5%. This fatality rate is very low when compared to the 29% fatality rate from Ho et al. [2021a]. One reason for this may be due to the sample type. This study only reviewed cases in which patients presented in a

stable condition with an amputation and does not account for deaths that occurred at the scene of the incident, deaths caused by non-amputation related injuries, or deaths occurring in the emergency department. Both studies show a high survival rate for patients who survive the initial presentation.

Rodier et al. [2018] also conducted a retrospective case series of 254 subway-related trauma patients at Bellevue Hospital, New York City from 2001 to 2016. This study included all subway related injuries, including those which do not involve the train. The most common injury mechanisms are being hit by a train (49%), falling onto the tracks (44%) and being pinned by the train (3%). When analysing the following injury data (Table 2.5), only 53% of cases involve direct contact with the train. When analysing fatalities only, the rates of any bone fracture, intracranial haemorrhage, amputation, and torso injury were 85%, 62%, 27%, and 42%, respectively, with many patients sustaining more than one injury. Of the patients who required surgery, lower extremity amputation was the most common at 64% with 3 patients needing both upper and lower amputations. A 13% mortality rate was associated with the need for amputation. This finding is higher than the previous study at the same trauma centre Maclean et al. [2006]. The overall survival rate is 90%, which is in line with other studies, further highlighting the importance of surviving the initial impact and transport to a trauma centre.

Table 2.5: Type and location of injuries at Bellevue Hospital, New York City from 2001 to 2016

Obtained from Rodier et al. [2018]

Injury	**Percentage of Patients**
Torso	34
Rib fracture	21
Pneumothorax	13
Hemothorax	4
Amputation	21
Upper	6
Lower	13
Both	1
Intracranial hemorrhage	27
Patients with at least one fracture	49
Long-bone fracture	38
Facial fracture	25
Vertebral fracture	15
Solid organ injury	17

The above papers review the injury characteristics of pedestrians who present to a trauma centre alive; they do not account for those who died at the scene of the incident. Together, Gershon et al. [2008a] and Lin and Gill [2009] characterise subway-related fatalities in New

York City from 1990-2007. Both studies review the Office of Chief Medical Examiner (OCME) medical records and Lin and Gill [2009] present the following injury data (table 2.6). This dataset includes fatalities which occurred at the scene (n = 180) and after a survival interval ranging from 1 h to 18 years (n = 31). This data is valuable as it offers insights into the full range of fatality events, from collision with the train to treatment in hospital. However, these papers do not provide detailed injury data for pedestrians who survived the collision and subsequent medical treatment.

Table 2.6: Injury Type (Fatalities) and Location from NYC OCME 2003-2007

Obtained from Lin and Gill [2009]

Physical Injuries (%)	**Accident (n=76)**	**Suicide (n=111)**
Head	84	90
Torso	70	80
Extremity (injury)	62	77
Extremity (amputation)	25	38
Skull fracture	53	65
Decapitation	1	7
Torso transection	3	8

2.3.5 Station Environment

A fully detailed and comprehensive fatality rate for subway to pedestrian collisions is difficult to determine based on the current literature. Comparisons between studies are limited by the dataset which is used, as well as the high variability in subway train geometry and station environments. One such variable in the station environment is the presence of drainage troughs.

Drainage Troughs

Drainage troughs are channels between the tracks which increase the clearance between the train and the ground, allowing for extra space such that an individual may avoid contact with the undercarriage or wheels. First used in the London Underground in 1932 [Cocks, 1987], drainage troughs are present in many subway systems worldwide. Analyses [Coats and Walter, 1999, O'Donnell and Farmer, 1994b, 1992] of the effect of drainage troughs (Table 5.1) show lower fatality rates in stations featuring them. For example, there is a clear positive relationship between the percentage of London Underground stations with drainage troughs and the percentage of survivors from 1973-1990 [O'Donnell and Farmer, 1994a].

Table 2.7: Published studies regarding effectivness of drainage troughs

Authors	Study Period	Fatality Rate No trough	Fatality Rate Trough
[O'Donnell and Farmer, 1994b, 1992]	1973-1990	506/764 (66%)	308/842 (45%)
[Coats and Walter, 1999]	1996-1997	16/21 (76%)	14/32 (44%)

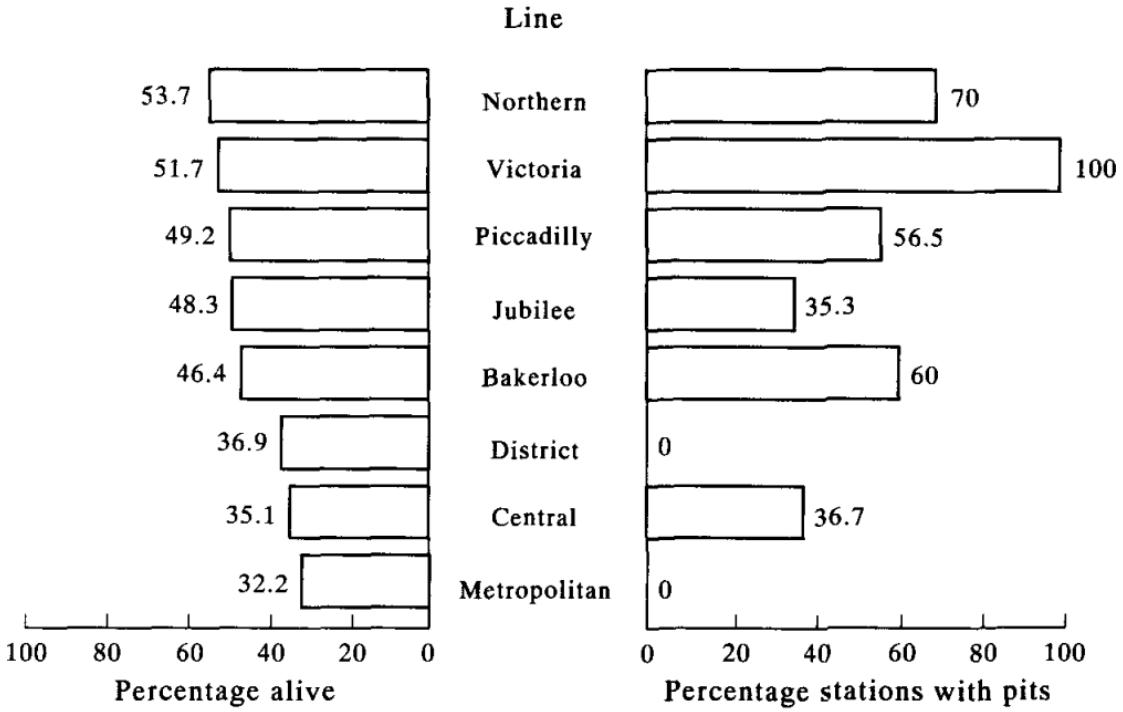

Figure 2.6: Incidents involving persons under London Underground trains (1973-1990). Survival according to line and presence of drainage troughs [O'Donnell and Farmer, 1994a]

A recent literature search into the effectiveness of drainage troughs showed a decline in references to these troughs since 2007 [Poirier et al., 2021]. Many different train models are used within a subway network introducing variability in train front geometry, the velocity of trains entering stations can depend on factors such as the track curvature and slope prior to the station and the track geometry itself may vary depending on the drainage needs at that specific station. While empirical evidence suggests that drainage troughs may act as a viable countermeasure in reducing fatality rates (Figure 2.6), the results of such studies were unable to attribute the reduction in fatality rates to drainage troughs due to the presence of these abovementioned confounding factors. [Barker et al., 2017], thus highlighting the need for biomechanical analysis studies.

Platform Screen Doors (PSDs)

Platform Screen Doors (PSDs), first used in 2002 in Hong Kong, are barriers erected at the edge of subway platforms that open and close only when the train is safely stopped at the station. The barriers may be full height, referred to as platform screen doors, or three-quarters to half height known as platform edge doors. While the intended use of the first PSDs was to conserve energy by keeping cool air in the underground stations, the most obvious advantage from a public safety standpoint is the reduction in accidental and suicidal subway-to-pedestrian collisions. The effect of PSDs on rail suicide is well documented. In a pioneering research report [Law et al., 2009], suicide statistics on the Hong Kong rail network MTR are reviewed both before and after the installation of the very first PSDs. This study provides empirical evidence that PSDs have minimised, if not eliminated, direct contact with moving trains, thus reducing the suicide attempts' success rate.

It is often argued that, due to individual intent, a person may simply substitute this platform for one that does not have PSDs or find an alternative method not involving subways. This is known as the method substitution hypothesis [Berman et al., 2022][Daigle, 2005][Almeida et al., 2023]. To investigate the possible suicide substitution to railways without PSDs, the KCR rail network was separately assessed alongside the MTR network. Figure 2.7 shows the number of rail suicides for MTR decreased by 81.6% post PSD installation, whereas the number of suicides on the KCR network remained steady. After the installation of PSDs, there was no sign of displacement to an unsealed platform, as the change in KCR figures was not significant ($p = 0.905$) Law et al. [2009].

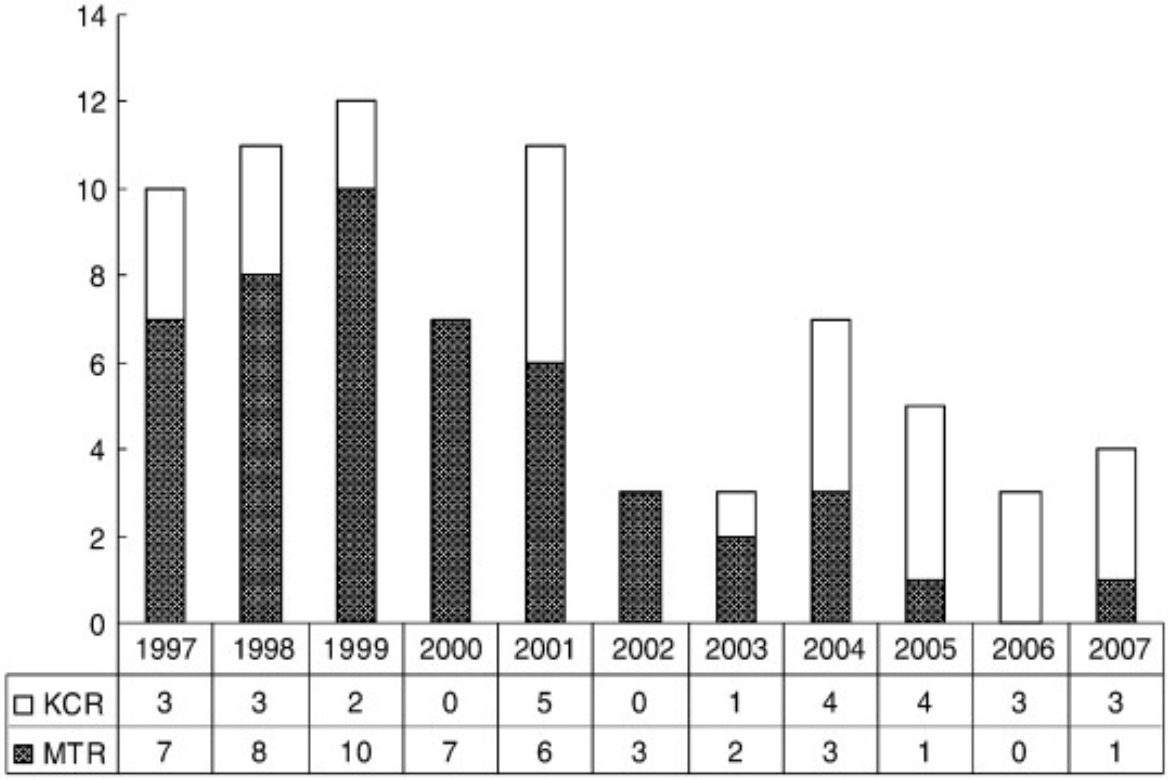

	1997	1998	1999	2000	2001	2002	2003	2004	2005	2006	2007
KCR	3	3	2	0	5	0	1	4	4	3	3
MTR	7	8	10	7	6	3	2	3	1	0	1

	Number of railway suicides (%)	
	Pre-installation period (1997 - 2001)	Post-installation period (2003 - 2007)
KCR	13 (25.5%)	15 (68.2%)
MTR	38 (74.5%)	7 (31.8%)

Figure 2.7: Railway suicides by railway system in Hong Kong, 1997–2007 [Law et al., 2009]

While restricting access to the track area has been shown to have positive outcomes, PSDs may also negatively impact pedestrian and passenger safety. In emergency situations such as fire or smoke in the station, loss of power, disabled or stopped trains, structural collapse, terrorist activity, or other criminal acts, the PSDs may hinder the safe evacuation of passengers. Misalignment between the PSDs and train doors reduces the available exit width, thus increasing evacuation time Qu and Chow [2012].

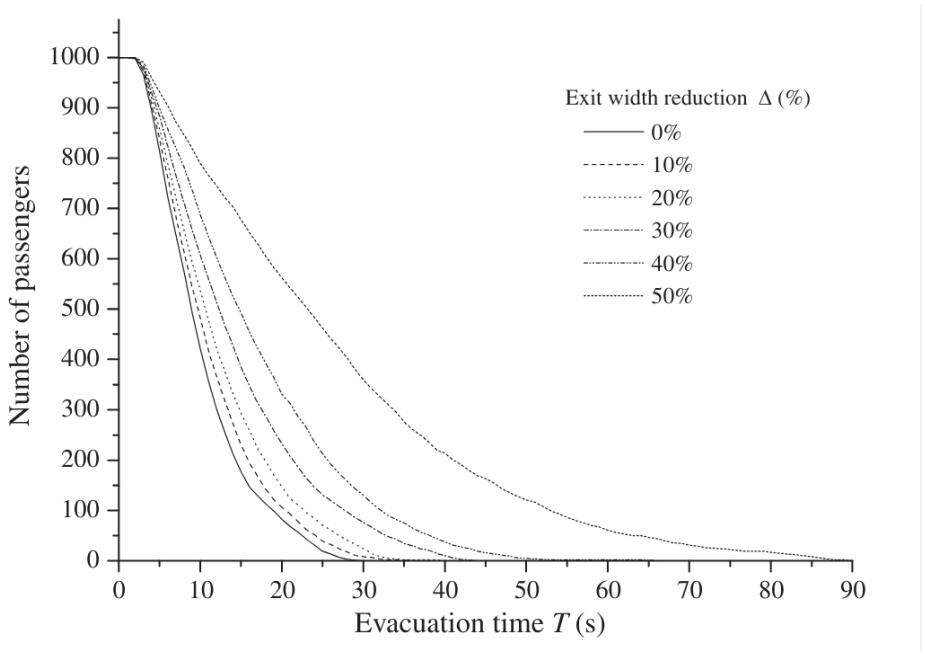

Figure 2.8: Evacuation time of a train compartment [O'Donnell and Farmer, 1994a]

A recent Metropolitan Transportation Authority (MTA) report outlines the feasibility and financial requirements of installing PSDs in the NYC subway network [Metropolitan Transportation Authority Track Trespassing Task Force, 2022]. This report estimates that only 128 out of 472 stations may structurally support PSDs, with an estimated cost of over $7 billion.

2.4 Impact Testing

2.4.1 Background

Pedestrian impact tests are evaluations conducted to assess the safety of vehicles in the event of a collision with a pedestrian. Epidemiological data are used to identify specific impact mechanisms, which are then reconstructed using Post-Mortem Human Surrogates (PMHS) or, more often, Anthropomorphic Test Devices (ATDs). These tests are crucial in understanding and mitigating the injuries that pedestrians may sustain in such accidents. The vast majority of pedestrian impact testing is in relation to automobile collisions, with a notable lack of published literature regarding rail pedestrian impacts. For this reason, the vehicle impact papers presented in this literature review will highlight flat faced vehicles and Light Truck Vehicles (LTVs) where possible, as this geometry is most similar to subway fronts.

2.4.2 Post-Mortem Human Surrogates Testing

Post-Mortem Human Subjects testing involves using human cadavers to conduct safety research, primarily in the field of automotive crash testing. PMHS subjects are instrumented with various sensors and markers to collect data on forces, accelerations, and deformations during impacts. The availability of experimental cadaveric data allows for the validation of pedestrian ATDs and numerical models to ensure model prediction capabilities. PMHS testing can be divided into two categories: full-scale tests using the full pedestrian body and localised testing using only the areas of interest, such as the head or leg.

The pioneering study in full-scale pedestrian PMHS testing was conducted in 1975 by Pritz et al. [1975]. A series of 15 experimental impacts were conducted using unembalmed cadavers, covering a range of speeds from 10-30mph. These tests used a basic test buck with two instrumented adjustable impactors to represent the hood edge and bumper of typical vehicles. The PMHS was supported by means of an exoskeleton in a realistic standing position. The simulated vehicle front is attached to a HYGE sled, which accelerates to the desired speed before striking the PMHS, after which it decelerates at a predefined braking rate. A padded area was placed immediately behind the PMHS to avoid any further damage that may confuse the injury assessment. High-speed video and force time histories on the bumper and hood edge were recorded during each event. A full X-ray injury analysis was conducted after each test. The conclusion of this study pointed towards vehicle front end design as the culprit for lower body injuries.

Between 1975 and the 1990s, there were many more PMHS pedestrian impact tests. For example, Cavallero et al. [1983] evaluated 50 cadaver tests performed at 32km/h to show the influence of passenger car front structures on injury outcomes in pedestrian impacts. No biomechanical data in terms of forces or acceleration were reported. Kallieris and Schmidt [1988] published data related to 11 PMHS pedestrians ranging from 19 to 78 years old. The front end of a medium sized production car was used at test speeds of 23-41km/h. In this study, no vehicle braking was used, which caused the subject to be thrown from the vehicle at high speeds. It was determined that the braking effect must be considered for future studies. The data presented in PMHS studies prior to the 1990s focused on injury severity, with little to no reporting on the vehicle's impact parameters such as stiffness, bonnet height, or bonnet edge configuration. This makes it difficult, if not impossible, to numerically simulate these impacts and highlighted the need for well-documented reports.

From 1993, PMHS impact tests started to provide material characteristics such as stiffness, as well as kinematic details [Ishikawa et al., 1993b]. Schroeder [2000] presented results for 5 PMHS tests using two different vehicle types. This study showed the change in kinematics, resulting in the pedestrian's arms becoming pinned between the car and thorax. To prevent this, a full-scale testing methodology using a sled was developed at the University of Virginia in 2005 [Kam et al., 2005]. This test plan and experimental design was developed based on the analysis of a combination of literature, multi-body modelling, and epidemiological studies. This methodology led to the development of kinematic corridors for the pelvis, head, and thorax for different vehicle types and speeds [Kerrigan et al., 2005, 2007a, 2008]. From here, full-scale PMHS tests have offered invaluable data for validating full body ATDs or numerical models.

These PMHS tests have led to a clear understanding of pedestrian injuries caused by contact with a motor vehicle. However, these tests focus mainly on vehicle/primary contact, with limited references to the subsequent contact between the pedestrian and the ground (secondary contact). These contacts involve complex pedestrian kinematics, such as any combination of rolling, sliding, or bouncing before coming to rest. This leads to significant challenges in predicting the kinematics; thus, this injury mechanism is not as well understood. An analysis of the German collision database GIDAS highlighted the importance of secondary contact injuries and showed that the head, thorax and spine dominate AIS4-5 ground contact injuries. The ground contact injury severity has been shown to increase with pedestrian age and vehicle speed [Shang et al., 2018]. Badea-Romero and Lenard [2013] came to similar conclusions when reviewing UK data.

Real world epidemiological data highlights the importance of ground contact on pedestrian injury risk; however, there is limited cadaver data. To address this, recent PMHS impact tests have been conducted, focusing on both primary and secondary impacts. In 2020, Shang et al. [2020] reported on 6 staged full body PMHS tests at 20-30km/h with 3 different vehicle types, with various Normalised Bonnet Leading Edge Heights (NBLEH). Each vehicle was tested twice, with full test details shown in Table 2.8 with the vehicles in figure 2.9.

Table 2.8: PMHS test details

[Shang et al., 2020]

Test Number	**Vehicle Speed (km/hr)**	**Pedestrian Data**	**Vehicle Data**
Test01	30.5	Male, 88y/o, 1.74m, 66kg	Peugeot 307 (sedan), NBLEH 0.7
Test02	30.4	Male, 83y/o, 1.72m, 69kg	Peugeot 307 (sedan), NBLEH 0.7
Test03	20.4	Male, 94y/o, 1.67m, 64kg	Citroen C4 (compact), NBLEH 0.9
Test04	21	Male, 83y/o, 1.67m, 55kg	Citroen C4 (compact), NBLEH 0.9
Test05	30.1	Female, 94y/o, 1.58m, 38kg	Renault Kangoo II (van), NBLEH 1.2
Test06	30.4	Male, 86y/o, 1.62m, 69kg	Renault Kangoo II (van), NBLEH 1.2



(a) Peugeot 307 (sedan)



(b) Citroen C4 (compact)



(c) Renault Kangoo II (van)

Figure 2.9: Vehicles used in PMHS tests
[Shang et al., 2020]

Six triaxial accelerometers were inserted into the cadavers. One was inserted in the chest, two were screwed onto the left and right thigh bones, two were inserted into the ilium (left and right side) and one was inserted in the mouth to represent an approximate head CG. High-speed video footage was used to track head trajectory during each event using Model Based Image Mapping (MBIM). Each case was reconstructed by two independent researchers. Three phases and four time points were identified in each case, describing head contact with the vehicle and the ground, which are shown in Figure 2.10.

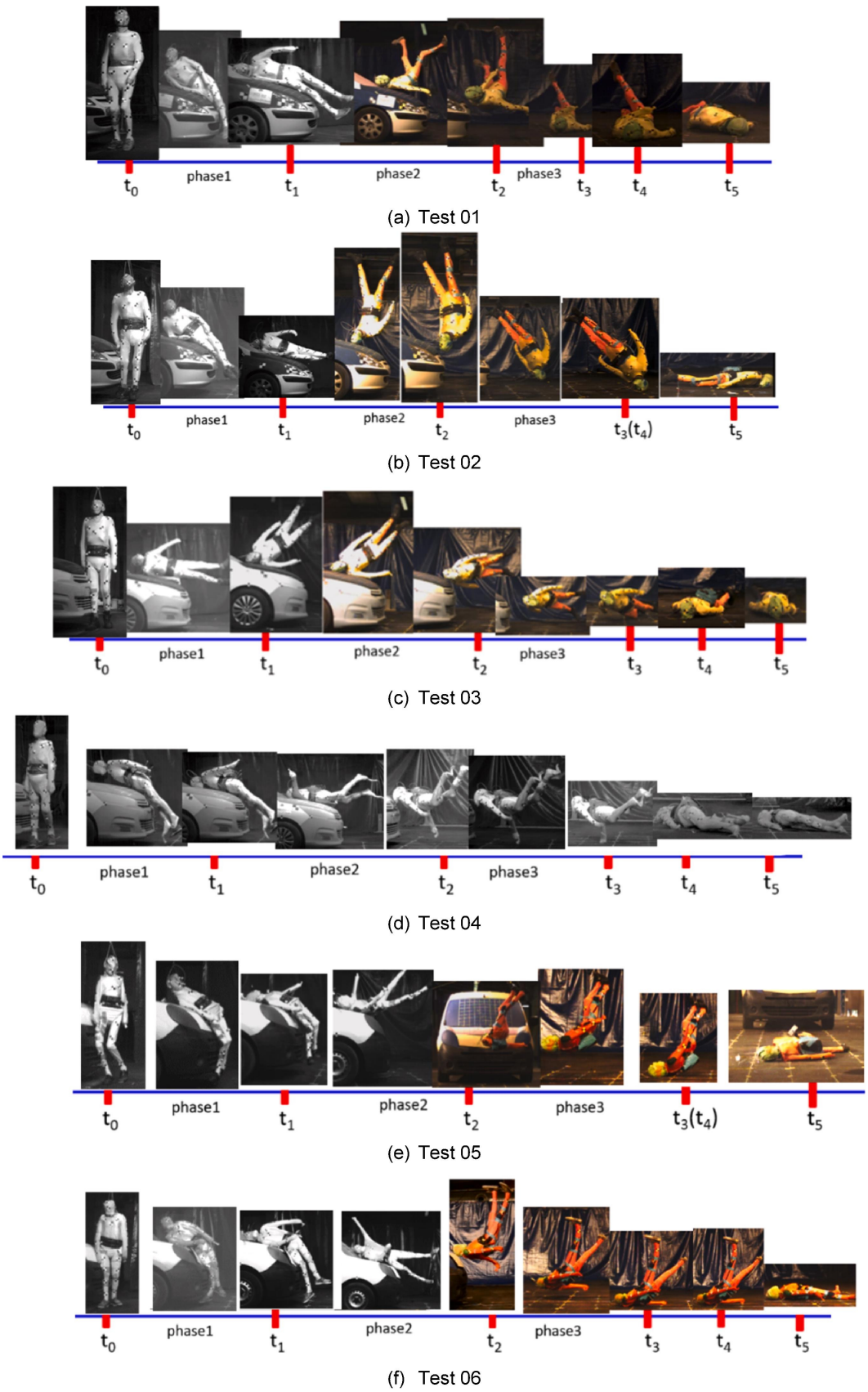

Figure 2.10: Sequences of vehicle-pedestrian impact for the six cadaver tests [Shang et al., 2020]

The head accelerometer data was used to calculate an approximate HIC score denoted $aHIC_{15}$ for both the vehicle and ground contact, with the MBIM data being used to estimate BrIC scores (figure 2.11). This shows that both the $aHIC_{15}$ and BrIC can be higher for ground contact compared to vehicle contact. The high stiffness of ground contact is evidenced by the shorter contact interval compared to vehicle contact.

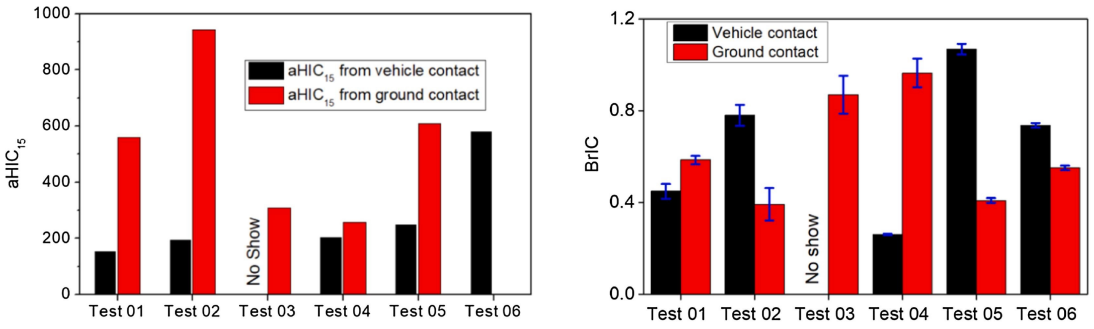

(a) HIC score (b) BrIC score

Figure 2.11: Summary of head injuries for vehicle and ground contact [Shang et al., 2020]

The ground contact mechanisms in tests 01,04 and 05 were considered suitable for estimating the ground contact stiffness using a spring-mass model. A head mass of 4.5kg was assumed for the Equation 2.5 with a calculated ground contact stiffness varying between 178 and 1741kN/m. The contact time interval Δt for both head-to-vehicle and head-to-ground contact was estimated by a combination of the filtered accelerometer and video data. This data would later be used in follow-up publications to investigate the MADYMO pedestrian model's head contact characteristics [Shang et al., 2021]. These contact characteristics are also used in the simulation research throughout this thesis.

$$k = \frac{M}{(\Delta t)^2}[\pi^2 + (\log e)^2] \tag{2.5}$$

where:

k = Stiffness ($\frac{N}{m}$)

M = Mass of head (4.5kg)

e = Coefficient of restitution,

2.4.3 Anthropomorphic Test Devices

Anthropomorphic Test Devices, commonly known as crash test dummies, are human-like models used in the automotive safety field. They are used to test and simulate the effects of vehicle impacts on the human body. These devices play a crucial role in understanding how different crash scenarios affect occupants and pedestrians, allowing for the design of safer vehicles. ATDs are principally designed for standard testing. While there are full-body ATDs used in crash safety research, such as the Thor and Hybrid III 50th Percentile Male dummy [White et al., 2023], ATDs such as headforms and legform impactors are used for more specific, localised injury analysis.

The closest equivalent to a subway train pedestrian impact test found in published literature was a pilot study involving an urban rail vehicle (URV) [Lopot et al., 2019]. A T6A5 ČKD Tatra tram with a "classic" front from the 1980s struck the Hybrid III 50th Percentile Male dummy at speeds of 10km/h and 20km/h on 200m of straight, flat tramway track.

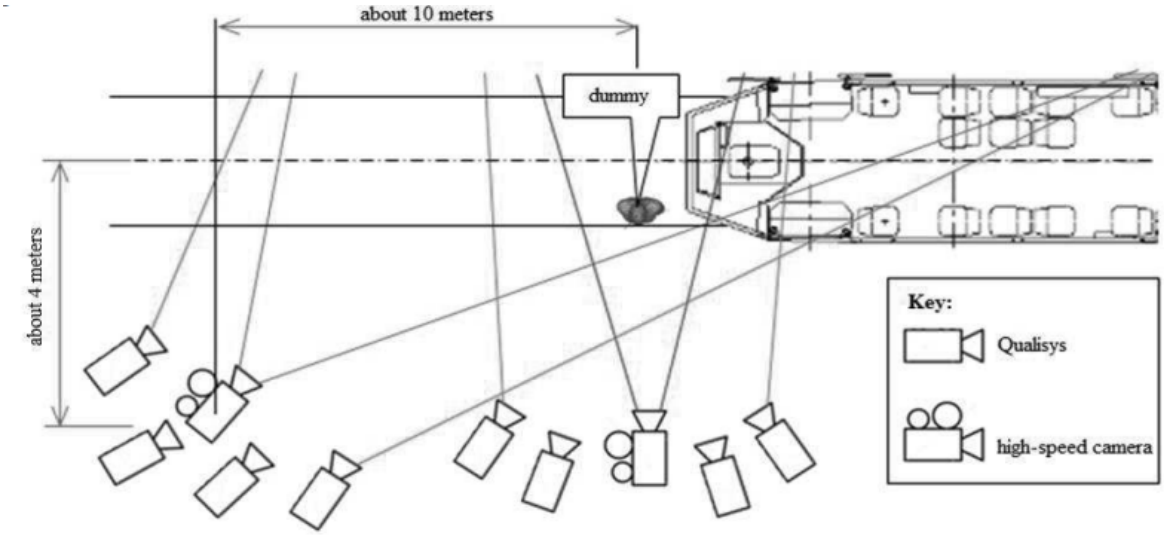

Figure 2.12: Pilot Tram Hybrid III Impact Setup
[Lopot et al., 2019]

The test setup involved two high-speed cameras, one with a recording frequency of 12,000Hz and the other a wide angle with 500fps. The Qualisys 3D cinematic system, in an eight-camera configuration with a recording frequency of 300Hz, was also used to capture the event from multiple angles (Figure 2.12). No accelerometers or other sensor instruments were used; therefore, no estimate of the dummy's loading conditions was available.



Figure 2.13: Impact between Hybrid III and a T6A5 ČKD Tatra tram
[Lopot et al., 2019]

The high-speed cameras were used to estimate the head's velocity during the collision (Figure 2.13). As the HYBRID III dummy did not use accelerometers, the acceleration time histories were acquired by numeric derivations of detected speed curves. This double derivation of position data is subject to increased numerical errors. The acceleration time histories were then used to calculate the HIC_{15} for both primary and secondary contact (Table 2.9). Both primary and secondary HIC_{15} scores are extremely high, corresponding to an almost 100% risk of critical head injury using Figure 2.5. The authors acknowledge that the values presented are only gross hypothetical values due to the lack of measured accelerations and compounding errors involved in numeric derivations. Despite this limitation, it is clear that for this test, the secondary impact poses much more of a risk to head injury. The authors attribute this to both the stiffness of the ground compared to the tram's deformable panels, as well as the accelerated falling velocity caused by the high friction between the dummy's feet and the ground. This friction rotates the pedestrian, resulting in a higher head-ground impact velocity above 12m/s. This paper continues to use numerical modelling to evaluate the effect of different front-end geometries on the presented HIC_{15} scores, which will be discussed in Section 2.5.

Table 2.9: Estimated hypothetical HIC scores for tram pedestrian collisions
[Lopot et al., 2019]

Time (s)	**Collisions Stage**	HIC_{15}
0.03	Dummy head first impact with tram front end	6201.8
0.48	Dummy head first contact with ground	24008.3

2.5 Numerical and Computational Modelling

2.5.1 Background

The costly nature of full-scale pedestrian impact tests using either PMHS or ATDs has led to normalised vehicle front-end geometry testing procedures using impactors at fixed velocities and impact angles. These tests are significantly cheaper, at the expense of not being able to replicate the full kinematic complexity and secondary contact implications of a vehicle-pedestrian collision.

One way to reconstruct pedestrian-vehicle collisions without the time and cost investment involved with crash tests is to use full-scale numerical Human Body Models (HBM). This allows for a wide range of testing environments as well as more control over the impact conditions. Two common approaches to creating and using computational pedestrian HBMs are Multibody Modelling (MB) and Finite Element Modelling (FE). These HBMs must be validated for their specific use cases using epidemiological and physical experimental data to ensure accuracy in accident reconstruction.

2.5.2 MADYMO Multibody Modelling

The principle behind the multibody modelling approach is to model mechanical systems as a series of kinematic chains consisting of rigid, non-deforming bodies connected by kinematic joints. Newton-Euler equations are used to describe the motion of these bodies. Multibody HBMs have been used since the early 1960s [McHenry, 1963] through multiple iterations of programming packages previously referred to as Crash Victim Simulation (CVS) packages, e.g., [McHenry, 1963, McHenry and Naab, 1966, Robbins et al., 1974]. These early CVS packages laid the groundwork for modern multibody modelling software packages such as MADYMO (MAthematical DYnamic MOdels) developed by the Netherlands Organisation for Applied Scientific Research (TNO) and currently owned by Siemens Industry Software and Services B.V. Multibody modelling using MADYMO will be the primary modelling technique used in this thesis.

MADYMO uses four main HBM types:

- **Facet occupant models**

  The outer surface of the facet models consists of massless, meshed shell type contact elements referred to as facet surfaces. These facet surfaces are fully connected to rigid and/or flexible bodies. This allows for more accurate geometric representations while still being considered as multi-body models, since no FE solver is used in simulations.

- **Facet active human model**

  The facet active human model is similar in design to the facet occupant model however the neck, arms and lower extremities are modelled in more detail with active behaviour to keep the initial position of the neck, spine, hips and elbows. This model is available in sitting and standing postures and is suitable for low severity loading applications.

- **Facet pedestrian model**

  The facet pedestrian mode is identical to the standing facet active human model, except that it does not include active behaviour. This model is more suited to simulation with an FE vehicle model.

- **Ellipsoid pedestrian models**

  Unlike the above mentioned models, the outer geometry of the MADYMO ellipsoid models is represented by ellipsoids. This offers a much faster computational time at the cost of a less geometrically accurate surface compared to facets. The inertial properties of the pedestrian segments are incorporated in the rigid bodies of the pedestrian models. A force penetration contact characteristic is used alogside friction and damping to describe the contact interactions of the pedestrian model with itself and with its environment. A small female model representing the 5th percentile female population, a mid-size male model representing the 50th percentile male model population, and a large male model representing the 95th percentile male model are available, and two child body sizes representing a 3 and 6-year-old are available (Figure 2.14 Table 2.10).

Table 2.10: Anthropometry of the ellipsoid pedestrian model

[Madymo, 2019]

Parameter	3 Year old	6 Year old	Small 5% Female	Mid Size 50% Male	Large 95% Male
Standing height (m)	0.95	1.17	1.53	1.74	1.91
Seated height (m)	0.55	0.64	0.81	0.92	1.00
Shoulder breadth (m)	0.25	0.28	0.4	0.47	0.52
Knee height (m)	0.28	0.35	0.47	0.54	0.59
Weight (kg)	14.5	23.0	49.77	75.7	101.1

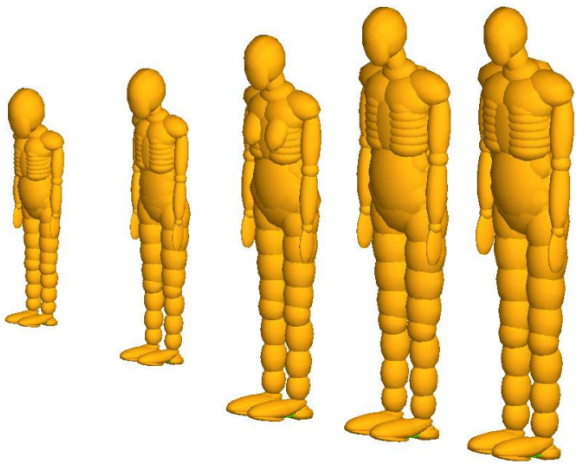

Figure 2.14: Ellipsoid pedestrian models, from left to right; 3-year-old child, 6-year-old child, small female, mid-size male and large male
[Madymo, 2019]

As mentioned above, epidemiological studies alongside full-scale impact tests are used to validate numerical models. The car-pedestrian tests used for the validation of the MADYMO ellipsoid 50th percentile male pedestrian models, often referred to as Average Male 50th percentile (AM50) are summarised in Table 2.11. The AM50 pedestrian model was scaled to the specific body dimensions of each PMHS subject prior to simulating the corresponding test.

Table 2.11: Anthropometry of the ellipsoid pedestrian model
[Madymo, 2019]

Model	**Description**	**Test**	**Specifications**	**Reference**
Scaled AM50	5 tests, large family car and optimized car	5 PMHS	32-39.8 km/h, deceleration 4.7-5.7 m/s2	EEVC [1998b]
Scaled AM50	10 tests, 3 different cars	10 PMHS	25, 32, 39, 40 km/h	Ishikawa et al. [1993a]
Scaled AM50	3 tests, small family car	3 PMHS	25, 32, 39 km/h	Yang et al. [2000]

Table 2.11 is adapted from the 2019 MADYMO Human Body Model Manual [Madymo, 2019] however, there have been other validation studies such as Kajzer et al. [1993] and De-Lange et al. [2007]. Up to the year 2021, these validation tests are for full body kinematics and segment kinematics for primary impact vehicle pedestrian collisions but offer no validation for pedestrian ground contact. Despite this, the AM50 model has been used in assessing ground contact injuries [Crocetta et al., 2015b, Zou et al., 2019]. In an effort to assess the capability of the MADYMO pedestrian model for use in ground contact head injury scenarios, Shang et al. [2021] reconstructed the six cadaver tests from Shi et al. [2018b] discussed

in Section 2.4.2 using scaled AM50 models (Figure 2.16). Simplified multibody models of the vehicles used in Shi et al. [2018b] were created in MADYMO, with each vehicle model consisting of a lower bumper, bumper, bonnet leading edge, bonnet, windshield, wheels and roof (Figure 2.15).

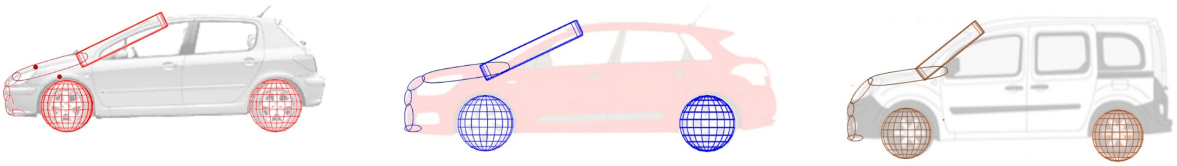

(a) Peugeot 307 (b) Citroen C4 (c) Renault Kangoo II

Figure 2.15: The vehicle models used in [Shi et al., 2018a] with simplified MADYMO models [Shang et al., 2021]

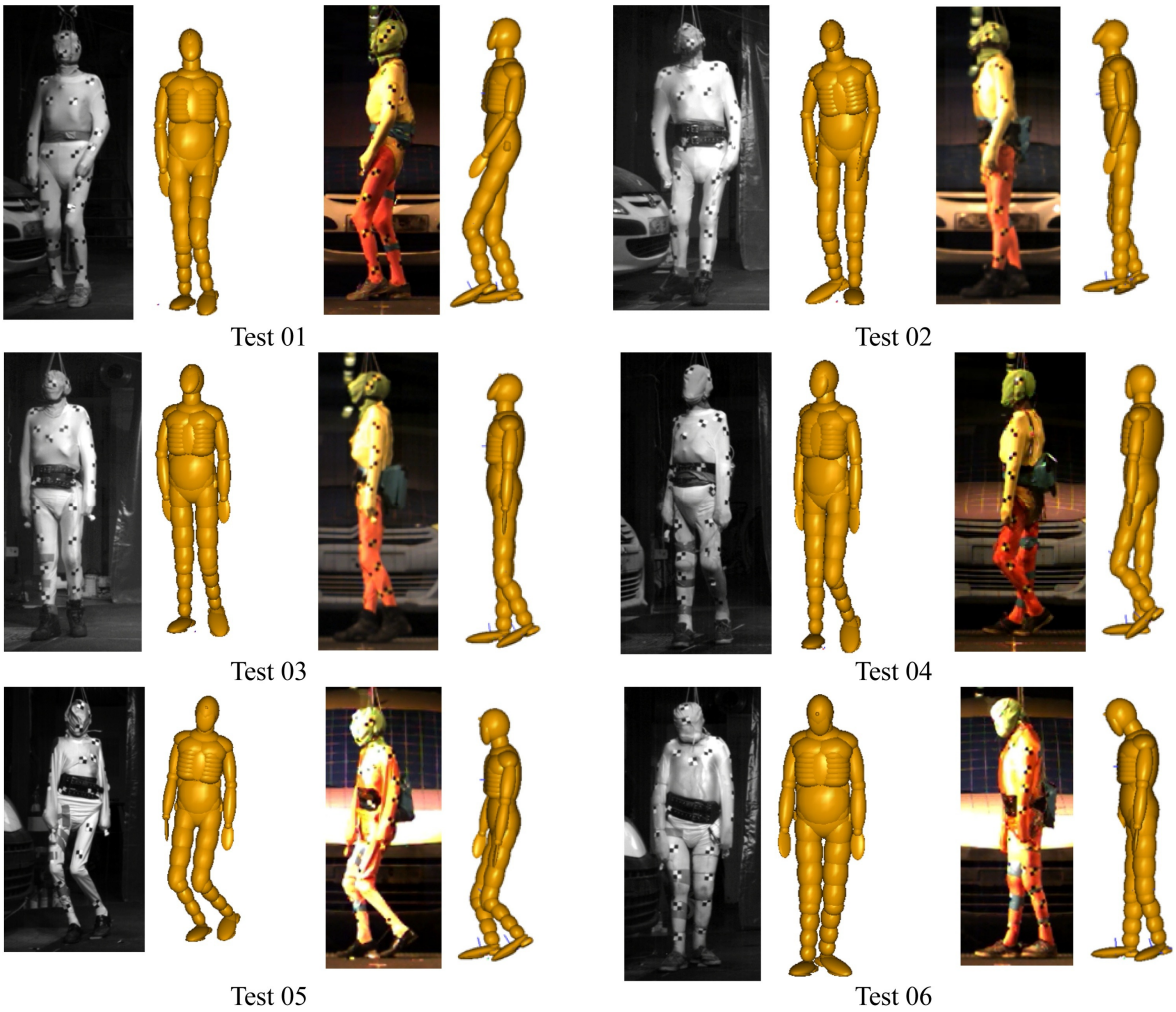

Figure 2.16: The initial postures of PMHS pedestrians and the corresponding scaled multi-body models

[Shang et al., 2021]

The contact characteristics applied to the MB vehicles used in this study were based on those derived from impactor tests, e.g.,[Hobbs and McDonough, 1998, Liu et al., 2002, Martinez et al., 2007], and summarised Euro-NCAP tests [Martinez et al., 2007]. For contact between the pedestrian's head and the ground, individual stiffness characteristics were calculated based on the location of impact (anterior/face or posterior). A multibody sphere with matching inertial and kinematic properties to the AM50 head just prior to impact was used to estimate the ground stiffness. The assumption is that a quarter wave of simple harmonic motion reasonably models the head acceleration up to the peak acceleration. From this, the stiffness is calculated based on peak acceleration and velocity change 2.7. The anterior stiffness Ka was found to be 97kN/m, while the posterior stiffness Kp was much higher at 1400kN/m.

$$\sqrt{\frac{k}{m}} = \omega = \frac{1}{\Delta T} = \frac{1}{\left(\frac{\Delta V}{Acc_{peak}}\right)} = \frac{Acc_{peak}}{\Delta V} \tag{2.6}$$

$$K = m\left(\frac{\Delta v}{Acc_{peak}}\right)^2 \tag{2.7}$$

Where m is the mass of the head, ω is the natural frequency, ΔT is the time duration of impact, ΔV is the total velocity change up to the peak acceleration, and Acc_{peak}.

The results of this study (Figure 2.17) show relatively high errors in comparing both the primary and secondary HIC scores between the PMHS tests and MADYMO models. The authors attribute some of the error in primary contact HIC scores to the lack of pedestrian voluntary motions, which are observed in real-life videos and cannot be replicated in PMHS tests. These voluntary motions may affect pedestrian post-impact kinematics and thus result in variable ground contact mechanisms. Another possible source of error may have been in the scaling of the AM50 models. As part of this study, a sensitivity analysis showed the effect of minor changes to the initial conditions on the ground contact HIC scores. For example, in one test, the AM50 models' ankle, knee, and hip joints were offset by +5 and -5 degrees from their baseline values. The results of these tests highlight the increased importance of initial conditions when evaluating secondary contact injuries. Small changes in impact conditions result in large kinematic differences and thus different head-ground contact mechanisms. This limits the capability of using the MADYMO AM50 models to accurately replicate the exact kinematics of both primary and secondary contact phases, though it is still useful in describing trends among different input conditions.

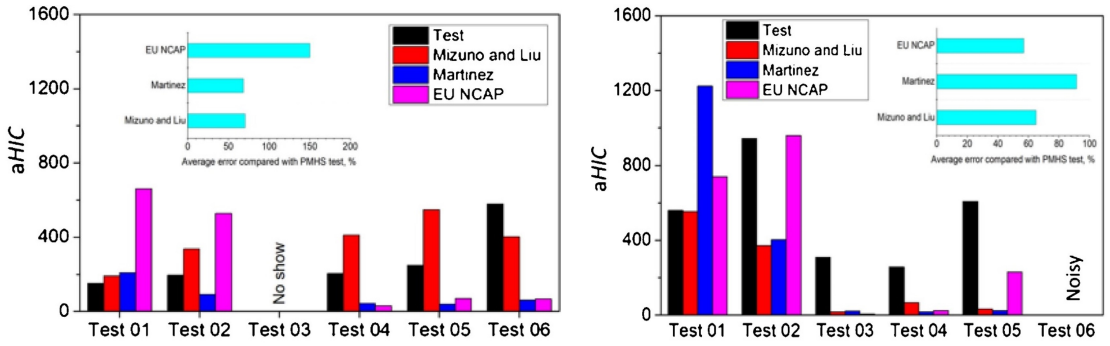

(a) HIC score from primary contact (b) HIC score from secondary contact

Figure 2.17: Comparison between PMHS and MADYMO HIC scores [Shang et al., 2021]

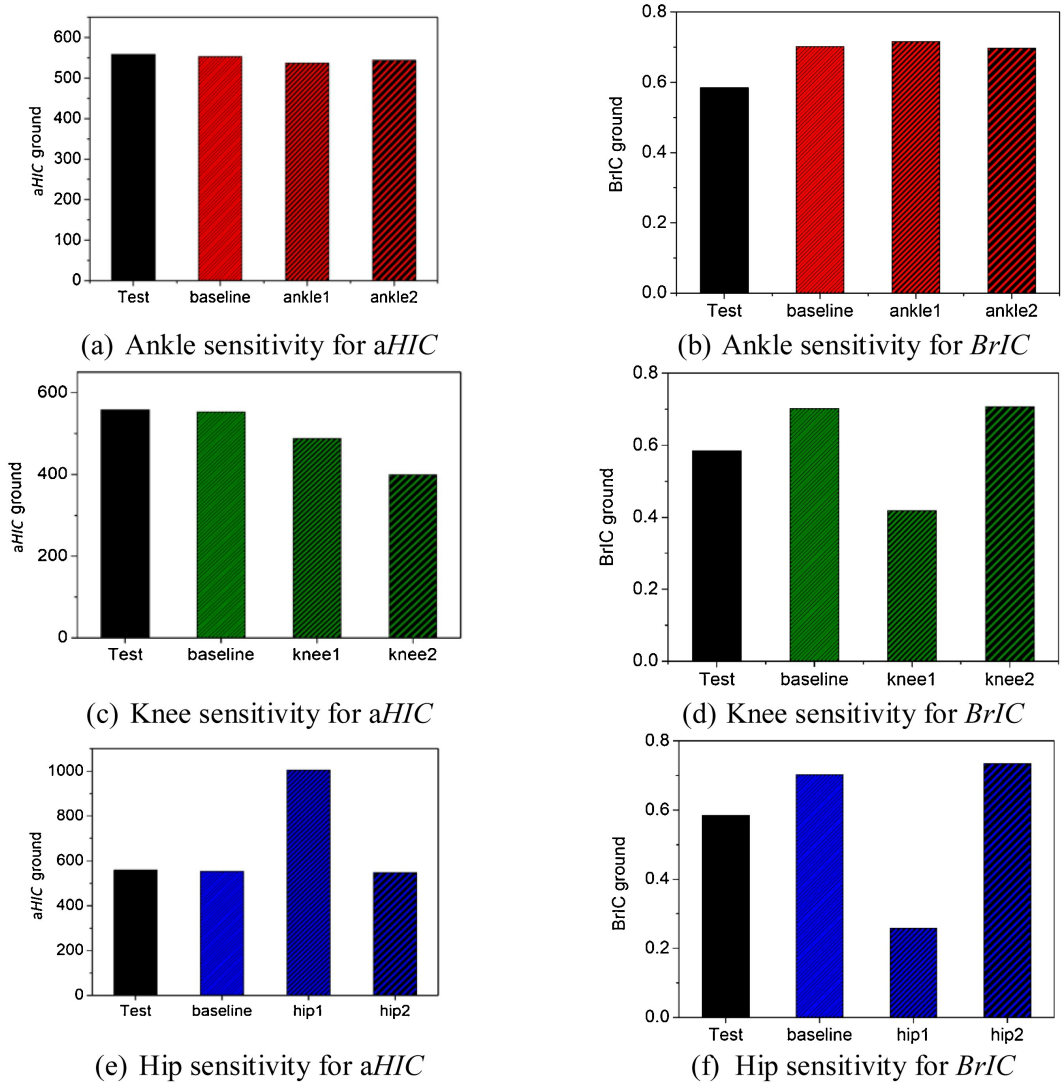

(a) Ankle sensitivity for a*HIC* (b) Ankle sensitivity for *BrIC*

(c) Knee sensitivity for a*HIC* (d) Knee sensitivity for *BrIC*

(e) Hip sensitivity for a*HIC* (f) Hip sensitivity for *BrIC*

Figure 2.18: Initial joint angle effect on aHIC and BrIC from ground contact for Test 01 [Shang et al., 2021]

While recreating the specific PMHS tests from Shi et al. [2018a] proved challenging, MADYMO has been used in literature to highlight the dangers of certain aggressive vehicle geometries. While no subway specific model is available, Grzebieta and Rechnitzer [2000] created MADYMO models of various classes of surface trams used in Melbourne, Australia. The HIC score was calculated for both pedestrian and car impacts with these trams using a Hybrid III model. The impact velocity was 35km/h, and injuries caused by ground contact were not considered. The tram with the most protruding bumper had the highest risk of injury caused by the pedestrian rotating around the thigh. This led to HIC scores of over 1000. The key takeaway from this study was that Melbourne's trams are overly aggressive toward other road users, even at low speeds, and that some padding on the tram's surface may lower the HIC score to desirable levels <1000.

Chevalier et al. [2019], used MADYMO to conduct a large-scale parameterised model of a tramway front-end based on 20km/h and 30km/h impacts with the MADYMO 50th percentile male, 95th percentile male, 5th percentile female, and 6-year-old child ellipsoid models. MADYMO was chosen for this study due to its fast computational time, making it more suited to large parametric-style studies. The parameters considered included the angles and dimensions for the tramway front end (Figure 2.19) and pedestrian sizes. The stiffness of the tram front was not altered, as the goal was to design simple geometric rules that can reduce head injury risk. Similar to the previous studies, injuries resulting from ground contact are not considered.

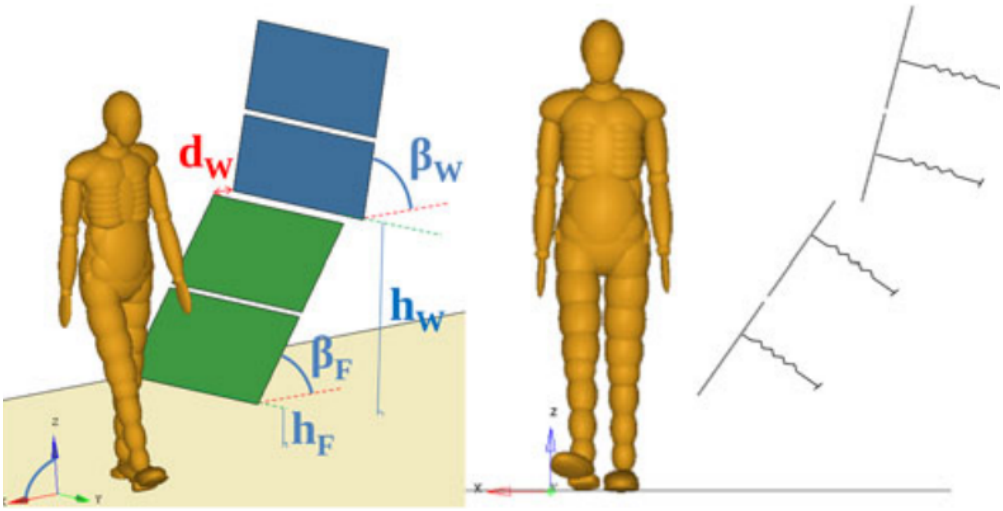

Figure 2.19: Tramway front end modeled using 2 portions of planes (blue = windshield, green = fairing)

[Chevalier et al., 2019]

In total, 8840 simulations were run with a computational time of approximately 1 minute per run, showcasing MADYMO's aptitude for parametric studies. Detailed kinematic observations of simulations show the following mechanisms (Figure 2.20):

- **Left** When the lower body is engaged, trunk rotation can increase the head's relative velocity upon impact with the windshield (fairing height of 1.05 m, relative head impact velocity of 6.77 m/s, and a Head Injury Criterion of 5,520).
- **Center** Shoulder loading can decrease the head's velocity when it hits the windshield (same fairing height, relative head velocity of 1.6 m/s, and a HIC of 80).
- **Right** A combination of shoulder loading by the fairing and a windshield offset at head level can prevent head impact with the windshield (fairing height of 1.30 m, HIC of 120).

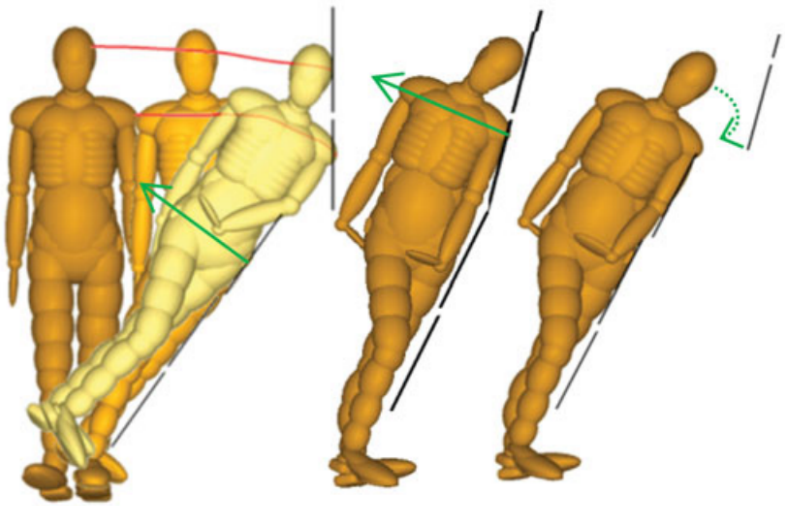

Figure 2.20: All scenarios involved a tram speed of 20 km/h and the AM50 model [Chevalier et al., 2019]

The key findings of this study suggest the pedestrian head was the most commonly injured body region. Lower extremity injuries showed patterns that differed greatly with pedestrian model size. Combinations of height and offset of the windscreen were observed to have an effect on the kinematics and HIC values due to the mechanisms listed above; however, these too were affected by pedestrian size. The most effective approach to reducing the risk of head injury from contact with the rigid windscreen appears to be a combination of shoulder loading by the fairing and adjusting the windscreen offset to lower the head impact velocity.

The limitations to this study listed by the authors include a lack of pedestrian posture variety. Each simulation involves the pedestrian in a walking posture (no initial velocity) at a 90 degree angle to the tram front. It is possible that the effect of the shoulder loading mechanism listed above will vary with impact position. The authors also highlight the need to investigate MADYMO's capacity for capturing the effect of impact angle on shoulder response. For application to large flat-fronted vehicles such as trams, there exists no PMHS data for validation. The simplified tram front-end geometry is represented by 2 flat surfaces with the same deviation angle. Most modern tram fronts now have curved panels in both the vertical and lateral directions, which would affect both the pre-head impact and ground contact kinematics. Another limitation is that, without consideration of ground contact, the overall safety is difficult to assess. Shi et al. [2018a] showed that ground contact HIC scores can be more severe than primary contact HIC scores at low impact velocities such as 20km/h. While this study offers insights into the mechanisms that lower primary contact HIC scores, it is unknown whether those same mechanisms may lead to higher secondary contact injury risk.

The effects of pedestrian posture (gait), vehicle-front geometry and impact velocity on the dynamic responses of the head were investigated by Peng et al. [2012]. The AM50 and 6-year-old ellipsoid models were used at 7 different initial gait positions (Figure 2.21) with 5 distinct vehicle shapes (Super Mini Car (SMC), Small Family Car (SFC), Large Family Car (LFC), Multi-Purpose Vehicle (MPV) and Sport Utility Vehicle (SUV)). In order to simulate a large range of impact conditions, four vehicle velocities (30km/h, 40km/h, 50km/h and 60km/h) were considered for each pedestrian position and vehicle type, resulting in a total simulation matrix of 280 simulations.

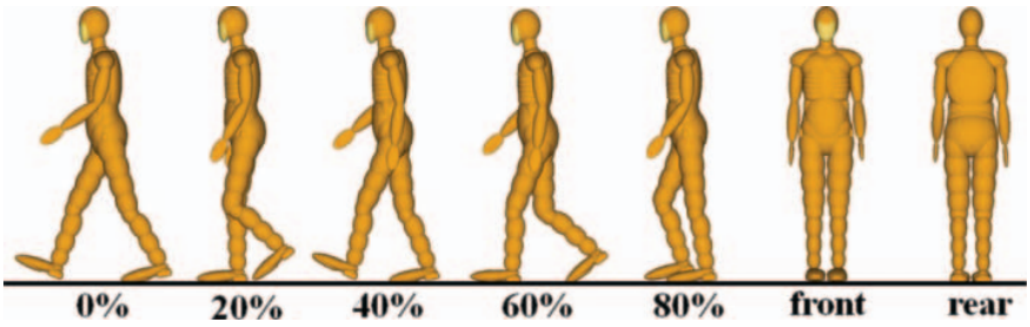

Figure 2.21: Pedestrian stances for different gait parameters (%)
[Peng et al., 2012]

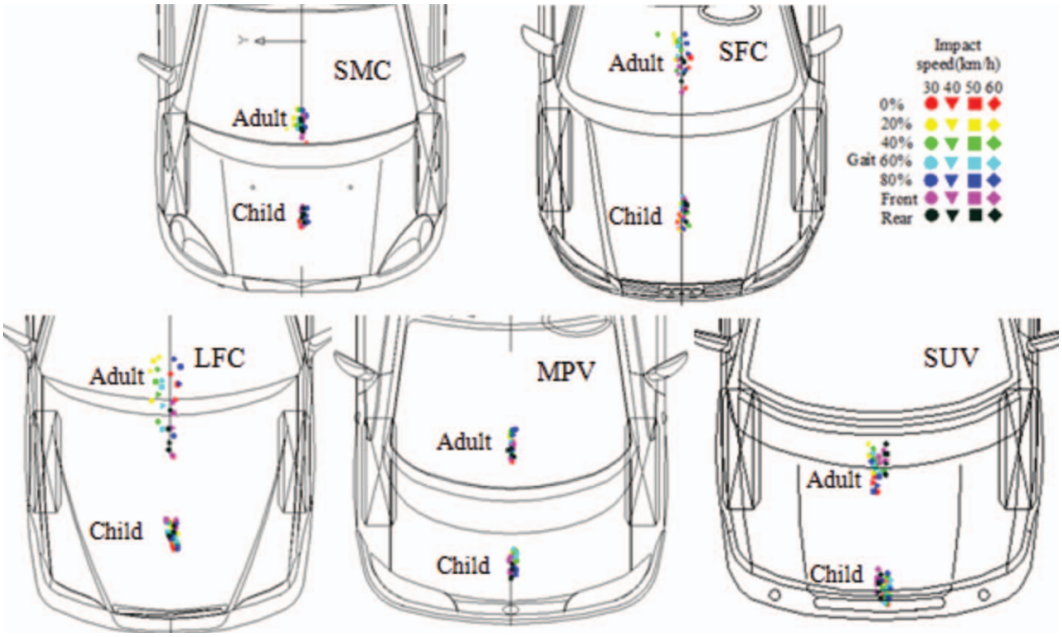

Figure 2.22: Comparison of the distribution of head contact point on different vehicle for different vehicle velocity and pedestrian gait
[Peng et al., 2012]

The results of this study suggest that the Wrap Around Distance (WAD), head impact location and head impact velocity are influenced both by vehicle geometry and pedestrian gait. The % gait of the pedestrian during the collision may determine the head impact location on the windscreen or bonnet (Figure 2.22). For adults, the impact angles are lower for SFC and MPV vehicles than for other types. For children, impact angles are larger for SMC, SFC, and LFC; smaller for MPV and SUV; and smallest for SUV. The authors recommend, based on this study, that test procedures should specify different impact angles for different vehicle types.

A limitation of this study is that, while pedestrian gait is altered, the impact position in all cases is the centre line of the vehicle. Given the curved geometry of some of the vehicles, off-centred impacts may yield different results. A larger parametric study involving a combination of multiple pedestrian gaits and impact positions would capture a larger portion of existing scenarios.

Despite the mentioned limitations these paper offer the most up to date and closest surrogate to a computational flat faced subway pedestrian model. The studies provides a good foundation to build on and highlight the importance of initial postures (gait), pedestrian sizes, impact velocity, vehicle geometry and ground contact or run over consideration.

2.5.3 Finite Element Modelling

Finite Element (FE) modelling also plays a critical role in pedestrian safety research, offering a more detailed analysis when compared to multibody modelling. Unlike multibody modelling, which simplifies the human body and vehicle components into interconnected rigid bodies with simplified joint and contact mechanics, FE modelling discretises both the human anatomy and vehicle structures into a mesh using nodes and elements. This allows for the simulation of complex material behaviours such as localised deformations at the cost of a much higher computational load and increased user inputs such as detailed material and meshing properties. In this way, FE modelling complements multibody modelling by providing a more detailed analysis of localised deformations and material responses. Together, these methods offer a comprehensive approach to pedestrian safety research, with multibody modelling providing the foundational understanding of impact kinematics and finite element modelling offering deeper insights when needed.

A finite element parametric study to assess the effect of vehicle front-end geometry on pedestrian injury risk was conducted by Han et al. [2012]. The studies were carried out using 2 Total HUman Model for Safety (THUMS) pedestrian models (177cm and 165cm) and 4 finite element vehicle models with different front-end shapes (Figure 2.23 from left to right: medium-size sedan, minicar, one-box vehicle, and sport utility vehicle (SUV)).

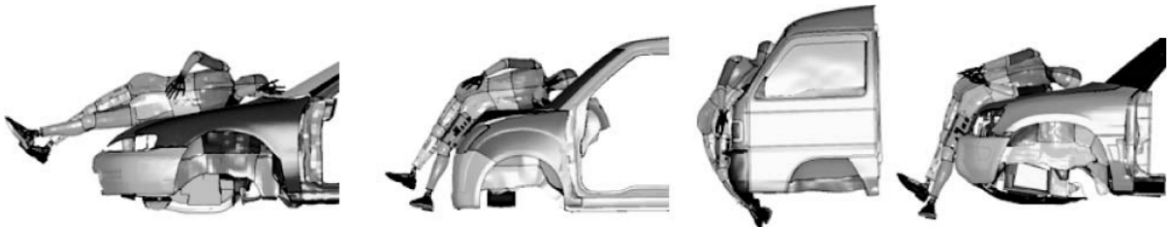

Figure 2.23: All scenarios involved a tram speed of 20 km/h and the AM50 model [Han et al., 2012]

In vehicle-to-pedestrian collisions, the impact velocities of different body regions, such as the head and chest, are influenced by the vehicle's shape and pedestrian size. The study found that head impact conditions vary with vehicle shape:

- **Medium-Size Sedan:** The head impact velocity was similar to the initial impact velocity due to upper body rotation. This is a similar finding to the multibody parametric study Chevalier et al. [2019] which cited trunk rotation as a factor of increased head injury risk.

- **One-Box Vehicle:** The head impact velocity was lower than the initial vehicle velocity. This too supports the findings from Chevalier et al. [2019] which attributed shoulder loading on the flat faced vehicles to lower relative head impact velocity.

- **Minicar and SUV:** Similar head impact velocities were observed due to similar rotation around the hood leading edges.

Head injury risk also varied with vehicle shape and hood length. Longer hoods and higher hood leading edges increased head injury risk in collisions with medium-size sedans and SUVs, while shorter hoods reduced head injury risk in minicar collisions. Additionally, as vehicle impact velocity increased from 20 to 50km/h, the time to head impact decreased, which is important for optimising active safety measures like hood pop-up mechanisms and pedestrian detection sensors.

Lopot et al. [2019] conducted full-scale ATD impact tests with a tram (Section 2.4.3). As part of that study, a virtual tram pedestrian impact using the Altair HyperWorks environment was used to investigate whether different front-end geometries could reduce the HIC scores shown in Table 2.9. The results suggest that the accelerated fall effect can be eliminated by using geometries that encourage first contact lower on the pedestrian. In these cases, the dummy hits the ground under significantly less harmful conditions. There are limitations to this work; however, it should be noted that this is a pilot study with the intention of encouraging future research in this area. This is not presented as a completed research piece. It is, however, the most up-to-date simulation of a tram-pedestrian collision using full-scale testing.



Figure 2.24: Primary stage of impact of modified front on the dummy in the simulation [Lopot et al., 2019]

2.6 Impact Energy Mitigation

Impact energy mitigation is a large research focus among biomechanical safety engineering studies. The head injury criterion (Section 2.2.3) is a linear acceleration-based metric for estimating skull fracture risk. By reducing the linear acceleration of the head during an impact, the associated HIC score will be reduced. This concept has been used in helmet design with both sports and military applications, e.g., [Fan, 1983, Franklyn and Laing, 2016, Johnston et al., 2015].

Sances Jr et al. [2000] evaluated the head injury mitigation with foam padding covering vehicular roll bars and brush bars. The first part of this study involved a 32mm diameter steel production brush/roll bar with three types of foam padding. A 5th percentile Hybrid III female head and neck was mounted at the end of a pendulum. The head was instrumented with three orthogonal uni-axial IC 500G sensors. The height of the pendulum was adjusted to obtain different impact velocities from 3.4 to 6.7m/s, with an impact location offset from the head Centre of Gravity (CG) by approximately 25mm (Figure 2.25). The three types of foam padding used were Simpson Race Products roll bar padding, cold-rolled steel metal air gap padding and production brush bar foam padding. In each case, the thickness of padding was approximately 25mm.

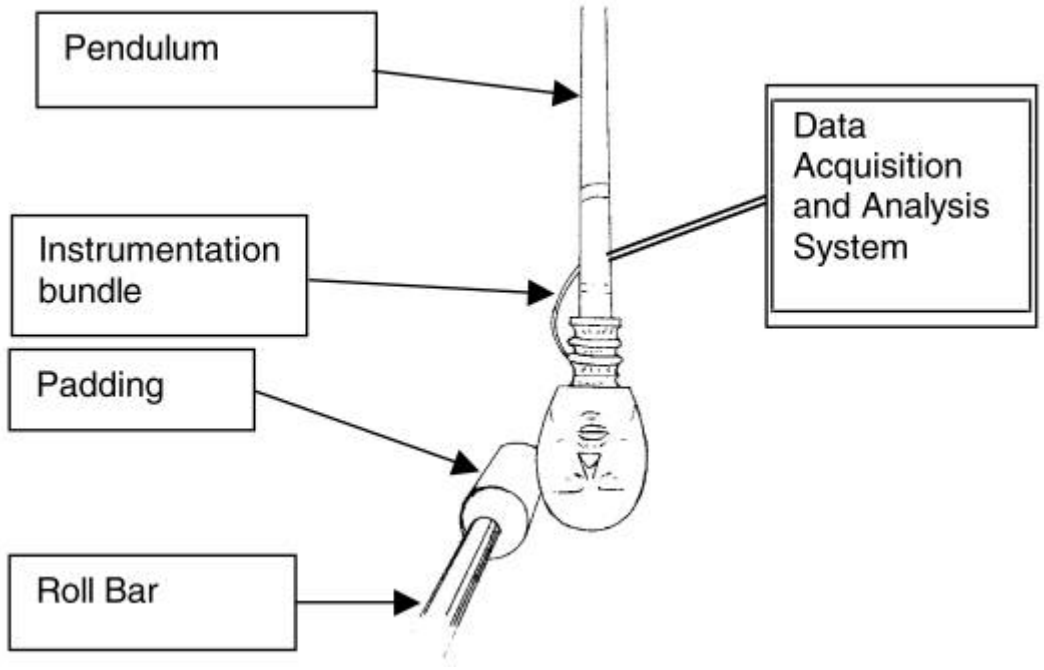

Figure 2.25: Illustration of overall test configuration
[Sances Jr et al., 2000]

The second and third parts of this study used 47mm diameter bare steel roll bars rigidly supported at each end. The padding used for these tests was stock vinyl and foam, commercial padding, Simpson Race Products padding, and the metal air gap padding. An instrumented free-falling Hybrid III 50% male head form at speeds of 5.4m/s with a 25mm CG offset was used for side impact and forehead impacts for the second and third studies, respectively.

The results of this study (Tables 2.12 & 2.13) report that the HIC and linear acceleration were markedly reduced with the addition of padding materials under all test conditions compared to the baseline no padding condition. This reduction was greater at higher impact velocities compared to lower. This is consistent with numerous other studies, which have similarly demonstrated that padding materials effectively mitigate impact forces across various conditions such as [Nazarian et al., 2015]. A similar observation was made regarding the test dummies, with the 50th percentile male dummy experiencing a larger reduction in HIC scores. The findings delineate the biomechanical importance of energy absorbing padding materials to mitigate head injuries. Some limitations of this study include the lack of neck injury consideration as well as slight differences in padding thickness (up to 6mm difference) which were attributed to manufacturing difficulties.

Table 2.12: Pendulum Head Side Impact with 25 mm offset from CG 5th percentile female Hybrid III Head and Neck

[Sances Jr et al., 2000]

Test	**Impact Velocity (m/s)**	**HIC**	**Peak Linear Acceleration (g)**
Production bar	3.4	202	135
Production bar	4.5	454	196
Production bar	4.5	582	245
Production bar	6.7	1966	500
Simpson Race Products padding	3.4	90	49
Simpson Race Products padding	4.5	200	71
Simpson Race Products padding	4.5	239	73
Simpson Race Products padding	6.7	710	167
Simpson Race Products padding	6.7	667	121
Metal air gap	3.4	126	71
Metal air gap	4.5	150	81
Metal air gap	6.7	423	141
Production brush bar padding	3.4	105	68
Production brush bar padding	4.5	239	92
Production brush bar padding	6.7	883	196

Energy absorbing systems are routinely used in the automotive industry worldwide. A car bumper can be considered an energy absorbing system. Passive energy absorbing systems are also of interest for pedestrian safety. Lakshminarayana et al. [2011] created a multibody model of a Tata SE 1613 Turbo EX BS II Heavy Goods Vehicle (HGV) to investigate the

Table 2.13: Free Fall Head Impacts 50% male Hybrid III 5.4 m/s and 25 mm CG offset [Sances Jr et al., 2000]

Test	**HIC Side**	**HIC Frontal**	**Peak Linear Acceleration Side (g)**	**Peak Linear Acceleration Frontal (g)**
Production bar	2626	1871	458	324
Stock vinyl and foam	2268	1348	414	279
Commercial padding	1130	794	248	208
Simpson Race Products padding	558	383	144	128
Metal air gap	240	192	68	64

effects of soft external frontal frames referred to as Deformable Energy Absorbing (DEA) systems on pedestrian collisions as a means of injury mitigation. This DEA frontal system is made from semi-rigid polyvinyl chloride foam having a density of 100kg/m^3 and a cell size of approximately 400µm. This simulated DEA was created in the LS_DYNA software programme as a Finite Element model to allow for deformations and then imported into MADYMO and attached to a multibody truck front end. This results in a coupled finite element to multibody simulation. The thickness of the entire system including the mounting bars is 100mm (Figure 2.26).

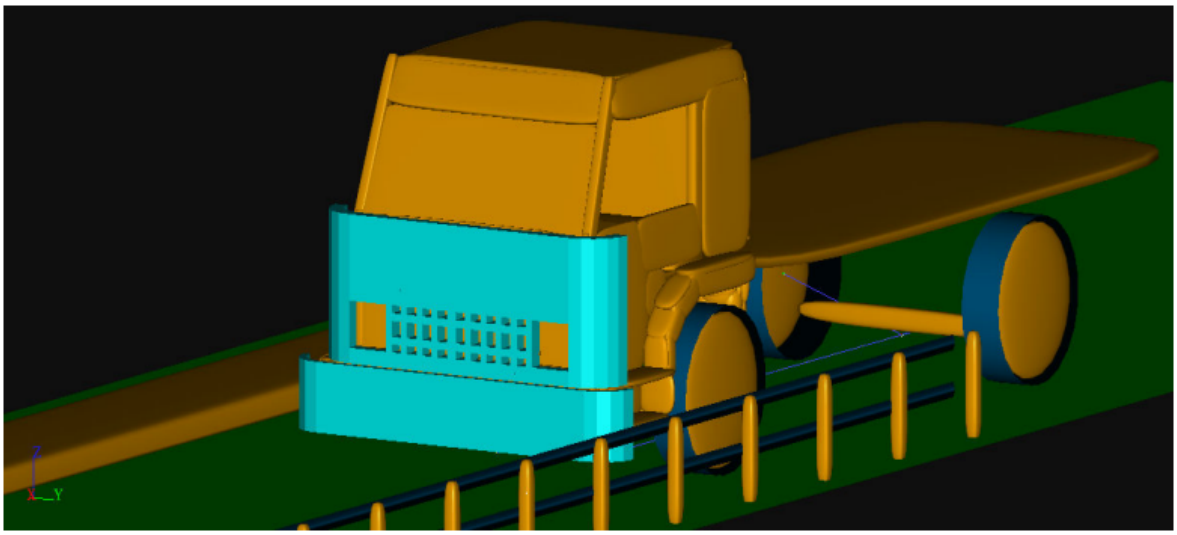

Figure 2.26: Tata SE 1613 Turbo EX BS II Truck with attached with DEA frontal system [Lakshminarayana et al., 2011]

The Hybrid III 50th percentile Male was utilised as the pedestrian model. Side and rear impact were analysed at speeds starting from 15km/h to 60km/h at 5km/h increments. The HIC score was calculated for both the primary (F) and secondary (S) impact, with and without the DEA. An initial velocity for the side impact pedestrian model was set at 2m/s; although a single standing posture was used in all simulations.

The results of these simulations suggest that the presence of a DEA reduces the head injury risk for both side and rear primary impacts. With an allowable HIC threshold of 1000, the DEA increases the maximum impact velocity from 30km/h to 50km/h for side impacts and 25km/h to 45km/h for rear impacts (Figure 2.27). When comparing secondary impacts, the reduction in HIC scores due to the DEA was not considered significant.

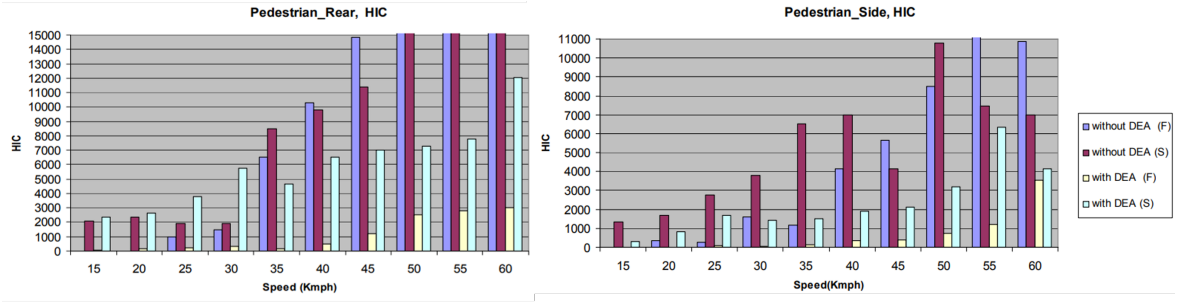

Figure 2.27: Plot for HIC at different speeds during first and secondary impacts for pedestrian rear impacts

[Lakshminarayana et al., 2011]

There are several limitations to this study. As shown by Peng et al. [2012], the position and gait of the pedestrian play a role in both primary and secondary impact kinematics, which in turn affect the associated HIC scores. In this study, the pedestrian is given an initial walking velocity, but a single unnatural standing position is used in all simulations. The resulting HIC scores presented in Figure 2.27 are noticeably higher than those in alternative literature. For example, Figure 2.27 reports a HIC score of 8500 for a side impact at 50km/h with the flat-faced truck, whereas Han et al. [2012] reported a HIC score of roughly 400 for the one box car at the same velocity. Chevalier et al. [2019] also reported significantly lower HIC scores for flat-fronted vehicles, with the exception that different HBMs were used for these publications. For ground contact, the simulated HIC scores ranged from 1800 to 6000 for side and rear impacts, while Shi et al. [2018a] reported HIC scores between 300-800 for 20km/h and 30km/h PMHS side impacts (Figure 2.11). While the HYBRID III model used in this study represents an ATD dummy and not a PMHS, the resulting HIC scores would ideally be expected to fall within a similar range. Figure 2.27 also indicates a drop in HIC score from roughly 1600 to 1200 for impact at 30km/h and 35km/h. This implies that the impact at 35km/h has a lower probability of injury than an impact at 30km/h. This same trend can be observed for speeds of 20km/h and 25km/h. Validation of the contact characteristics used this model are not presented in this paper. Figure 2.5 showed that HIC scores above

3000 have a 99.9% probability of a maximum untreatable head injury. In practice, large HIC scores, such as those over 5000, are unlikely to be representative of the impact scenario due to the deformation of the skull. As the HIC score is based on peak acceleration, skull fracture and larger deformations would occur before a HIC score the likes of 10,000 could be reached.

The same authors would later publish a follow-up study [Mitra et al., 2018] that addresses the abovementioned limitations. The objective of this study was the same as Lakshminarayana et al. [2011] however, all the individual model components used in this study have been validated against available experimental research. Additional pedestrian postures have been incorporated into the simulation test matrix with a gait cycle of 0-40%. The resulting HIC scores have been directly compared to similar studies [Chawla et al., 2000]. The primary and secondary HIC scores are presented for side impacts at various speeds and gait cycles, both with and without the deformable energy absorbing system (DEA). The results show a slight variation in primary impact HIC score with gait for impacts without the DEA; however, large variations are observed when the DEA is introduced to the model (Figure 2.28).

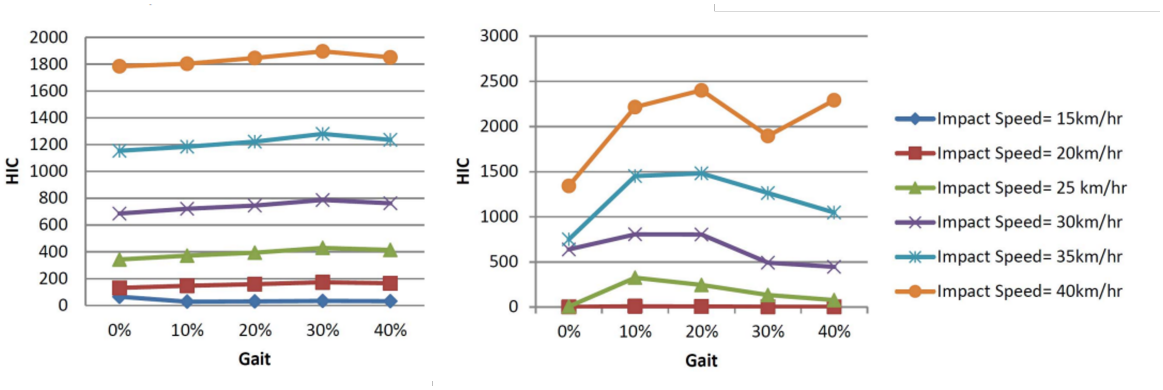

Figure 2.28: Primary impact HIC vs gait with DEA (Right) and without DEA (Left) [Mitra et al., 2018]

The secondary impact HIC scores (Table 2.14) are significantly higher than the primary impact, which is in line with previous studies such as [Shi et al., 2018b]. This is true for both with and without the DEA. The effect of gait on the secondary impact HIC is prominent in both cases. For an impact velocity of 35km/h with no DEA, the secondary contact HIC score varies from 5281 at 10% gait to 12543 at 40% gait. The findings from this study further highlight the importance of pedestrian initial conditions on the secondary impact injury analysis.

Table 2.14: Secondary impact HIC scores

[Mitra et al., 2018]

Speed (km/hr)	**Without DEA (gait cycle)**					**With DEA (gait cycle)**				
	0%	10%	20%	30%	40%	0%	10%	20%	30%	40%
15	13341	8841	13623	6872	13458	5198	10285	3421	8363	9998
20	9224	9961	16341	18508	14067	9731	10700	7633	2509	2086
25	8669	11506	20321	19945	12815	9759	11202	4216	11822	14795
30	6095	3738	8906	5280	9700	10124	9915	7092	16440	15157
35	9729	5281	9217	5824	12543	13070	17367	12184	14749	16015
40	14200	9492	11895	8163	14428	16538	27952	19355	16366	20164

2.7 Summary and Research Gap

A literature review into the topic of improved subway to pedestrian collision safety was conducted. The key areas identified in safety research are epidemiological studies, physical impact testing, computational modelling, and safety device design.

The review of the epidemiological studies produced a large dataset of subway pedestrian collision data from the 1950s up to the late 2010s. However, direct comparison between these studies is not always possible due to many confounding factors. The range of fatality rates presented in Table 2.2 may be explained by differences in the structural environments across each rail network, as well as the intent of the pedestrian or data collection methods. Even within rail networks, structural differences at each platform may affect the risk of fatality, as shown by O'Donnell and Farmer [1994a] however, this effect has not been quantified. Specific biomechanically relevant information such as impact velocities, pedestrian initial position and injury mechanisms are not present in the literature. Epidemiological data specific to the NYC subway system is limited to Lin and Gill [2009] and Gershon et al. [2008a]. No additional studies have emerged since 2009 which include all NYC subway pedestrian collisions.

There have been no full-scale PMHS or ATD subway pedestrian impact tests found in this literature search. The closest testing scenario found was a non-instrumented HYBRID III dummy used by Lopot et al. [2019] in a pilot study to assess the kinematics of street car/tram pedestrian collisions. The lack of full impact tests for subway to pedestrian collisions is likely due to the financial cost of such tests. This, however, presents a challenge for future computational modelling studies, as there is a lack of validated models for this collision type.

Computational modelling has been used extensively for road vehicle safety research; however, no specific subway pedestrian model has been found in the literature. While some computational modelling studies have investigated flat-faced vehicles [Lakshminarayana et al.,

2011] or street-level tram impacts [Chevalier et al., 2019, Grzebieta and Rechnitzer, 2000], the complex secondary contact interactions between the pedestrian and the tracks are not well understood. The effect of secondary contact on head injury risk has been shown to be of significant concern when dealing with a flat roadbed [Shi et al., 2018b]. With the additional complexity of a railway track with a live third rail, drainage trough, and cross ties, secondary contact injury risk must be considered to adequately determine the overall risk of head injury.

In summary, while there are epidemiological data sources for subway pedestrian collisions, confounding factors between rail networks make comparisons and compilations difficult. PMHS and ATD impact tests have been conducted for automotive road vehicles, but to date, no subway-specific test data has been found. The computational modelling studies found include flat-faced vehicles and trams, but focus mainly on primary impact injuries and omit injuries caused by run-over and secondary contact. No subway pedestrian model has been found. Figure 2.29 outlines the results of this literature review as well as the gaps found in each section, which this thesis aims to address.

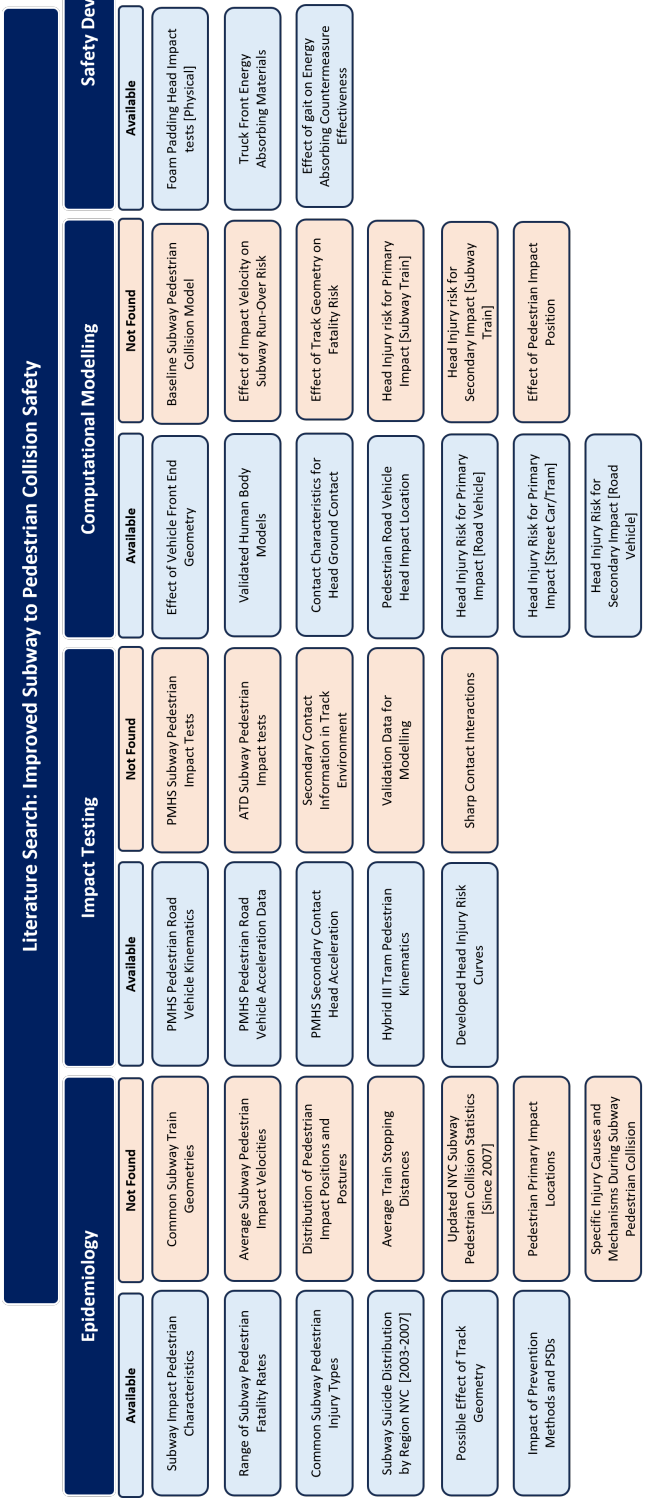

Figure 2.29: Summary of literature review findings

Chapter 3

A Detailed Analysis of New York City Subway Pedestrian Incidents from 2019

The results from this study are published in Transportation Research Record (TRR)

doi.org/10.1177/0361198123116669

3.1 Introduction

Large metropolitan cities have invested in urban subway systems to help tackle the challenges of high carbon emissions, high road traffic and urban sprawl [Wey, 2019]. The number of cities with operational subway systems increased from 50 in the 1970s to over 219 in 2019, with a global subway track length in excess of 15,000km [Mao et al., 2021]. With this increase in subway stock usage, ridership and track length, it can be expected that there will be an increase in subway-related injuries. While there are a small number of assault cases where pedestrians were pushed in front of a subway train, most incidents relate to voluntary trespassing. This is reflected in literature reporting on the increase in subway trespassing related fatalities. Trespassing related cases include both intentional (suicide/suicide attempts) and unintentional (accidental) subway train human collisions. The mean annual number of suicidal acts on the London Underground system increased from 36 (1940–1949) to 94 (1980–1989) with a further 644 recorded suicide attempts between 2000 and 2010 [Martin and Rawala, 2017, O'Donnell and Farmer, 1994b]. The Toronto subway system has reported a statistically significant increase in its subway suicides since 2013, with an average of 23 suicide incidents per year in 2018 [Ho et al., 2021b].

Chapter 2 highlights the importance of epidemiological studies as a first foundational step towards improved safety design. This chapter also describes the difficulties in comparing data from different rail networks due to many confounding factors such as vehicle type, mean velocity and station geometry. The main focus of this research is based around the New York City subway system, which is one of the oldest and largest in the world, with 5.5 million daily passengers in 2019. There are 472 stations operating 24 hours a day. There are two primary papers which offer insight into the nature of these incidents. Gershon et al. [2008b] collected medical examiner records for all 668 New York City subway-related fatalities from 1990 to 2003; see Table 3.1. Between 1990 and 2003, the most frequent borough for NYC subway fatalities was Manhattan (43.1%) and most cases involved males (84%), often in their late thirties or early forties (25.3%). For males, there are more cases of accidental fatalities, while for females there are more cases of suicide. In total, suicide accounted for about half of NYC subway train human fatalities (51.4%) between 1990 and 2003.

The second paper [Lin and Gill, 2009] examined medical records for 211 NYC subway-related fatalities between 2003 and 2007. Table 2 shows that between 2003 and 2007, the majority of both NYC subway accidental (86%) and intentional (81%) fatalities involved

Table 3.1: 1990-2003 NYC fatality data adapted from [Gershon et al., 2008a]

	Suicide N (%)	**Accident N (%)**	**Total N (%)**
Sex			
Male	269 (78%).4	286 (90.8%)	561 (84%)
Female	74 (21.6%)	29 (9.2%)	107 (16%)
Age			
0-24	42 (12%)	44 (14%)	89 (13%)
25-34	96 (28%)	71 (22.5%)	169 (25.3%)
35-44	88 (25.7%)	88 (27.9%)	177 (25.3%)
45-54	56 (16.3%)	55 (17.5%)	112 (16.8%)
55-64	24 (7%)	40 (12.7%)	66 (9.9%)
65-74	18 (5.3%)	10 (3.2%)	29 (4.3%)
75+	19 (5.5%)	7 (2.2%)	26 (3.9%)
Borough			
Manhattan	137 (40.3%)	146 (47.3%)	288 (43.1%)
Bronx	37 (10.9%)	39 (12.6%)	79 (11.8%)
Brooklyn	95 (28%)	88 (28.5%)	185 (27.7%)
Queens	70 (20.6%)	34 (11.0%)	104 (15.6%)
Staten Island	1 (1%)	2 (2%)	3 (0.4%)
Total	(51.4%)	(47.2%)	

males, with an average age between 43 and 45. The authors distinguished between suicides and accidents using toxicology reports, witness statements, police reports, and autopsy reports for each case. The results show very close agreement with the previous paper [Gershon et al., 2008a], with suicide accounting for 52% of fatalities and accidents accounting for 36%. The remaining 12% of fatalities are categorised as "other", which is not included in Table 2. Temporal data was collected; however, no noticeable trends for month and day were observed. Incident rates do show a peak in accidental fatalities at 04:00am, corresponding to the closing time of bars and nightclubs, and reinforcing the conclusions of another study on rail-related death [Pelletier, 1997], which called for more effort on the education of alcohol abuse to reduce rail-related deaths.

Table 3.2: 2003-2007 NYC fatality data adapted from Lin and Gill [2009]

	Suicide n(%)	**Accident n(%)**
Male	81	86
Female	19	14
Average Age (Years)	43.9	45.2
Total	52	36

It is thus clear that more effective safety measures are needed to combat the rising number of subway incidents. However, to effectively design such countermeasures, a more detailed understanding of the nature of subway collisions is required. The two above papers present the most up-to-date understanding of NYC Subway's fatal incidents from 1990 to 2007. Since then, there has been a lack of published literature on NYC subway incidents, and our understanding of existing subway collision configurations is therefore poor. Most importantly, there is little known about the configuration of pedestrian subway collisions in any subway system. Previously published literature is also limited only to fatal subway human interactions.

This chapter aims to deliver a comprehensive analysis of NYC Subway incidents, identifying key biomechanical parameters such as impact velocity, impact position, pedestrian pre-collision behaviour, and post-collision outcomes. By generating new insights into the patterns and mechanics of subway-to-pedestrian collisions, this study provides critical data to support the development of biomechanical models, inform the design of effective countermeasures, and guide evidence-based policies to reduce fatalities and enhance passenger safety in subway environments.

3.2 Methodology and Data Collection

This study focused on the collection and evaluation of Public Transportation Safety Board (PTSB) case reports for 263 New York City Subway incidents for the year 2019. The New York Subway system saw a 95% reduction in ridership in 2020 due to the Covid-19 pandemic. Since then, subway ridership has been slowly increasing; however, by June 2021, which is the time this study took place, the NYC Subway had risen to only 30% of its pre-Covid-19 ridership [Wang and Noland, 2021]. Therefore, the 2019 data is considered the most recent representation of an average year of NYC Subway incidents. This conclusion is supported by a preliminary review of 2018 NYC Subway incident data, which had a similar number of incidents and fatalities. In addition, the number of 2019 fatalities is similar to the average numbers of annual fatalities reported by Gershon et al. [2008a] and Lin and Gill [2009]. A total of 526 case reports detailing 263 incidents (2 separate reports per incident) were supplied directly from the New York Metropolitan Transportation Authority (MTA) and manually reviewed. Of these 263 incidents, 185 involved subway human interaction, which was further analysed as part of this study. Ethical approval was granted by the School of Engineering Research Ethics Committee for the analysis of this data.

A sample of 10 cases was reviewed to create a set of 32 categories for data collection and evaluation based on the available comparable data recorded from the investigators in the case reports (Table 3.3). As the purpose of this study is to aid in the design of safety equipment, these categories were chosen with consideration of biomechanical modelling for countermeasure design evaluation. For example, it was decided that track elevation (elevated or below ground) was to be recorded. This information can be used to evaluate the effectiveness of equipment in different environments.

Table 3.3: Relevant information recorded from PTSB incident reports

Event	**Train**	**Pedestrian**	**Outcome**
ID Number	Division	Pre-impact action	Witness Description
Date	Train number	Impact position	Injury outcome
Time	Train model	Age	KABCO
Borough	Interaction	Sex	Injured body region
Station name	Final position	Employee status	
Station elevation	Stopping distance	Final position	
Line and Direction	Impact velocity		
Incident type	Braking type		
Intention	Stopping time		
Hours delayed	Train contact area		
Response time	Contact evidence		

The impact velocity was estimated using an event recorder that was installed in 65 of the incident trains. This event recorder gives the velocity at the time the emergency brakes were activated. In most cases involving emergency brake activation, the train operator witnessed a pedestrian on the track in front of the train or in the act of jumping in front of the train, prompting brake activation. Due to the limited deceleration, the train generally slowed but did not stop prior to contacting the pedestrian. This slow deceleration is to protect the occupants during emergency braking. The exact velocity at the time of impact is unobtainable in many cases; therefore, the event recorder speed at the time of emergency brake activation can be considered an upper bound speed estimate. The train surface contact region was reported based on evidence of human tissue or bodily fluids found on contact surfaces or from the subway train operator's or other witness accounts. The final rest position of the pedestrian was based on the position where the pedestrian was first found. A body found on the tracks by an oncoming train was coded as "behind train". The categorisation of suicide and accident was determined by using the train operator's witness statement. Pre-impact action and impact condition are differentiated due to the reports of a pedestrian "jumping in front of a train" only to land on the tracks and lay down or change their posture. The pre-impact action is not always the impact position.

The cases contain a wide range of injuries from no injury to fatality. The 5-point injury scale known as KABCO, which is used by police to assign an injury metric in road traffic accidents, was applied [Compton, 2005]. KABCO categorises injuries as Fatal (K), Severe (A), Moderate (B), Minor (C), and None (O). A simplified injury categorisation is also used for graphical purposes. Fatalities are equated to K, injuries are equated to A and B, and no injury is equated to C and O in reference to the KABCO Scale.

The database was stored on an Excel sheet. Two coders analysed the case reports, with each coder assigned a subset of cases. Both coders then read each of their cases individually and extracted the desired information, inputting it into the Excel sheet. Lists and drop-down menus were used when appropriate to reduce entry error. Two intercoder reliability tests showed above 98% agreement between the two coders.

3.3 Results

3.3.1 Literature Comparison

A total of 263 New York City Subway incident cases were made available for 2019. We first assessed if the 2019 data showed similar trends to published findings. Figure 3.1 compares distributions of age and location for the 2019 data with the 1990-2003 data from [Gershon et al., 2008b]. Table 3.4 shows age and sex comparisons of the 2019 data to the 1990-2007 data [Gershon et al., 2008b, Lin and Gill, 2009]. Both Figure 3.1 and Table 3.4 contain only fatal cases. Both Figures show little change in the overall trends from previous studies.

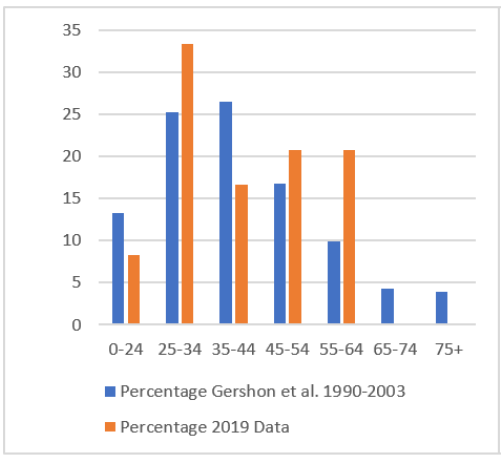

(a) Age distribution of NYC subway fatalities

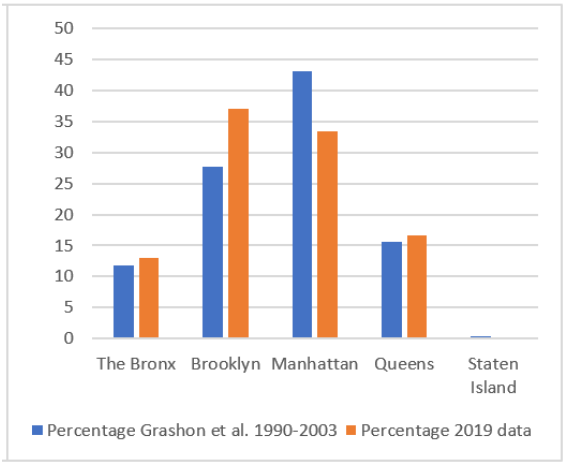

(b) Distribution of NYC fatalities by borough

Figure 3.1: Fatality data comparison between Gershon et al., 2008 and 2019 data

Table 3.4: 1990-2003 Gershon et al. [2008a], 2003-2007 Lin and Gill [2009] and 2019 Data

	1990-2003 N(%)	**2003-2007 N(%)**	**2019 N(%)**
Male	561 (84%)	156 (83%)	63 (83%)
Female	107 (16%)	41 (17%)	13 (17%)
Mean Age	35-44	44	39

3.3.2 Event Type and Location

Of the 263 New York City Subway incident cases from 2019, 185 (70%) involved train to human contact. The remaining 30% related to falls (with no train contact), assaults, derailments and other unrelated categories. Figure 3.2 shows the breakdown of accidental impacts (n=106) and intentional impacts (suicide/suicide attempts n=53) using the KABCO scale. A small number of cases were excluded from this comparison (n=26) due to incidents not fitting within either the suicide or accident categories. Examples of cases removed include homicides, undetermined cases and assaults. The overall fatality rate is 29% with a further 41% of pedestrians presenting at the nearest hospital alive. Since medical records were not available, it is unknown how many of those pedestrians survived. The 2021 paper [Ho et al., 2021b] found a mortality rate of 29% for patients who presented to the emergency department after a subway human collision, with a survival rate of 88% for those who survived the initial presentation. Thus, an overall estimated fatality rate of 31% is presented with the assumption that 12% of the severely injured (A on the KABCO Scale) resulted in a fatality.

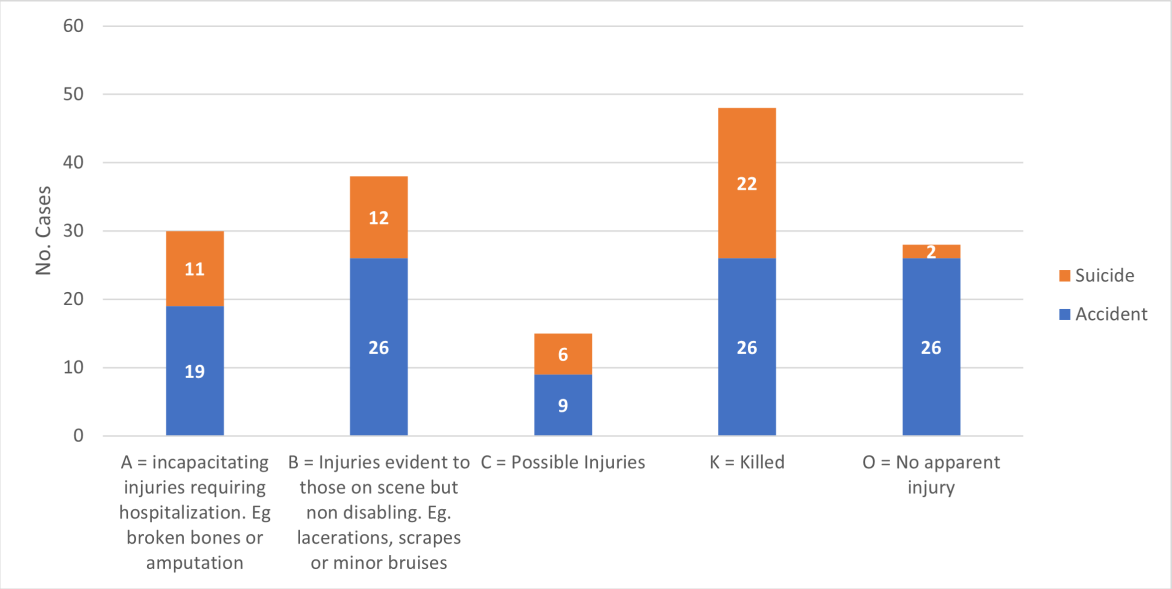

Figure 3.2: KABCO Accident vs Suicide for NYC Subway 2019, n = 159

The New York City Subway has 472 stations, of which 283 (60%) are below ground, 149 (32%) are elevated, and the remaining 8% are a mix of surface/at-grade and embankments. Table 3.5 shows the breakdown of the NYC 2019 subway incident data in relation to track type (elevated/surface and below ground) and incident location relative to the station. Figure 3 shows a stacked representation of the KABCO categories with track type, showing a 40% fatality rate (19/48) for above-ground stations compared to a 27% fatality rate (35/130) for below-ground stations.

Figure 3.3 shows that the fatality rate is 50% higher in an elevated station (40%) than in a below-ground station (27%). The train geometry and entry velocity are similar in both station types; however, there is a significant difference in track geometry.

Table 3.5: 2019 NYC Subway incidents by station type and location

	Below Ground	**Elevated/Surface**	**Total**
At station at platform	111	43	154
At station away from platform (Within 200ft)	18	6	24
Not at Station	5	1	6
Total	134	50	184

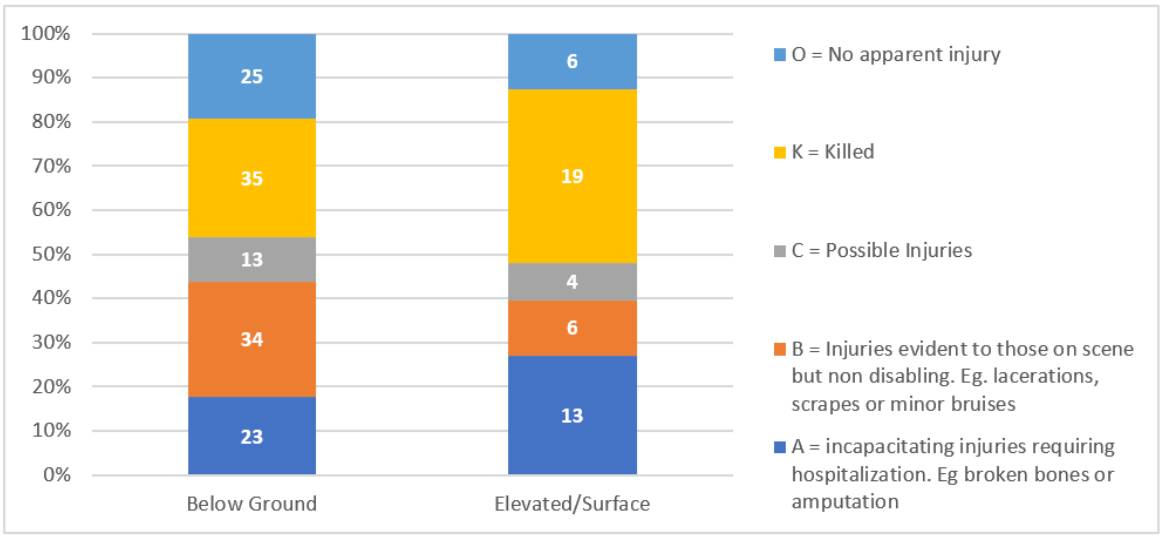

Figure 3.3: KABCO proportions vs track type for NYC Subway 2019, n = 178

3.3.3 Impact Data

Figure 3.4 shows the most common types of pre-impact behaviour reported by the train operator and eyewitnesses. Figure 3.5 shows the impact positions of the pedestrians using the simplified injury categorisation. Figure 3.6(a) shows the estimated impact velocity with the same simplified injury scale. Figure 3.6(b) shows the proportion of fatality/injury/no-

injury outcomes as a function of estimated impact velocity (mph). Figure 3.7 shows the train surface contact area for primary impacts categorised according to the KABCO scale. Figure 3.8 shows the final position of the pedestrian with the KABCO scale.

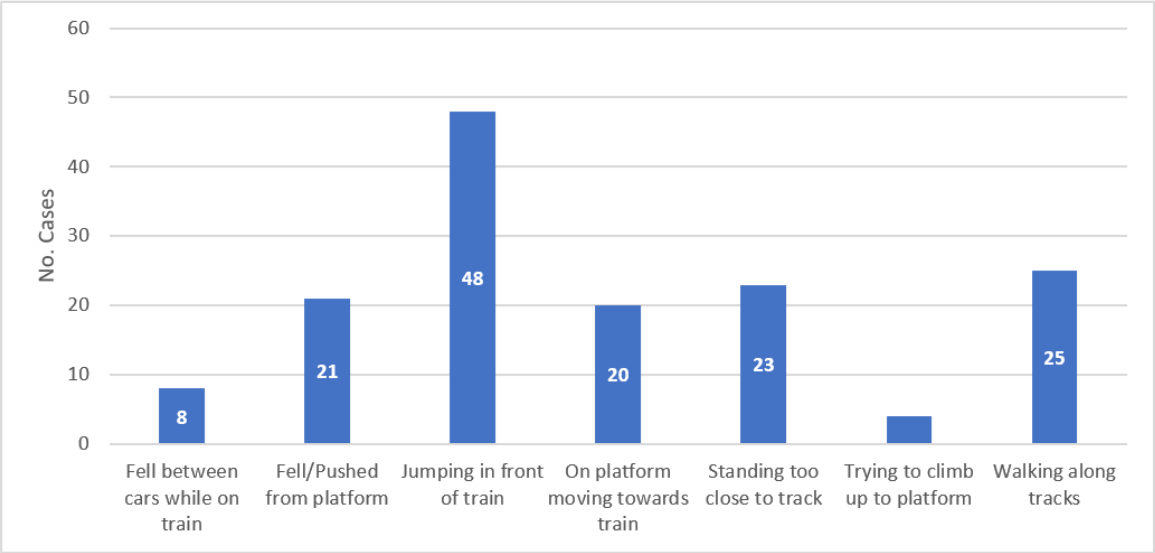

Figure 3.4: Pre-Impact behaviour for for NYC Subway 2019, N = 159

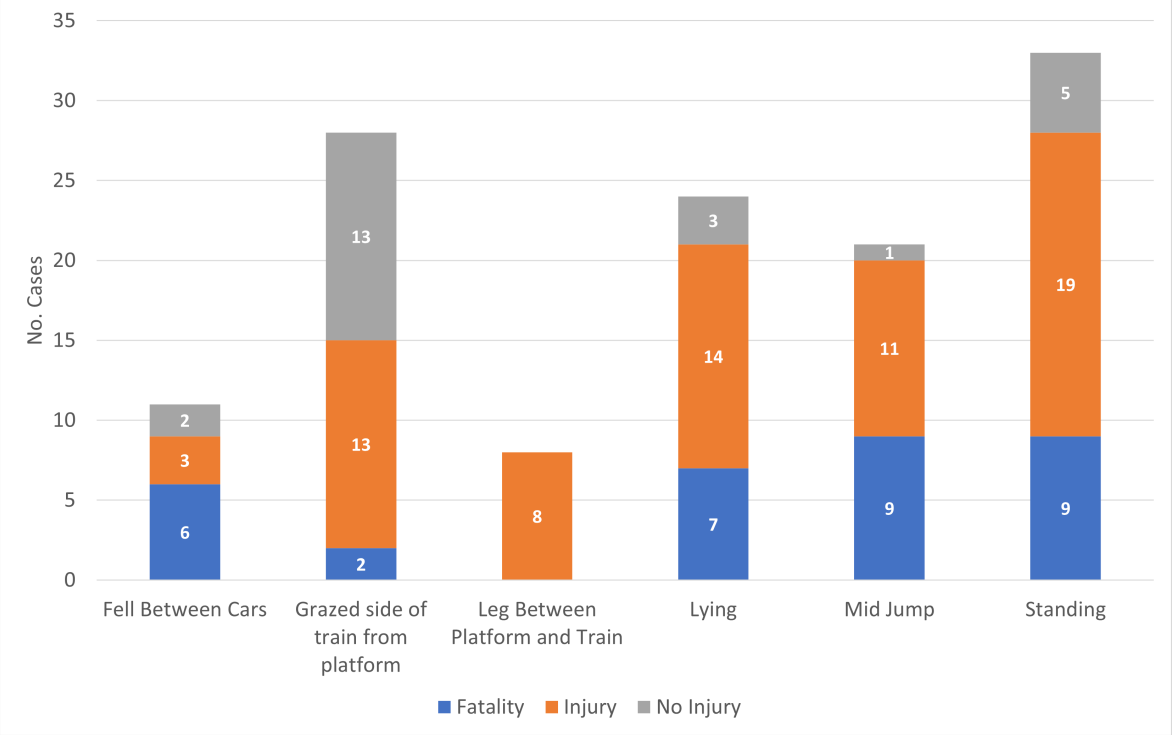

Figure 3.5: Impact positions for for NYC Subway 2019, N = 125

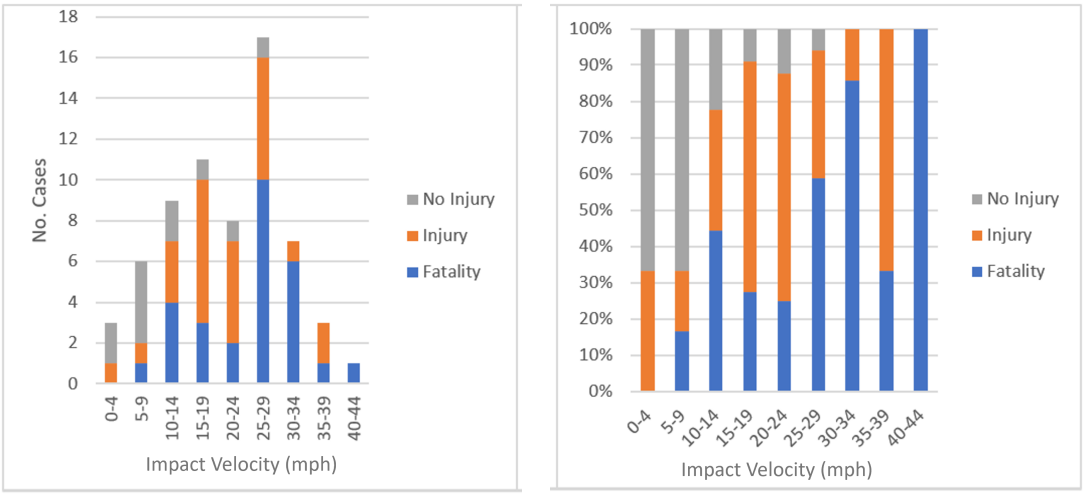

(a) Estimated impact velocity (mph) with incident outcome fatalities

(b) Proportion of fatality/injury/no-injury outcomes as function of estimated Impact Velocity

Figure 3.6: 2019 NYC Subway data with estimated impact velocity (mph), N = 65

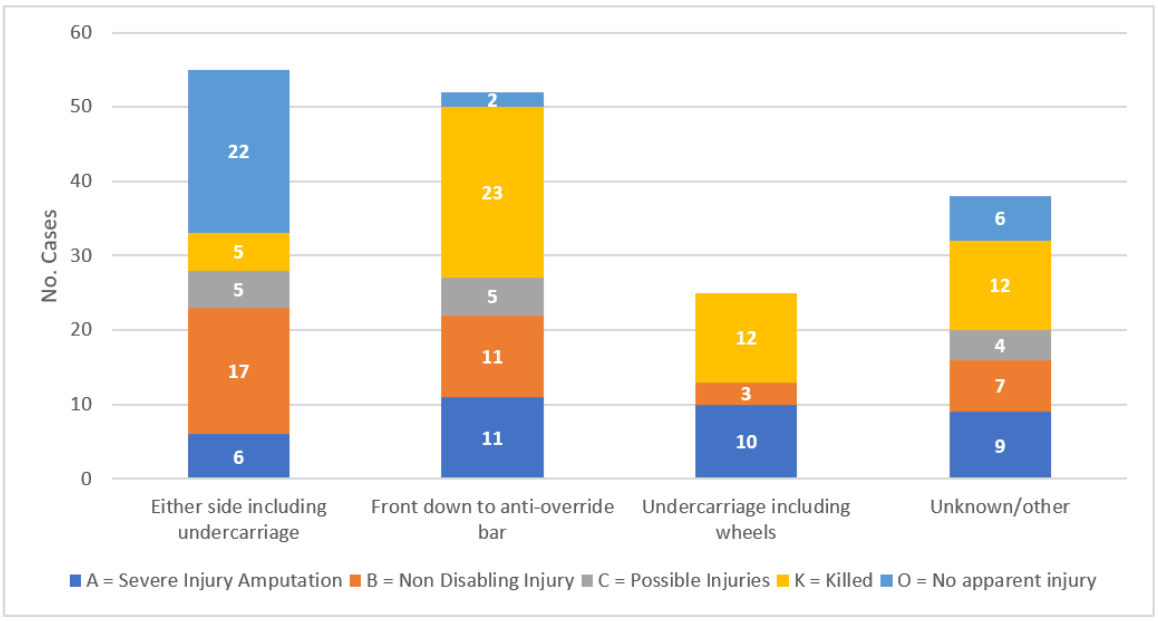

Figure 3.7: 2019 NYC Subway KABCO data with primary contact area, N = 170

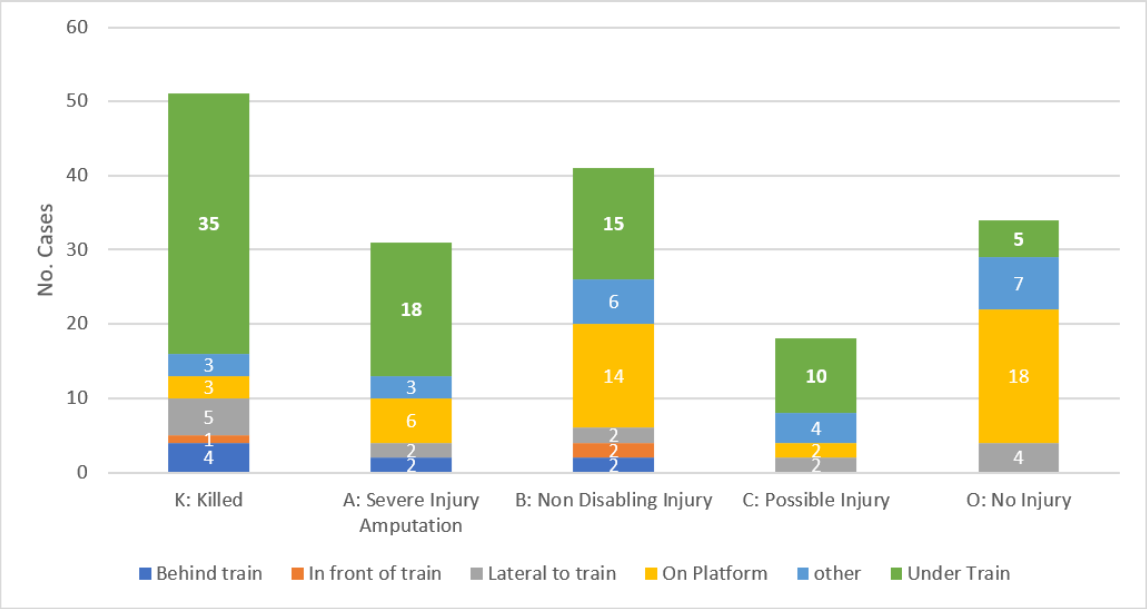

Figure 3.8: 2019 NYC Subway KABCO data with pedestrian final position, N = 175

3.4 Discussion

Table 3.4 compares published literature (1990-2007) on New York City subway incidences with the 2019 fatal data. The former covers a 17-year timespan, whereas this study presents data for one year only. The percentage distributions show reasonable alignment despite slight differences in peak values. Thus, the age, sex, and geographical distribution of subway collisions in the New York City transit system have not changed substantially over a 30-year period, further justifying the conclusion that 2019 can be considered a typical year for more detailed analysis. Moreover, this analysis of New York City subway pedestrian incident cases presents significant new insights into the nature of subway-to-pedestrian collisions, and these are considered in detail below.

3.4.1 Event Type and Location

The breakdown of suicide and accidental train human collisions (Figure 3.2) differs slightly from previous literature (Tables 3.1-3.2). The reliance on eyewitness accounts only may account for this. The fatality rate for suicidal train-to-human impacts is 42%, while accidental impacts have a 25% fatality rate. Suicidal acts tend to be on the roadbed and thus have a much more violent impact, with a high risk of rollover by the train wheels. A large portion of accidental impacts are side impacts, with the pedestrian standing too close to the edge of

the platform. This distinction further highlights the difficulty in comparing epidemiological data from multiple subway pedestrian collision studies, as some studies focus only on suicidal acts which will skew the reported fatality rate.

Figure 3.9 presents photographs of both an elevated and below-ground NYC Subway station. One possible reason for the higher fatality and amputation rate in above-ground and elevated stations compared to below-ground stations could be the drainage trough (often referred to as a suicide pit) (Figure 3.9(b)) which is not present in elevated stations (Figure 3.9(a)). However, track geometry can differ even within stations. A single below-ground station may contain both one track with a deeper drainage trough with crossties and another track with a shallower drainage trough without crossties. Further study on the effects of track geometry on secondary impacts is needed to better understand the effect of track geometry on pedestrian injury outcomes. This work will be presented in Chapter 5.



(a) R142 Entering an Elevated NYC Subway Station (b) NYC Below ground Station tracks

Figure 3.9: Elevated and Below ground NYC Subway Stations. Images taken by Author

3.4.2 Impact Data

A significant proportion (15%) of NYC Subway train to human collisions occur due to the pedestrian standing too close to the platform edge (Figure 3.4). Further, the most common pre-impact manoeuvre is a pedestrian jumping from the platform to the roadbed, followed by the pedestrian walking along the tracks. Accordingly, limiting access to the platform edge (e.g. via platform doors) would likely be an effective countermeasure in many cases. However,

the space available on existing platforms may limit the viability of platform doors in many cases.

In terms of biomechanical modelling for countermeasure development and assessment, the initial position of the pedestrian model is of great importance; see Figure 3.5 and Chapter 2. The conditions coded as "Grazed the side of the train from platform" and "Leg between platform and train" have the highest survival rate. Of the three frontal impact positions, mid-jump has the highest fatality rate (43%). Mid-jump incidents often occur at the highest train velocity as the train operator has not initiated the emergency brakes; however, they occur less frequently. When considering fatalities only, standing, jumping and lying should be given equal consideration for safety countermeasure design. Future policies aimed at injury/fatality mitigation and associated computational modelling efforts would therefore benefit from a comprehensive impact position comparison involving the abovementioned postures.

The most common estimated impact velocity is 11-13m/s or 25-29mph (Figure 3.6(a)), and there is unsurprisingly a positive correlation between impact velocity and fatality rate (Figure 3.6(b)). However, due to run-over and the risk of electrocution from the third rail, even low velocity impacts in the 2-4m/s (5-9mph) range can result in a fatality. Secondary impact can be fatal at any speed, especially due to the presence of the third rail which carries a lethal electrical current. Secondary contact can also result in serious injuries due to track stiffness and geometry.

Figure 3.7 shows the primary impact location, with side impacts presenting the lowest fatality rate (9%) and wheel/undercarriage presenting the highest (40%). Not surprisingly, therefore, policies aimed at reducing the capacity of pedestrians to be run over by the subway should be the main safety consideration.

3.4.3 Countermeasure Summary

Most train to human impacts occurred at a platform or within the station area (200ft either side of the platform) (Table 3.6), reflecting limited access to the subway track. Thus, the following suggested countermeasure designs should focus on the station area.

Table 3.6: Summary of possible countermeasures based on findings

Findings	**Possible Countermeasures Requiring Further Study**
- Lower fatality rate in below ground stations - Higher fatality rate in suicidal impacts compared to accidental impacts	- Optimised drainage through design for all stations
- Large portion of accidental collisions caused by pedestrians standing too close to platform edge	- Platform edge doors where possible - Further education on dangers posed to pedestrians at the platform (Mishara, 1999, Mishara, 2007, Poirier et al., 2021) - Additional platform Personnel at peak times
- Similar number of fatal incidents are observed for standing lying and mid jump impact positions	- Equal importance given to the three impact positions mentioned for future studies.
- Fatal incidents observed in low-speed impacts	- Third rail/wheel contact prevention such as wheel guards

3.4.4 Limitations

The analysis in this study is based on the data available in the New York City Transit Authority's incident reports. These have been completed based on the train operators' and other eyewitnesses' accounts. Thus, the level of detail available in the incident reports is variable. The reliance solely on eyewitness accounts may explain the slight discrepancies in suicide and accident fatality numbers compared to the published literature, as medical records, toxicology results, patient history and medication data were not available for this study (Figure 3.2). The speed estimates should be considered as an upper bound. The precise position of the pedestrian at the instant of contact with the subway cannot be established with certainty. Due to variability in available data between incident reports, direct comparison can be difficult. For example, impact velocity is only reported for trains which have an event recorder installed, whereas the train model is recorded for all cases. If a direct comparison was made between impact velocity and train type, there would be many missing datapoints which may change the reader's interpretation. It is for this reason the total number of cases n is different for Figures (3.2-3.8). Notwithstanding all these limitations, the information presented in this chapter provides the most detailed available analysis of the configurations of subway-to-pedestrian collisions.

3.5 Conclusion

This analysis of 2019 NYC Subway incidents shows little has changed in terms of borough, age and gender distribution of NYC subway fatalities since 1990. Further, the data shows most cases (97%) occur at or close to the station area, emphasising that policies aimed at limiting track access would inhibit most collision cases. The fatality rate appears to be substantially influenced by track geometry, with the presence of the drainage trough reducing fatality rates, suggesting secondary impacts play a major role. Grazing the side of the train from the platform is the second most frequent impact position. This type of impact could be prevented with additional policies focused on ensuring passengers are standing clear of the platform edge while a train is approaching. For example, additional education with personnel ensuring the platform edge is clear during peak times may yield beneficial results (Mishara, 1999, Mishara, 2007, Poirier et al., 2021).

For biomechanical modelling for future intervention design, scenarios involving pedestrians standing, lying and jumping are all important. The fatality rate increases with impact speed as expected; however, impacts of 16-18m/s (35-40mph) can be survivable, and some very low speed events are fatal. An effective countermeasure at 8m/s (30mph) impact speed would mitigate the injury for the vast majority of cases. The most common final resting position for pedestrians was under the train, associated with the highest fatality rate. This suggests future policies promoting countermeasures that protect against contact with the underside of the train, the wheels, and the track bed. This information is pivotal to the initial conditions used in the following chapters of this thesis.

Chapter 4

Experimentally Derived Contact Characteristics for Hard Shell Energy Absorbing Material: Application to Subway-to-Pedestrian Collisions

4.1 Introduction

In automotive safety, significant safety advances have been achieved through combining accident data analysis, physical testing, computational modelling and accident reconstruction. For example, relationships between car front shape and pedestrian injury risk have been evaluated using the German In Depth Accident Study (GIDAS) database [Li et al., 2017]. Data derived from impact testing involving either an anthropomorphic test device or a post-mortem human surrogate (e.g. Arregui-Dalmases et al. [2015], Richardson et al. [2021]) can be utilised to enhance computational modelling studies. Collisions between subway vehicles and pedestrians, although less frequently addressed in comparison to road vehicle accidents, constitute a significant safety concern within urban settings.

The focus of this chapter is to bridge the gap between the epidemiological data presented in Chapter 3 and future computational modelling studies on subway-to-pedestrian impact safety design. Although epidemiological analysis has revealed key insights into the frequency, severity, and circumstances surrounding these incidents, Chapter 2 highlights the lack of available impact test data specific to subway-to-pedestrian collisions. While some comparisons can be made to existing studies involving heavy goods vehicles with frontal energy absorbing materials [Chevalier et al., 2019, Lakshminarayana et al., 2011, Mitra et al., 2018], additional consideration is needed to apply this data to a subway-specific environment. For example, an operational concern may be that any energy-absorbing safety device would need to be contained within a hard shell to protect against weathering and impacts with light debris while maintaining its energy absorbing and lightweight properties [Jiang et al., 2022]. The effect of this hard shell on the risk of head injury in pedestrians would need to be minimal to offer a worthwhile benefit.

The aim of this chapter is therefore

1. Design and fabricate a test rig to accelerate a headform ATD to a predetermined velocity (based on Chapter 3) and impact an energy absorbing material with a hard shell covering.

2. Use the acceleration, mass and position of the headform to derive the force deformation relationships for energy absorbing material with and without a hard shell.

3. Assess the capacity to replicate the impact conditions using MADYMO.

4.2 Material Selection

4.2.1 Analytical model

To make an informed decision on the type of energy-absorbing material to use, an analytical model was developed in MATLAB to simulate the position of a spring-mass system $x(t)$ during a collision. The model incorporates base support motion, represented as a ramp function $X(t)$, to simulate the movement of the train during impact (Figure 4.1).

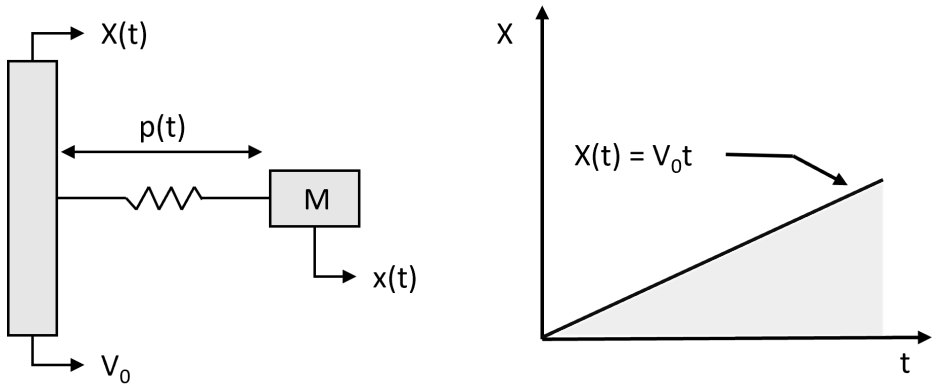

Figure 4.1: Analytical model ramp function schematic

$$x(t) = A\cos(\omega_n t) + B\sin(\omega_n t) + V_0(t) \tag{4.1}$$

In this system (Figure 4.1):

- The mass M (kg) represents the mass of a human head or headform impactor.
- The base support position $X(t)$ represents the train's motion, modeled as $X(t) = V_0 t$, where V_0 is the train's velocity.
- The penetration (m) or crush depth $p(t) = X(t) - x(t)$ represents the minimum required depth of a countermeasure.

The equations of motion for the spring-mass system are derived with the initial conditions $x(0) = 0$ and $\dot{x}(0) = 0$. Solving for the constants A and B, the displacement (m), velocity (m/s), and acceleration (m/s^2) of the mass are expressed as Equations 4.2-4.4. The user provides the stiffness k (N/m) and mass m (kg) to calculate the natural frequency ω_n (Hz).

$$x(t) = -\frac{V_0}{\omega_n}\sin(\omega_n t) + V_0 t \tag{4.2}$$

$$\dot{x}(t) = -V_0\cos(\omega_n t) + V_0 \tag{4.3}$$

$$\ddot{x}(t) = V_0\omega_n\sin(\omega_n t) \tag{4.4}$$

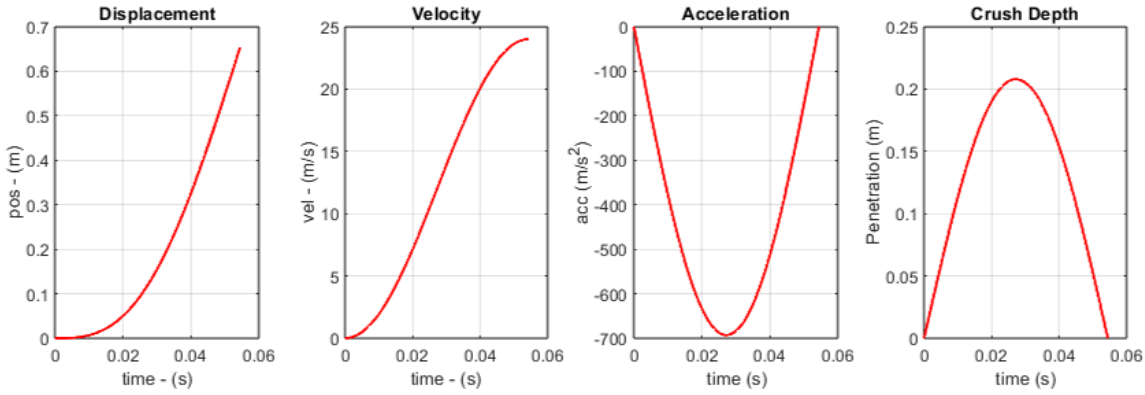

Figure 4.2: Analytical model estimates for a 15kN/m EAC with a 4.5kg mass at 12m/s

The results of the analytical model indicate that an energy-absorbing countermeasure with a stiffness of 15kN/m would require a minimum crush depth of 20cm to effectively halt a 4.5kg headform travelling at an impact velocity of 12m/s, with an estimated peak acceleration for this scenario being approximately 70G, as shown in Figure 4.2.

Following the fabrication of the physical headform (Section 4.3.1), which has a revised mass of 10kg, the analytical model was amended. It proposed that a crushable material thickness of at least 30cm would be necessary for conducting impact testing under comparable conditions.

This approach presumes a linear spring stiffness, thereby simplifying the material behaviour; however, it does not encompass non-linear stiffness characteristics at elevated strain levels or potential rotational effects during impact. Notwithstanding these limitations, the model provides a valuable initial approximation for ascertaining the theoretical stiffness and geometric requirements of energy-absorbing countermeasures.

4.2.2 Quai-static Compression Testing

To identify the suitable foam type for the proposed impact tests, three distinct commercial foam samples, sourced from [Foam2Home] were subjected to compression testing with an Instron 3366 (Figure 4.3). The foam types examined included firm foam (40 kg/m^3), a mixed firm foam with a memory foam topper (50 kg/m^3) and a mixed bound foam (35 kg/m^3) with a memory foam topper. Two samples of each foam type were tested to a maximum strain of 80% employing the full top surface area and two cylindrical indentors. The dimensions of the foam samples were 0.15x0.15x0.1m with the two cylindrical indentors possessing radii of 0.02m and 0.06m.

The resulting stress-strain curves from each compression test involving the bound-memory foam are presented in Figure 4.4 with the other foam types detailed in Appendix A. This foam exhibited the highest stress per unit strain, indicating that it possesses the greatest stiffness. Consequently, it emerges as the most suitable candidate for the intended testing purposes. Furthermore, these results also highlight the influence of impactor size on the corresponding stress-strain curves. Parts a-f of Figure 4.4 show that with smaller impactors, the top surface area is under additional forces such as tension and friction against the impactors' sides as the compression is not uniform.

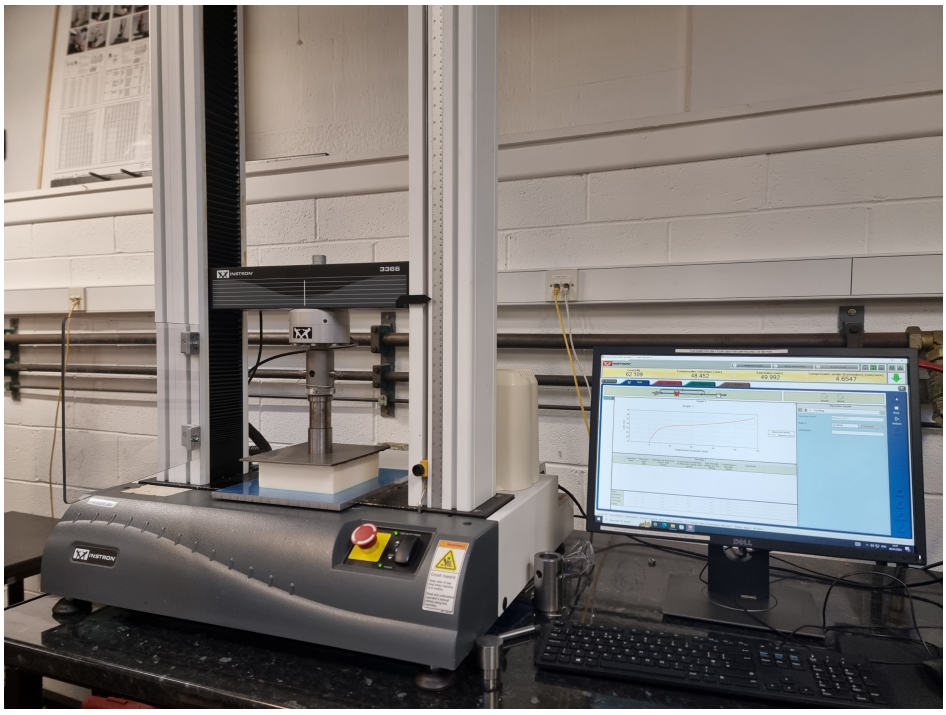

Figure 4.3: Instron 3366 compression test machine using Bluehill software package

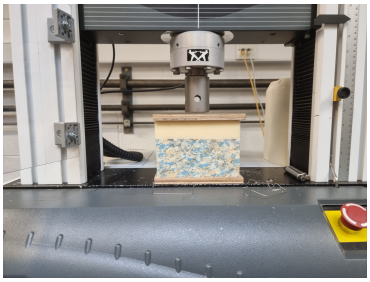

(a) Full Plate No Strain

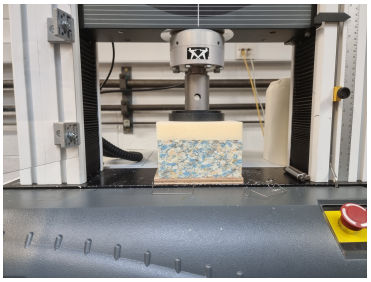

(b) Large Indentor No Strain

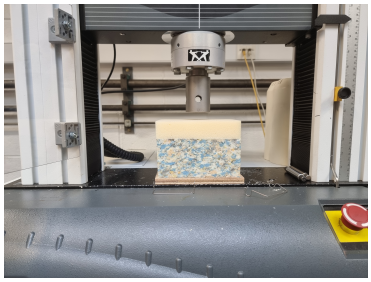

(c) Small Indentor No Strain

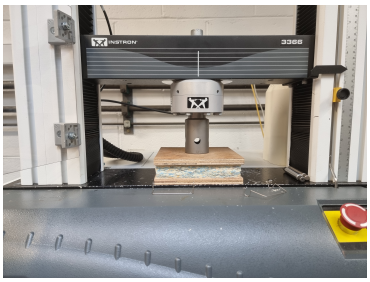

(d) Full Plate 80% Strain



(e) Large Indentor 80% Strain



(f) Small Indentor 80% Strain

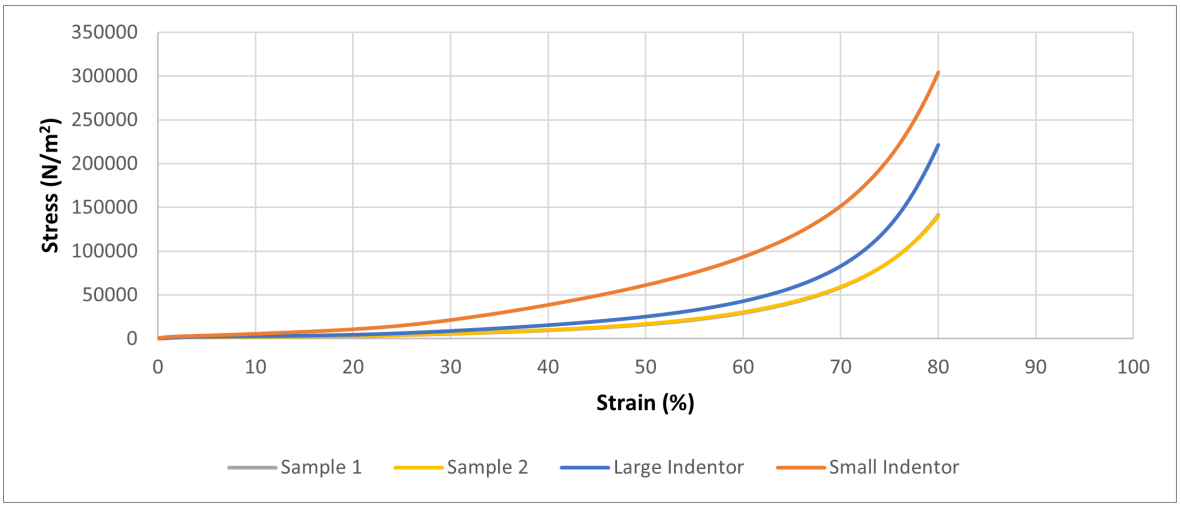

(g) Bound Foam with Memory Foam Topper Stress Strain Curves

Figure 4.4: Bound Foam with Memory Foam Topper

A force-penetration relationship for the full-scale test was estimated utilising the stress-strain curves presented in Figure 4.4 for a foam block measuring $0.5 \times 0.5 \times 0.3$m and a spherical indenter with a radius of 0.08m, selected to replicate the contact area of a headform ATD. The effective Young's modulus was calculated for specific regions of the stress-strain curves, corresponding to different levels of foam deformation. This analysis provides a stiffness corridor that accounts for variations in the foam's behaviour under different impactor conditions. The upper bound of the corridor reflects higher stiffness values associated with smaller impactor sizes, while the lower bound represents the reduced stiffness observed during full-surface-area compression.



(a) Instron 5589 quasi static compression test using full scale equipment

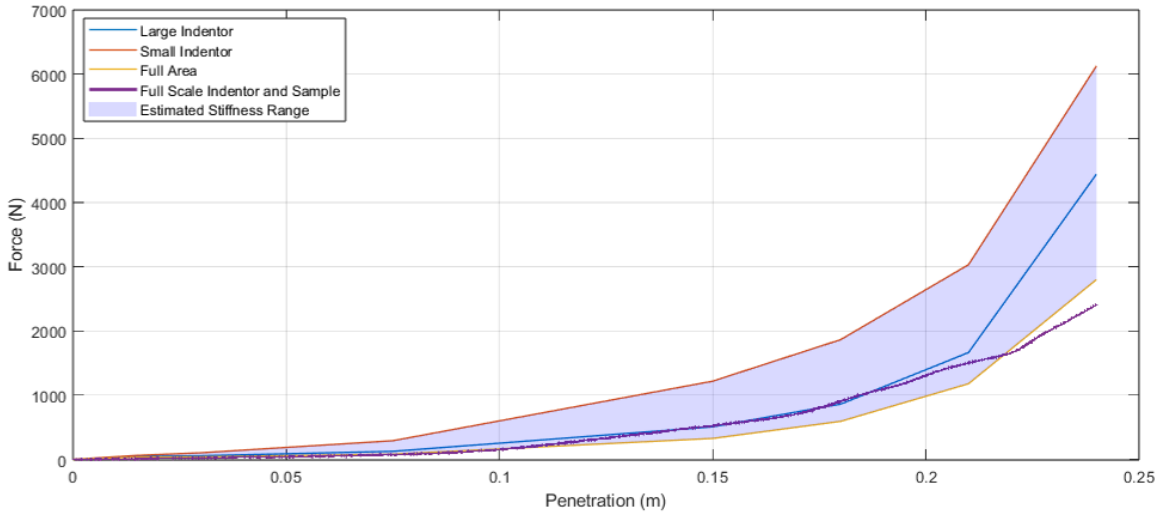

(b) Estimated stiffness corridor from small foam samples with full scale quasi static compression results

Figure 4.5: Full scale, quasi static compression test setup

Following the fabrication of the headform (Figure 4.7), an additional quasi-static test was conducted using an Instron 5589 compression testing machine. In this test, the headform was securely fixed to the Instron and employed as the indentor. The full 0.5x0.5x0.2m bound foam with a 0.5x0.5x0.1m memory foam topper was used (Figure 4.5(a)). The resulting force-displacement data from these tests fall within the calculated stiffness corridor up to 0.23m or 75% strain, thereby enhancing confidence in the force penetration calculation (Figure 4.5(b)). The strain rate was assessed in intervals of 50mm/min, ranging from 50mm/min to 250mm/min. No significant strain rate effects were noted at the quasi-static test velocity.

4.3 Full Testing Methodology

4.3.1 Acceleration

Headform

Typically, pedestrian headform ATDs can be bought from companies such as Cellbond or Humanetics, which specialise in crash testing equipment. Figure 4.6 shows a Humanetics adult pedestrian headform, characterised by an aluminium partial sphere encased in a flexible elastomer (PVC) skin. Provisions for accelerometer mountings are incorporated at the geometric centre of the sphere. The application of this headform is intended for impact testing against the hoods or windshields of vehicles to ascertain the associated HIC_{15} score. Despite their technical sophistication, the financial cost of most commercial ATDs exceeds $100,000, surpassing the budgetary constraints of this project.



Figure 4.6: Pedestrian headform ATD from Humanetics

An instrumented rigid headform with appropriate geometry was developed to support future multibody modelling initiatives. Fabricated in the workshop at Trinity College Dublin, the headform comprises a solid aluminium dome with a radius of 0.0825m and integrated accelerometer mounting points at its base. This dome is connected to a 0.32m long aluminium cylinder with a wall thickness of 0.02m (Figure 4.7). The cylinder serves two primary functions: it stabilises the headform during the acceleration phase with the assistance of small plastic fins, and it adjusts the centre of gravity towards the flat side of the dome, positioning it closer to the accelerometer mounting locations to ensure accurate measurements. The overall mass of the headform is 10kg, which has been incorporated into all post-processing calculations and the analytical model approach detailed in Section 4.2.1. This mass also enables the headform to effectively simulate impacts involving body regions with similar geometries, such as the shoulder.

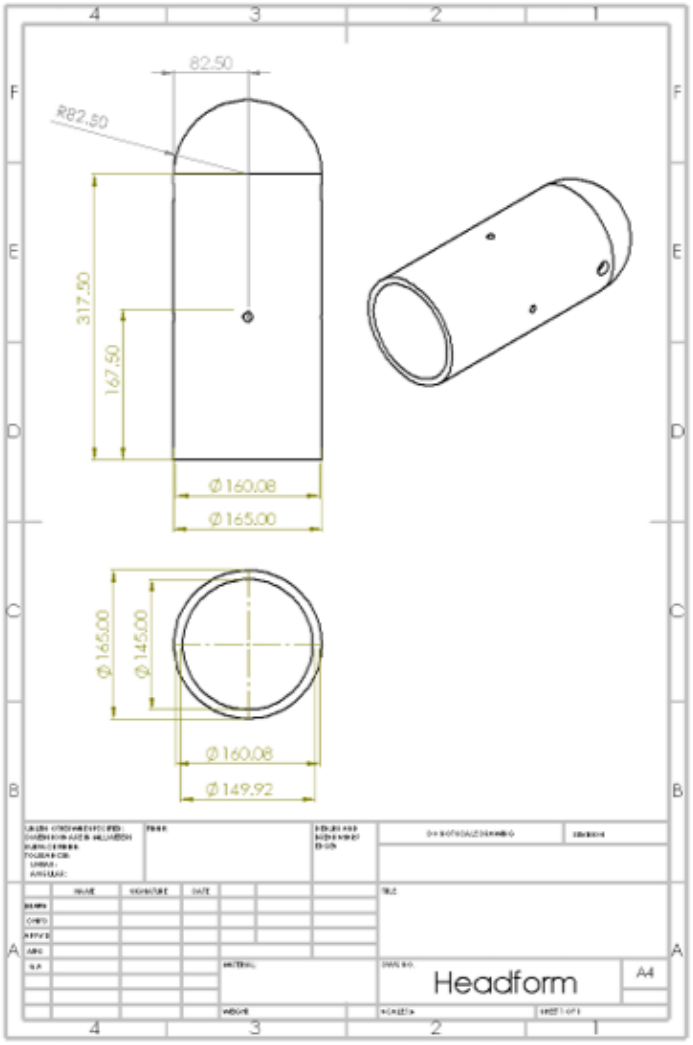

Figure 4.7: Pedestrian headform dimensioned drawings for fabrication at TCD

Dynatest 500 Impact System

To achieve the required headform velocities, a HYGE Dynatest 500 Component Crash Simulation System was used (Figure 4.8). This system utilises differential gas pressure acting upon two surfaces of a thrust piston within a sealed cylinder. The cylinder comprises a high (load) pressure side and a low (set) pressure side, which are separated by an orifice plate. The entire piston is subjected to dry nitrogen gas pressure in chamber A, whilst gas pressure is applied to a smaller area of the piston within chamber B (Figure 4.9). Upon activation of the system, the seal at the orifice opens, disrupting the equilibrium and exposing the piston area to the pressure, which results in a thrust on the piston. The comprehensive operational procedure is detailed in Appendix B.

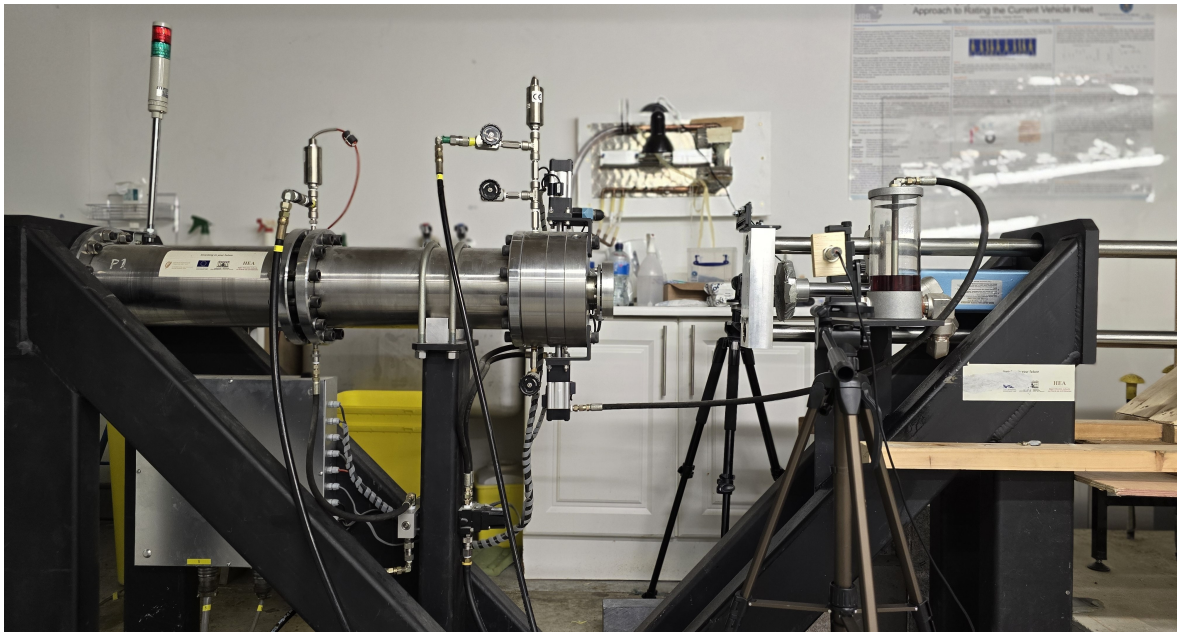

Figure 4.8: Dynatest 500 Impact System

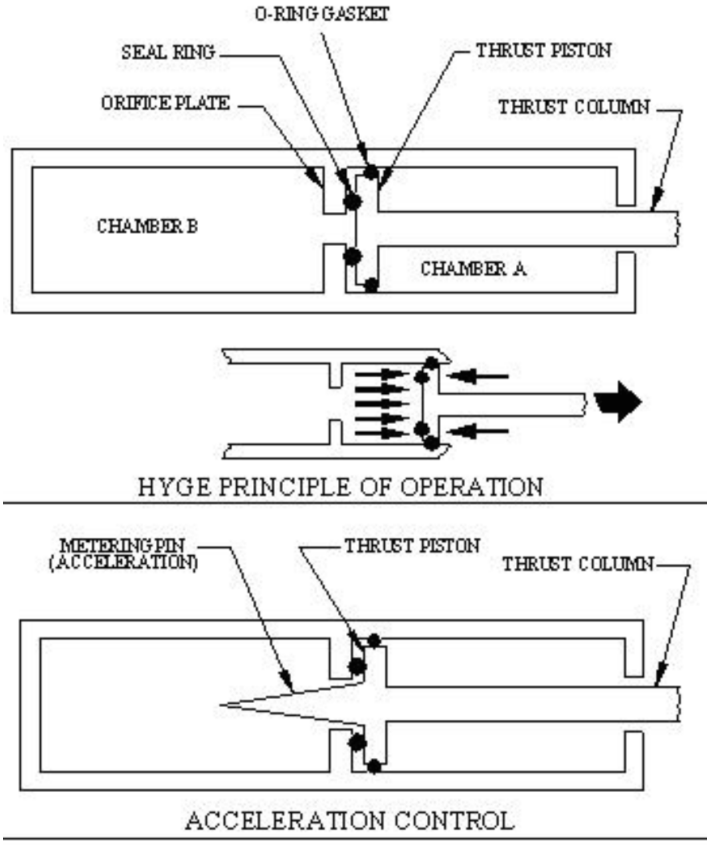

Figure 4.9: Dynatest 500 Impact System operating principles

Dynatest 500 Headform Mount

A 0.01m thick, 0.085m internal radius, 0.28m long aluminium cylinder was rigidly mounted to the Dynatest 500 to secure the headform during acceleration (Figure 4.10). The cylinder serves as a barrel, holding the headform in position while allowing its plastic fins to move freely through rectangular slits, restricting internal rotation. During testing, the mounting block and headform accelerate together as the Dynatest thrust piston is activated. Upon piston impact with the damping system, the mounting block decelerates rapidly, while the headform, unattached to the mount, exits the barrel at the target velocity due to inertia. A minimum impact velocity of 7m/s, calculated via projectile theory, ensures contact with the EAC before ground impact.

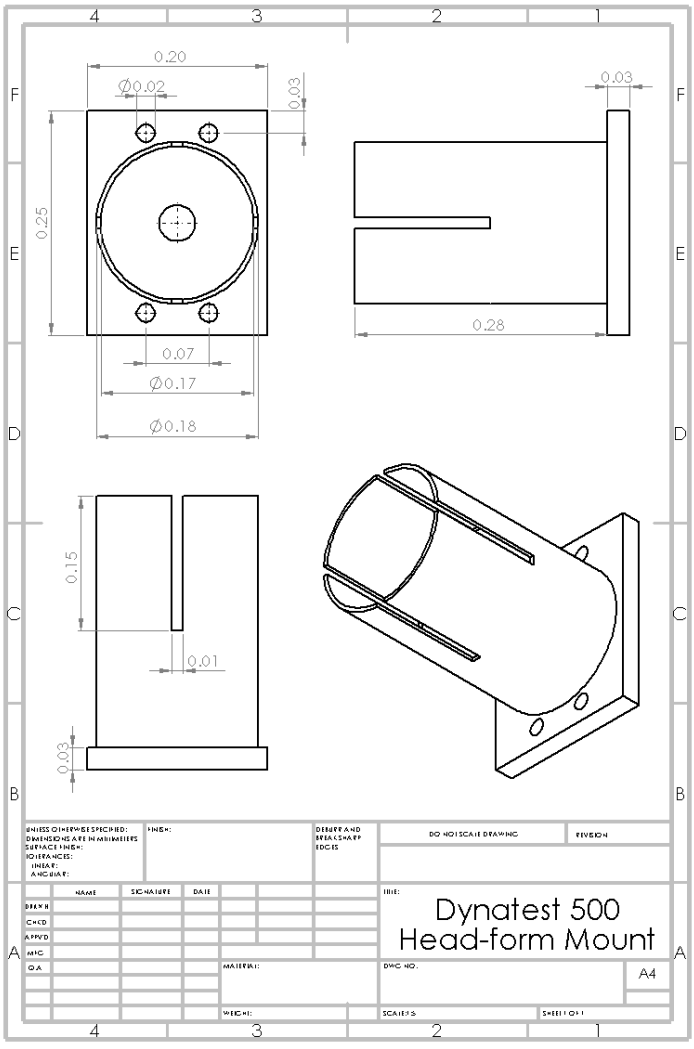

Figure 4.10: Dynatest 500 headform mount, dimensioned drawing for fabrication at TCD

4.3.2 Impact

As the aim of this study is to conduct a series of impact tests to derive force penetration relationships usable in multibody modelling software such as MADYMO, the mounting conditions of the impact surface must be considered. It is crucial that the block of foam remains securely fixed during the impact tests to ensure the accuracy of the force-penetration relationship. If the foam were allowed to move or slide backwards upon impact, it would absorb energy in a way not related to material deformation, but rather through the foam's displacement. This unintended movement would distort the measured force response, leading to inaccurate data on how the foam material behaves under impact.

To achieve this, the foam was placed within a four-sided aluminium enclosure with the front and top faces exposed. This enclosure was subsequently mounted to an existing crash barrier within the Biomechanics Impact Lab at Trinity Biomedical Science Institute (Figure 4.11). This crash barrier was securely bolted to a concrete runway using pre-existing 16mm threaded rods and two M12 rawl bolts for each rear support of the barrier. Considering the relatively low mass of the headform in comparison to the crash barrier, along with the bolted mounting points, this arrangement was deemed adequate to prevent any unintended movement during the impact phase. This was verified using high-speed video footage.

A total of six hard shells were created using 1mm aluminium and 3mm ABS (Figures 4.12 and 4.13). The material was ordered in large sheets and then bent into shape using rolling pins and a heat strip. The side panels of the mounting box are removed when using the hard shells to facilitate lateral flexion.

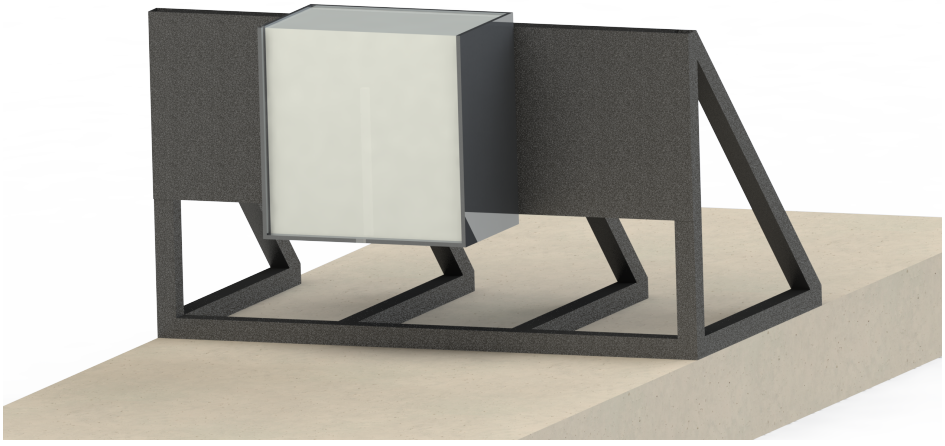

Figure 4.11: Solidworks render of foam EAC held within mount on crash barrier

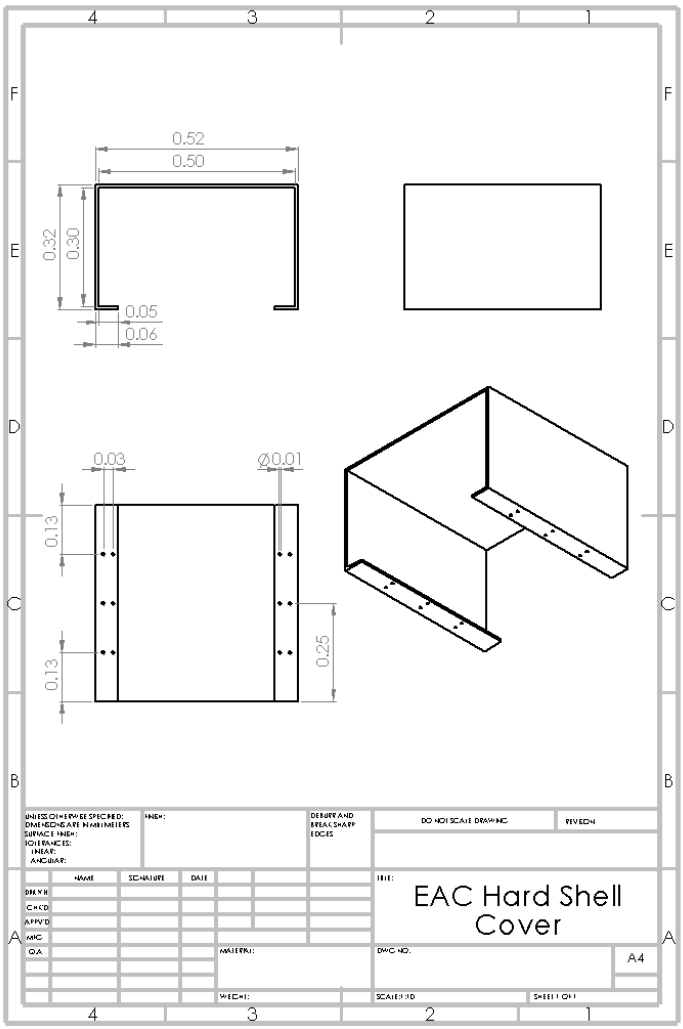

Figure 4.12: Solidworks part drawing for EAC hard shell covers

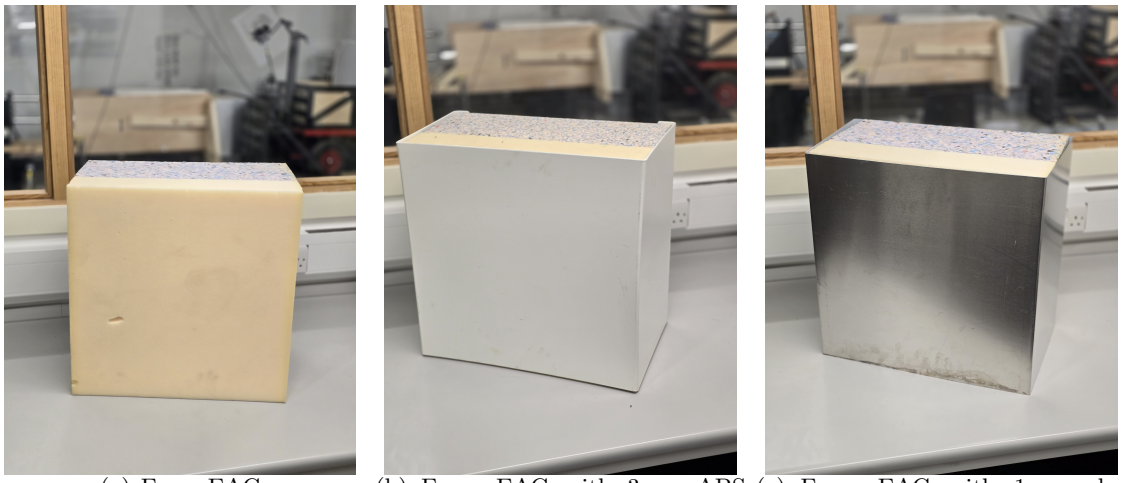

(a) Foam EAC (b) Foam EAC with 3mm ABS shell (c) Foam EAC with 1mm aluminium shell

Figure 4.13: All energy absorbing countermeasure surfaces

4.3.3 Containment

Numerous safety concerns must be addressed during high-velocity impact testing. Throughout each test, all personnel are evacuated from the laboratory and enter a separate viewing area. However, an additional structure is required to contain the headform after its rebound from the energy absorption chamber (EAC). It is likely that the hard shells may induce significant rebound velocities if they do not plastically deform. The containment unit, first designed in SolidWorks (Figures 4.14), was constructed in situ with 1/2 inch plywood sheets and timber (Figure 4.15). Additional foam padding was incorporated at the base of the containment unit to safely capture the headform and mitigate the risk of equipment damage.

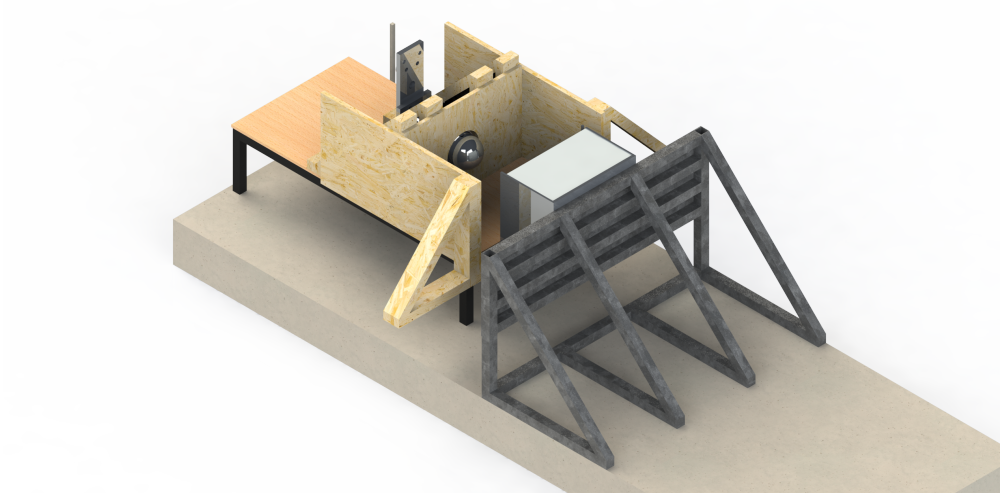

Figure 4.14: Solidworks render of containment unit

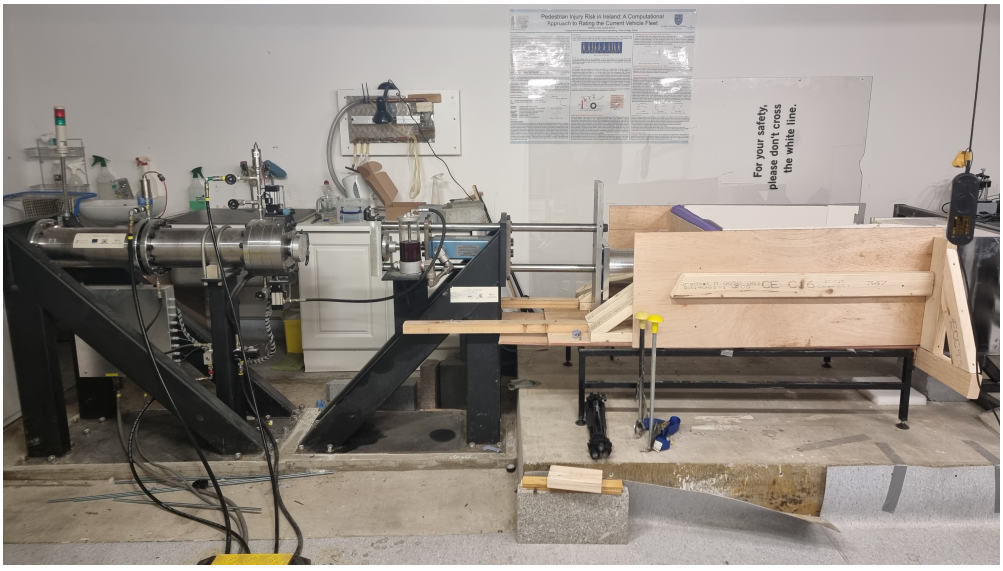

Figure 4.15: Completed containment unit

4.3.4 Instrumentation

Figure 4.16 outlines the basic instrumentation schematic for the headform impact tests. A Fastec 5G high-speed camera is mounted from the ceiling, facing the top surface of the energy-absorbing countermeasure. The camera's frame rate is set at 2500 fps, with the foam illuminated by two spotlights. A MEMS piezoresistive PCB 726ch accelerometer is positioned inside the headform, with its sensitive axis oriented in the direction of motion. The accelerometer's sample rate is regulated by the 24-bit ADC PCB9234 data acquisition device. The sample rate used in this study is 51.2kHz. The accelerometer is powered by a battery pack housed within a Faraday cage, as the PCB9234 does not provide excitation voltage to piezoresistive accelerometers. Both the camera and accelerometer are activated via an RS PRO Retroreflective Photoelectric Sensor, positioned as close as possible to the headform within the Dynatest mount. This arrangement ensures a synchronous start time for both the accelerometer and video footage for each test. The software utilised in this study comprises LABVIEW, Matlab, and MADYMO.

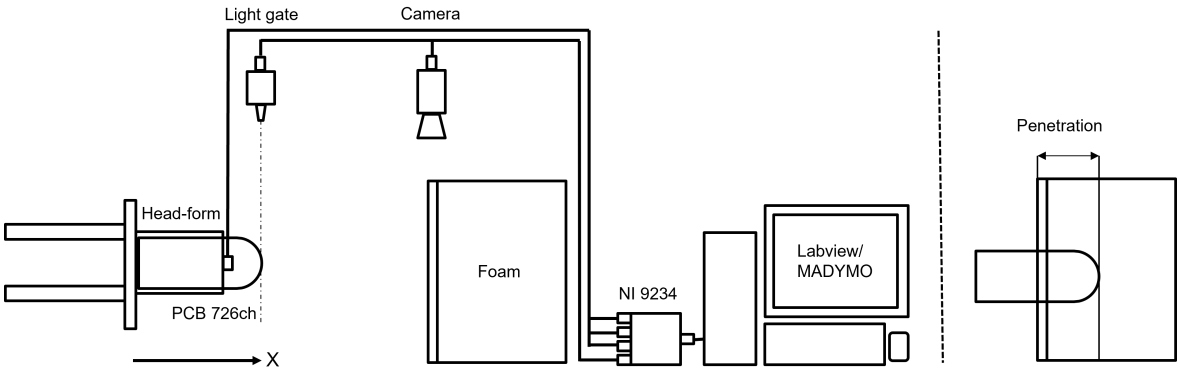

Figure 4.16: Instrumentation schematic for headform impact tests

4.3.5 Test Matrix

This study presents nine impact tests, encompassing three velocities for each countermeasure type: foam, 3mm ABS, and 1mm aluminium (Table 4.1). The impact velocities were determined using high-speed video footage from the Fastec Hi-Spec camera, which operated at 2500fps. Markers positioned at 0.1m intervals along the trajectory of the headform enabled precise measurements of velocity (Figure 4.18). The time required for the headform to traverse each interval was converted into seconds, and the average velocity across the

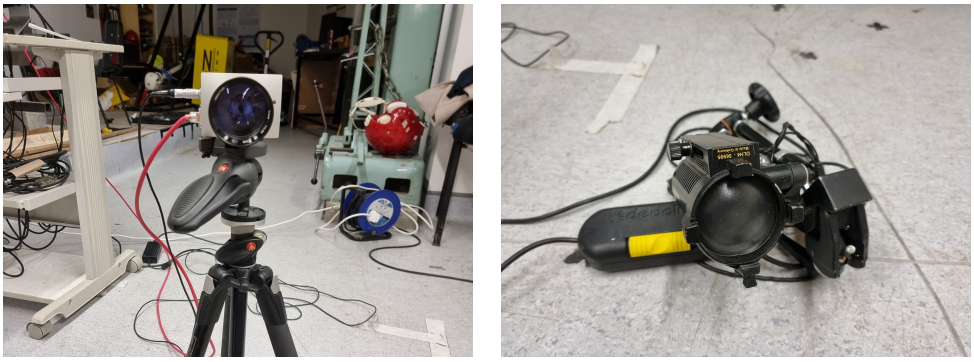

(a) Fastec Hi-spec 5G camera (b) High intensity spotlight

Figure 4.17: Recording apparatus used for impact testing

0.1m intervals was used as the impact velocity. The total travel distance before reaching the energy-absorbing countermeasure (EAC) was 0.9m.

For elevated velocities, the Dynatest 500 launcher was calibrated to a maximum pressure of 220PSIG, resulting in an impact velocity of 11.4m/s, which is within 0.5m/s of the prevalent collision speed indicated in the 2019 epidemiological data (Chapter 3, [Hall et al., 2023]). Three foam blocks were available for use. For each test, a different foam block was used, ensuring that each block had time to recover between impacts. Hard shells were replaced after each test due to damage caused by the tests' destructive nature.

Table 4.1: Impact Test Matrix

Foam EAC	**3mm ABS Shell**	**1mm Aluminium Shell**
7.32m/s	7.86m/s	7.45m/s
9.85m/s	10.01m/s	9.85m/s
11.36m/s	11.47m/s	11.22m/s



Figure 4.18: Positions of markers used for impact velocity calculations

4.4 Post Processing

A total duration of 1 second of accelerometer and video data was recorded for each test. The acceleration time history during impact with the EAC is determined through visual inspection of both the raw accelerometer data and video footage. This data is subsequently processed using a Butterworth low-pass filter with a cutoff frequency of 150Hz (Figure 4.19(a)). Considering the duration of the acceleration pulse and the rigid construction of the headform, the dominant frequencies of interest are situated well below 150Hz.

The calibration certificate provided with the accelerometer gives a sensitivity of 0.03833mV per m/s^2 for a 10V excitation voltage. Using this value the resulting acceleration time history for the impact phase can be found. By applying the fundamental principles of calculus and kinematics, the area beneath the acceleration time curve signifies the change in velocity over the specified time interval. Thus, the point of zero velocity, and consequently maximum penetration, can be determined through integration. The acceleration curve up to this point represents the loading phase (Figure 4.19(b)). For all tests, the timing of the loading phase, obtained from video footage, closely corresponded with the timings recorded by the accelerometer.

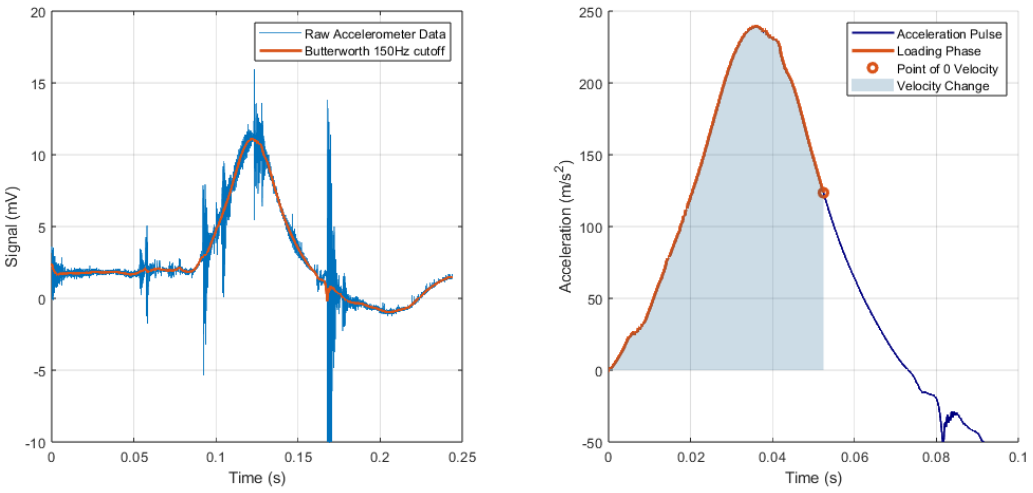

(a) Raw and filtered accelerometer data

(b) Acceleration loading curve

Figure 4.19: Accelerometer data processing

4.5 Results

4.5.1 Impact Test Results

Figure 4.20 illustrates the acceleration-time histories for all test conditions outlined in Table 4.1. Notably, the foam EAC exhibited the most prolonged pulse duration across all test velocities in comparison to the covered EAC configurations. At lower velocities (below 10m/s), the foam EAC generated peak accelerations of approximately 24G, whereas both covered EACs achieved marginally higher peaks, near 27G (Figure 4.20(a)). Interestingly, as the impact velocity increases, the relative differences in peak acceleration between the EAC types shift. At 11.5m/s, the foam EAC produced a larger peak acceleration (53G) compared to both the aluminium and ABS variants (48G), thereby reversing the trend previously observed at lower velocities.

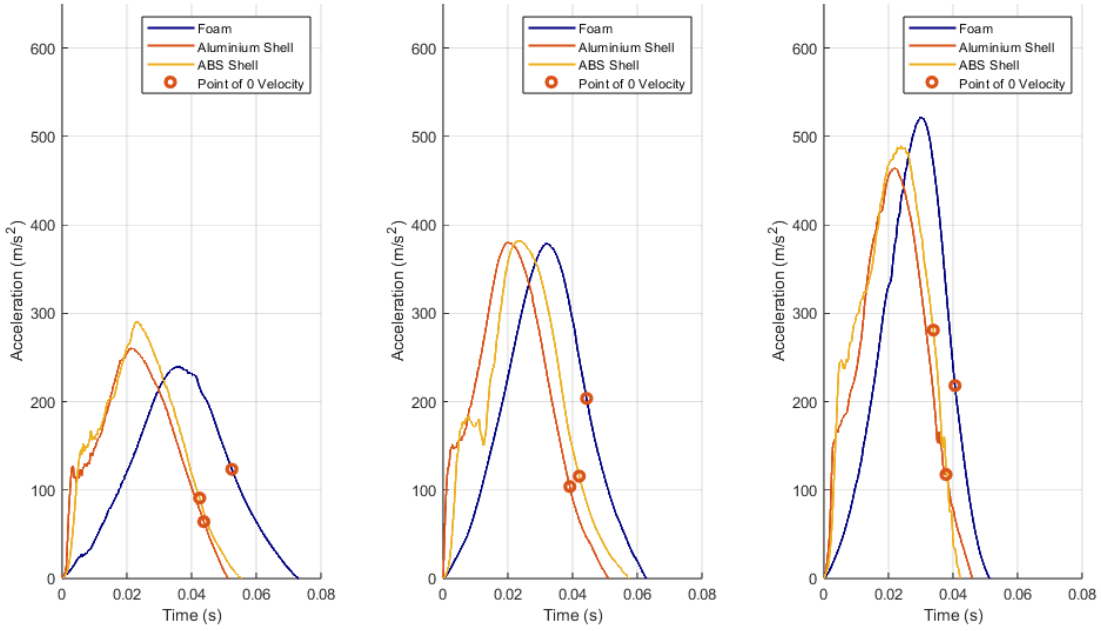

(a) Impact velocity 7.5m/s (b) Impact velocity 10m/s (c) Impact velocity 11.5m/s

Figure 4.20: Acceleration data for each test condition

To track the penetration of the headform into the EAC, high-speed video footage was analyzed frame-by-frame. A specific point on the headform was manually tracked in MATLAB by selecting its position in each video frame. These pixel coordinates were then converted into physical distances by utilising known distances and addressing parallax effects based on the cameras' position relative to the headform's motion. The red points in Figure 4.21

display the total position change of the tracking point throughout the headform's penetration during impact at 11m/s into the aluminium-covered EAC. The pixel distance between each of these red points is used to determine the position time history. Figure 4.22 presents the total measured penetration during the loading phase under all test conditions.



Figure 4.21: Position of tracking points throughout the loading phase shown as red circles

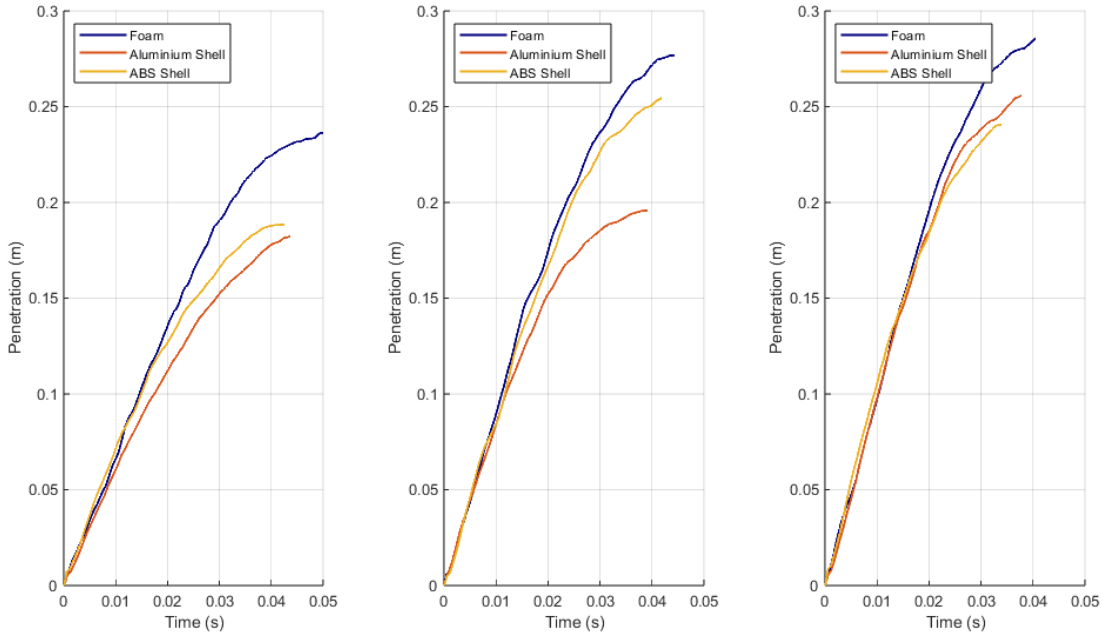

(a) Impact velocity 7.5m/s (b) Impact velocity 10m/s (c) Impact velocity 11.5m/s

Figure 4.22: Penetration time histories during the impact loading phase

4.5.2 Force Penetration Characteristics

The acceleration time histories (Figure 4.20) were combined with the mass of the headform and the penetration data captured from the high-speed camera footage (Figure 4.22) to derive the force-penetration relationships illustrated in Figure 4.23. For all impact velocities, the covered EACs exhibit an intially high-stiffness region at low penetration, followed by a reduction in stiffness at roughly 0.05m of penetration. This is most evident in Figure 4.23(b), after which another high-stiffness region is observed. In contrast, the foam EAC demonstrates a more linear response, with lower overall contact stiffness in comparison to the covered EACs.

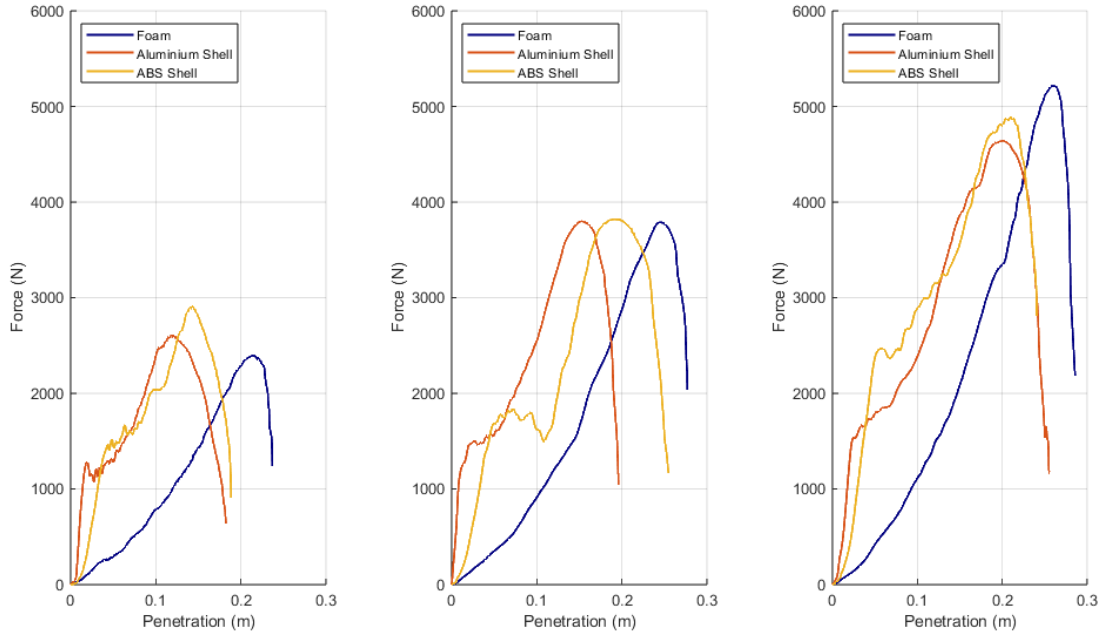

(a) Impact velocity 7.5m/s (b) Impact velocity 10m/s (c) Impact velocity 11.5m/s

Figure 4.23: Derived force penetration relationship for each test condition

4.5.3 Viscoelastic Behaviour

The peak forces illustrated in Figures 4.23 do not signify the conclusion of the loading phase, as penetration persists beyond these peaks. This leads to a drop in stiffness and a reduction in elastic force as the loading phase progresses. The behaviour observed implies the presence of viscoelastic properties, particularly as the velocity of the headform approaches zero. Figure 4.24 presents the headform linear velocity throughout the force penetration curves for the three foam EAC collisions.

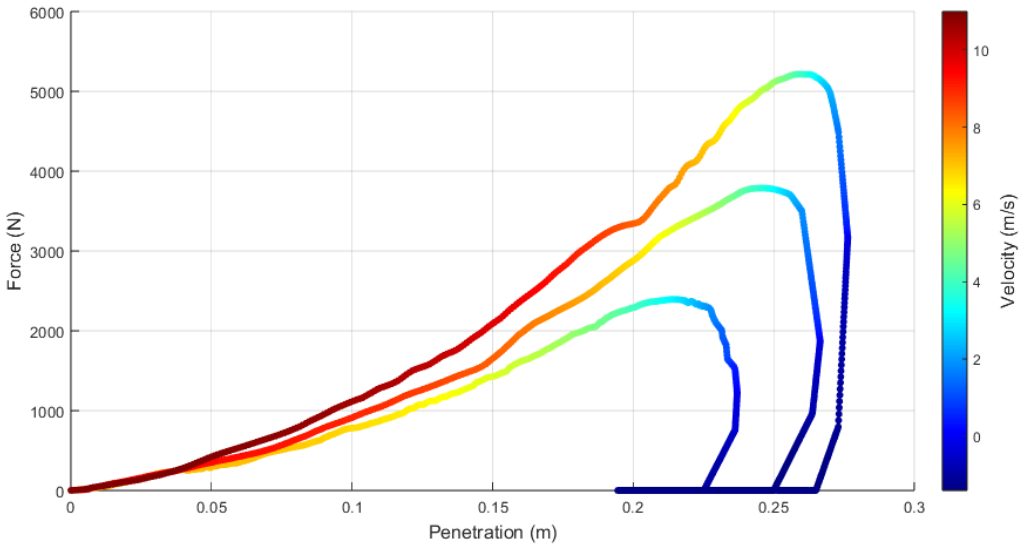

Figure 4.24: Headform linear velocities for foam EAC force penetration curves [Impact Velocities, bottom to top 7.5-10-11,5m/s]

Figure 4.25(a) presents the force-penetration relationships obtained from both dynamic and static foam EAC tests using the same full scale indentor and foam block. The Instron compression velocity of 0.0008m/s is considered representative of static conditions. Stiffness values were calculated for each of the identified stiffness regions and are depicted in Figure 4.25(b). The comparison highlights that viscoelastic behavior is apparent only under dynamic testing conditions, becoming evident as the headform decelerates to zero velocity.

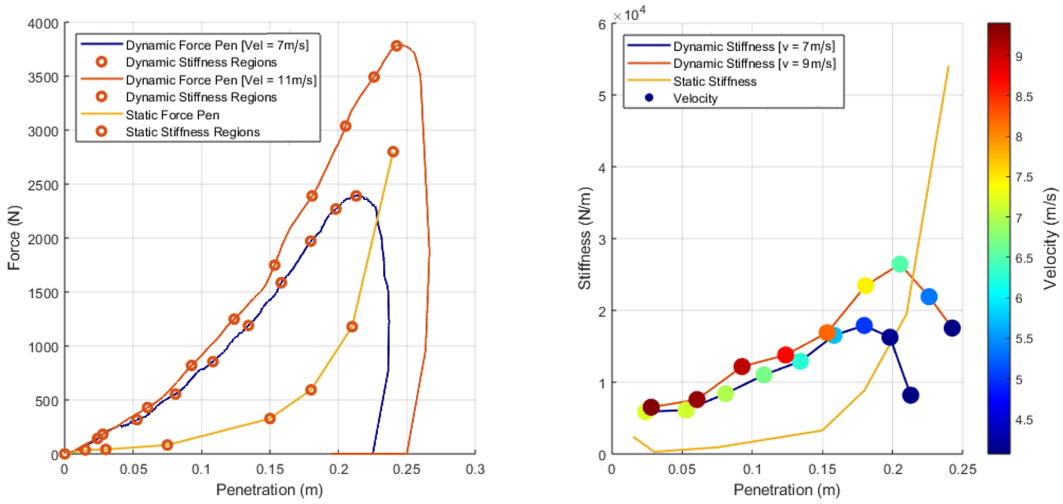

(a) Static vs dynamic force penetration relationships

(b) Effect of linear velocity on contact stiffness

Figure 4.25: Viscoelastic behaviour observed for dynamic tests only

4.5.4 MADYMO Reconstruction

The experimental impact environment was reconstructed in MADYMO using two rigid bodies, each with an ellipsoid: one representing the EAC and the other representing the headform. The EAC was fixed in place, while the headform was assigned initial velocities as specified in Table 4.1. The mass, geometry, and centre of gravity of the physical headform were used. Each force-penetration relationship was paired with its corresponding impact velocity. No friction or damping coefficients were applied in the simulation, and neither were the foam's inertial values, as the effects of these factors were accounted for in the derived force-penetration characteristics. Unloading curves and hysteresis slopes were manually determined through trial simulations. The results of the simulation are presented in Figure 4.26 with dashed lines alongside the physical experimental acceleration data. While both hysteresis and the unloading curve had minimal impact on the overall acceleration profile, hysteresis had a slightly greater effect. However, both variables only influenced the final 15% of the curve.

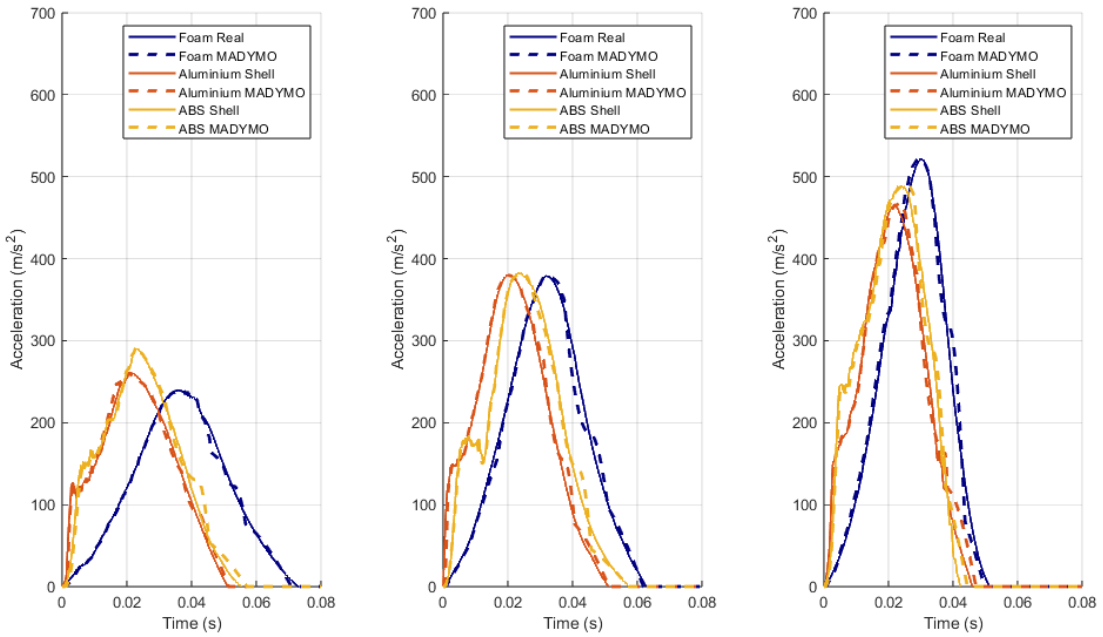

(a) Impact velocity 7.5m/s (b) Impact velocity 10m/s (c) Impact velocity 11.5m/s

Figure 4.26: Real (solid) and simulated (dashed) acceleration time histories

4.6 Discussion

The data presented in Figures 4.20(a) and 4.20(b) demonstrate that the foam EAC exhibits a lower amplitude but a longer-duration acceleration pulse compared to the covered EAC. The peak acceleration of all EACs increases with the impact velocity, however, the rate of increase is most pronounced in the foam EAC. Notably, at an impact velocity of 11m/s, the foam EAC achieves a peak acceleration that exceeds that of the covered variants. This may be attributed to the increasing stiffness of the foam in regions experiencing higher deformation as well as the faster initial deceleration caused by the shells.

During the quasi-static testing, as depicted in Figure 4.4(g), there is a notable rise in stress beyond 60% strain. However, these tests are conducted at a constant low velocity, which does not give rise to the viscoelastic effects observed in the dynamic tests. As the headform penetrates into the foam, air is expelled through the open cell pores within the foam block. The rate at which the air is expelled from the foam would likely alter the contact stiffness. Figure 4.25 shows how the contact stiffness changes with both penetration and velocity. This effect may explain why, for the 10m/s tests, both the aluminium and ABS shells experience similar acceleration pulses (Figure 4.20(b)) despite differences in the penetration time history (Figure 4.22(b)). The total penetration of the headform into the foam EAC during this test reached 0.27m, equivalent to 90% of the total length, positioning it within a higher stress region relative to total strain. However, in contrast, the velocity of the headform within this region is very small and decelerating towards zero. This placed the headform in a lower stiffness region. Both the aluminium and ABS shell EACs demonstrate an initially higher stiffness compared to the foam EAC, but a lower penetration. This reduced penetration into the foam effectively limits exposure to the foam's higher stiffness region, thereby providing a protective advantage at higher impact velocities. For lower impact velocities where both the penetration into the foam and velocity are low, the initial stiffness of shells creates a higher peak acceleration.

Figure 4.26 demonstrates that the MADYMO model accurately replicates the acceleration-time history during both the impact loading and unloading phases, using the derived contact characteristics. The loading curve was derived based on the velocity change matching the initial impact velocity, determined via integration. However, due to the strong velocity dependency of the contact stiffness, the simulations are limited to this specific impact speed. Using these contact characteristics to simulate higher impact velocities would result in an

insufficient velocity change, causing the simulated headform to decelerate but fail to stop, potentially passing completely through the foam.

4.6.1 Limitations

There are several limitations to this study which must be considered. Significant time was spent repairing and refurbishing the Dynatest 500 impact ram to the point at which it was suitable for this project. To reduce the risk of damage to the solenoid valves used in the Dynatest, the maximum set pressure was set to 220PSIG. This limits the impact velocity to 11.5m/s. While this is close to the most common subway-to-pedestrian impact velocity (Figure 3.6), under ideal conditions, the full range of subway-to-pedestrian impact velocities would be tested. This would increase future modelling capabilities as currently, only the tested velocities can be simulated due to the strong viscoelastic effects. Averaging the calculated force-penetration curves is not a viable approach in this case, as the countermeasure's total depth is fixed. If the total force is insufficient to stop the headform's linear displacement before reaching maximum penetration, the simulation will result in the headform passing through the foam block.

Another limitation of this study is the use of a single-axis accelerometer. Due to hardware constraints with the data acquisition system, only one accelerometer was employed. While high-speed video footage confirmed minimal rotation during the loading phase, rotational effects were observed late into the unloading phase. A DEWE-43-A data acquisition system was available for use for a limited time at the tail end of this project. During this time, an additional impact test was conducted with two single-axis accelerometers facing in the X and Z directions. The results from this test show only a slight increase to the overall acceleration profile due to z direction (downwards) acceleration (Appendix D Figure D.1). Despite this, incorporating multi-axis sensors in future experiments could enhance the precision of data used for model validation.

Notwithstanding these limitations, this study designed, manufactured, and conducted a series of impact tests which informed a multibody model regarding the effects of hard shell coverings on energy-absorbing materials across a range of impact velocities.

4.7 Conclusions

This study highlights the velocity-dependent influence of hard shells on the acceleration pulse of foam-based EACs. At lower velocities (below 10m/s), 1mm aluminum and 3mm ABS shells produced shorter-duration, higher-peak acceleration pulses than pure foam EACs. At higher velocities, however, peak accelerations in hard-shelled EACs were similar to or lower than those of pure foam EACs. This shift reflects the shells' ability to limit foam penetration, balancing the foam's velocity-dependent stiffness increase with the shells' higher initial stiffness. Optimizing hard-shell designs for lower impact velocities could enhance their effectiveness as safety countermeasures.

The multibody software package MADYMO successfully reproduced the experimental acceleration time histories by using the derived force-penetration relationships. For subway-pedestrian impacts, an EAC wrapped in a thin, hard shell could offer increased protection for impacts occurring at velocities above 10m/s. Chapter 3 indicates that in 2019, 73% of recorded NYC subway-pedestrian fatalities with velocity data involved impact speeds over 10m/s. Further modeling efforts using the contact characteristics derived in this study could provide valuable insights into the overall safety effects of implementing EACs on the front of subway trains.

Chapter 5

Baseline Multibody Model of Subway-to-Pedestrian Collisions: Effect of Impact Velocity and Drainage trough Depth on Injury Risk

The results from this study are published in the Journal of Applied Sciences

doi.org/10.3390/app142210738

5.1 Introduction

The high number of pedestrian deaths worldwide is a well-documented problem, with the World Health Organisation (WHO) reporting 280,000 pedestrian fatalities in 2022 [WHO, 2022]. Extensive research has been conducted to improve pedestrian road vehicle safety (e.g. [Kerrigan et al., 2007b, Martin, 2006, Shang et al., 2021, Tiwari, 2020]). However, much less attention has been given to pedestrian incidents involving subway trains, despite deaths per 1,000,000 train miles increasing from 1.1 to 2.1 in the United States from 2013 to 2023 [FRA, 2022]. Existing subway crashworthiness research has focused on occupant protection (e.g. Han and Koo [2003], Li et al. [2016], Peng et al. [2017], Xu et al. [2019], Xue et al. [2007]) for subway vehicles and does not address subway-to-pedestrian collisions. There is thus a lack of published literature regarding this form of rail incident.

Major advancements in automotive safety have been driven by a combination of accident data analysis, physical testing, computational modelling, and accident reconstruction. A significant challenge in replicating this approach for subway safety is the cost of physical impact tests. Automotive pedestrian ground contact typically involves interaction with a flat surface (e.g Shi et al. [2018b], Yin et al. [2017]. Recent street level tram-pedestrian collision studies utilise flat surfaces for secondary impact [Tomsovsky et al., 2022], or focus only on primary contact injuries [Chevalier et al., 2019]. In contrast, secondary contact for subway-pedestrian collisions involves a more complex geometry with different track types. These tracks introduce new dangers such as live electrically charged running rails (third rail), sharp corners and drainage troughs, which may affect kinematics and run-over risk.

Chapter 3 shows a substantial number of cases with incapacitating injuries including amputation, likely resulting from wheel contact. While empirical evidence suggests that drainage troughs may act as a viable countermeasure in reducing fatality rates, these studies have been purely epidemiological (Chapter 2). There have been no proposed baseline models of subway-pedestrian interactions, and there is no biomechanical analysis on the effect of drainage troughs on these events. Therefore, due to confounding factors such as variations in vehicle impact velocities and train geometries, the results of the studies mentioned in Chapter 2 were unable to attribute the reduction in fatality rates to drainage troughs [Barker et al., 2017].

While infrastructure such as Platform Screen Doors (PSD) have been installed in modern subway systems, only 8.5% of NYC Subway platforms were deemed feasible for this approach

as of 2020, with this number increasing to a maximum of 27% by 2033 [Metropolitan Transportation Authority Track Trespassing Task Force, 2020]. This warrants continued research into subway pedestrian safety. In particular, further research is needed to better quantify the effect of drainage troughs on pedestrian safety. Of particular interest is the required drainage trough depth to prevent wheel-pedestrian and third rail (high voltage) contact risk and the potential effect on secondary head impact injury.

The aim of this chapter is therefore to use the multibody modelling software MADYMO to create a New York City (NYC) subway-pedestrian model. The purpose of the model is to provide biomechanical insights into:

- The effect of impact velocity on train to pedestrian run-over risk.
- The effect of drainage trough depth on third rail contact and run-over probability as well as the minimum trough depth needed to avoid wheel or undercarriage contact.
- The effect of impact velocity on both primary and secondary contact head injury risk.

5.2 Methodology

Multibody modelling and injury weighting methods were used to create the baseline model and assess the effects of speed, third rail and drainage troughs on injury outcome. Accordingly, the methodology addresses the following

- Multibody Train and Station Environments (2 track types)
- Adapted Multibody Pedestrian Model (AM50)
- Pedestrian Posture and Train Speed
- Simulation Test Sample (STS) with Injury Criteria, Contact Scores and Weighted Scoring
- Sensitivity Study

5.2.1 Multibody Train Model and Impact Velocity

According to Chapter 3, the R160 train has the largest fleet within the NYC Subway system (1600 trains) and is associated with the highest number of fatal subway-pedestrian interactions for the NYC Subway in 2019. The multibody R160 train front was created in MADYMO using thirteen cylinders and fourteen ellipsoids based on dimensions supplied by the Federal Transit Administration (Figure 5.1). The train front was split into eight separate

groups for contacts (front panels, door, window, anti-climber, coupler, wheels, truck, and under-carriage). As the train front is significantly stiffer than the human model, the contact characteristics used were those of the MADYMO pedestrian model; i.e. the train was treated as completely rigid.

The most common estimated subway-pedestrian impact velocity is 11-13m/s, but low impact velocity may also be fatal due to the stiffness of the train front and the possibility of wheel or third rail contact. The impact velocities used in this study therefore range from 2-16m/s in 2m/s increments. Based on the available NYC event recorder data from Chapter 3, the R160 train's emergency braking was modelled as a linear deceleration of 1.43m/s^2.

The geometry of the NYC Subway track bed varies across stations, but two representative track types were selected for modelling. The first features a flat track bed without crossties (Figure 5.2), while the second includes a 0.25m drainage trough with crossties (Figure 5.3). Multibody models of each track type were created using cylinders and a ground plane, extending 60m to capture secondary impacts and possible roll-over events. Each track setup was modelled to resemble a station environment, as most impacts occur within 60m of a station (Chapter 3). The ground plane's vertical position was adjusted to represent drainage trough depth for each track type.

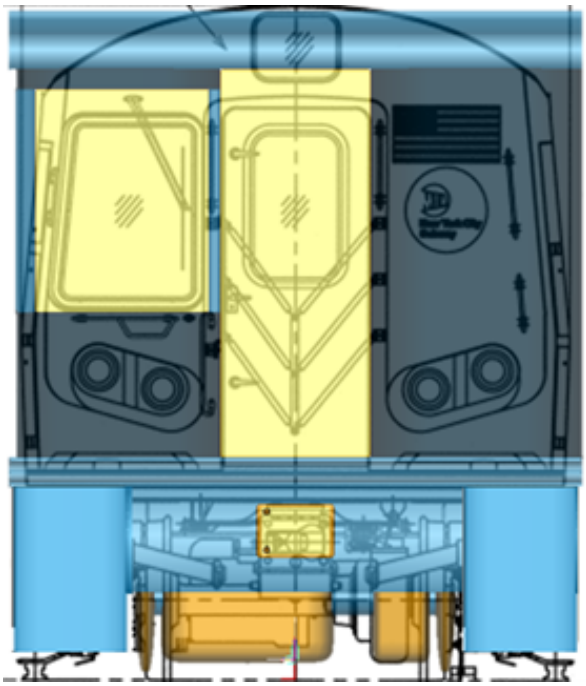

Figure 5.1: MADYMO Multibody Model of an R160 Subway Train

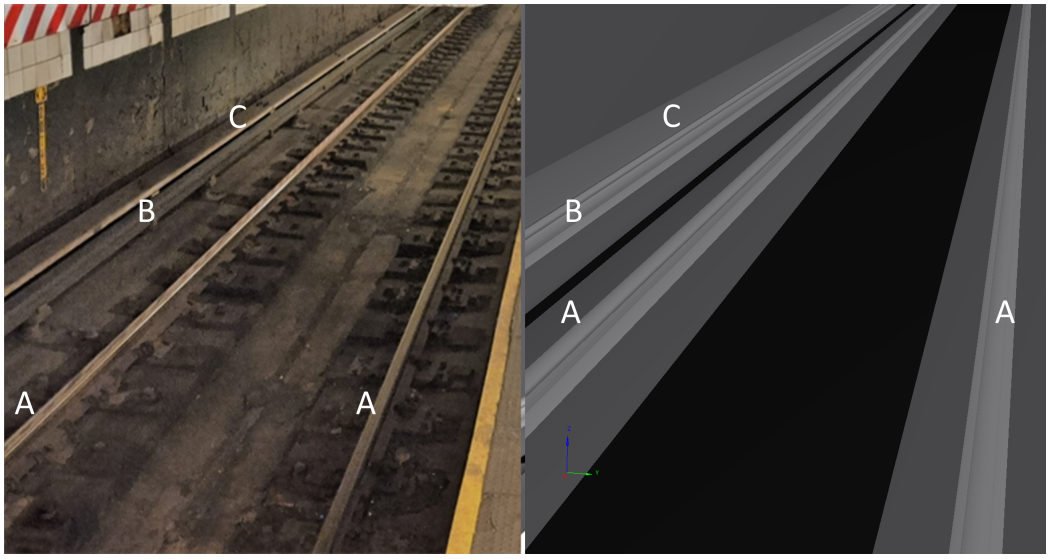

Figure 5.2: NYC flat track bed with no crossties & multibody model (Images taken by author)
A – Running Rail B – Third Rail (Live) C – Third Rail Guard

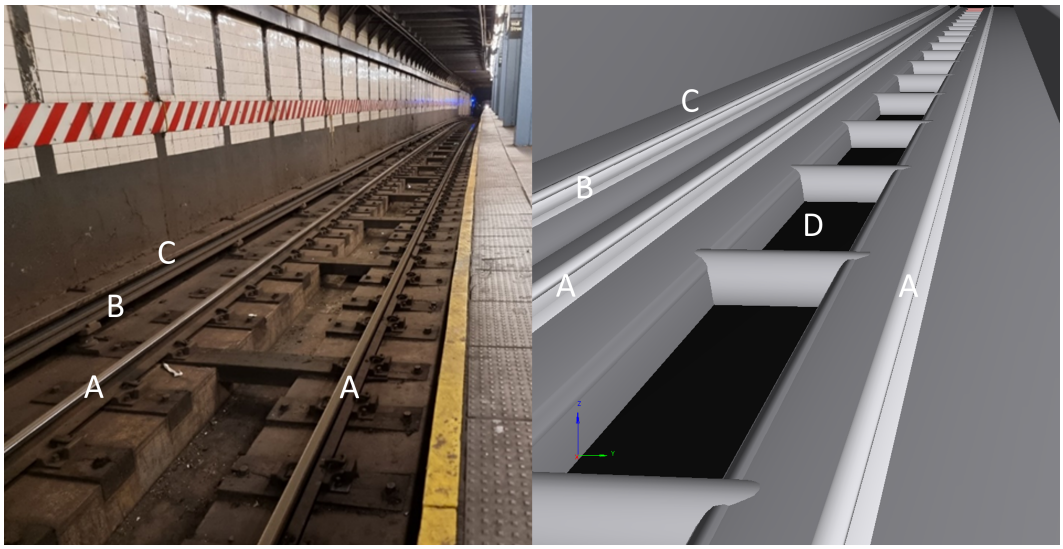

Figure 5.3: NYC track bed with drainage trough and crossties & multibody model (Images taken by author)
A – Running Rail B – Third Rail (Live) C – Third Rail Guard D – Drainage Trough (Suicide pit) D – Crossties

5.2.2 Adapted MADYMO Human Pedestrian Model

Based on the average age and sex distribution for 941 fatal NYC Subway human collisions (Table 2), the MADYMO Adult Male 50th Percentile (AM50) ellipsoid model was chosen. This model has been used extensively; for example, to assess the influence of impact velocity and pedestrian posture during vehicle contact [Elliott et al., 2012].

Table 5.1: Age and Sex percentage for NYC Subway fatalities [Gershon et al., 2008b] [Lin and Gill, 2009] [Hall et al., 2023]

	1990-2003 N(%)	**2003-2007 N(%)**	**2019 N(%)**
Male Female	561 (84%) 107 (16%)	156 (83%) 41 (17%)	63 (83%) 13 (17%)
Mean Age	35-44	44	39

The MADYMO AM50 model makes use of frangible joints in the legs to account for fracture. By default, these joints remain locked until a fracture threshold is met, following which the connected segments are free to rotate relative to each other. Minor damping forces are used to prevent numerical instabilities (e.g. gimbal lock). However, preliminary analysis showed that, due to the high impact force and complex positioning used in this study, this damping force was insufficient. Given the high likelihood of amputation, limb fracture was not the focus of this study. Thus, these joints remained locked to allow simulations to run to completion and focus on head injuries. A sensitivity study was conducted to assess the effect of this on the overall findings.

To address the limited head contact data available for model validation, the default MADYMO AM50's head contact characteristics were altered to reflect those calculated based on the ground contact for 6 published PMHS tests [Shi et al., 2018b]. The MADYMO AM50 and calculated linear head stiffness can be seen in Figure 5.4. Initially, the linear model outputs a higher force per unit of penetration compared to the MADYMO model up to 0.003m; thereafter, this is reversed.

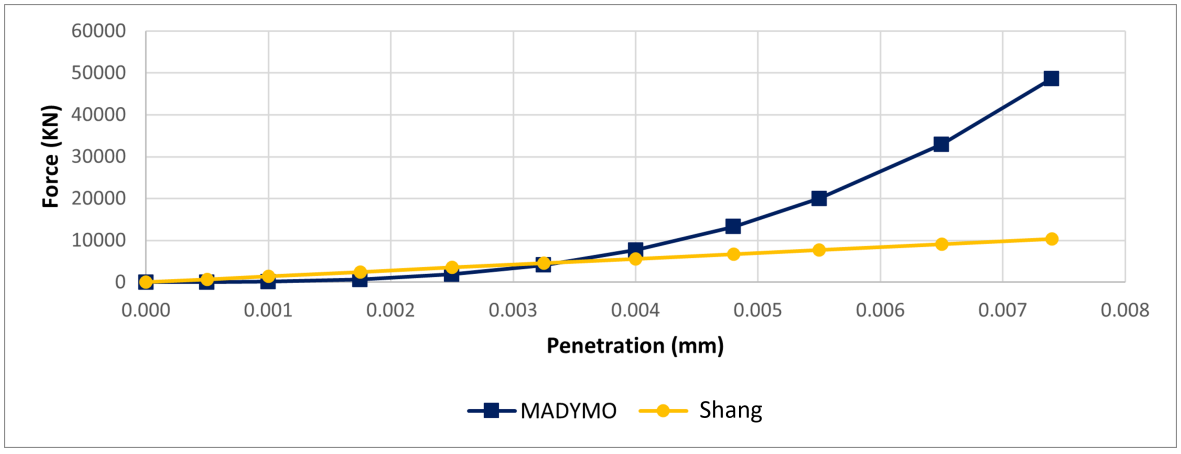

Figure 5.4: Force-Penetration data for the existing AM50 model compared to calculated linear stiffness [Shi et al., 2018b]

5.2.3 Pedestrian Position and Pose

Pedestrian impacts are highly sensitive to initial conditions, with minor changes in pedestrian pre-impact pose sometimes having a significant effect (e.g., change of head contact location from a soft to a stiff region) [Simms and Wood, 2006]. To improve the validity of our simulations, we sourced real-world videos and employed pose estimation techniques to define plausible pedestrian pre-impact poses. Firstly, 2D poses were manually annotated, defining the pixel coordinates for each key point on the pedestrian. GAST-Net was then applied to lift the 2D poses to 3D [34]. An inverse kinematics optimisation technique (KinePose) was developed to infer joint orientations in a user-customisable biomechanical model for 3D pose estimates [Liu et al., 2021]. The approach was adapted for use with the MADYMO ellipsoid models using reorientable joints. The resulting poses are shown in Figure 5.6

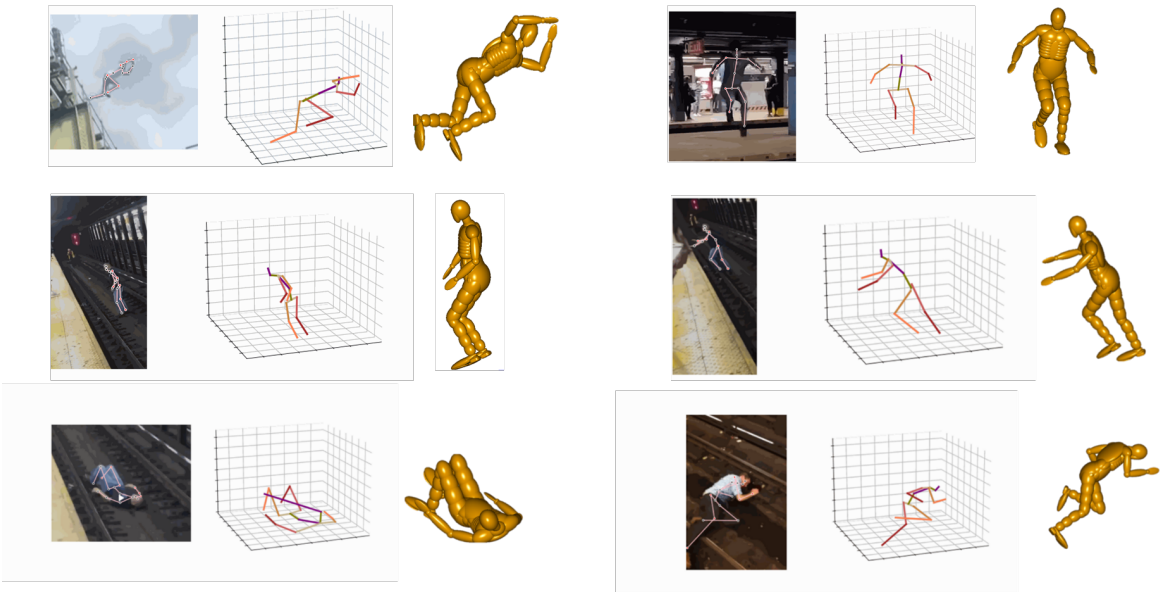

Figure 5.5: Representative stills from YouTube videos, illustrating 2D keypoints, 3D keypoints, and the subsequent MADYMO pe-destrian modeling configuration via KinePose [Gildea et al., 2022]

5.2.4 Simulation Test Sample (STS)

Full STS

A simulation test sample (STS) was developed to represent the range of possible impact configurations in subway-pedestrian incidents, using the NYC incident report data from Chapter 3 as the primary source. This resulted in 1920 unique Impact Scenarios (IS) across 24 positions, 8 velocities, 5 trough depths and 2 track types. Further, a weighting system was applied

to also address the likelihood of each scenario, similar to Li et al. [2017]. This weighted STS was then used to assess the likelihood of wheel run-over across a range of impact positions, impact velocities and track geometries. The full STS conditions are presented in Table 5.2 and Figure 5.6.

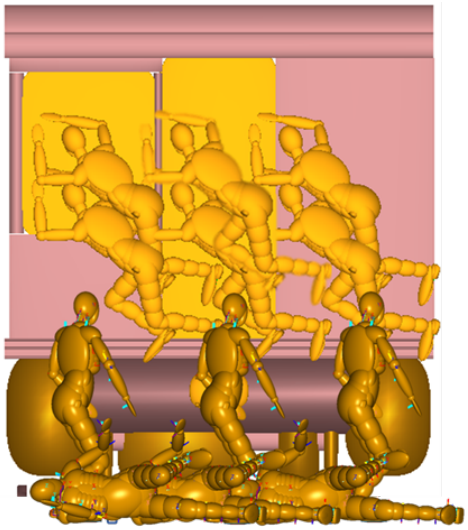

Figure 5.6: Pedestrian position and poses used in full STS

Table 5.2: Full Simulation Test Sample (N = 1920)

Impact position	**Posture**	**Impact Location**	**Track Type**	**Trough Depth (m)**	**Impact Velocity (m/s)**	**Total Simulations**
Lying	Lying 1 Lying 2	Left Right Middle	Flat bed Crossties	5 [0 0.25 0.5 0.75 1]	8 [2 4 6 8 10 12 14 16]	480
Mid Jump	Jump 1 Jump 2	Left upper Right upper Middle upper Left lower Right lower Middle lower	Flat bed Crossties	5 [0 0.25 0.5 0.75 1]	8 [2 4 6 8 10 12 14 16]	960
Standing	Standing 1 Standing 2	Left Right Middle	Flat bed Crossties	5 [0 0.25 0.5 0.75 1]	8 [2 4 6 8 10 12 14 16]	480

Baseline Simulation Test Sample (BSTS)

A subset of this STS was used to develop the baseline (as-is) risk for comparison. This Baseline Simulation Test Sample (BSTS) consists of 24 impact positions, 8 velocities and 2 track types, but with only one trough depth for each track type (0m for flat track bed (Figure 5.2) & 0.25m for the track bed with crossties (Figure 5.3). This results in 384 impact scenarios representing the existing NYC Subway environment. This BSTS allows for comparisons to

be drawn between the existing environment and one with a different drainage trough depth, and in future potentially also the assessment of other proposed countermeasures.

5.3 Injury Criteria & Contact Score

Head Injury Criteria (HIC)

The Head Injury Criterion (HIC_{15}) was used to quantify the head injury risk for each simulation [Versace, 1971b]. HIC scores are frequently used in automotive safety research (e.g. Su [2019], Suntay et al. [2020]). The primary impact time window for distinguishing primary head contact from either secondary or run-over head contact was set at 0-0.4s for lying, 0-0.5s for jumping and 0-0.28s for standing impacts (Figure 5.7). An additional contact phase between the pedestrian and the train is present in IS which involves run-over. Based on the calculated HIC scores, the probability of Abbreviated Injury Scale (AIS) head injury risk was determined using correlation [Hayes et al., 2007]. A nominal HIC_{15} threshold was set at 2000, corresponding to an 88% probability of an AIS4+ injury, and this was chosen as a reasonable upper limit of survivability.

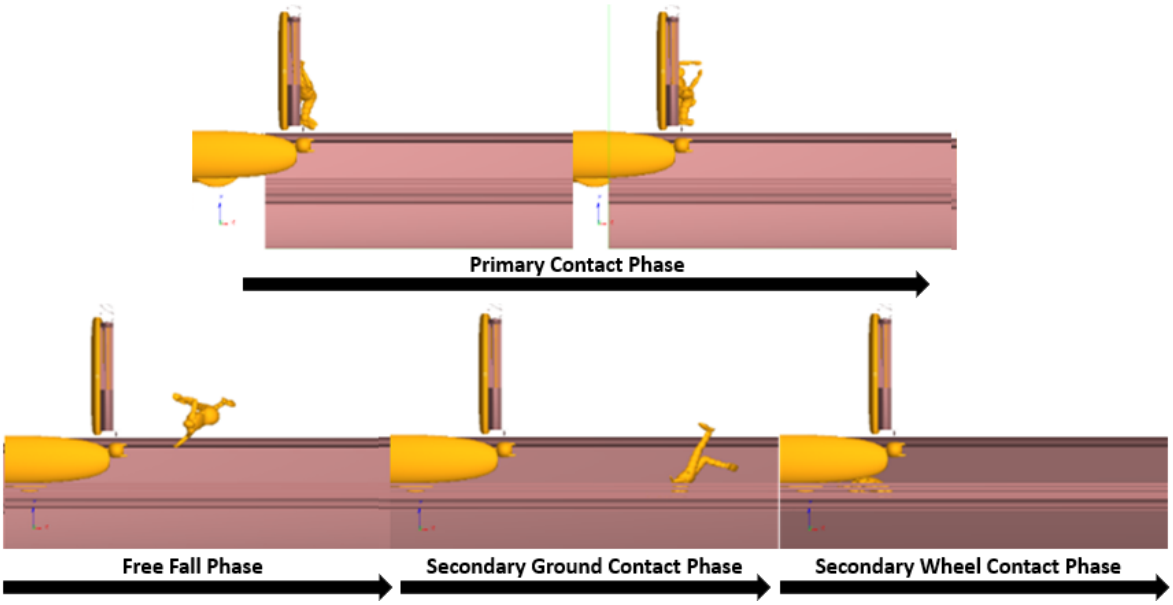

Figure 5.7: Contact phases for jumping case at 16m/s impact velocity

Contact Score (CS)

To investigate the effect of track geometry on electrocution by the third rail, a contact probability system was used. The contact score (CS) was defined as the number of simulations

predicting at least one wheel/third rail contact, divided by the total number of simulations for that configuration. Wheel and third rail contacts were defined as a binary measure (1 for one or more contacts and 0 for no contacts).

5.4 Weighted Injury Scores (WIS)

Not all impact scenarios occur at the same frequency. The NYC Subway Public Transportation Safety Board (PTSB) case reports from Chapter 3 were used to calculate the proportional frequency of each simulated impact scenario. There were 25 cases with both a recorded impact velocity between 2-16m/s and a recorded impact position of either standing, jumping or lying. Over 40% of these incidents occurred at 12-14m/s, while only 4% occurred at 14-16m/s, indicating the need for a Weighted Injury System (WIS) and Weighted Contact Score (WCS).

The Impact Scenario Proportion (ISP) was defined as the product of the Impact Velocity Proportion (IVP) and Impact Position Proportion (IPP), where the sum of each proportion is equal to 1 5.1 5.2. The full set of ISPs are presented in Table 5.3. The Weighted Contact Score was defined as the sum of the products for the base CS with the associated ISP divided by the sum of the ISPs 5.3.

$$ISP = IVP * IP \tag{5.1}$$

$$\sum_{i=1}^{N} ISP_i = \sum_{i=1}^{N} IVP_i = \sum_{i=1}^{N} IPP_i = 1 \tag{5.2}$$

$$WCS = \frac{\sum_{i=1}^{N} CS_i * ISP_i}{\sum_{i=1}^{N} ISP_i} \tag{5.3}$$

Table 5.3: All Impact Scenario Proportions (ISPs) for baseline model

Impact Velocity	**2m/s**	**4m/s**	**6m/s**	**8m/s**	**10m/s**	**12m/s**	**14m/s**	**16m/s**
Lying	0.0178	0.0266	0.0266	0.0266	0.0178	0.0976	0.0089	0.0089
Mid Jump	0.0266	0.0399	0.0399	0.0399	0.0266	0.1464	0.0133	0.0133
Standing	0.0325	0.0488	0.0488	0.0488	0.0325	0.1790	0.0163	0.0163

5.5 Sensitivity Study

A sensitivity study was conducted to evaluate the effects of contact hysteresis and fracture joint damping on the relationship between trough depth, run-over risk, and head injury risk. This analysis aimed to determine how variations in these parameters influence pedestrian kinematics and injury outcomes in subway-to-pedestrian collisions. To ensure computational efficiency while capturing key trends, a smaller subset of nine jumping impact scenarios was selected for this assessment (Figure 5.8. The full range of tested variables, including impact velocity, pedestrian posture, and trough depth variations, is detailed in Table 5.4.

Table 5.4: Sensitivity study initial conditions and variables

Variable	Value	Impact Velocity (m/s)	Trough Depth (m)	Position	Total
Hysteresis	Standard x10 Off	10	0 0.5 1	9	81
Joint Damping Forces	Standard (5N) Double Locked	10	0 0.5 1	9	81

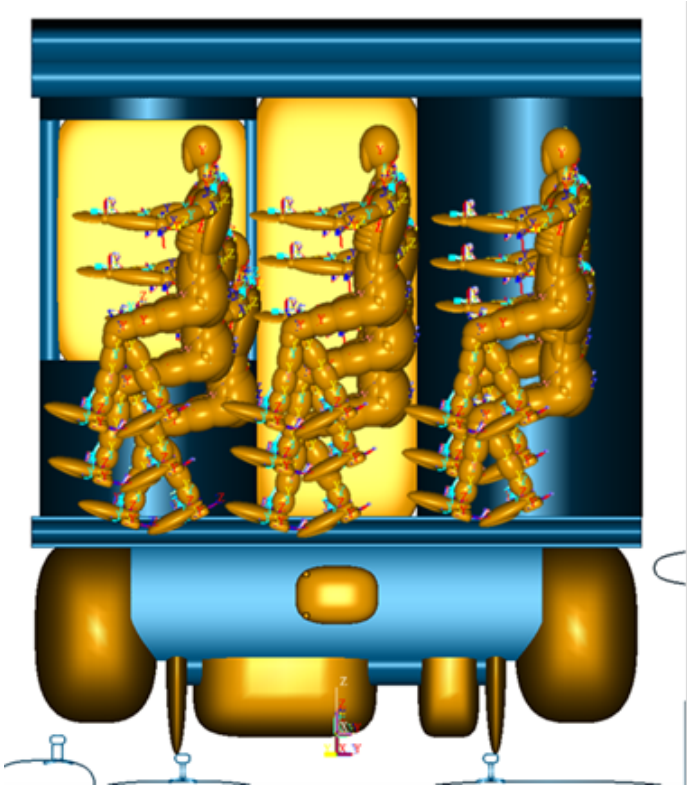

Figure 5.8: Sensitivity study pedestrian impact position and posture

5.6 Results

5.6.1 Sensitivity Study

A direct comparison of how CS or HIC scores are affected by fracture joint changes is not possible, as data is unavailable for simulations that failed due to gimbal lock. This issue arose in cases where excessive joint rotation led to numerical instability, preventing the simulation from progressing. To address this, Table 5.5 illustrates that locking the fracture joints allowed all simulations to run to completion without encountering instability. Given this constraint, the results presented in this chapter are based on the AM50 model with locked leg fracture joints, ensuring consistency and comparability across all simulated scenarios.

Table 5.5: Sensitivity study, simulations with modelling instabilities with various fracture joint damping

Number of Simulations:	**Completed (N)**	**Fracture Error from Gimbal Lock (N)**	**Complete (%)**
Standard Joint Damping (5N)	10	17	37
Double Joint Damping (10N)	16	11	60
Locked joints	27	0	100

Figure 5.9 illustrates the effect of varying hysteresis on contact scores (CS). While individual CS values fluctuate depending on the chosen hysteresis level, the overall trend between CS and trough depth remains consistent. Specifically, an increase in trough depth leads to a reduction in CS values, irrespective of the hysteresis setting applied. This suggests that although energy absorption influences localised variations in contact severity, it does not significantly alter the broader trend in model predictions. These findings indicate that the model's assessment of drainage trough depth as a mitigating factor for roll-over risk remains robust across different hysteresis values.

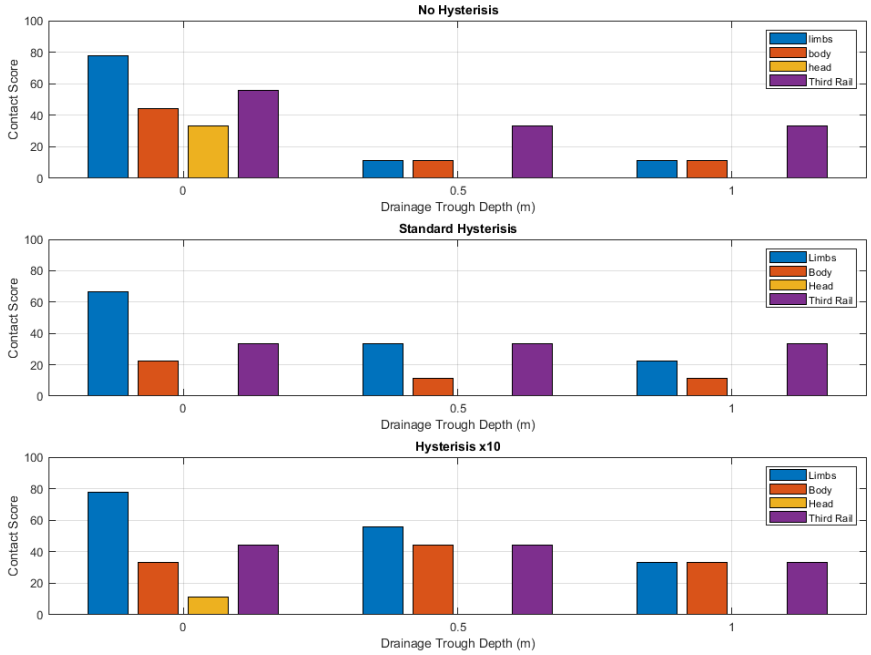

Figure 5.9: Sensitivity study contact scores at different hysteresis values

5.6.2 Baseline Run-Over Risk

Figure 5.10 shows the BSTS contact and weighted contact score separated by impact conditions. Lying has the highest weighted contact score (WCS) across all regions, while jumping IS show a relatively lower WCS for the limbs compared to lying or standing. The third rail contact scores are 0.2-0.3 for all impact positions.

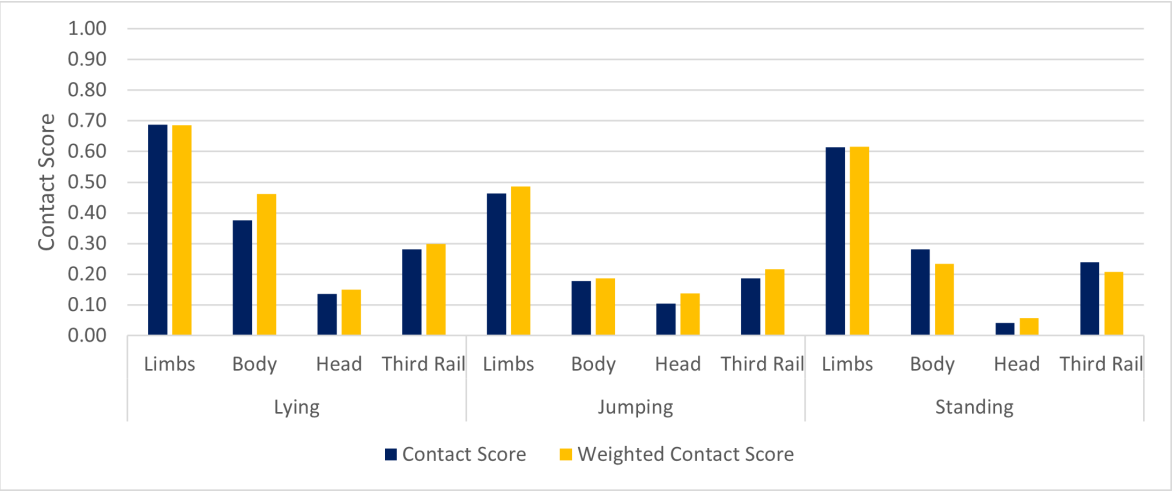

Figure 5.10: Contact Scores and Weighted Contact Scores for baseline model. All impact positions

Figure 5.11 shows the combined CS and WCS for the Baseline Simulation Test Sample (BSTS). The modelling results suggest that a typical collision between an R160 subway train and a 50th percentile male pedestrian in the existing NYC track environment has a contact likelihood of 59% for limb-to-wheel contact, 27% for body-to-wheel, 11% for head-to-wheel and 23% for third rail contact.

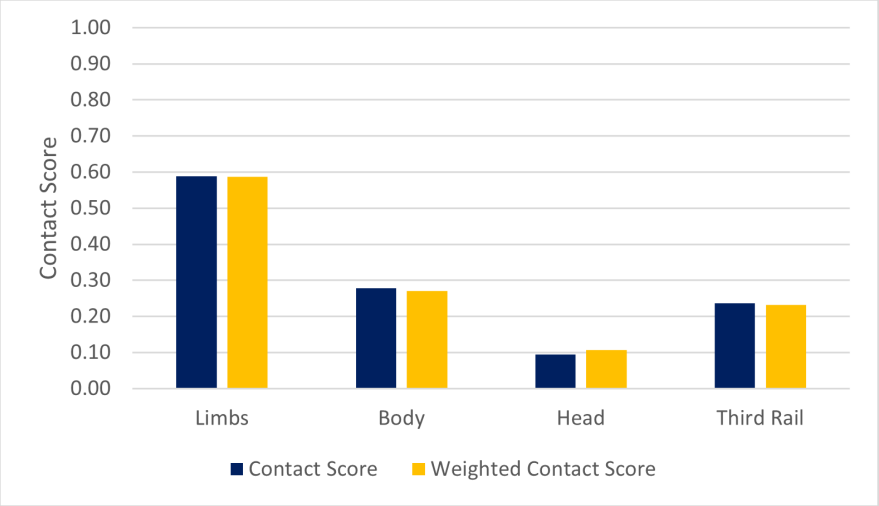

Figure 5.11: Overall combined Contact Scores and Weighted Contact Scores for Baseline Simulation Test Sample

Figure 5.12 presents the relationship between the CS and impact velocity, where above a train speed of 4m/s the impact velocity does not greatly affect the contact scores. The weighted contact scores do not substantially differ from the unweighted contact scores, implying that the CS are independent of impact position and velocity.

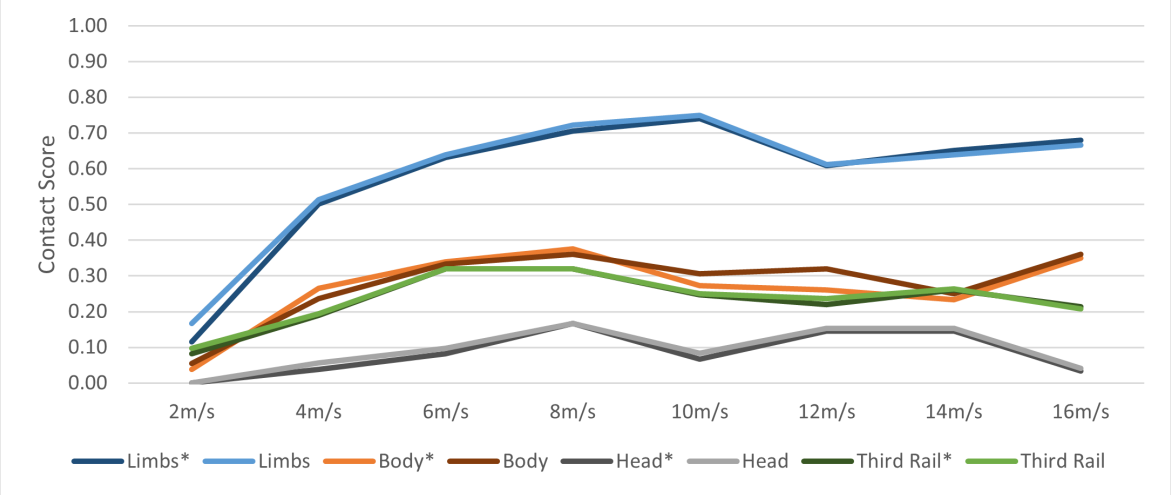

Figure 5.12: Effect of impact velocity on contact scores (weighted*)

5.6.3 Baseline Head Injury Risk

Figure 5.13 shows the range of primary and secondary HIC_{15} scores for the BSTS. The notches in the box plot represent an approximation of the 95% confidence interval (CI) for the median, as described by McGill et al. [1978]. The notch width is calculated using an asymptotic normality approximation, where non-overlapping notches between two box plots suggest a statistically significant difference in medians at approximately p≈0.05 (Equation 5.4). Jumping ISs result in the highest range of HIC_{15} scores, while the standing ISs show a smaller range but higher HIC_{15} values. Secondary contacts show similar HIC_{15} scores in both jumping and standing, and a lower dependency on impact velocity. HIC_{15} scores above the 2000 threshold correspond to a greater than 88% probability of AIS4+ head injury.

$$Notch = Median \pm 1.57x\frac{IQR}{n^{0.5}} \tag{5.4}$$

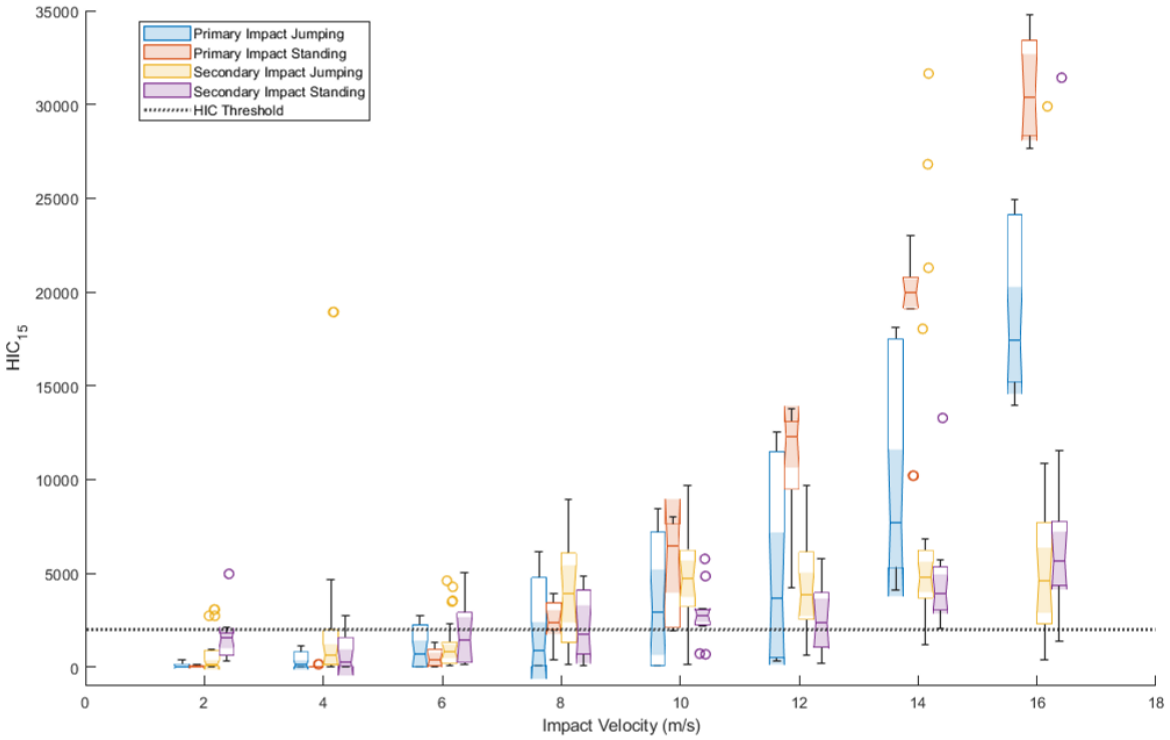

Figure 5.13: Baseline Simulation Test Sample (BSTS) primary and secondary HIC_{15} scores

Figure 5.14 shows the proportion of jumping and standing HIC_{15} scores that fall below the threshold HIC_{15} score of 2000. The models suggest that only 29% of incidents will result in an AIS4+ head injury probability of less than 88%. Primary impact shows a similar proportion of cases below this threshold (47% compared to the 44% of secondary contact HIC_{15} scores).

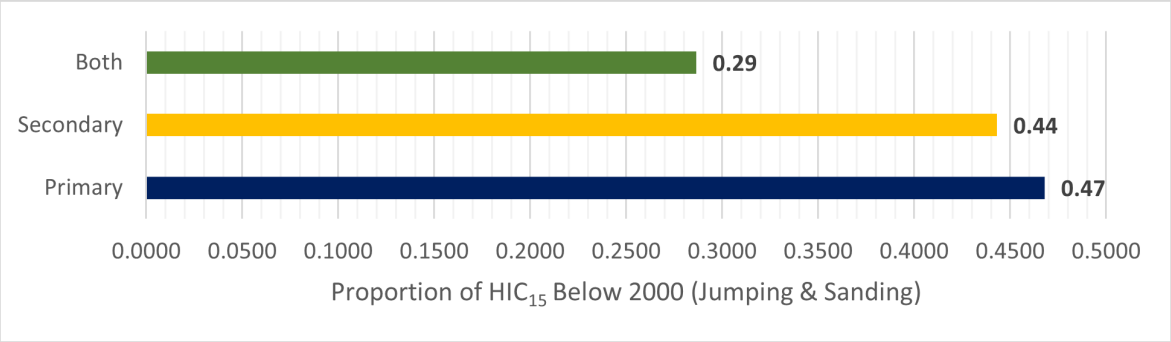

Figure 5.14: Baseline Simulation Test Sample proportion of jumping and standing $HIC_{15} < 2000$

5.6.4 STS Run-Over Risk

Figure 5.15 shows the relationship between drainage trough depth and wheel/third rail contact for the full simulation test sample. There is a general reduction in CS with increasing drainage trough depth. This relationship is strongest for jumping, with less effect for standing or lying. Jumping scenarios also show the lowest CS for limbs, body and third rail contacts, with similar head CS to standing. There is no clear relationship between drainage trough depth and wheel/third rail contact probability for lying. Overall, the model shows a general decline in wheel and third rail contacts as trough depth increases for the limbs and in some cases, for the head and body. This relationship is most prominent between 0-0.5m of trough depth, with little to no additional benefit beyond 0.5m.

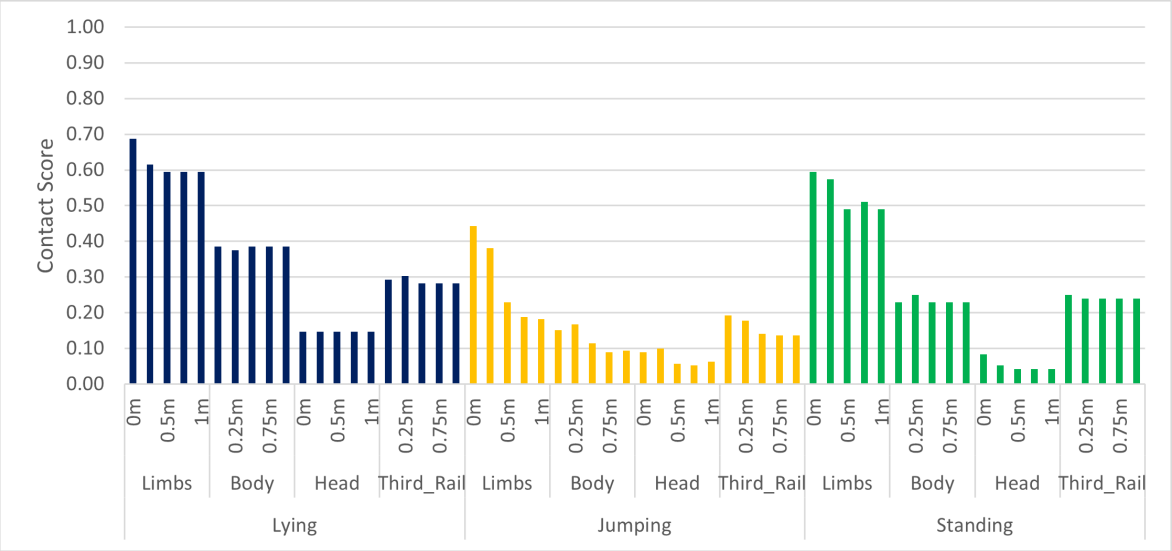

Figure 5.15: Full Simulation Test Sample contact scores separated by impact position and drainage trough depth

5.6.5 STS Head Injury Risk

Figure 5.16 shows the effect of drainage trough depth on secondary contact HIC_{15} score for jumping and standing scenarios. There are only small changes in the median HIC_{15} score with each increment in trough depth, but a significant difference with a 95% confidence for jumping can be found when comparing HIC_{15} at 0m and 1m trough depth. The significance level is based on a normal distribution assumption.

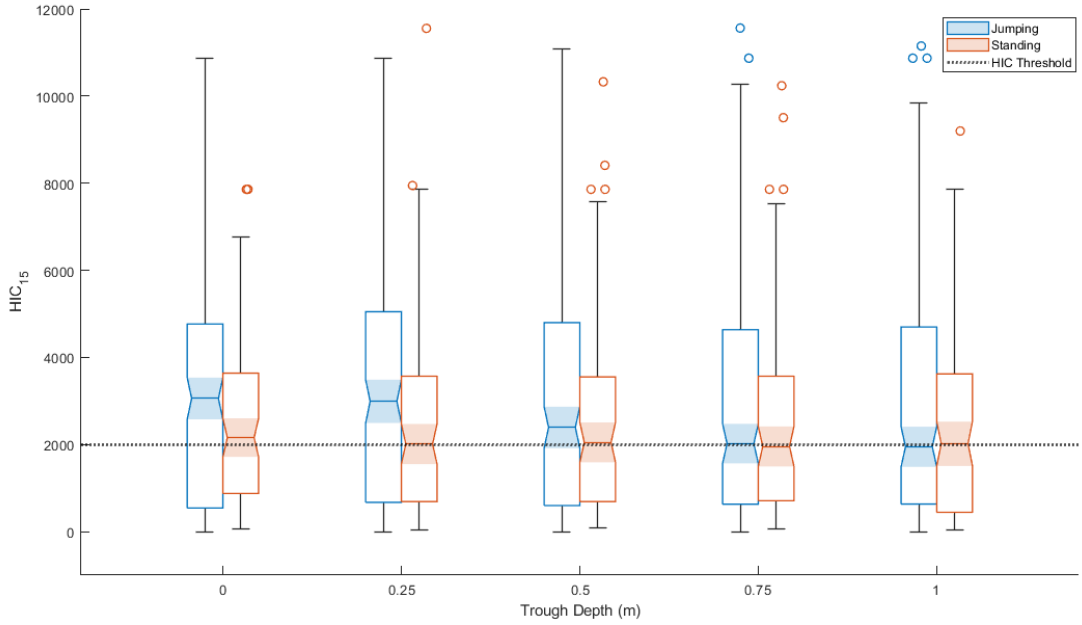

Figure 5.16: Relationship between drainage trough depth and secondary contact HIC_{15} score for jumping and standing impact scenarios

5.7 Discussion

Subway-to-pedestrian collisions are increasing [FRA, 2022], but there is a lack of biomechanical analysis. To the best of our knowledge, this is the first model of subway-to-pedestrian collision interactions. As there is no validation data against which to assess this model, predicted trends offer more significance than absolute values, similar to the approach taken in [Li et al., 2015]. The sensitivity study shows that the trends in modelling results are not greatly sensitive to the uncertainty in contact hysteresis. Further locked leg fracture joints are required for modelling to proceed.

5.7.1 Main Findings

The risk of direct contact with the wheels is highest for the limbs and lowest for the head. Lying on the tracks is not surprisingly generally worse than jumping or standing (Figure 5.10), but this does not account for any voluntary movement such as intentional positioning in the centre of the track. The models therefore more closely resemble a pedestrian falling onto the tracks and not moving. Third rail contact occurs about 20% of the time; however, this may be an overestimate due to high penetration into the third rail guard, which is a

modelling limitation. There is a weak impact velocity dependency on contact scores for impact velocities above 4m/s (Figure 5.12). Conversely, there is a strong impact velocity dependency on primary contact HIC_{15} scores, but not on secondary contact HIC_{15} (Figure 5.13), which is similar to findings from vehicle to pedestrian collisions [Simms and Wood, 2009]. Regarding head injury risk, about 30% of the Baseline Simulation Test Sample (BSTS) cases are potentially survivable, with a $HIC_{15} < 2000$ for both primary and secondary impacts (Figure 5.14). The contact scores decrease with drainage trough depth up to 0.75m, with the largest benefit in jumping impact scenarios (Figure 5.15). Increasing trough depth beyond 0.75m shows little benefit. Trough depth shows a significant difference in secondary contact HIC_{15} between 0 and 0.5m trough depth (Figure 5.16), and this is likely caused by a deeper trough reducing the likelihood of a pedestrian hitting the ground headfirst. This does not account for any potential change in other body region injuries.

5.7.2 Baseline Run-Over Risk

The current risk of a pedestrian to train interaction resulting in a limb amputation is almost 60% for the full baseline impact scenarios (Figure 5.11). The pre-impact position is an influencing factor in calculating this risk. The limb contact risk varies between 69% and 46% for lying and jumping impact scenarios respectively (Figure 5.10). The high contact scores for lying impact scenarios are expected, as the left and right lying positions are in the direct path of the train wheels for primary contact. The standing and jumping impact scenarios result in a primary impact location higher up on the train front, requiring an additional train contact phase for roll-over to occur (Figure 5.7). Potential actions taken by the pedestrian to avoid contact (such as lying between the rails) have not been modelled, as the models are passive. The lying postures thus more closely represent an individual who has fallen on the tracks and does not move before impact.

The head contact probability with the wheels is lowest for the standing impact scenarios (Figure 5.10), likely due to the kinematics during the free fall phase. Figure 5.17 shows that for standing impact positions, the pedestrian is rotated away from the wheels, such that the head is the furthest body part from the wheels during secondary contact. The secondary contact for the jumping pedestrian shows no rotation away from the wheels during free fall.

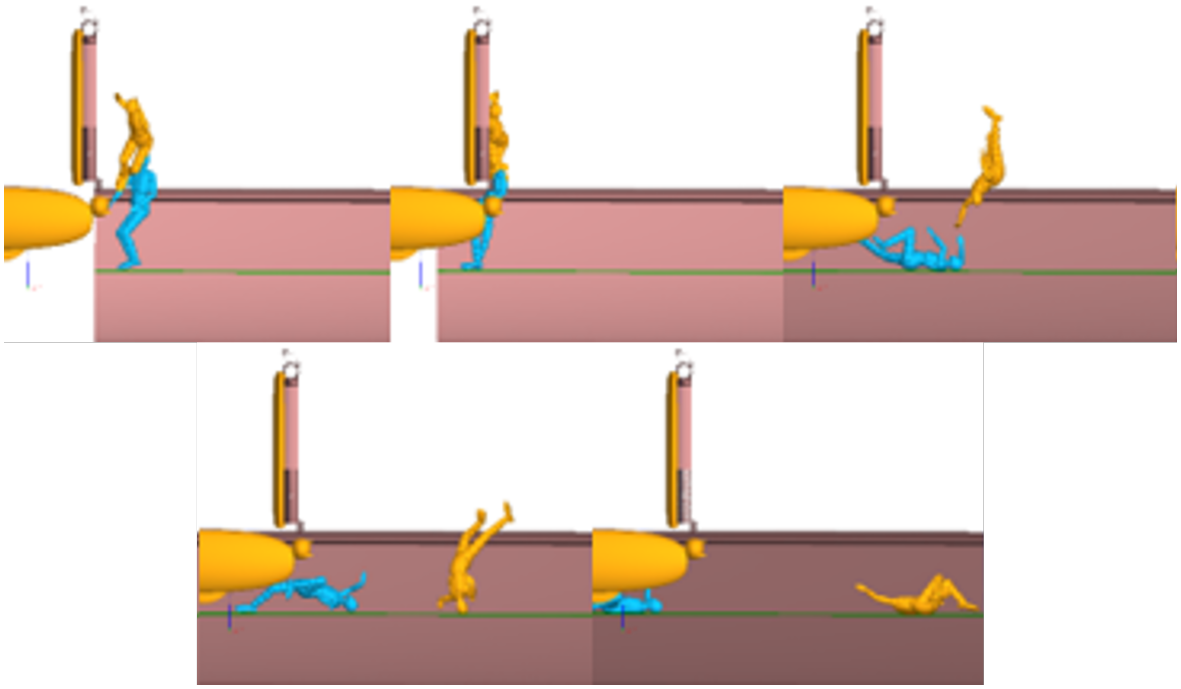

Figure 5.17: Standing (blue) and jumping (yellow) kinematics for a 16m/s impact

Figure 5.12 shows that impact velocity has a marginal influence on contact scores. Impact velocities between 6-16m/s show little to no change in contact scores. However, the contact score is significantly lower between 2-4m/s. This may be caused by the complete absence of a run-over due to the emergency braking of 1.43m/s^2. This suggests that train to pedestrian impacts pose similar run-over risks independent of the impact velocity at speeds above 4m/s. Epidemiological data from Chapter 3 highlights 12m/s as the most common impact velocity. The study finds the impact velocity must be decreased to below 4m/s before any substantial benefit will be found in reducing pedestrian to wheel contact injuries. Given the passive nature of the pedestrian models, the lower velocity (<4m/s) contact scores are likely an overestimation as no active avoidance manoeuvres are made by the pedestrian model. During a real pedestrian collision at 2m/s, sufficient time might be available to physically manoeuvre into a more advantageous position. At higher impact velocities, the ability to move out of the path of the wheels is less likely.

5.7.3 Effect of drainage trough on Run-Over Risk

Figure 5.15 shows the contact scores for jumping impact scenarios are heavily influenced by drainage trough depth. The limb contact score falls from 44% to 18% as the trough depth increases from 0 to 1m. Contact scores from standing and lying show less dependency

on trough depth. The secondary contact phase for a jumping pedestrian occurs later than for standing and lying. This yields two benefits: there is additional time for the train to decelerate before run-over can occur and there is more time for the pedestrian to fall into the trough before roll-over.

Figure 5.15 shows that contact scores for jumping impact scenarios are heavily influenced by drainage trough depth. The limb contact score falls from 44% to 18% as the trough depth increases from 0 to 1m. Contact scores from standing and lying show less dependency on trough depth. The difference in secondary contact kinematics may be a factor in the effectiveness of trough depth. The secondary contact phase for a jumping pedestrian occurs later than for standing and lying. This yields two benefits: there is additional time for the train to decelerate before roll-over can occur and there is more time for the pedestrian to fall into the trough before roll-over (Figure 5.17).

The greatest change in contact scores can be seen between as trough depth increases from 0-0.5m, while additional trough depths yield little further benefit. This is likely due to the secondary contact position of the pedestrian. Cases which yielded no benefit from a 0.5m trough due to their secondary contact positioning are unlikely to benefit from a 1m trough. Conversely, pedestrians who avoided the train due to a 0.5m trough will not further benefit from a 1m trough. Third rail contacts do not significantly depend on trough depth, with a 2% reduction between 0 and 0.5m, and the contact score for third rail contacts remains between 20-25% for the full simulation test sample. Due to the nature of rigid multibody modelling, this is likely an overestimation as the pedestrian's limbs or other body regions cannot be severed. This can cause the pedestrian in the model to be dragged along the rails, increasing the likelihood of third rail contact. Overall, a drainage trough with a depth of 0.5m may reduce the risk of wheel to pedestrian contacts but will offer no benefit for third rail contact prevention. Future studies optimising the geometry of the trough through both width, depth and curvature may offer further insights into the safety benefit. This research could be used to inform future track design policy.

5.7.4 Baseline Head Injury Risk

In this study, HIC_{15} score was used as the primary metric to evaluate head injury risk due to its widespread acceptance in biomechanical research. While rotational head injury metrics, such as those derived from the Brain Injury Criterion (BrIC) score or Head Impact Power (HIP), are indicators of brain injury risk, previous studies have demonstrated a strong cor-

relation between high HIC_{15} values and elevated rotational injury metrics [Marjoux et al., 2008]. Chapter 2 Figure 2.4 suggests that efforts to mitigate linear acceleration can simultaneously reduce rotational injury risk. This correlation supports the use of HIC_{15} as a proxy for overall head injury risk.

Figure 5.13 shows a strong dependency of primary impact HIC_{15} score on train impact velocity, while secondary impact HIC_{15} scores show little to no velocity dependency between 6-16m/s. Impact velocities between 12-16m/s show a significant difference with 95% confidence in the median primary HIC_{15} scores for jumping (lower primary HIC_{15} scores) compared to standing (higher primary HIC_{15} scores) impacts. There are more outliers detected for secondary contacts, as the variability in impact conditions is much greater, as previously observed for secondary contact for vehicle to pedestrian collisions [Crocetta et al., 2015c].

Figure 5.14 shows that 29% of the jumping and standing impacts result in a HIC_{15} score of less than 2000 for both primary and secondary impacts. This implies that countermeasure design must incorporate both primary and secondary impact mitigation to be effective.

Figure 5.16 shows the secondary contact HIC_{15} surprisingly decreases with trough depth. Upon further investigation, it was found that the addition of the trough changes the kinematics of the ground contact, reducing the likelihood of headfirst collisions, thus reducing pedestrian head to ground contact velocity. This does not account for any change in injury probability associated with other body regions, such as the chest or spine. Regarding HIC_{15} scores alone, these findings show no negative consequence of increasing trough depth.

5.7.5 Limitations

There are several limitations to this work. The lack of experimental data needed for model validation means that the results are focused on trends rather than individual simulations. However, the sensitivity study to assess the dependency of these trends on unknown factors showed no significant reliance. Future model validation research utilising full-scale staged tests would be most beneficial; however, the financial cost of such tests would be high. Retrospective injury analysis of similar impact cases to those used in the STS would advance model validation; however, NYC medical examiner records and injury data were not available at the time of this study. While multibody modelling allowed for a large simulation test sample to be evaluated, amputations, decapitations and bisections could not be modelled. This may cause an overestimation of third rail contact likelihood as the body can be

dragged alongside the train instead of becoming separated from the body region in contact with the wheels. Further, the subway environment includes more sharp or edge contacts compared to automotive collisions. For primary contact, potential sharp interactions include the anticlimber, coupler and train wheels. For secondary contact, sharp interactions could include the rails, crossties and trough edges. The contact characteristics used in this study are based on force-penetration relationships; as such, any change in head acceleration due to the object geometric sharpness is not considered in head injury risk calculations. The initial conditions, track environment and train front geometry used in this study are based on the NYC Subway system. At the time of this study, the NYC Subway is one of the largest subways in the world and offers the most up to date pedestrian incident information. However, to represent the growing global issue of subway-to-pedestrian collisions, further studies using different pedestrian characteristics such as sex, height and weight, as well as track and train types are needed; this will be the focus of future work.

Notwithstanding these limitations, this research offers the first model of subway-to-pedestrian interactions and assesses the effect of drainage troughs as a potential means of improving pedestrian safety.

5.8 Conclusion

A model of subway-to-pedestrian collisions is presented, taking into account variability in impact configurations. The model predicts substantial risk of wheel contact during run-over and shows this is not strongly speed dependent, except at very low speeds. On the other hand, increasing the drainage trough depth reduces the likelihood of contacts with both the wheel and the third rail. Further, the model shows that increasing drainage trough depth does not significantly influence the injury risk in secondary contact with the ground. Similar to vehicle pedestrian collisions, primary contact with the subway is much more sensitive to subway speed than the secondary contact with the ground. Finally, the high injury severity predicted by the model for both primary and secondary contact indicates that pedestrian protection interventions must address both of these impact phases. The results of this model offer a baseline injury risk against which future countermeasure studies may be compared. For potential subway-to-pedestrian safety advancements, roll-over likelihood would be reduced with the implementation of a drainage trough with a minimum depth of 0.5m. This may inform future subway track design policies incorporating pedestrian safety into drainage

trough systems. Reducing the approach velocity of incoming subway trains into the station would decrease primary contact head injury risk, but a substantial velocity reduction (station entry velocity <4m/s) would be required to reduce run-over likelihood. Countermeasures to address secondary contact head injury risk are required. Future studies of track guards utilising the available drainage trough space while providing softer ground contact surfaces may be a promising area of research.

Chapter 6

Subway to Pedestrian Collision Safety: Multibody Models of Energy Absorbing Countermeasure Designs

6.1 Introduction

Advancements in biomechanical safety research have drastically transformed vehicle designs over the last century (e.g. Crocetta et al. [2015a], Kianifar and Campean [2019]). This is evident in the vast improvements in automotive safety standards and crashworthiness, as well as the visual geometric difference in vehicle design. Pedestrian safety research involving Heavy Goods Vehicles (HGV) has shown that run-over collisions may be improved through the optimisation of the vehicle front-end design (e.g. Feist et al. [2009], Hamacher et al. [2009], Martin et al. [2020]), however subway train designs have seen minimal changes. Despite decades of knowledge and technological progress, the design of subway vehicle front ends has remained largely static, with limited adaptations for pedestrian safety. For subway-to-pedestrian collisions, a focus on collision avoidance measures, such as platform screen doors, can be found in the literature. While studies show the benefit of Platform Screen Doors (PSD) (e.g. Chung et al. [2016a], Law et al. [2009]), this type of large-scale infrastructural investment is not always practical in older subway environments such as New York City [Metropolitan Transportation Authority Track Trespassing Task Force, 2020]. The gap between complete collision avoidance and more passive fatal injury reduction methods underscores the critical need for dedicated safety research specific to subway-pedestrian interactions.

Building upon the findings from the previous chapters, this final study centres on the practical application of the collected epidemiological, experimental, and modelling data in an effort to move towards the design of effective safety interventions for subway-to-pedestrian collisions. Chapter 3 provided crucial insights into the prevalence and circumstances of subway-related pedestrian injuries, helping to identify the most critical impact conditions. Chapters 4 and 5 then utilised these parameters to conduct impact tests, deriving contact characteristics and establishing a baseline multibody model to simulate and assess head injury risks associated with these types of collisions.

The aims of this study are to use the multibody modelling software MADYMO to assess the effectiveness of various Energy Absorbing Countermeasures (EAC) designs on:

- Pedestrian head injury risk using Head Injury Criterion (HIC_{15}).
- Pedestrian to wheel run-over risk using Contact Scores (CS)

6.2 Countermeasure Design

6.2.1 Design Targets

Effective Impact Velocity [8-12m/s]

For the NYC subway, pedestrian impact velocities range from 2-16m/s, with the most common velocity of 12m/s (Chapter 3 Figure 3.6). Experimentally derived EAC contact characteristics are based on a maximum impact velocity of 11.5m/s (Chapter 4 Table 4.1). While there is a strong velocity dependency on primary contact HIC_{15} scores, secondary contact HIC_{15} scores lose this correlation above 8m/s (Chapter 5 Figure 5.13).

Impact Conditions [Standing & Jumping]

Chapter 3 Figure 3.5 shows that standing, jumping, and lying positions are each common at impact, with similar numbers of associated fatalities and injuries. Chapter 5 Table 5.2 outlines the Simulation Test Sample (STS) used in developing a baseline multibody model. In this study, a subset of that test matrix has been created using the jumping and standing positions listed in Table 5.2, along with the impact velocities from Chapter 4. Since drainage trough depth is not a focus of this study, all simulations will use a single depth of 0.75m with crossties. To account for operational concerns regarding the proximity of train equipment to the rail, all train-mounted countermeasures will maintain a minimum clearance of 0.2m from the rail top. As a result, lying impact positions are excluded from this study.

Injury Reduction [Median Primary HIC_{15} <1000 & 50% Reduction in CS]

Chapter 5 has identified three key areas for injury mitigation: primary contact, secondary contact, and run-over. Each of these areas must be considered for effective countermeasure design. Euro NCAP proposed criteria for automotive vehicles to primary contact HIC_{15} scores between 650-1700. Vehicles with HIC_{15} scores below 650 would receive a green safety rating, while HIC_{15} scores above 1700 would receive a red rating. Yellow, orange, and brown ratings are equally dispersed between HIC_{15} scores of 650-1700 [Euro, 2018]. This study will rate each proposed countermeasure using this system. Chapter 5, Figure 5.13 shows a large range of HIC_{15} scores for impact velocities between 8-12m/s, each with median values above 1000. Therefore, an initial target of HIC_{15} <1000 has been set which corresponds to a Euro NCAP pedestrian rating of Yellow.

6.2.2 Train Front Panels (FP)

Three countermeasure design concepts have been developed for this study, each targeting a specific area of injury causation: primary contact, secondary contact, and run-over injuries. These designs are intended to work synergistically, complementing one another to provide a holistic approach to injury mitigation. While their combined use holds the potential for significant safety benefits, their effectiveness remains subject to further evaluation, and practical challenges such as manufacturing feasibility and integration into existing subway systems must also be considered.

The first countermeasure design features hard-shelled energy-absorbing panels mounted directly on the train-front, with the objective of reducing head injuries during primary contact. To achieve this, the panels are filled with a deformable material engineered to replicate the contact characteristics of an aluminium-covered EAC, as experimentally determined in Chapter 4. This chapter established that contact characteristics are highly sensitive to impact velocity and exhibit viscoelastic behaviour. Therefore, in the simulations, the aluminium EAC contact characteristics specific to each impact velocity were applied using the corresponding velocity-dependent loading curves.

Beyond mitigating head injuries, this design also addresses run-over risks through the strategic geometry of the panels. The panel's shape is specifically designed to work in tandem with the drainage trough, leveraging its safety potential to redirect pedestrian kinematics away from hazardous areas such as the third rail (Chapter 5). The geometry consists of two circles with radii of 0.15m and 0.25m, connected by an arc with a radius of 0.75m, creating a contour with a minimum depth of 0.3m and a maximum of 0.5m. By positioning the larger curve at the outer edge of the train-front, this configuration is designed to guide pedestrians during the free-fall phase of impact, influencing their trajectory toward the drainage trough and potentially reducing the likelihood of critical run-over injuries.

In the MADYMO simulations, this panel design was represented using a facet surface (shown in blue in Figure 6.1(a)) to visualise its shape and placement. However, to define contact interactions, three ellipsoids were modelled on each side of the train front to approximate the panel geometry (Figure 6.1(b)). This approach allowed for a detailed evaluation of the panel's potential effectiveness in altering pedestrian kinematics and mitigating injuries across multiple scenarios.

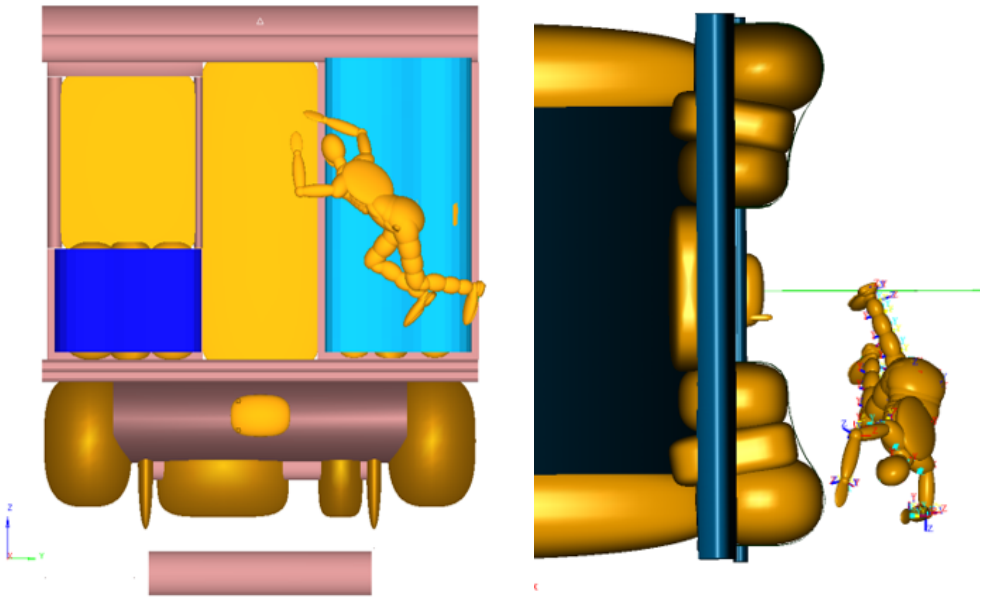

(a) Front view of MADYMO front panel countermeasure

(b) Aerial view of MADYMO front panel countermeasure

Figure 6.1: Multibody model of subway pedestrian collision with front panel EAC concept

The panels can be mounted to the front of the R160 train using existing brackets currently employed for handles and door chains. To enhance compatibility across different train models, the design incorporates a modular approach (Figure 6.2(a)). Since the panels are attached directly to the train front, their effective coverage extends from the front face down to the override bar (anticlimber), with sufficient space for the vision glass and door (Figure 6.2(b)). As shown in Chapter 3, Figure 3.7, this area accounts for 31% of recorded impact incidents from 2019.

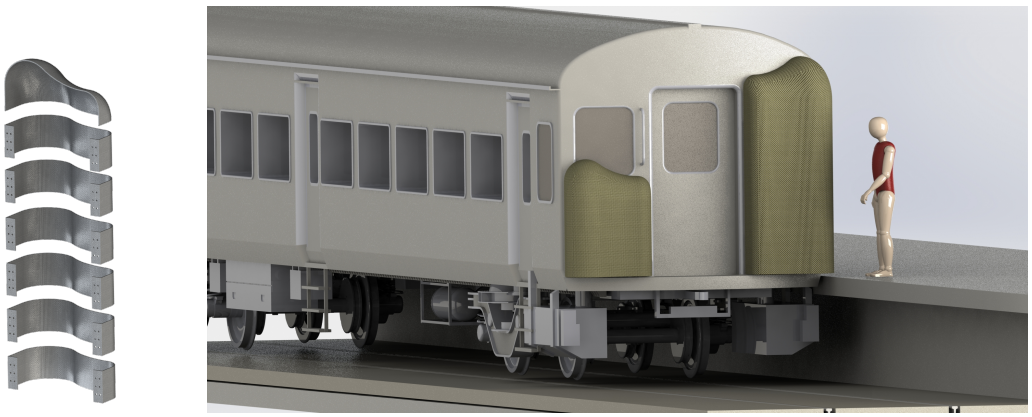

(a) Front panels modular design shells

(b) Front panels attached to subway train front

Figure 6.2: Solidworks renderings of modular front panels countermeasure design

6.2.3 Full Frontal Guard (FFG)

While the front panel EAC concept has an effective coverage range extending from the train front to the anticlimber, to ensure standing pedestrians receive the full benefit, this range must be extended. While maintaining the same contact characteristics and geometry as the front panel concept, the vertical dimension of the countermeasure has been extended such that the panels maintain a clearance of 0.2m from the rail top. An additional panel has been placed in the centre covering the coupler while leaving sufficient spacing for the operation of the door. This panel has been angled to 45 degrees to further influence pedestrian kinematics toward the drainage trough and away from the third rail (Figure 6.3).

This design concept adds a large operational challenge, as components such as the anti-climber, coupler, and ladder have been covered by the panels, as each poses a substantial risk of injury to a pedestrian. There are also no clear mounting points from first inspection below the anticlimber. Although more challenging in implementation compared to front panels, the full frontal guard concept is expected to have an effect on at least 70% of incidents involving a frontal subway-to-pedestrian collision, according to Chapter 3 Figure 3.5.

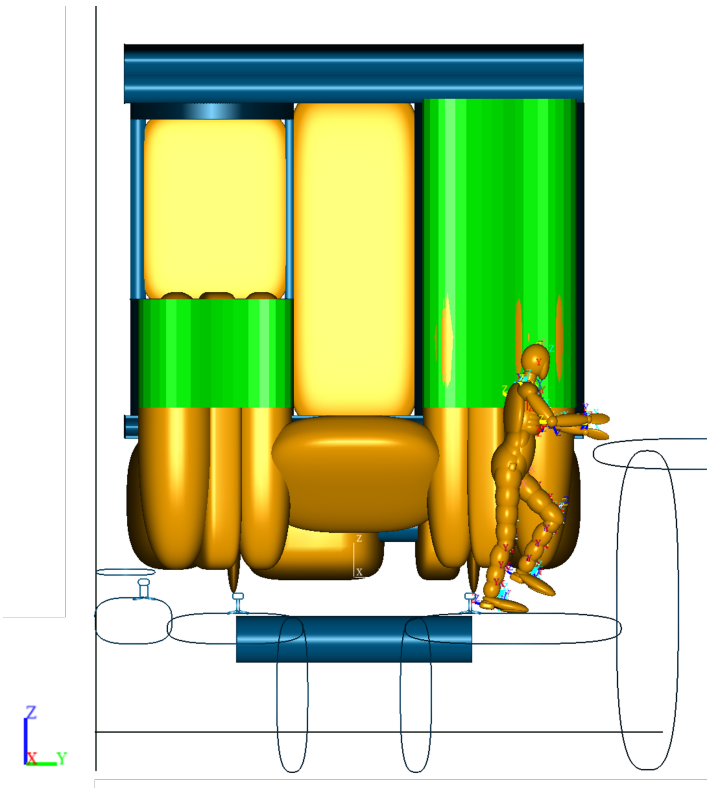

Figure 6.3: Multibody model of standing pedestrian to subway collision with full frontal guard countermeasure concept

6.2.4 Rail Guard (RG)

The FP and FFG countermeasure design concepts address primary contact head injury risk and run-over risk; little benefit is expected in terms of secondary contact head injury reduction. To address secondary contact, a rail covering has been designed that uses the ABS force penetration curve derived in Chapter 4. The intention of this rail covering is to provide a softer landing surface while also rounding out edges along the drainage trough and crossties. The geometry of this rail guard is similar to the FP concept and further guides the pedestrian kinematics towards the drainage trough (Figure 6.4).

This design concept is intended to be installed over the existing rail infrastructure, specifically targeting high-risk areas in order to minimise financial and operational impact. To keep installation costs and required downtime manageable, coverage would be limited to station zones and extend only 60 metres beyond each end of the platform. This approach is based on incident data, which indicates that just 3% of subway-to-pedestrian collisions occur beyond this distance from the platform edge. By implementing the rail guard system in tandem with the proposed full frontal train guard, it would be possible to address 97% of all recorded standing and jumping collisions from 2019 (Chapter 3).

For the purpose of evaluating its impact on head injury severity and run-over risk, the rail guard design has been integrated into the multibody simulation model. In this model, the rail guard is represented as a series of cylindrical elements positioned over the rails and across the crossties. These cylindrical elements use force-deformation characteristics derived from impactor tests with vehicle bonnets [Mizuno and Kajzer, 2000] to modify the kinematics of a pedestrian during a collision, reducing the likelihood of run-over.

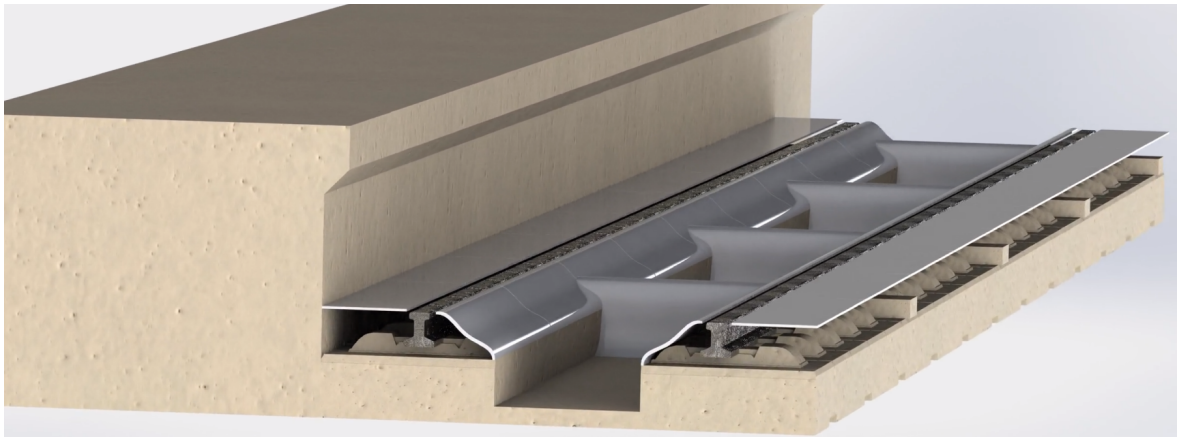

Figure 6.4: Solidworks rendering of rail guard design

6.2.5 Simulation Test Matrix

A total of 216 multibody simulations (Table 6.1) were analysed to determine the primary and secondary collision HIC_{15} score and Contact Score (CS) between the pedestrian's limbs, body, and head with the train wheels or third rail.

Table 6.1: Countermeasure design simulation test sample N = 216

Countermeasure	Impact Posture	Impact Position	Impact Velocity (m/s)	Total (N)
No Countermeasure	Jumping 1 Standing	Jumping Low (Left Middle Right) Jumping High (Left Middle Right) Standing (Left Middle Right)	8 10 12	54
Front Panels (FP)	Jumping 1 Standing	Jumping Low (Left Middle Right) Jumping High (Left Middle Right) Standing (Left Middle Right)	8 10 12	54
Full Frontal Guard (FFG)	Jumping 1 Standing	Jumping Low (Left Middle Right) Jumping High (Left Middle Right) Standing (Left Middle Right)	8 10 12	54
Rail Guard with FFG (RG+FFG)	Jumping 1 Standing	Jumping Low (Left Middle Right) Jumping High (Left Middle Right) Standing (Left Middle Right)	8 10 12	54

6.3 Results

Figure 6.5 shows the primary and secondary impact HIC_{15} score for each countermeasure concept. Each countermeasure design substantially decreases the median primary impact HIC_{15}. The front panel's design shows a slight increase in secondary contact HIC_{15}; however, only the track guard displays a statistically significant effect (Figure 6.5(b)).

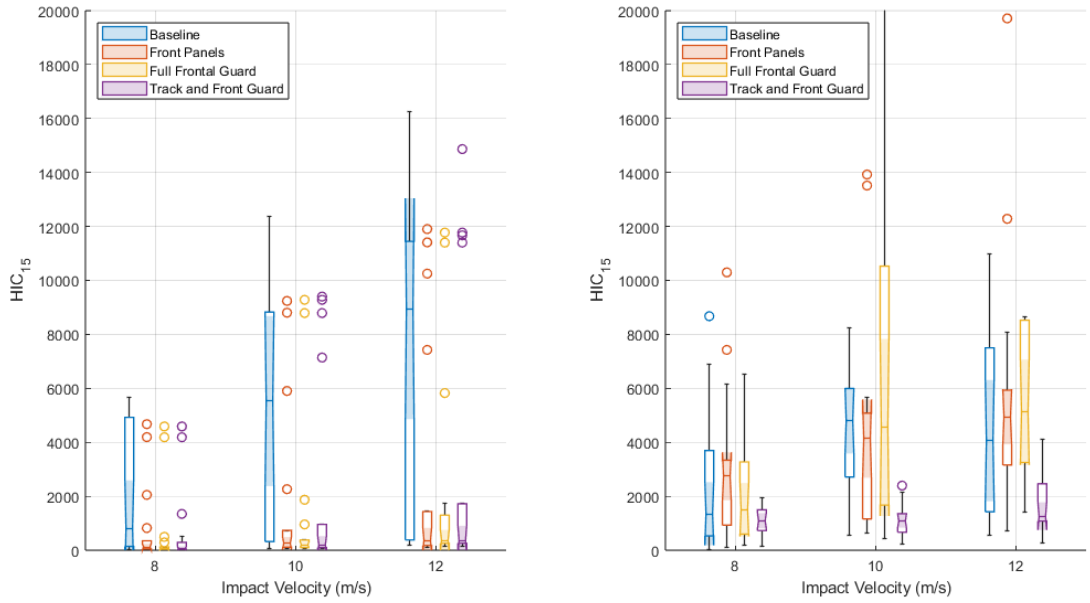

(a) Primary Impact

(b) Secondary Impact

Figure 6.5: Range of HIC_{15} scores for each countermeasure design

Figure 6.6 presents a scatter plot of both primary and secondary HIC_{15} values for each countermeasure concept. Circular and triangular markers indicate standing and jumping postures, respectively, while marker colours represent different impact velocities. The baseline results (6.6(a)) exhibit a wide distribution of HIC_{15} values, whereas the track and front guard configuration (6.6(d)) shows a tighter cluster around lower HIC_{15} values.

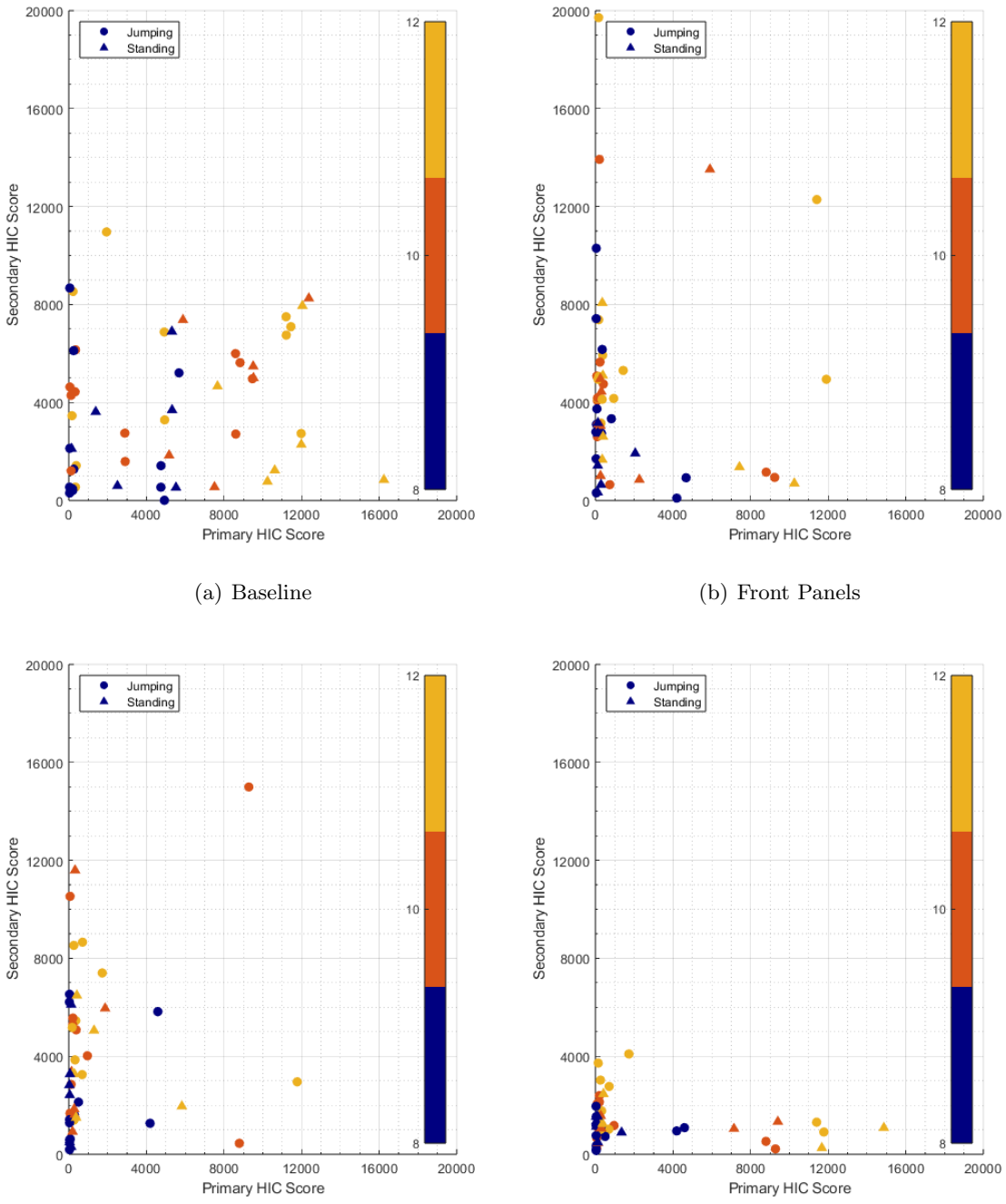

(a) Baseline

(b) Front Panels

(c) Full Front guard

(d) Track and Front Guard

Figure 6.6: HIC_{15} scores for each countermeasure design

Figure 6.7 outlines the effect of each countermeasure design on the risk of contact between the train wheel and pedestrian body region. The risk of contact with the third rail is also shown. The baseline limb to wheel contact score of 0.5 (50%) is reduced to 0.35 with the front panels. This is further reduced to 0.2 with the full front guard, as the effect is greater for standing pedestrians. Surprisingly, the addition of the track guard increased the limb CS to above the baseline risk. This will be further discussed in Section 6.4

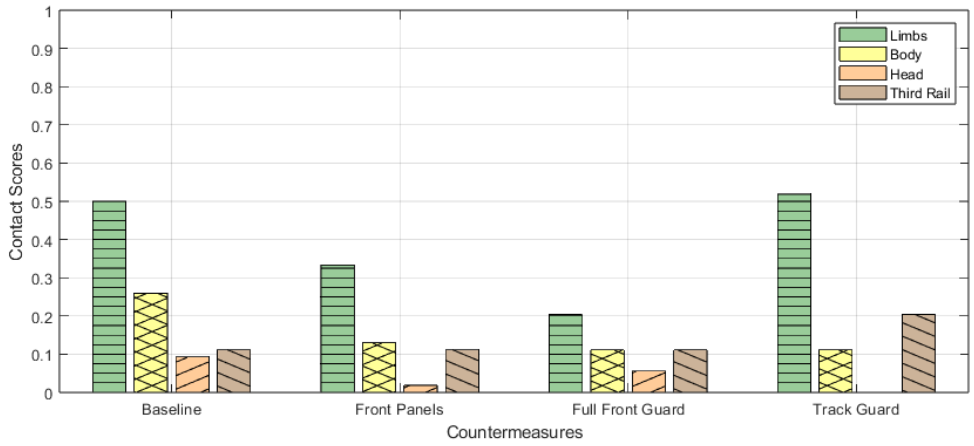

Figure 6.7: Contact scores for each countermeasure deign

Figure 6.8 illustrates the cumulative impact of each countermeasure design on both head injury risk and the likelihood of run-over. Across 54 simulations per countermeasure, the bars indicate the distribution of HIC_{15} scores, categorised according to the EURO NCAP safety scale [Euro, 2018]. The hatched regions highlight the subset of simulations where pedestrians avoid contact with both the train wheels and the third rail.

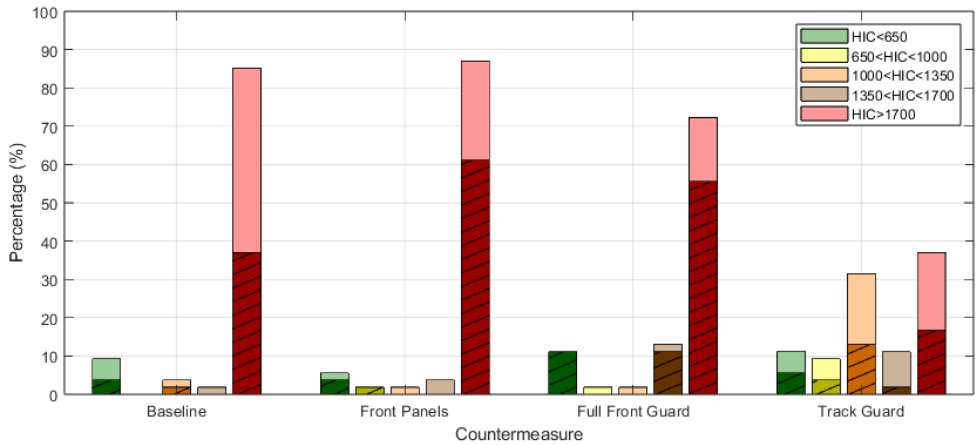

Figure 6.8: Countermeasure effect on head injury and run-over risk [Hatched = No run-over]

6.4 Discussion

6.4.1 Head Injury Risk

Primary Contact

Both the median value and range of primary contact HIC_{15} scores for the baseline subway-to-pedestrian model show a strong velocity dependence. Figure (6.5(a) shows the median primary contact HIC_{15} score increasing by a factor of 10 from an 8m/s to a 12m/s impact. This has also been discussed in Chapter 5 Section 5.7.4. For impacts which use either the front panels or full frontal guard, the median value and magnitude of the velocity dependency are significantly smaller. The front panel countermeasure concept results in an 85% reduction in the median HIC_{15} score at 8m/s, with a 95% reduction in HIC_{15} at 12m/s. While not statistically different to the front panels, the full front guard further decreases the median HIC_{15} by 95% of the baseline at 8m/s. The range of calculated HIC_{15} scores is also much smaller. This is likely due to the increased effectiveness of standing pedestrians who may not have fully contacted the front panel design. As both concepts use the same contact definitions, the expected HIC_{15} score is similar; however, the full frontal guard captures more of the simulated pedestrian postures, resulting in a tighter overall range of HIC_{15} scores. As expected, the rail guard will have no effect on primary contact HIC_{15} scores.

Secondary Contact

The front panels and full frontal guard show no statistical difference on median HIC_{15} scores for secondary contact compared to the baseline model, though in some instances they do increase the overall range of calculated HIC_{15} scores (Figure 6.5(b)). This is likely due to the curvature of the countermeasure altering the fall kinematics of the pedestrian. The rail guard is the only countermeasure concept that produced a statistically significant reduction in secondary contact HIC_{15} score compared to the baseline model. This is expected, as a softer contact stiffness is used for the rail guard compared to ground contact.

Figure 6.6 presents the combined effects of each countermeasure on both primary and secondary HIC_{15} scores. The baseline model (Figure 6.6(a)) reveals a wide distribution of HIC_{15} values for both primary and secondary contacts. In contrast, the front panels and full frontal guard concentrate more values toward the lower end of the primary HIC_{15} axis. However, significant variation remains on the secondary axis, with 87% (Figure 6.6(a)) and 72% (Figure 6.6(c)) of values exceeding the 1700 threshold in either primary or secondary

contact. The combined use of full front panels and a rail guard (Figure 6.6(d)) achieves the most substantial clustering within the target range, with only 38% of values exceeding the HIC_{15} scores threshold of 1750. These results emphasise the importance of addressing both impact types, as reducing primary HIC_{15} scores alone is insufficient to lower the overall fatality risk from ground contact.

6.4.2 Run-Over Risk

The contact score used in this study matches the definition in Chapter 5, representing the ratio of simulations where pedestrian body regions contact train wheels or the third rail. For example, Figure 6.7 shows a baseline limb contact score of 0.5, indicating that 50% of the 54 baseline simulations resulted in at least one limb-wheel contact. This aligns with the baseline score in Chapter 3. Using the front panel countermeasure reduces the limb contact score by 30%, to 0.35, demonstrating that the panel's geometry improves pedestrian fall kinematics to reduce wheel contact. The full frontal guard enhances this effect further by influencing standing pedestrians. Figure 6.9 illustrates the altered kinematics leading to avoided wheel contact.

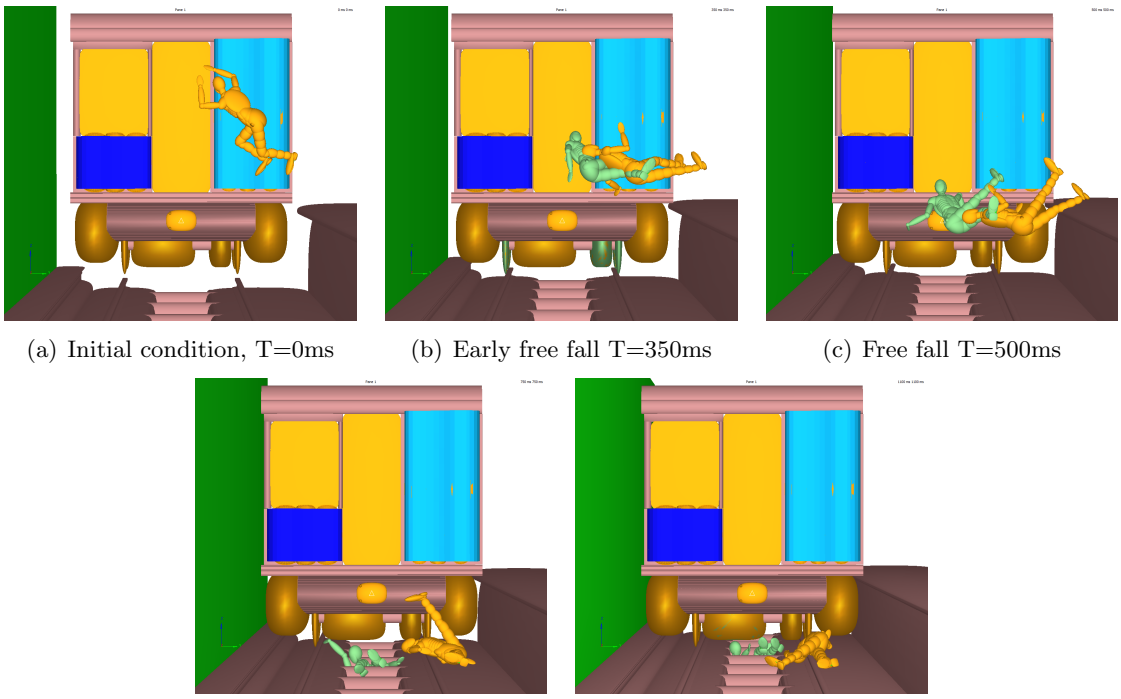

(a) Initial condition, T=0ms (b) Early free fall T=350ms (c) Free fall T=500ms

(d) Secondary contact position T=750ms (e) Run-over position T=1100ms

Figure 6.9: Baseline (yellow) and front panels (green) effect on fall kinematics

The primary objective of the rail guard design was to reduce the secondary contact HIC_{15} scores, which was successfully achieved as illustrated in Figure 6.6(d). An additional goal was to lower overall contact scores by guiding the pedestrian into the drainage trough following secondary contact. The rail guard's geometry (Figure 6.4) was modeled in MADYMO using cylinders positioned over the cross ties, maintaining a 0.1m clearance. Ideally, the curvature of these cylinders would influence pedestrian kinematics so that if a person fell near the track edges, steering them toward the centre and into the drainage trough. However, Figure 6.7 reveals this intended effect was not fully realized. Although there is a modest reduction in body and head contact scores compared to the baseline model, the limb and third rail contact scores are unexpectedly higher. A detailed review of the .kn3 animation files, suggests that the rounded cross tie geometry, combined with a narrower trough from the rail guards, caused pedestrians to rebound upward after ground contact, increasing the risk of wheel impact. This is because the pedestrian's linear velocity remains predominantly horizontal, and the large radius of the rounded cross ties acts like a ramp, propelling the pedestrian upward after contact. An example of this is depicted in Figure 6.10.

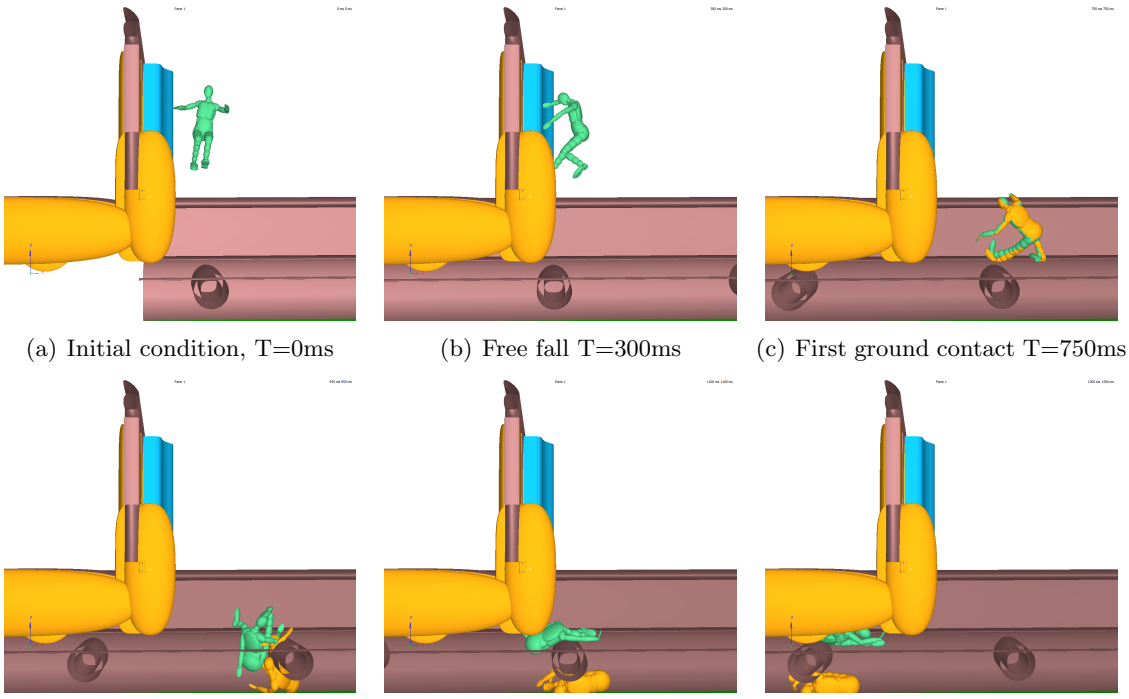

(a) Initial condition, T=0ms (b) Free fall T=300ms (c) First ground contact T=750ms

(d) First crosstie contact T=950ms (e) Run-over position T=1100ms (f) Wheel contact position T=1300ms

Figure 6.10: Baseline (yellow) and rail guard (green) effect on fall kinematics

6.4.3 Overall Fatality Risk

Figures 6.5 and 6.7 demonstrate that while the rail guard can reduce secondary contact head injury risk, it comes at the expense of an increased run-over risk. To evaluate the overall safety impact of each countermeasure design, Figure 6.8 presents the combined effects on head injury and run-over risk. Maximum HIC_{15} scores (from either primary or secondary contact) are grouped and colour-coded based on EURO NCAP pedestrian safety ratings [Euro, 2018], with the bar heights indicating the percentage of simulations (54 per countermeasure) falling within each safety range. As anticipated, the baseline model has a large proportion (85%) of simulations with HIC_{15} scores exceeding 1700. Interestingly, while the front panel design demonstrates a significant reduction in primary contact HIC_{15} scores, the slight increase in median secondary contact HIC_{15} scores results in a marginally higher overall percentage of simulations exceeding the threshold, at 87%. The full frontal guard reduces this proportion to 72%, as more cases achieve HIC_{15} scores below 1700. While Figure 6.6 also reflects this trend, Figure 6.8 provides additional insight by hatching regions to highlight cases without train wheel contact. This distinction emphasizes that reducing head injury risk alone is insufficient for preventing fatalities in severe wheel impact scenarios that lead to decapitation or limb severance. Notably, while the track guard increased the number of wheel contacts, it reduced the overall percentage of HIC_{15} scores exceeding 1700 and slightly outperformed the full front guard when considering cases below the threshold and without wheel contact (23% compared to 22%).

6.4.4 Limitations

There are several limitations in this study that warrant consideration. As highlighted in Chapter 5, the absence of Post-Mortem Human Subject (PMHS) test data necessary for robust model validation limits the analysis to identifying trends rather than interpreting individual simulations. While the use of experimentally derived contact characteristics for countermeasure interactions enhances model reliability, these characteristics were only evaluated at three specific velocities, resulting in a constrained test matrix. This limited scope reduces the strength of comparisons to the epidemiological data from Chapter 3, which includes only 36 cases within the tested velocity range. Nevertheless, this velocity range does capture the most prevalent impact speed of 12m/s. Additionally, only jumping and standing impact postures were modelled, with lying conditions excluded due to operational constraints

involving moving components near the top of the rail. Consequently, the safety benefits assessed in this study are applicable solely to jumping and standing impacts, which account for 70% of frontal subway train-to-pedestrian collisions reported in Chapter 3. Despite these limitations, this research provides the first multibody assessment of passive pedestrian safety countermeasures, effectively covering 70% of impact scenarios and 55% of impact velocities observed in 2019.

6.5 Conclusions

This study set out to design and evaluate the effect of three countermeasure concepts on the primary and secondary contact head injury risk, as well as the run-over risk using contact scores. Each countermeasure concept was designed to minimise head acceleration during the primary contact phase and to modify pedestrian kinematics, guiding them towards a safer secondary contact position to reduce the risk of run-over. The likely manufacturing and maintenance costs range in increasing complexity from the front panel concept to the full frontal guard with rail guards. However, this study aims to act as a proof of concept to encourage future research.

The experimentally derived contact characteristics implemented in each countermeasure enable 0.5m of energy-absorbing material to achieve a significant reduction in primary contact head injury risk, resulting in a 95% decrease in median HIC_{15} scores for 12m/s impacts. Although the effect on secondary contacts is limited, the front guard concept achieves 28% of HIC_{15} scores within a range comparable to automotive safety evaluations, with 10% of cases meeting the maximum safety rating under the EURO NCAP scoring system. When the full front guard is combined with a track guard, this proportion increases substantially, with 63% of maximum HIC_{15} scores falling within the comparable range. In contrast, without these countermeasures, only 14% of impacts achieve scores comparable to those observed in automotive pedestrian collisions.

As well as reducing the head injury risk, the geometric effect of the front panels and full front guard also decreases the risk of pedestrian-to-train and third rail contact. The full frontal guard resulted in a 40% reduction in amputation risk. This improvement was only possible due to the drainage trough. For elevated stations or networks without sufficient space between the rails, the magnitude of this benefit would likely be reduced.

A rail guard was simulated alongside the full front guard concept to decrease the secondary contact HIC_{15} score and while this was achieved, the increase in wheel contacts resulted in an overall similar level of effectiveness compared to the full front guard alone. A balance between reduced head injury risk and increased amputation risk may be a promising area of future research. Medical examiner records and detailed injury reports for surviving pedestrians would greatly aid in this area.

Overall, this study presents the first multibody evaluation of a passive approach to subway pedestrian fatality reduction, which indicates that with 0.5m of allowable space on the train front, both the head impact risk and wheel contact risk have the potential for significant improvement.

Chapter 7

Discussion

7.1 Discussion of Results

7.1.1 Background

The popularity and use of subway and metro systems have been expanding worldwide, with 14 new metro systems between 2018 and 2020, taking the total number to 193 [Brief, 2022]. Alongside this, the rate of pedestrian collisions has been increasing. In the United States of America (USA), the Federal Railroad Administration (FRA) Office of Safety Analysis reports a total of 941 train collisions involving trespassing pedestrians in 2023, a 64% increase in collisions since 2013 [FRA, 2022]. The key areas identified in safety research are epidemiological studies, physical staged tests, computational modelling and safety device design. A comprehensive literature review was conducted regarding each of the above mention areas.

7.1.2 Epidemiology - A Detailed Analysis of New York City Subway Pedestrian Incidents from 2019

The review of epidemiology studies produced a large dataset of subway-to-pedestrian collision statistics from the 1950s to the late 2010s (Chapter 2 Table 2.2). However, there are many confounding factors that make direct comparison between statistics difficult. Fatality rate may be influenced by the inclusion or omission of accidental impacts. The data collection methods, as well as structural and environmental factors such as drainage troughs, have been shown to affect the overall survival rates and injury data. When focused on the NYC Subway directly, the most current available literature was from 2008 [Lin and Gill, 2009]. This paper included a detailed injury analysis; however, biomechanically relevant information such as impact velocity, train front end geometry, and pedestrian initial positions was not fully understood in the literature.

To address this gap and expand on the current biomechanical knowledge of subway-to-pedestrian collisions, 263 PTSB incident reports for the year 2019 were collected and analysed (Chapter 3). At the time of this study (June 2021), 2019 represented the last typical year as the NYC Subway saw a 95% reduction in ridership during the Covid-19 pandemic. This study was able to update the current literature regarding the age, sex, and geographical distribution of subway-to-pedestrian collisions in NYC, which showed no substantial change since 1990.

Significant new insights into the nature of these events are outlined and explored in Chapter 3. The fatality rates differed greatly between accidental (25%) and suicidal (42%)

collisions, which further highlights the need for careful comparison between fatality rates in the literature, as those which focus only on suicidal impacts will skew the reported fatality rates. The three frontal impact conditions (Standing, Mid Jump, Lying) occurred at relatively similar frequencies (Figure 3.5), though mid-jump cases had the highest fatality rates (43%). Unsurprisingly, a positive correlation was found between impact velocity and fatality. The most common impact velocity was 40-47km/hr or 25-29mph however, even at lower velocities, fatalities are still possible due to the risk of run-over or electrocution by the third rail (figure 3.6(a)). The most common train model involved in collisions was the Kawasaki R160, with 97% of cases occurring within 60m of the platform.

The results from this study, which are published in the Transportation Research Record Journal of Transportation Research Board [Hall et al., 2023], provide future biomechanical accident reconstruction/modelling studies with the proportion of impact velocities, pedestrian positions, and expected fatality rates for each position. There are limitations to this study, such as the lack of available medical records; however, this data can provide the first foundational step towards subway-to-pedestrian model validation.

7.1.3 Impact Testing - Experimentally Derived Contact Characteristics for Hard Shell Energy Absorbing Material: Application to subway-to-pedestrian Collisions

Staged automotive road vehicle testing, using PMHS or ATDs, has often been employed to validate computational models, as demonstrated in studies such as [DeLange et al., 2007, EEVC, 1998b, Ishikawa et al., 1993a, Kajzer et al., 1993, Yang et al., 2000]. However, the literature review revealed no full-scale, staged PMHS or ATD subway-to-pedestrian impact tests. The closest relevant research utilised a non-instrumented HYBRID III Dummy for a surface-level tram pedestrian impact [Lopot et al., 2019]. The lack of available test data for validation is a significant limitation for future computational studies.

For multibody simulations using contact stiffness models, the equivalent stiffness K_{eq} for two springs in series K_a and K_a is given by Equation 7.1. When one spring is significantly stiffer than the other ($K_a >> K_b$) the equivalent stiffness approximates the stiffness of the softer spring, as shown in Equation 7.2. In subway-to-pedestrian simulations without a countermeasure, where the subway train front is assumed to be infinitely rigid compared to the pedestrian, the effective contact stiffness is determined by the MADYMO ellipsoid model's contact characteristics.

$$K_{eq} = \frac{K_a K_b}{K_a + K_b} \tag{7.1}$$

where $K_a >> K_b$

$$K_{eq} \approx \frac{K_a K_b}{K_a} = K_b \tag{7.2}$$

This approximation is not the case; however, once a softer train front countermeasure is introduced. While the exact countermeasure design was unknown during the conception of this study, the general principle of reducing head acceleration through softer contact stiffness and larger penetration was understood. It was also accepted that a soft energy-absorbing countermeasure must also be wrapped in a stiffer outer shell to protect against general wear and tear. To increase confidence in future multibody models, a specific contact characteristic was experimentally derived in this study (Chapter 4).

A headform impactor was propelled at velocities of 7.5, 10, and 11.5m/s using a DYNATEST-500 impact ram, with the acceleration pulse during contact with various EACs recorded. Figure 4.20 presents the acceleration data for each test, while Figure 4.23 illustrates the derived force-penetration relationships. The results indicate that EACs covered with a 1mm aluminium or 3mm ABS shell exhibit a higher initial contact stiffness compared to pure foam EACs. As the shell deforms, the stiffness decreases, after which the response aligns with that of pure foam. This initial increase in force at lower penetration values leads to higher peak accelerations at low impact velocities (Figure 4.20(a)) but reduces overall penetration depth. Conversely, due to the reduced penetration, the hard shell helps lower the overall peak acceleration during higher velocity impacts as the peak force caused by the shells is less than the peak force experienced at high strain regions. The effectiveness of these designs should be evaluated in the context of typical impact velocities; for instance, Chapter 3 identifies 12m/s as the most common impact speed in 2019. The derived force penetration characteristics were used in MADYMO to recreate the acceleration time histories shown in Figure 4.26. The addition of a hysteresis slope and unloading curve help to increase the accuracy of the falling edge of the acceleration time history 4.26.

The findings of this study demonstrate that a hard shell surrounding an energy-absorbing material can either increase or decrease the peak acceleration of a headform, contingent on the impact velocity and penetration depth. It also highlights the significant viscoelastic effects on contact stiffness and the need for specific force penetration curves for each im-

pact velocity. This could not have been predicted through multibody modelling methods alone. Preliminary tests, video analysis and subsequent testing prior to the completion of this study indicate minimal rotational effects during the loading phase (Appendix D Figure D.1). Future impact tests incorporating tri-axial accelerometers and gyroscopes may offer deeper insights into potential rotational dynamics, particularly during the unloading phase. The contact characteristics derived from this research have been directly integrated into the multibody modelling presented in Chapter 6, thereby enhancing the reliability of that study's conclusions. Beyond subway-to-pedestrian safety, this work holds relevance for automotive pedestrian countermeasures, such as pop-up hoods, which raise the bonnet during a collision to allow greater penetration before the pedestrian encounters high-strain-related stiffness [Ames and Martin, 2015]. In line with this chapter's methodology, future studies aimed at optimising the balance between initial stiffness and overall penetration could further reduce head accelerations and consequently lower the risk of head injuries.

7.1.4 Computational Modelling - Drainage Troughs as a Protective Measure in subway-to-pedestrian Collisions: A Multibody Model Evaluation

A literature review found no subway-to-pedestrian impact computational model. While computational modelling studies have been conducted that focus on surface-level tram-to-pedestrian collisions [Chevalier et al., 2019, Grzebieta and Rechnitzer, 2000], the ground contact mechanisms either involve a flat surface or are ignored. For subway-to-pedestrian collisions, the complexity of the ground contact mechanism is an important factor due to the presence of the live electrical third rail, crossties, and run-over risk from the train, which has a much slower deceleration compared to trams. It has long been thought that the drainage trough, a channel between the rails, would decrease the risk of run-over related injuries due to the additional space to avoid wheel contact [Coats and Walter, 1999, O'Donnell and Farmer, 1994a, 1992]. However, as this was based only on empirical findings and due to confounding factors, no quantifiable evidence of any safety benefit has been reported [Barker et al., 2017]. To address this gap in the literature as well as offer a new quantifiable insight into the effect of the drainage trough on pedestrian run-over risk, a subway train-to-pedestrian multibody model was created in Chapter 5.

Based on findings that 83% of incidents involved males with an average age of 40 years (Chapter 3), the MADYMO 50th percentile male (AM50) ellipsoid pedestrian model was

employed. As described earlier in Section 7.1.3, the existing contact characteristics of the pedestrian model were used, while the train front was treated as infinitely rigid in comparison. The AM50 head contact properties were adjusted to align with recent PMHS test data [Shi et al., 2018b]. To accurately reconstruct pedestrian postures, video footage sourced from publicly available online platforms was analysed, capturing people jumping across or standing on train tracks. Although no impacts were observed, these postures were recreated in MADYMO using KinePose [Gildea et al., 2022]. Two types of track geometries—representing a typical elevated station (without crossties) and an underground station (with crossties)—were modelled. The resulting test matrix consisted of 1920 unique input conditions, each of which was then weighted against the frequency of those particular conditions according to Chapter 3. This weighting showed little overall change in the conclusions drawn from the results. While the initial conditions reflect recent location-specific epidemiological data, pedestrian collisions with subway trains are a global issue. Expanding the modelling approach to incorporate data from other subway systems could yield even broader safety benefits.

Although the epidemiological data from Chapter 3 does not include detailed injury analysis due to the absence of available medical records, the findings indicate that 50% of pedestrian impact cases result in either fatality or incapacitating injury requiring immediate hospitalisation. This figure may serve as an upper limit when accounting for amputations. The results of this study suggest that, with no modifications to drainage trough depth, the risk of amputation during a subway train to pedestrian collision stands at 59% (Figure 5.11), indicating a possible slight overestimation. This overestimation is likely influenced by the placement of the lying pedestrians (Figure 3.5), as this posture yielded the highest contact scores (Figure 5.10), compounded by the passive nature of the models. At lower impact velocities, the potential effect of active avoidance maneuvers is greater, which would not be represented in a numerical model. Primary contact head injury risk increased with impact velocity, whereas secondary contact risk showed less dependence on velocity above 10m/s. In contrast, the contact score demonstrated no dependency on impact velocity beyond 4m/s (Figure 5.12). The drainage trough was shown to significantly decrease the run-over risk by 40% up to a depth of 0.5m, without any statistical increase in head injury risk (Figures 5.15 & 5.16).

The findings from this study provide critical insights into subway pedestrian collisions that are difficult or impossible to obtain through empirical or epidemiological methods alone.

Prior to this work [Hall et al., 2024], no subway-to-pedestrian baseline model has been available in academic literature. Notably, the analysis suggests that contact score remains unaffected by impact velocities above 4m/s. This insight implies that policies focused solely on reducing train entry speeds may have limited impact on mitigating the risk of fatal run-over injuries. Instead, a comprehensive approach must consider three interrelated factors: primary contact injury, secondary contact injury, and the risk of run-over or third rail contact. The study demonstrates that a trough depth of 0.5m is adequate to contain pedestrians and prevent wheel contact. Further research into the influence of both trough width and depth could establish important design criteria for future subway system construction or upgrades. Additionally, the baseline injury risks and data presented here can serve as a benchmark for assessing the effectiveness of future countermeasures. Moreover, comparing these results with baseline models from other systems, such as the London Underground, could reveal previously unrecognised factors influencing pedestrian fatality risk.

7.1.5 Safety Device Design - subway-to-pedestrian Collision Safety: Multibody Models of Energy Absorbing Countermeasure Designs

A review of the literature revealed no academic studies specifically addressing passive subway-to-pedestrian impact mitigation, though related research has examined energy-absorbing front ends for heavy goods vehicles [Feist et al., 2009, Lakshminarayana et al., 2011, Mitra et al., 2018]. As noted, however, these studies do not address the unique challenges of run-over risk, third rail hazards and track geometry specific to subway environments. Consequently, this final study (Chapter 6) combines the findings from Chapters 3 to 5 to design and evaluate three concepts for mitigating pedestrian fatalities in subway impacts. A new simulation matrix incorporates each countermeasure along with a baseline model, covering a single track type, three impact velocities, and two pedestrian positions (jumping and standing), resulting in a total of 216 simulations (Table 6.1). The initial conditions are informed by Chapter 3; countermeasure contact characteristics are derived in Chapter 4, and the subway-to-pedestrian multibody model is developed in Chapter 5. Each countermeasure concept and its estimated effectiveness are discussed separately below:

Front Panels

The first EAC concept involves modular front panels mounted directly to the front of the train using existing attachment points currently designated for handrails. These panels are

designed to cover the entire train front down to the anticlimber, leaving adequate clearance for the emergency exit door. The geometry features two curved arcs, with radii of 0.15m (inner edge) and 0.3m (outer edge), providing a minimum penetration depth of 0.3m before contact with the train front. The contact characteristics of the EAC, based on aluminium-covered materials detailed in Chapter 4, are used for modelling.

By incorporating a larger radius curve on the outer edge of the panels, this design aims to redirect the pedestrian's kinematics toward the centre of the track during a free fall, as illustrated in Figure 6.9. For this countermeasure, the limb contact score decreased from 50% in the baseline model to 35%. The HIC_{15} score, using a threshold of 1700 based on the EURO NCAP pedestrian safety scoring system [Euro, 2018], showed a substantial improvement. However, while the primary HIC_{15} score has significantly reduced, the secondary contact HIC_{15} showed a slight increase (Figure 6.8).

While this countermeasure significantly impacts the safety of jumping pedestrians, its effectiveness for standing pedestrians is limited. This is because the area between the countermeasure and the train wheels remains unchanged, leaving standing pedestrians vulnerable.

Full Frontal Guard

The second EAC concept builds upon the modular front panel design by extending the protective coverage vertically, leaving only a 0.2m clearance from the bottom edge to the top of the rail. Additionally, an angled panel is strategically placed over the coupler in the centre of the train, sloped at 45 degrees to further guide the pedestrian into the drainage trough, as depicted in Figure 6.3. This extended design is anticipated to offer a significant improvement in safety, especially for standing pedestrians, who are now more effectively captured by the softer front surface of the train.

Despite these safety benefits, the design introduces new operational challenges. Covering critical components such as the anticlimber and coupler raises concerns, particularly because there are no obvious mounting points for panels positioned below the anticlimber. Nevertheless, the purpose of this study is to serve as a proof of concept, demonstrating the potential of such designs if operational constraints can be addressed. Future research will be necessary to evaluate the practicality of these designs in real-world scenarios, but this study marks an important initial step toward that goal.

Compared to the front panel concept, the full frontal guard design shows a marked increase in effectiveness across all measured outcomes. The risk of limb amputation is reduced from

50% in the baseline model to 20%, a significant improvement over the 35% risk achieved with the front panels alone. Additionally, the percentage of simulations where the HIC_{15} score falls below the safety threshold of 1700 increases from 15% in the baseline model to 28% (Figure 6.8).

Combined Full Frontal Guard with Rail Guard

To directly address the risk of secondary contact head injuries, the third countermeasure concept integrates the full frontal guard with an additional rail guard. This rail guard is mounted on top of the existing track environment and features rounded edges to cover the crosstie edges and rail mounting blocks, maintaining a 0.1m clearance between them. The contact characteristics for this design are modelled similarly to a pedestrian leg's interaction with a car bumper, as referenced in [Shang et al., 2021]. The geometry of the rail guard was specifically designed to further direct pedestrian kinematics into the drainage trough. The goal of this analysis was to evaluate the potential of rail guards to reduce secondary contact HIC_{15} scores and mitigate the risk of run-over injuries, with the anticipation that future research could optimise the design.

The simulation results reveal a notable increase in the percentage of HIC_{15} scores below the safety threshold of 1700, rising from 28% with the full frontal guard alone to 63% with the added rail guard. This improvement clearly correlates with a reduction in secondary contact head injury risk, as depicted in Figure 6.8. However, an unexpected outcome was observed: the risk of limb amputations from wheel contact increased to 55%, surpassing even the baseline model's 50% risk. A detailed analysis of the fall kinematics indicated that the combination of the rail guard's curvature and the reduced trough width caused pedestrians to bounce and slide back into the train's path due to their predominantly horizontal velocity (Figure 6.10). While this design successfully reduces head injury risk, it also increases the likelihood of run-over fatalities.

7.2 Limitations

There are several limitations to the work presented in this thesis, primarily concerning model validation, which could be addressed through additional studies in the future. In Chapter 3, the absence of detailed medical examiner records and specific injury data—commonly used in previous studies like [Lin and Gill, 2009], hampers the depth of comparison possible between

epidemiological findings and modelling results. Efforts are ongoing to secure these records from the 2019 PTSB reports for future analysis, which could enrich the findings in Chapters 3 & 5. The epidemiological study was conducted during the Covid-19 pandemic. Using the most up to date data would lead to skewed results from global lockdowns and travel restrictions. Therefore, only 2019 data was reviewed to avoid these anomalies. Preliminary analyses using 2018 data yielded similar results, but a broader review covering multiple years would strengthen the study's conclusions.

Additionally, the lack of staged tests involving PMHS or ATDs with subway systems necessitated a reliance on observed trends rather than individual simulation outcomes. Sensitivity analyses exploring the effect of variables like hysteresis slopes and damping forces revealed effects on individual Contact Scores but did not alter the key conclusions, such as the reduction of Contact Scores with increased pit depth. The models employed in this study feature a single train front (R160) and a 50th percentile male pedestrian model (AM50). Given the global nature of subway-pedestrian collision risks, future research should consider a wider array of train and pedestrian models to enhance the representation of the results.

The countermeasure contact characteristics were derived from the force-penetration curves experimentally obtained in Chapter 4. Ideally, full-scale staged testing using PMHS subjects would be performed, but this was beyond the scope of this thesis. Within the existing setup, the absence of a fully instrumented pedestrian dummy head equipped with a tri-axial accelerometer and gyroscopes limited the accuracy of the data. The countermeasure designs presented are proof-of-concept models, with minimal consideration given to installation or maintenance complexities beyond a protective shell. However, addressing such practical implementation concerns of full sized countermeasures falls outside the primary objectives of this study.

7.3 Addition To Known Literature

Notwithstanding the limitations outlined above, this thesis has made significant contributions to the existing body of knowledge. It provides substantial new epidemiological data and introduces the first comprehensive subway-to-pedestrian baseline model, along with a quantifiable assessment of the safety benefits of drainage troughs. Efforts are currently underway to synthesise the findings from Chapters 5 and 6 into an additional journal publication,

which will further highlight the impact and relevance of this work. Figure 7.1 illustrates the contributions made in the context of the literature review findings summarised in Figure 2.29.

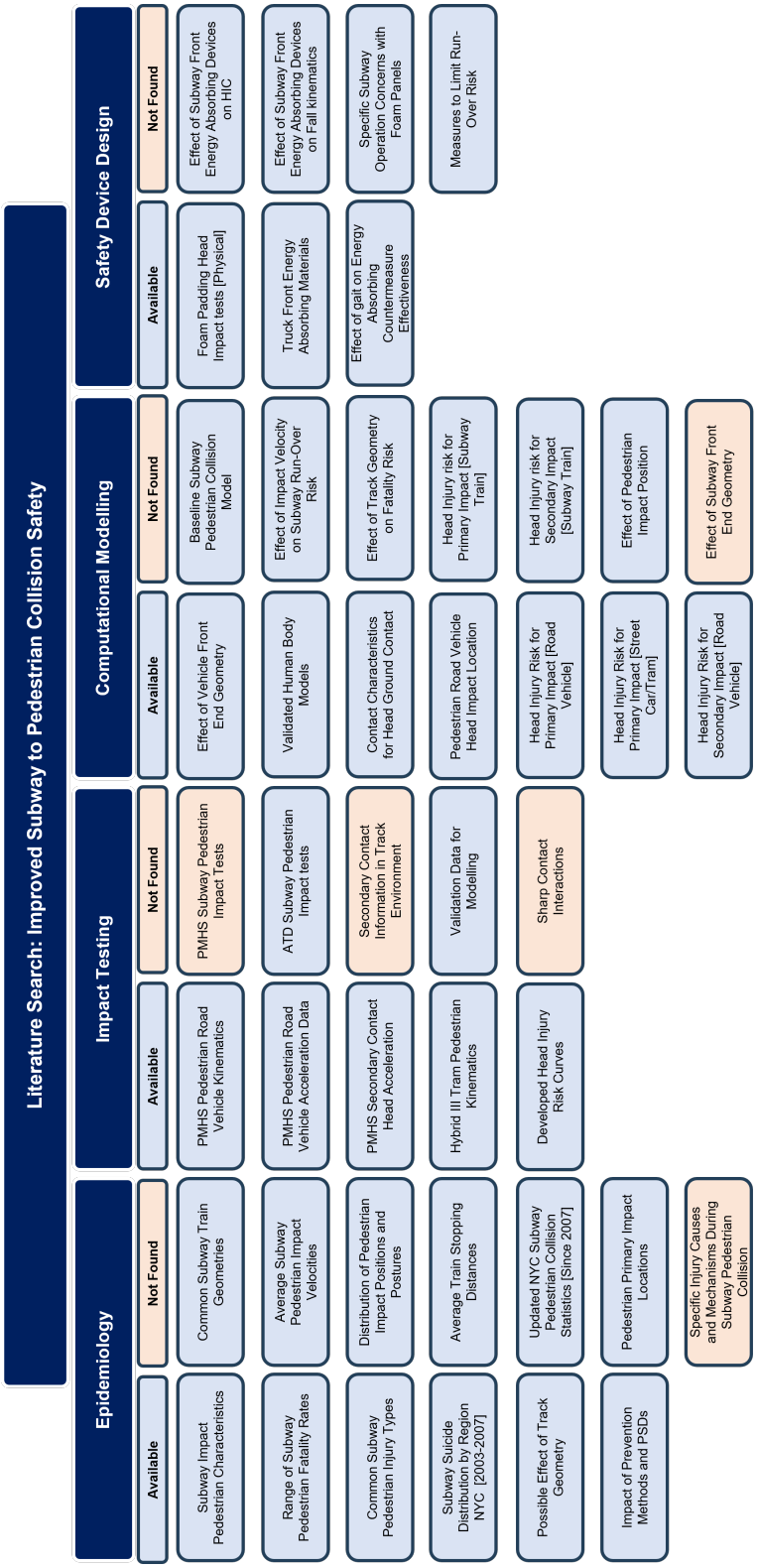

Figure 7.1: Summary of literature review findings

Chapter 8

Conclusions

8.1 Main Conclusion

The objectives set out by this thesis involved contributing to the overall understanding of subway pedestrian collisions across four biomechanical safety research methodologies (Chapter 1). The main conclusions from each of these contributions are listed below:

Epidemiology

This thesis highlights that for the NYC subway system, the sex and geographical distribution of subway-to-pedestrian incidents have remained largely unchanged since the early 1990s. Interventions and policies focusing on areas within 60m of the platform could address 97% of such incidents, underscoring the critical need for targeted safety measures in these zones. The most common collision type involved contact with the train front, occurring across standing, mid-jump, and lying positions at similar rates. Contact with the train edge, often due to pedestrians standing too close or walking into the side of a moving train, was the second most frequent impact type. Although this category had the lowest fatality rate, it did include some fatal cases, emphasising the need for preventive strategies. Impact velocities in these incidents ranged from 2–20m/s (5–45mph), with fatalities increasingly likely at higher speeds but still present at low speeds. The most frequently observed velocity was 12m/s (25mph), providing a crucial benchmark for modelling efforts. These findings provide invaluable baseline data for developing representative models of subway-to-pedestrian collisions and inform future research into mitigation strategies.

Impact Testing

The absence of relevant subway-to-pedestrian force penetration data in the academic literature underscores a critical gap in validation data for modelling efforts. While it can be assumed that the effective stiffness during a collision with a rigid train front is predominantly influenced by pedestrian contact stiffness, the introduction of softer energy-absorbing countermeasures complicates this assumption. To address this, contact characteristics for three countermeasure types were experimentally derived at velocities of 7.5, 10, and 11.5m/s. These force-penetration relationships enabled accurate replication of experimental acceleration time histories using MADYMO, thereby strengthening confidence in its application to baseline models. These findings contribute to the foundational understanding needed for designing and evaluating effective subway-to-pedestrian collision countermeasures.

Baseline Model

Taking into account the variability of impact conditions, including velocity, track types, pedestrian posture, and impact position, this study introduced a baseline multibody model for subway-to-pedestrian impacts. The model highlighted a significant risk of wheel contact during run-over, which was found to be independent of train entry velocity. As such, policies solely focused on reducing entry speed would likely have minimal impact on mitigating these injuries. This chapter also demonstrated the substantial safety benefits of drainage troughs, showing a 50% reduction in limb amputations with the implementation of a 0.5m deep trough. These findings confirm the life-saving potential of such features, colloquially referred to as "suicide pits." To improve overall pedestrian safety, efforts should address the three primary injury mechanisms identified: primary contact, secondary contact, and wheel/third rail contact.

Countermeasure Design Concepts

Two countermeasure concepts were developed to address the risks of primary impact and run-over injuries in subway-to-pedestrian collisions. Simulations demonstrated that modular panels attached to the train front significantly reduced both head injury risk (90%) and the risk of contact between the train wheels and pedestrian (58%), with increased effectiveness when covering a larger frontal area. A third concept, the rail guard, showed promise in lowering secondary contact injury risk but inadvertently increased run-over and amputation risks due to altered pedestrian kinematics. Among the designs tested, the full frontal guard combined with the track guard emerged as the most effective countermeasure, offering a slightly greater overall safety benefit compared to the full front guard alone. These findings suggest that a well-designed, energy-absorbing countermeasure with a depth of 0.5m could substantially reduce the lethality of subway-pedestrian collisions. Future research and development should prioritise optimising such designs for practical implementation and operational feasibility.

8.2 Future Work

Model validation represents a critical area for future research. Staged tests, which are standard practice in biomechanical safety research for automotive pedestrian safety, are notably absent for subway-to-pedestrian collisions. As highlighted in Chapter 2, the lack of PMHS and ATD impact data for subway scenarios limits the validation of current models. Future efforts to obtain such data would significantly enhance the accuracy and reliability of subway-to-pedestrian impact studies. In addition, future epidemiological studies incorporating detailed medical examiner records and injury data from surviving pedestrians could provide valuable insights for model validation. Subway-to-pedestrian collisions are a global issue, and comparative analyses across diverse cultural and infrastructural contexts could uncover previously unrecognised trends or risk factors.

While Chapter 3 identified grazing the side of the train from the platform as a frequent but underexplored collision type, this thesis did not directly address countermeasures for such scenarios. Although these incidents typically result in lower fatality rates, severe injuries are still possible. Developing countermeasure designs specifically targeted at preventing side collisions would be an important step towards improving overall pedestrian safety.

Finally, Chapter 6 explored three countermeasure concepts for injury mitigation but did not address the practical challenges of maintenance and operational feasibility. Optimising these designs for real-world application, balancing safety benefits with practical considerations, should be a priority for future research to transition these concepts from academic theory to actionable solutions.

8.3 Final Statement

The overarching aim of this research was to challenge the notion that improving pedestrian safety in subway collisions is an insurmountable challenge due to the massive size and weight of these vehicles. This work demonstrates that meaningful reductions in fatalities are possible, even with just 0.5m of available space on the train front. While this study has limitations and identifies areas for further improvement, it ultimately concludes that subway-to-pedestrian fatalities are preventable. Continued research in this field holds the potential to save lives that might otherwise be deemed unsavable.

Bibliography

FRA, administration, f.r., 3.02 - Accident Trends - Charts & Graphs, fra, editor. 2022., 2022. URL `https://safetydata.fra.dot.gov/officeofsafety/publicsite/graphs.aspx`.

World health organisation, death on the roads, 2022. URL `https://extranet.who.int/roadsafety/death-on-the-roads/#ticker/all_road_users`.

R. Alexandrescu, S. J. O'Brien, and F. E. Lecky. A review of injury epidemiology in the uk and europe: some methodological considerations in constructing rates. *BMC public health*, 9:1–22, 2009.

J. Almeida, C. Barber, R. K. Rosen, A. Nicolopoulos, and K. H. M. O'Brien. "in the moment i wanted to kill myself, and then after i didn't": A qualitative investigation of suicide planning, method choice, and method substitution among adolescents hospitalized following a suicide attempt. *Youth & Society*, 55(1):29–43, 2023.

E. Ames and P. Martin. Pop-up hood pedestrian protection. In *Materiały 24 Miedzynarodowej Konferencji ESV. Pobrane z: http://www-esv. nhtsa. dot. gov/Proceedings/24/isv7/main. htm (dostep: 24.06. 2022 r.)*, 2015.

C. Arregui-Dalmases, J. R. Kerrigan, D. Sanchez-Molina, J. Velazquez-Ameijide, and J. R. Crandall. A review of pelvic fractures in adult pedestrians: experimental studies involving pmhs used to determine injury criteria for pedestrian dummies and component test procedures. *Traffic Injury Prevention*, 16(1):62–69, 2015.

S. Azami-Aghdash, H. Sadeghi-Bazargani, H. Shabaninejad, and H. A. Gorji. Injury epidemiology in iran: a systematic review. *Journal of Injury and Violence Research*, 9(1):27, 2017.

A. Badea-Romero and J. Lenard. Source of head injury for pedestrians and pedal cyclists: Striking vehicle or road? *Accident Analysis & Prevention*, 50:1140–1150, 2013.

S. P. Baker and B. O'Neill. The injury severity score: an update. *Journal of Trauma and Acute Care Surgery*, 16(11):882–885, 1976.

F. Bandak, R. Eppinger, M. Haffner, N. Khaewpong, S. Kuppa, M. Maltese, T. Nguyen, R. Saul, E. Sun, E. Takhounts, et al. Development of improved injury criteria for the assessment of advanced automotive restraint systems: Ii. 1999.

E. Barker, K. Kolves, and D. De Leo. Rail-suicide prevention: Systematic literature review of evidence-based activities. *Asia-Pacific Psychiatry*, 9(3):e12246, 2017.

A. L. Berman, A. Athey, and P. Nestadt. Effectiveness of restricting access to a suicide jump site: a test of the method substitution hypothesis. *Injury prevention*, 28(1):90–92, 2022.

S. Brief. World metro figures 2021. 2022.

R. Buehler and J. Pucher. The growing gap in pedestrian and cyclist fatality rates between the united states and the United Kingdom, Germany, Denmark, and the Netherlands, 1990–2018. *Transport reviews*, 41(1):48–72, 2021.

C. Cavallero, D. Cesari, M. Ramet, P. Billault, J. Farisse, B. Seriat-Gautier, and J. Bonnoit. Improvement of pedestrian safety: influence of shape of passenger car-front structures upon pedestrian kinematics and injuries: evaluation based on 50 cadaver tests. Technical report, SAE Technical Paper, 1983.

A. Chawla, D. Mohan, V. Sharma, and J. Kajzer. Safer truck front design for pedestrian impacts. *Journal of Crush Prevention and Injury Control*, 2(1):33–43, 2000.

M.-C. Chevalier, D. Brizard, and P. Beillas. Study of the possible relationships between tramway front-end geometry and pedestrian injury risk. *Traffic Injury Prevention*, 20(1): 107–113, 2019.

Y. W. Chung, S. J. Kang, T. Matsubayashi, Y. Sawada, and M. Ueda. The effectiveness of platform screen doors for the prevention of subway suicides in south korea. *Journal of Affective Disorders*, 194:80–83, 2016a.

Y. W. Chung, S. J. Kang, T. Matsubayashi, Y. Sawada, and M. Ueda. The effectiveness of platform screen doors for the prevention of subway suicides in south korea. *Journal of Affective Disorders*, 194:80–83, 2016b.

T. Coats and D. Walter. Effect of station design on death in the london underground: observational study. *BMJ*, 319(7215):957–957, 1999.

R. A. Cocks. Study of 100 patients injured by london underground trains 1981-6. *British Medical Journal (Clinical research ed.)*, 295(6612):1527, 1987.

C. P. Compton. Injury severity codes: A comparison of police injury codes and medical outcomes as determined by nass cds investigators. *Journal of Safety Research*, 36(5), 2005.

G. Crocetta, S. Piantini, M. Pierini, and C. Simms. The influence of vehicle front-end design on pedestrian ground impact. *Accident Analysis & Prevention*, 79:56–69, 2015a.

G. Crocetta, S. Piantini, M. Pierini, and C. Simms. The influence of vehicle front-end design on pedestrian ground impact. *Accident Analysis & Prevention*, 79:56–69, 2015b.

G. Crocetta, S. Piantini, M. Pierini, and C. Simms. The influence of vehicle front-end design on pedestrian ground impact. *Accident Analysis & Prevention*, 79:56–69, 2015c.

M. S. Daigle. Suicide prevention through means restriction: Assessing the risk of substitution: A critical review and synthesis. *Accident Analysis & Prevention*, 37(4):625–632, 2005.

R. DeLange, L. VanRooij, R. Happee, and X. Liu. Validation of human pedestrian models using laboratory data as well as accident reconstruction. In *2nd International Conference on ESAR "Expert Symposium on Accident Research"*, pages 186–193, Germany, 2007. Bundesanstalt für Straßenwesen (BASt). Additional collaboration with TNO Automotive China.

EEVC(1998b). Pedestrian protection - synthesis of experimental and simulation researches performed in france. *INRETS*, 1998.

H. O. Eid and F. M. Abu-Zidan. Pedestrian injuries-related deaths: a global evaluation. *World Journal of Surgery*, 39:776–781, 2015.

J. Elliott, C. K. Simms, and D. P. Wood. Pedestrian head translation, rotation and impact velocity: The influence of vehicle speed, pedestrian speed and pedestrian gait. *Accident Analysis & Prevention*, 45:342–353, 2012.

E. U. A. f. R. ERA. Report on railway safety and interoperability in the eu, 2018.

N. Euro. European new car assessment programme (euro ncap), pedestrian testing protocol. Technical report, Version 8.5. Tech. Rep. October, European New Car Assessment Programme, 2018.

W. R. Fan. Head impacts with roof-pillar support structures-problem identification. Technical report, SAE Technical Paper, 1983.

F. Feist, J. Gugler, C. Arregui-Dalmases, E. Del Pozo de Dios, F. López-Valdés, D. Deck, and R. Willinger. Pedestrian collisions with flat-fronted vehicles: injury patterns and importance of rotational accelerations as a predictor for traumatic brain injury (tbi). In *21st International Technical Conference on the Enhanced Safety of Vehicles (ESV)*, pages 15–18, 2009.

Foam2Home. Foam cut to size. URL `https://www.foam2home.ie/product-category/foam-cut-to-size/?_gl=1*1rjdbdt*_up*MQ..*_gs*MQ..&gclid=Cj0KCQiA0fu5BhDQARIsAMXUBOK9ThnPKqR751irzz92TFe-khsfVv_FSDkzFEcxXT-91ccHBeatHe4aAvMYEALw_wcB`. Accessed: 2024-11-21.

M. Franklyn and S. Laing. Evaluation of military helmets and roof padding on head injury potential from vertical impacts. *Traffic Injury Prevention*, 17(7):750–757, 2016.

M. Frérot, A. Lefebvre, S. Aho, P. Callier, K. Astruc, and L. S. Aho Glélé. What is epidemiology? changing definitions of epidemiology 1978-2017. *PloS one*, 13(12):e0208442, 2018.

C. W. Gadd. Use of a weighted-impulse criterion for estimating injury hazard. Technical report, SAE technical paper, 1966.

M. S. Gaylord and D. Lester. Suicide in the hong kong subway. *Social Science & Medicine*, 38(3):427–430, 1994.

R. R. Gershon, J. M. Pearson, V. Nandi, D. Vlahov, A. Bucciarelli-Prann, M. Tracy, K. Tardiff, and S. Galea. Epidemiology of subway-related fatalities in new york city, 1990-2003. *Journal of safety research*, 39(6):583–588, 2008a.

R. R. Gershon, J. M. Pearson, V. Nandi, D. Vlahov, A. Bucciarelli-Prann, M. Tracy, K. Tardiff, and S. Galea. Epidemiology of subway-related fatalities in new york city, 1990-2003. *Journal of safety research*, 39(6):583–588, 2008b.

K. Gildea, C. Mercadal-Baudart, R. Blythman, A. Smolic, and C. Simms. Kinepose: A temporally optimized inverse kinematics technique for 6dof human pose estimation with biomechanical constraints. *arXiv preprint arXiv:2207.12841*, 2022.

R. H. Grzebieta and G. Rechnitzer. Tram interface crashworthiness. In *Proceedings of the International Crashworthiness Conference-ICRASH*, 2000.

F. G. Guggenheim and A. D. Weisman. Suicide in the subway: publicly witnessed attempts of 50 cases. *The Journal of Nervous and Mental Disease*, 155(6):404–409, 1972.

E. S. Gurdjian. Intracranial pressures and acceleration accompanying head impacts in human cadavers. *Surg Gynec Obstet*, 113:185, 1961.

E. S. Gurdjian, V. Roberts, and L. M. Thomas. Tolerance curves of acceleration and intracranial pressure and protective index in experimental head injury. *Journal of Trauma and Acute Care Surgery*, 6(5):600–604, 1966.

D. Hall, J. Linogao, L. Zentz, G. Shaw, T. Lamb, and C. Simms. Detailed analysis of new york city subway pedestrian incidents from 2019. *Transportation Research Record*, page 03611981231166692, 2023.

D. Hall, K. Gildea, and C. Simms. Drainage troughs as a protective measure in subway–pedestrian collisions: A multibody model evaluation. *Applied Sciences*, 14(22):10738, 2024.

M. Hamacher, S. Fassbender, F. Feist, and J. Gugler. Modification of a truck front for improved kinematics in run over accidents. In *Proc. 21st Int. Tech. Conf. Enhanc. Saf. Veh. Stuttg. Ger*, pages 15–18, 2009.

H.-S. Han and J.-S. Koo. Simulation of train crashes in three dimensions. *Vehicle System Dynamics*, 40(6):435–450, 2003.

Y. Han, J. Yang, K. Mizuno, and Y. Matsui. Effects of vehicle impact velocity, vehicle front-end shapes on pedestrian injury risk. *Traffic Injury Prevention*, 13(5):507–518, 2012.

W. C. Hayes, M. S. Erickson, and E. D. Power. Forensic injury biomechanics. *Annu. Rev. Biomed. Eng.*, 9:55–86, 2007.

E. Hertz. A note on the head injury criterion (hic) as a predictor of the risk of skull fracture. In *Proceedings: Association for the Advancement of automotive medicine annual conference*, volume 37, pages 303–312. Association for the Advancement of Automotive Medicine, 1993.

J. Ho, M. Mansour, and D. Gomez. Subway-related trauma at a level 1 trauma centre in toronto, ontario. *Canadian journal of surgery*, 64(6):E588, 2021a.

J. Ho, M. Mansour, and D. Gomez. Subway-related trauma at a level 1 trauma centre in toronto, ontario. *Canadian journal of surgery*, 64(6):E588, 2021b.

C. A. Hobbs and P. J. McDonough. Development of the european new car assessment programme (euro ncap). *Regulation*, 44(3):2439–2453, 1998.

H. Ishikawa, J. Kajzer, and G. Schroeder. Computer simulation of impact response of the human body in car-pedestrian accidents. Technical report, SAE Technical Paper, 1993a.

H. Ishikawa, J. Kajzer, and G. Schroeder. Computer simulation of impact response of the human body in car-pedestrian accidents. Technical report, SAE Technical Paper, 1993b.

W. JE and L. HR. Observations on the mechanism of brain concussion, contusion, and laceration. *Surgery, gynecology & obstetrics*, 101(6):680–690, 1955.

M. Jiang, J.-m. Xiao, et al. Research on lightweight laminate for car body with excellent cushioning and energy absorption characteristics. *Heliyon*, 8(11), 2022.

D. Johnston and J. Waddell. Death and injury patterns, toronto subway system 1954–1980. *Journal of Trauma and Acute Care Surgery*, 24(7):619–622, 1984.

J. M. Johnston, H. Ning, J.-E. Kim, Y.-H. Kim, B. Soni, R. Reynolds, L. Cooper, J. B. Andrews, and U. Vaidya. Simulation, fabrication and impact testing of a novel football helmet padding system that decreases rotational acceleration. *Sports Engineering*, 18: 11–20, 2015.

J. Kajzer, C. Cavallero, J. Bonnoit, A. Morjane, and S. Ghanouchi. Response of the knee joint in lateral impact: Effect of bending moment. In *Proceedings of the IRCOBI Conference*, pages 105–116, 1993.

D. Kallieris and G. Schmidt. New aspects of pedestrian protection loading and injury pattern in simulated pedestrian accidents. *SAE Transactions*, pages 1261–1272, 1988.

C. Kam, J. Kerrigan, M. Meissner, C. Drinkwater, D. Murphy, J. Bolton, C. Arregui, R. Kendall, J. Ivarsson, J. Crandall, et al. Design of a full-scale impact system for analysis of vehicle pedestrian collisions. *SAE transactions*, pages 2268–2282, 2005.

J. Kerrigan, C. Kam, C. Drinkwater, D. Murphy, D. Bose, J. Ivarsson, and J. Crandall. Kinematic comparison of the polar-ii and pmhs in pedestrian impact tests with a sport-utility vehicle. *Proceedings of the 2005 International Research Council on the Biomechanics of Impact (IRCOBI), Prague, Czech Republic*, 2005.

J. R. Kerrigan, J. R. Crandall, and B. Deng. Pedestrian kinematic response to mid-sized vehicle impact. *International journal of vehicle safety*, 2(3):221–240, 2007a.

J. R. Kerrigan, J. R. Crandall, and B. Deng. Pedestrian kinematic response to mid-sized vehicle impact. *International journal of vehicle safety*, 2(3):221–240, 2007b.

J. R. Kerrigan, J. R. Crandall, and B. Deng. A comparative analysis of the pedestrian injury risk predicted by mechanical impactors and post mortem human surrogates. Technical report, SAE Technical Paper, 2008.

M. R. Kianifar and F. Campean. Global optimisation of car front-end geometry to minimise pedestrian head injury levels. In *Proceedings of the Design Society: International Conference on Engineering Design*, volume 1, pages 2873–2882. Cambridge University Press, 2019.

K. Lakshminarayana, S. Mitra, and N. Mitra. Trucks with different external frontal frames: Comparing vulnerable road user's injury severities using madymo. In *3rd international conference on road safety and simulation, Indianapolis, USA*, 2011.

C.-K. Law, P. S. Yip, W. S. Chan, K.-W. Fu, P. W. Wong, and Y. Law. Evaluating the effectiveness of barrier installation for preventing railway suicides in hong kong. *Journal of affective disorders*, 114(1-3):254–262, 2009.

M. R. Lemov. *Car safety wars: one hundred years of technology, politics, and death*. Rowman & Littlefield, 2015.

G. Li, J. Yang, and C. Simms. The influence of gait stance on pedestrian lower limb injury risk. *Accident Analysis & Prevention*, 85:83–92, 2015.

G. Li, M. Lyons, B. Wang, J. Yang, D. Otte, and C. Simms. The influence of passenger car front shape on pedestrian injury risk observed from german in-depth accident data. *Accident Analysis & Prevention*, 101:11–21, 2017.

R. Li, P. Xu, Y. Peng, and Y.-q. Xie. Scaled tests and numerical simulations of rail vehicle collisions for various train sets. *Proceedings of the Institution of Mechanical Engineers, Part F: Journal of Rail and Rapid Transit*, 230(6):1590–1600, 2016.

P. T. Lin and J. R. Gill. Subway train-related fatalities in new york city: Accident versus suicide. *Journal of forensic sciences*, 54(6):1414–1418, 2009.

H. Lissner, M. Lebow, and F. G. Evans. Experimental studies on the relation between acceleration and intracranial pressure changes in man. *Surgery, gynecology & obstetrics*, 111:329–338, 1960.

J. Liu, J. Rojas, Y. Li, Z. Liang, Y. Guan, N. Xi, and H. Zhu. A graph attention spatio-temporal convolutional network for 3d human pose estimation in video. In *2021 IEEE international conference on robotics and automation (ICRA)*, pages 3374–3380. IEEE, 2021.

X. Liu, J. Yang, and P. Lövsund. A study of influences of vehicle speed and front structure on pedestrian impact responses using mathematical models. *Traffic Injury Prevention*, 3 (1):31–42, 2002.

K. L. Loftis, J. Price, and P. J. Gillich. Evolution of the abbreviated injury scale: 1990–2015. *Traffic Injury Prevention*, 19(sup2):S109–S113, 2018.

F. Lopot, P. Kubovỳ, K. Jelen, M. Šorfová, E. Tlapáková, V. Rulc, H. Purš, R. Ježdík, and M. Svoboda. Collision between a pedestrian and tram—pilot experiment. *Manufacturing Technology*, 19(6):998–1002, 2019.

M. Mackay. The increasing importance of the biomechanics of impact trauma. *Sadhana*, 32 (4):397–408, 2007.

A. A. Maclean, A. M. O'Neill, H. L. Pachter, and M. A. Miglietta. Devastating consequences of subway accidents: traumatic amputations. *The American Surgeon*, 72(1):74–76, 2006.

S. Madymo. Madymo human body models manual. *Release 7.8*, 2019.

R. Mao, Y. Bao, H. Duan, and G. Liu. Global urban subway development, construction material stocks, and embodied carbon emissions. *Humanities and Social Sciences Communications*, 8(1):1–11, 2021.

D. Marjoux, D. Baumgartner, C. Deck, and R. Willinger. Head injury prediction capability of the hic, hip, simon and ulp criteria. *Accident Analysis & Prevention*, 40(3):1135–1148, 2008.

A. Martin. *Factors influencing pedestrian safety: a literature review*. Number PPR241. TRL Wokingham, Berks, 2006.

P. Martin, J. Radcliffe, M. Qasim, and I. Guy. Enhanced bus front end geometries for improved pedestrian crashworthiness. In *Proceedings of the International Research Council on the Biomechanics of Injury Conference, Online*, pages 8–10, 2020.

S. Martin and M. Rawala. Suicide patterns on the london underground railway system, 2000–2010. *BJPsych bulletin*, 41(5):275–280, 2017.

L. Martinez, L. J. Guerra, G. Ferichola, A. Garcia, and J. Yang. Stiffness corridors of the european fleet for pedestrian simulation. In *Experimental Safety Vehicles Conference*, volume 6, page 2007, 2007.

R. McGill, J. W. Tukey, and W. A. Larsen. Variations of box plots. *The american statistician*, 32(1):12–16, 1978.

R. R. McHenry. Analysis of the dynamics of automobile passenger-restraint systems. In *Proceedings: American association for automotive medicine annual conference*, volume 7, pages 207–249. Association for the Advancement of Automotive Medicine, 1963.

R. R. McHenry and K. N. Naab. Computer simulation of the crash victim-a validation study. Technical report, SAE Technical Paper, 1966.

Metropolitan Transportation Authority Track Trespassing Task Force. System-wide platform screen door feasibility study, 2020. URL `https://new.mta.info/document/73241`.

Metropolitan Transportation Authority Track Trespassing Task Force. Addressing track trespassing: Actions for rider safety & system reliability, 2022. URL `<insertURLifavailable>`. Chartered by Janno Lieber, Chair & CEO.

B. L. Mishara. Suicide in the montreal subway system: characteristics of the victims, antecedents, and implications for prevention. *The Canadian Journal of Psychiatry*, 44(7): 690–696, 1999.

B. L. Mishara. Railway and metro suicides: Understanding the problem and prevention potential. *Crisis*, 28(S1):36–43, 2007.

S. Mitra, N. Mitra, and K. Lakshminarayana. Pedestrian injury severity in the event of a collision with a truck: are energy absorbing adaptive deformable fronts suitable? *International journal of vehicle safety*, 10(3-4):235–252, 2018.

K. Mizuno and J. Kajzer. Head injuries in vehicle-pedestrian impact. *SAE transactions*, pages 232–243, 2000.

O. Nazarian, M. Begley, and F. Zok. A concept for mitigating head injury under translational blunt impact. *International journal of crashworthiness*, 20(5):483–494, 2015.

J. A. Newman and N. Shewchenko. A proposed new biomechanical head injury assessment function-the maximum power index. Technical report, SAE Technical Paper, 2000.

L. Nokes, A. Roberts, and B. Knight. Use of the gadd severity index in forensic medicine: a case study. *Forensic science international*, 76(2):85–90, 1995.

R. Norton, A. Hyder, and M. Peden. The epidemiology of road traffic injuries: what exists, gaps and the role of public health. In *Proceedings of WHO Meeting to Develop a 5-year Strategy for Road Traffic Injury Prevention*, volume 26, page 14, 2001.

I. O'Donnell and E. Farmer. The epidemiology of suicide on the london underground. *Social science & medicine*, 38(3):409–418, 1994a.

I. O'Donnell and E. Farmer. The epidemiology of suicide on the london underground. *Social science & medicine*, 38(3):409–418, 1994b.

I. O'Donnell and R. Farmer. Suicidal acts on metro systems: an international perspective. *Acta Psychiatrica Scandinavica*, 86(1):60–63, 1992.

L. M. Patrick, H. R. Lissner, and E. S. Gurdjian. Survival by design: Head protection. In *Proceedings: American Association for Automotive Medicine Annual Conference*, volume 7, pages 483–499. Association for the Advancement of Automotive Medicine, 1963.

A. Pelletier. Deaths among railroad trespassers: the role of alcohol in fatal injuries. *JAMA*, 277(13):1064–1066, 1997.

Y. Peng, C. Deck, J. Yang, and R. Willinger. Effects of pedestrian gait, vehicle-front geometry and impact velocity on kinematics of adult and child pedestrian head. *International journal of crashworthiness*, 17(5):553–561, 2012.

Y. Peng, L. Hou, M. Yang, and H. Tian. Investigation of the train driver injuries and the optimization design of driver workspace during a collision. *Proceedings of the Institution of Mechanical Engineers, Part F: Journal of Rail and Rapid Transit*, 231(8):902–915, 2017.

C. Poirier, S. Adelé, and J.-M. Burkhardt. Individual accidents at the interface between platform, train and tracks (pt 2 i) in the subway: a literature review. *Cognition, Technology & Work*, 23:203–224, 2021.

H. Pritz, C. Hassler, J. Herridge, and E. Weis. Experimental study of pedestrian injury minimization through vehicle design. Technical report, SAE Technical Paper, 1975.

L. Qu and W. K. Chow. Platform screen doors on emergency evacuation in underground railway stations. *Tunnelling and Underground Space Technology*, 30:1–9, 2012.

R. Richardson, J.-P. Donlon, M. Jayathirtha, J. L. Forman, G. Shaw, B. Gepner, J. R. Kerrigan, M. Östling, K. Mroz, and B. Pipkorn. Kinematic and injury response of reclined pmhs in frontal impacts. Technical report, SAE Technical Paper, 2021.

D. H. Robbins, B. M. Bowman, and R. O. Bennett. The mvma two-dimensional crash victim simulation. Technical report, SAE Technical Paper, 1974.

L. S. Robertson. *Injury epidemiology*. Lulu. com, 2015.

S. G. Rodier, C. J. DiMaggio, S. Wall, V. Sim, S. G. Frangos, P. Ayoung-Chee, M. Bukur, M. Tandon, S. R. Todd, and G. T. Marshall. Subway-related trauma: an urban public health issue with a high case-fatality rate. *The Journal of Emergency Medicine*, 55(2): 165–171, 2018.

B. Rowson and S. M. Duma. A review of head injury metrics used in automotive safety and sports protective equipment. *Journal of biomechanical engineering*, 144(11):110801, 2022.

A. Sances Jr, F. H. Carlin, B. Herbst, S. Forrest, S. Meyer, A. Khadilkar, K. Friedman, and J. Bish. Studies of vehicular padding materials. In *Annual Proceedings/Association for the Advancement of Automotive Medicine*, volume 44, page 133. Association for the Advancement of Automotive Medicine, 2000.

G. Schroeder. Injury mechanism of pedestrians during a front-end collision with a late model car. In *JSAE Spring Convention, 2000*, 2000.

S. Shang, D. Otte, G. Li, and C. Simms. Detailed assessment of pedestrian ground contact injuries observed from in-depth accident data. *Accident Analysis & Prevention*, 110:9–17, 2018.

S. Shang, C. Masson, D. Teeling, M. Py, Q. Ferrand, P.-J. Arnoux, and C. Simms. Kinematics and dynamics of pedestrian head ground contact: A cadaver study. *Safety science*, 127: 104684, 2020.

S. Shang, C. Masson, M. Llari, M. Py, Q. Ferrand, P.-J. Arnoux, and C. Simms. The predictive capacity of the madymo ellipsoid pedestrian model for pedestrian ground contact kinematics and injury evaluation. *Accident Analysis & Prevention*, 149:105803, 2021.

L. Shi, Y. Han, H. Huang, Q. Li, B. Wang, and K. Mizuno. Analysis of pedestrian-to-ground impact injury risk in vehicle-to-pedestrian collisions based on rotation angles. *Journal of safety research*, 64:37–47, 2018a.

L. Shi, Y. Han, H. Huang, Q. Li, B. Wang, and K. Mizuno. Analysis of pedestrian-to-ground impact injury risk in vehicle-to-pedestrian collisions based on rotation angles. *Journal of safety research*, 64:37–47, 2018b.

C. Simms and D. Wood. *Pedestrian and cyclist impact: a biomechanical perspective*, volume 166. Springer Science & Business Media, 2009.

C. K. Simms and D. P. Wood. Effects of pre-impact pedestrian position and motion on kinematics and injuries from vehicle and ground contact. *International Journal of Crashworthiness*, 11(4):345–355, 2006.

G. Sonneck, E. Etzersdorfer, and S. Nagel-Kuess. Imitative suicide on the viennese subway. *Social science & medicine*, 38(3):453–457, 1994.

J. P. Stapp. Tolerance to abrupt deceleration. *Collected Papers on Aviation Medicine*, (14): 122–169, 1955.

Y. Su. A comparative study of pedestrian fatalities and new car assessment programs in the us and japan. 2019.

B. Suntay, J. Stammen, et al. Assessment of hood designs for pedestrian head protection: Active hood systems. Technical report, United States. Department of Transportation. National Highway Traffic Safety . . . , 2020.

E. G. Takhounts, M. J. Craig, K. Moorhouse, J. McFadden, and V. Hasija. Development of brain injury criteria (bric). Technical report, SAE Technical Paper, 2013.

G. Tiwari. Progress in pedestrian safety research. *International journal of injury control and safety promotion*, 27(1):35–43, 2020.

L. Tomsovsky, F. Lopot, P. Kubovy, R. Jezdik, B. Hajkova, V. Rulc, and K. Jelen. Tram-pedestrian collisions: The severity of head injuries due to secondary impact with the surrounding infrastructure (ground). In *2022 International Conference on Electrical, Computer, Communications and Mechatronics Engineering (ICECCME)*, pages 1–6. IEEE, 2022.

U.S. Department of Transportation. Departmental guidance on valuation of a statistical life in economic analysis, 2023. URL `https://www.transportation.gov/office-policy/transportation-policy/revised-departmental-guidance-on-valuation-of-a-statistical-life-in-economic-analysi` Accessed: 2025-02-13.

M. Vander Vorst, J. Stuhmiller, K. Ho, N. Yoganandan, and F. Pintar. Statistically and biomechanically based criterion for impact-induced skull fracture. In *Annual Proceedings/Association for the Advancement of Automotive Medicine*, volume 47, page 363. Association for the Advancement of Automotive Medicine, 2003.

J. Versace. A review of the severity index. 1971a.

J. Versace. A review of the severity index. 1971b.

H. Wang and R. B. Noland. Bikeshare and subway ridership changes during the covid-19 pandemic in new york city. *Transport policy*, 106:262–270, 2021.

W.-M. Wey. Constructing urban dynamic transportation planning strategies for improving quality of life and urban sustainability under emerging growth management principles. *Sustainable Cities and Society*, 44:275–290, 2019.

S. D. White, J. L. Salmon, P. Prasad, R. A. Burnett, A. Kim, and J. Buckman. A current assessment of the thor 50m in rear impacts. *Traffic Injury Prevention*, 24(3):208–212, 2023.

P. Xu, S. Lu, K. Yan, and S. Yao. Energy absorption design study of subway vehicles based on a scaled equivalent model test. *Proceedings of the Institution of Mechanical Engineers, Part F: Journal of Rail and Rapid Transit*, 233(1):3–15, 2019.

X. Xue, F. Schmid, and R. Smith. Analysis of the structural characteristics of an intermediate rail vehicle and their effect on vehicle crash performance. *Proceedings of the Institution of Mechanical Engineers, Part F: Journal of Rail and Rapid Transit*, 221(3):339–352, 2007.

J. Yang, P. Lövsund, C. Cavallero, and J. Bonnoit. A human-body 3d mathematical model for simulation of car-pedestrian impacts. *Traffic Injury Prevention*, 2(2):131–149, 2000.

S. Yin, J. Li, and J. Xu. Exploring the mechanisms of vehicle front-end shape on pedestrian head injuries caused by ground impact. *Accident Analysis & Prevention*, 106:285–296, 2017.

T. Zou, S. Shang, and C. Simms. Potential benefits of controlled vehicle braking to reduce pedestrian ground contact injuries. *Accident Analysis & Prevention*, 129:94–107, 2019.

Appendix A

Quasi-static Compression Testing Used in Chapter 4

A.1 Firm Foam F2H 40F

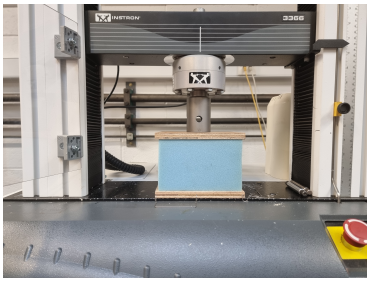

(a) Full Plate No Strain

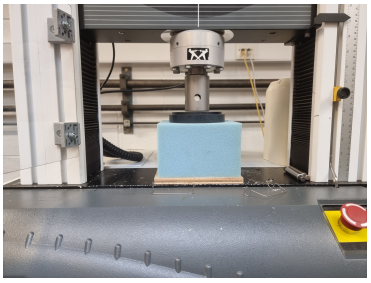

(b) Large Indentor No Strain

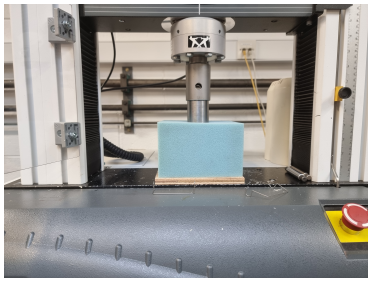

(c) Small Indentor No Strain

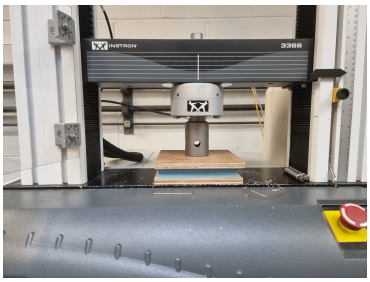

(d) Full Plate 80% Strain

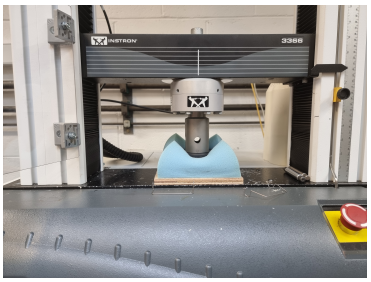

(e) Large Indentor 80% Strain

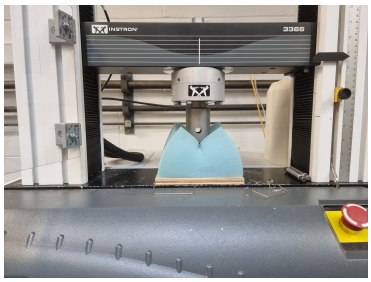

(f) Small Indentor 80% Strain

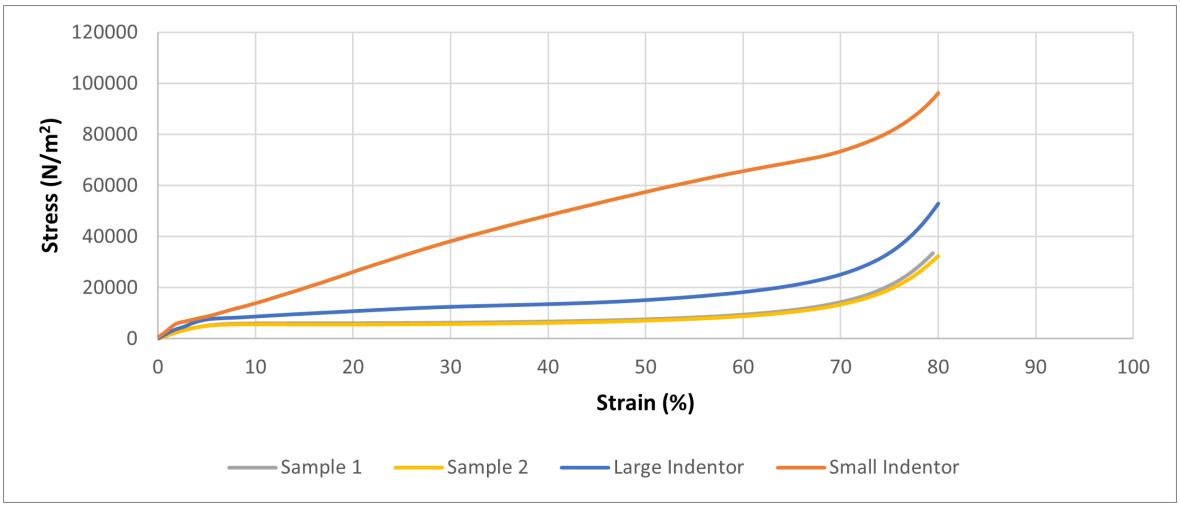

(g) Firm Foam Stress Strain Curves

Figure A.1: Firm foam compression test results

A.2 Mixed Firm and Memory Foam F2H 36M

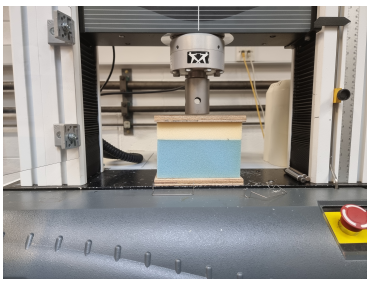

(a) Full Plate No Strain

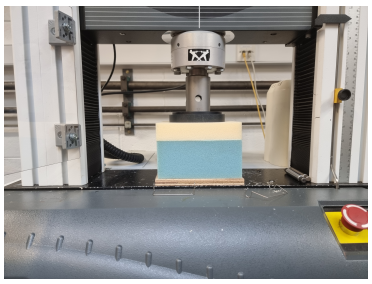

(b) Large Indentor No Strain

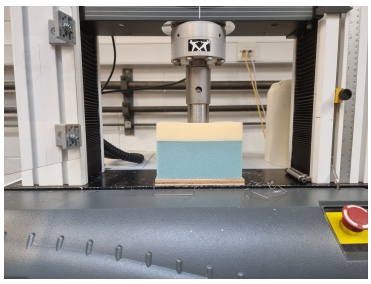

(c) Small Indentor No Strain

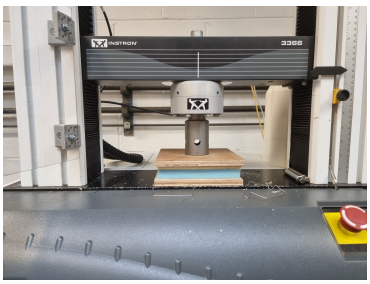

(d) Full Plate 80% Strain

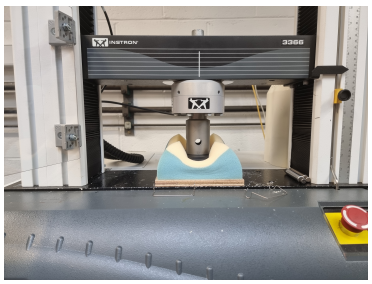

(e) Large Indentor 80% Strain

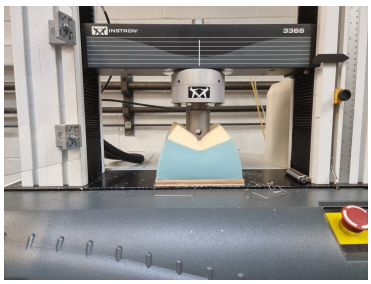

(f) Small Indentor 80% Strain

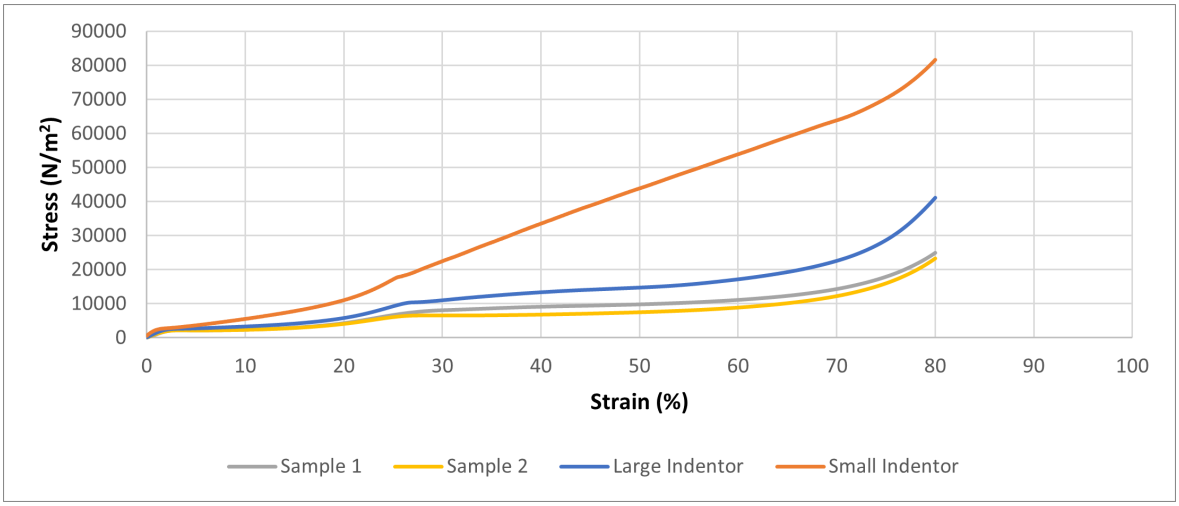

(g) Mixed Firm and Memory Foam Stress Strain Curves

Figure A.2: Firm foam with memory compression test results

Appendix B

DYNATEST Operational Procedure Used in Chapter 4

The operating procedure for the Dynatest 500 is as follows:

1. Connect the nitrogen bottles to the cylinder using the compressed gas quick release connector.
2. Open the nitrogen bottles using a key.
3. Switch on the control panel. The available pressure from the nitrogen bottles will be displayed in the top left screen.
4. Fill the set pressure as required for the test using the dial.
5. Engage the set isolation using the set isolation button on the right side of the control panel.
6. Fill the load pressure as required for the test. A load to set pressure ratio of 5:1 is recommended. Load to set pressure ratios above 6:1 should be avoided as this may cause premature activation.
7. Set the trigger pressure as required. This is used to open the seal at the orifice
8. Ensure all personnel are at a safe location, then disengage the lock yokes. This will sound the alarm and a ten second timer will be displayed.
9. Hold down the trigger button until zero and the piston will activate.
10. Once complete the system should be vented using the vent button on the load side of the control panel. This will vent the remaining nitrogen in the cylinder and retract the piston.
11. Once fully retracted, reengage the lock yokes. The alarm will stop sounding and the light will return to green indicating it is safe to approach.
12. To carry out additional tests, repeat the above steps.
13. To finish testing, isolate the nitrogen bottles and vent the system.

Appendix C

Construction of Containment Unit Used in Chapter 4



(a) No containment unit

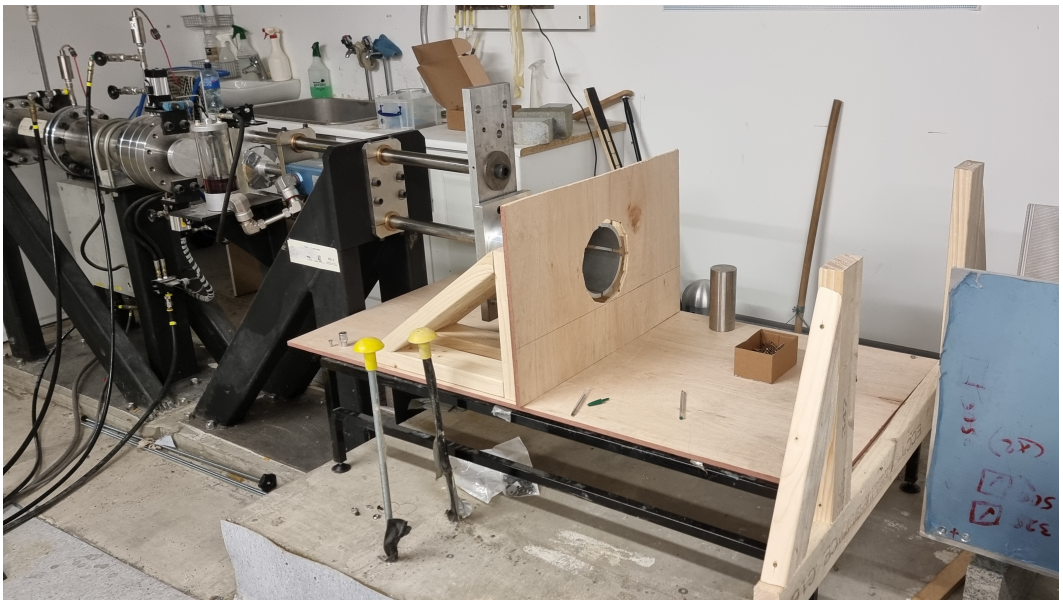

(b) Containment unit in construction

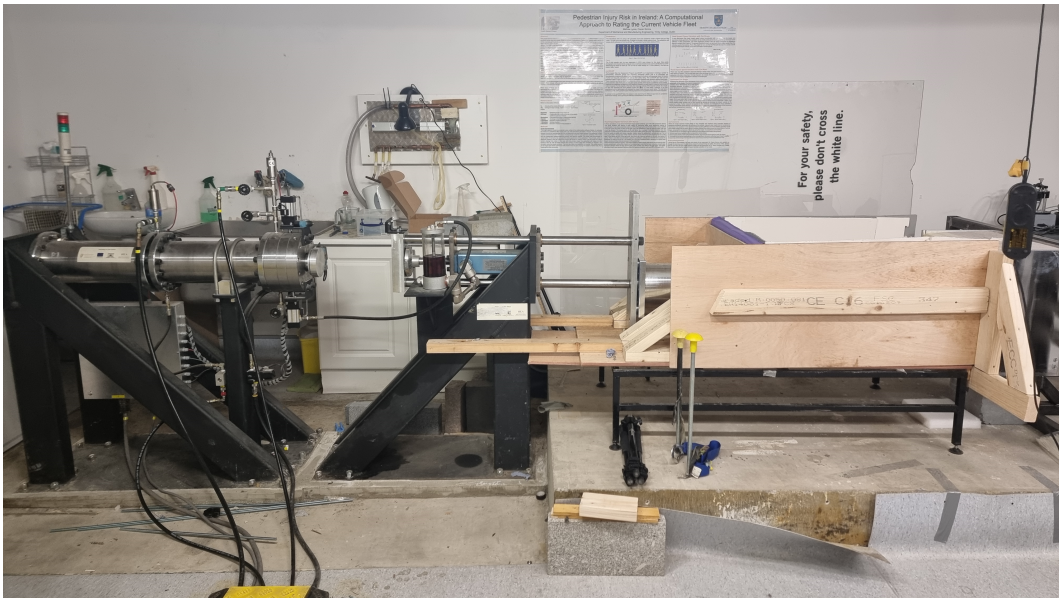

(c) Completed containment unit

Figure C.1: Dynatest 500 impact ram with containment unit and EAC mounting block

Appendix D

Effect of Z Axis Acceleration on Foam Impact Tests [Chapter 4]

D.1 Investigation of Multi-Axis Rotational Effects on Acceleration Time History

Figure D.1 shows the acceleration time history for a 7.5m/s impact with the foam countermeasure as described in Chapter 4. The addition of a second accelerometer with the sensitive axis in the direction of gravity results in only a slight change in the acceleration profile and thus the conclusions drawn from Chapters 4 and 6.

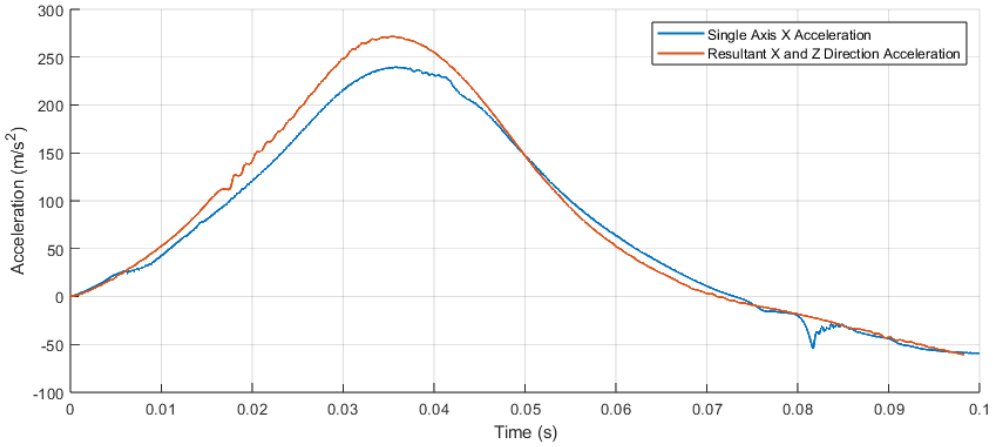

Figure D.1: Effect of incorporating Z axis acceleration to 7m/s foam impact tests